Department for Environment Food & Rural Affairs

Department for Business, Energy & Industrial Strategy

Met Office Hadley Centre

Environment Agency

UKCP18 Marine report

November 2018

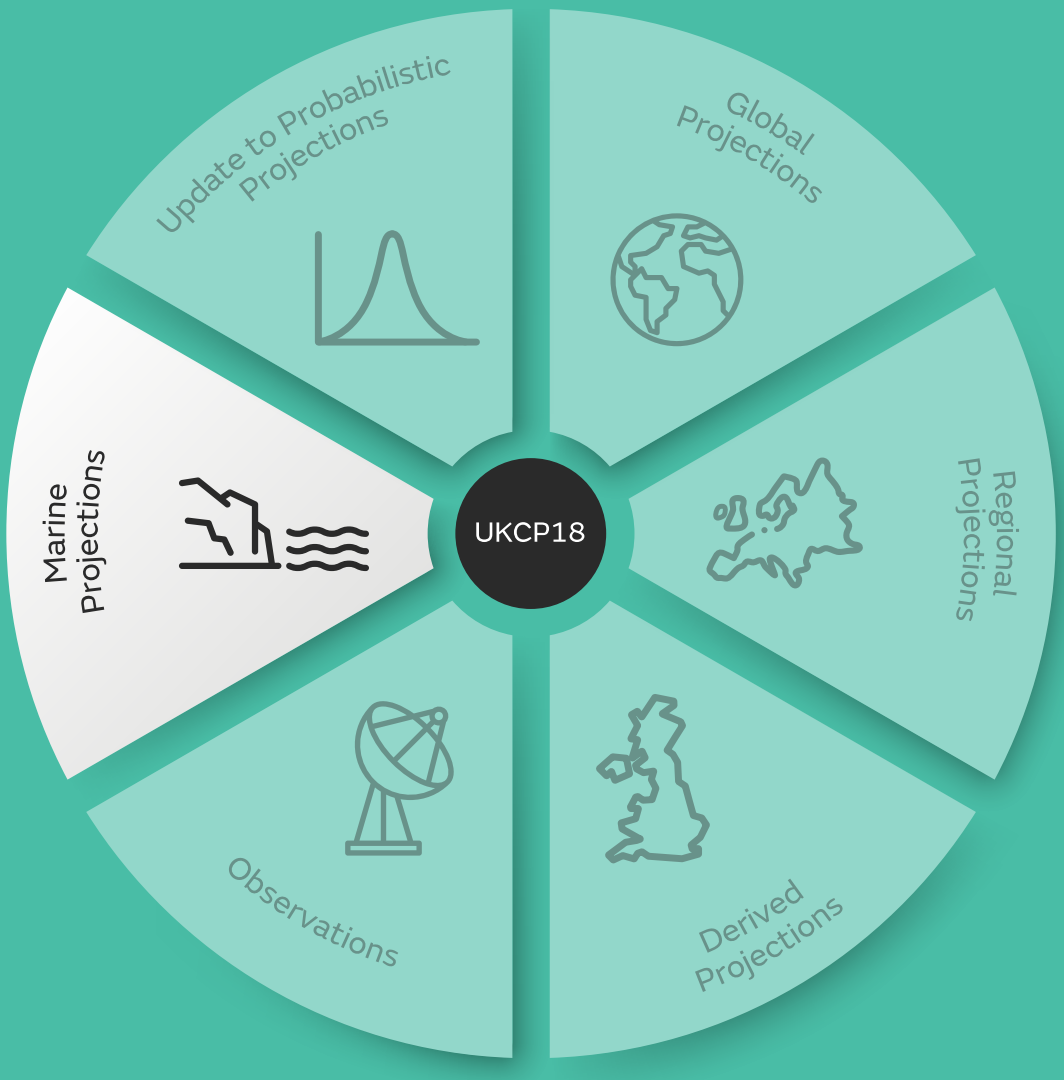

Matthew Palmer, Tom Howard, Jonathan Tinker, Jason Lowe, Lucy Bricheno[1], Daley Calvert, Tamsin Edwards[2], Jonathan Gregory, Glen Harris, Justin Krijnen, Mark Pickering[3], Chris Roberts and Judith Wolf[1].

[1] National Oceanography Centre, Liverpool, UK [2] King's College, London, UK [3] University of Southampton, UK

www.metoffice.gov.uk

Contents

Summary

In this section we present a summary of the key findings and caveats associated with the marine projections of UKCP18. Where appropriate, we include a reference to the relevant chapter where further details and discussion on these points can be found.

1.1 Background to the UKCP18 marine projections

The UKCP18 marine projections have been devised in consultation with a variety of UK stakeholder groups. The purpose of this report, along with the associated data products, is to facilitate vulnerability assessments to aid coastal decision makers. The emphasis of the UKCP18 marine projections is on changes in coastal sea level, including extreme water levels that arise from storm surges and surface waves. Users should be aware that the scope of work is different to that presented in UKCP09 (Lowe et al, 2009) as discussed further in section 5. In particular, we do not update the work to assess changes in coastal water properties and we have developed extended time-horizon sea level projections to meet stakeholder requirements.

As with UKCP09 (Lowe et al, 2009), the UKCP18 sea level projections take a simpler approach to quantifying uncertainty than the Bayesian methods employed for the Land Scenarios (Murphy et al, 2018). Our methods essentially follow those described in the IPCC 5th Assessment Report of Working Group 1 (IPCC AR5; Church et al, 2013) and do not include any weighting of the climate model ensemble used. All the projections presented in this report are premised on the RCP climate change scenarios described by Meinshausen et al, (2011). Following IPCC AR5, the ranges of the time-mean sea level projections presented in this report (Sections 3.1 and 4.2) are based on the 5th and 95th percentiles of the underlying model simulations, for a given RCP scenario. However, there may be a greater than 10% chance that the real-world response lies outside these ranges and this likelihood cannot be accurately quantified. In particular, we cannot rule out substantial additional sea level rise associated primarily with dynamic ice discharge from the West Antarctic Ice Sheet (see section 3.2.1). We recommend that decision makers make use of the projections presented in this report alongside multiple strands of evidence, including H++ scenarios[1], when assessing vulnerabilities to future extreme water levels.

1.2 Key findings

- UK coastal flood risk is expected to increase over the 21st century and beyond under all RCP climate change scenarios. This means that we can expect to see both an increase in the frequency and magnitude of extreme water levels around the UK coastline. This increased future flood risk will be dominated by the effects of time-mean sea level rise, rather than changes in atmospheric storminess associated with extreme coastal sea level events.
- 21st century projections of time-mean sea level change around the UK vary substantially by climate change scenario and geographic location. The ranges for UK capital cities at 2100 are summarised below for each RCP climate change scenario included in this report.

[1] "High-plus-plus" or "H++" scenarios are designed to explore the high-end plausible future sea level rise and complement the process-based sea level projections presented in IPCC assessments.

	Sea level change at 2100 (m) relative to 1981-2000 average		
	RCP2.6	RCP4.5	RCP8.5
London	0.29-0.70	0.37-0.83	0.53-1.15
Cardiff	0.27-0.69	0.35-0.81	0.51-1.13
Edinburgh	0.08-0.49	0.15-0.61	0.30-0.90
Belfast	0.11-0.52	0.18-0.64	0.33-0.94

- UK tide gauge records show substantial year-to-year changes in coastal water levels (typically several centimetres). We recommend that coastal decision makers account for this variability in risk assessments, particularly for shorter-term planning horizons. Numerical modelling results presented in this report suggest that variability observed at tide gauge sites is typically representative of long sections of coastline (section 3.1.4).
- The risk of coastal flood events will rise in accord with the projections of increase in time-mean sea level. However, based on storm surge modelling work, we suggest a best estimate of no significant additional increase in the statistics of extreme water levels associated with atmospheric storminess change only. The largest trend found in our ensemble of surge simulations of this additional component corresponds to a change of approximately 10cm per century for the 1-year return level, i.e. about 10% of the time-mean sea level change under the same RCP climate change scenario (section 3.2). We cannot rule out larger trends in storm surge due to this additional component. This additional component could be either positive (augmenting the time-mean sea level change) or negative (partially offsetting the time-mean sea level change).
- 21st century projections of average wave height suggest changes of the order 10-20% and a general tendency towards lower wave heights. Changes in extreme waves are also of order 10-20%, but there is no agreement in the sign of change among the model projections. High resolution wave simulations suggest that the changes in wave climate over the 21st century on exposed coasts will be dominated by the global response to climate change. However, more sheltered coastal regions are likely to remain dominated by local weather variability over the 21st century (section 3.3).
- Exploratory, time-mean sea level projections to 2300 suggest that UK sea levels will continue to rise over the coming centuries under all RCP climate change scenarios. For London and Cardiff the projection ranges at 2300 are approximately 0.5 - 2.2m, 0.8 - 2.6m and 1.4 - 4.3m for RCP2.6, RCP4.5 and RCP8.5, respectively. The values for Edinburgh and Belfast are substantially lower, with corresponding ranges at 2300 of approximately 0.0 - 1.7m, 0.2 - 2.1m and 0.7 - 3.6m. Compared to the 21st century projections, there is a much larger degree of unquantified uncertainty associated with sea level information on these extended time horizons. Therefore, these projections should be considered as illustrative of the potential future changes and provide an approximate set of scenarios against which vulnerabilities can be assessed.
- Idealised tidal simulations suggest that time-mean sea level change greater than about 1m could have a substantial impact on tidal amplitude and other tidal characteristics around the UK, with large spatial variations. This finding is qualitatively consistent with previous research, but the details vary among studies.

Further work is needed to better quantify the full impact these changes might have (e.g. coastal flooding, tidal currents, sediment transport, ecology, tidal profile for shipping etc). However, our results suggest that time-mean sea level change will have only a small effect on the size of storm surges over and above the effect on the tides (section 4.3).

1.3 Caveats and limitations

- The UKCP18 21st century time-mean sea level projections are based upon the 5th to 95th percentiles of the underlying model distributions. There may be a greater than 10% chance that the real-world response lies outside the 5th to 95th percentile range and this likelihood cannot be accurately quantified. We cannot rule out substantial additional sea level rise associated primarily with dynamic ice discharge from the West Antarctic Ice Sheet. We recommend that decision makers make use of multiple strands of evidence, including H++ scenarios when assessing vulnerabilities to future extreme water levels.
- The 21st century projections presented in this report are predicated on the CMIP5 climate models and the RCP climate change scenarios. The results are therefore subject to any inherent limitations of the underlying model ensembles and assumed climate change scenarios.
- The 21st century surge and wave projections are based upon relatively small CMIP5 model ensembles. It is unlikely that these simulations span the full range of CMIP5 model responses under climate change. These projections should be viewed as indicative of the overall magnitude of changes we might see over the 21st century. For both these sets of simulations, we cannot be sure of the relative influence of the climate change signal versus natural variability.
- The extended time-mean sea level projections have much lower confidence than the 21st century projections. These projections can be considered as sensitivity studies and should not be interpreted as showing the full range of post 2100 behaviour, or the most likely behaviour. The potential for additional sea level rise from Antarctic dynamic ice discharge is even more uncertain on these time horizons, with some studies suggesting several additional metres of rise by 2300 under RCP8.5.
- The simulations of changes in tide and surge characteristics make the simple assumption of a fixed coastline under all levels of future sea level rise. However, several global tide model studies (e.g. Pickering et al, 2017) find that tidal changes are very sensitive to coastal management practices. Thus, the findings presented here should be interpreted as illustrative of potential changes. Further work is needed under more realistic model configurations to make progress in this research avenue.
- One of the limitations of the storm surge and waves projections presented in this report was the availability of high frequency CMIP5 climate model output needed to drive surge and wave model simulations. The storm surge projections (presented in section 3.2) made use of dynamically downscaled data provided as part of the Euro-CORDEX project. Only a handful of Euro-CORDEX simulations had the high frequency surface wind and pressure data required to drive the storm surge model. The wave projections (presented in section 3.3) were limited to existing global and regional wave model simulations that had already been carried out as part the EU RISES-AM and COWCLIP projects. It was not possible to include the GFDL-ESM2M model (which provides our largest increase in the atmospheric drivers of surge) among our wave simulations. This limited the degree of consistency we were able to achieve across the surge and wave modelling components and resulted in model ensembles that are much smaller than for the time-mean sea level projections.

- The primary effect of mean sea level increase on waves is to increase the mean height around which the waves fluctuate, leading to increased over-topping and coastal flooding. An important secondary inshore effect arises as follows. The maximum amplitude of waves before breaking in shallow water is limited by the water depth (e.g. Goda, 2000). Thus, an increase in mean sea level will in general have the secondary effect of moving the surf zone further inshore, increasing the wave energy available at the coast for over-topping and coastal erosion, thereby exacerbating the primary effect. We do not assess this secondary inshore effect here: our assessment of changes in the wave climate focuses on offshore wave changes.

2. Introduction

Section summary: Changes in global and regional sea level arise from a wide variety of geophysical processes that operate on different time and space scales (the sea level "jigsaw puzzle"). Global mean sea level (GMSL) rise occurs from thermal expansion of seawater and the addition of water to the ocean from the loss of land-based ice and water. Changes in land-based ice and water storage result in spatial patterns of regional sea level change through the associated impact on Earth's gravity field and other effects. Local changes in seawater density and ocean circulation also give rise to a spatial pattern of change, which varies markedly among climate models, and is therefore highly uncertain. In addition, the ongoing response of the Earth system to the last deglaciation brings about a spatial pattern of regional sea level change across the UK that is dominated by the effect of vertical land motion. At local scales, the impacts of coastal sea level change typically arise primarily from extreme water level events. These deviations from the regional mean water level are often associated with storm surges and extreme wave conditions combined with the local tide. The UKCP18 sea level work focuses on 21st century projections of: (i) regional time-mean sea level; (ii) changes in surge extremes; (iii) potential changes in tide and surge characteristics; and (iv) changes in local wave climate. In addition, we present exploratory projections of regional time-mean sea level change out to 2300. All projections are rooted in, or traceable to, CMIP5 climate model simulations under the RCP climate change scenarios.

2.1 The sea level "jigsaw puzzle"

Changes in sea level occur due to a broad range of geophysical processes that operate on different spatial scales and time scales. Like the pieces of a jigsaw puzzle, it is important to have an appreciation of how these different processes combine, and in some cases interact, to see the whole picture. In this section we present a schematic of the different sea level components that are included in the UKCP18 sea level projections (Figure 2.1.1) and discuss the different terms and their interactions.

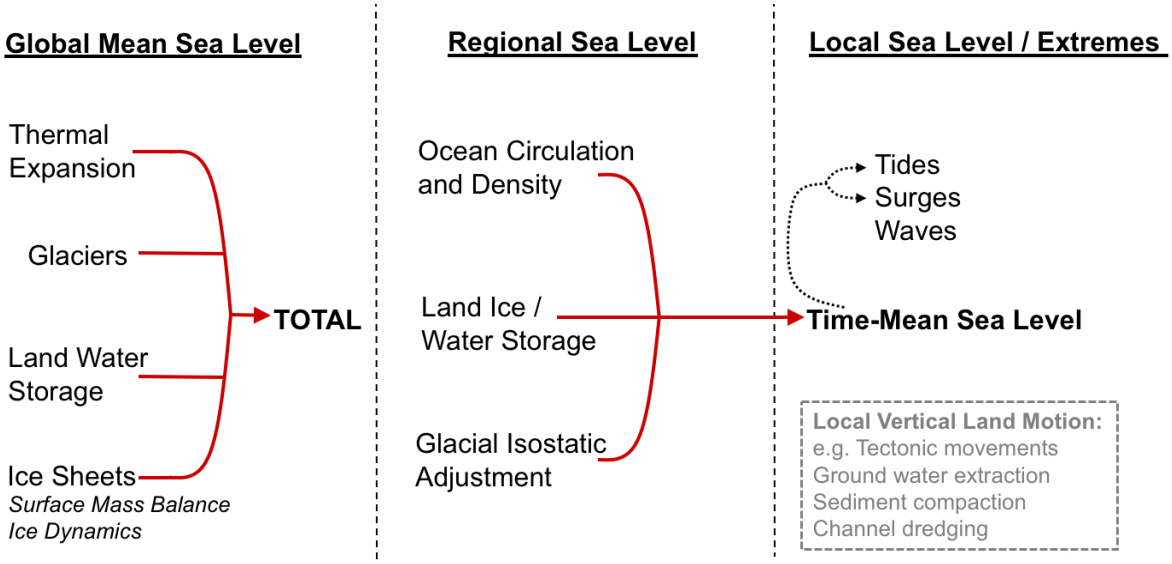

Figure 2.1.1. The sea level "jigsaw puzzle" including the various components that are represented in the UKCP18 sea level projections. The schematic summarises the major contributors to changes in: global time-mean sea level (left-hand column); regional sea level (middle column); and local sea level and extremes (right-hand column). The potential interaction between local time-mean sea level and tide and surge characteristics is indicated by the black dashed lines. The grey text highlights some of the non-climatic processes that can give rise to sea level change through vertical land motion. These processes are not included in the UKCP18 sea level projections.

Changes in global mean sea level (GMSL, Figure 2.1.1, left column) arise due to either: (i) changes in the average ocean density (e.g., if the ocean becomes less dense, the volume increases and GMSL rises); or (ii) a change in global ocean mass through input or removal of water. For GMSL, changes in density are overwhelmingly dominated by thermal expansion, i.e. the tendency for seawater to become less dense as temperature increases (e.g. Griffies et al, 2014). Under anthropogenic climate change, freshwater input to the ocean arises from loss of land-based ice from mountain glaciers and the Greenland and Antarctic ice sheets. Following IPCC AR5 (Church et al, 2013) and other studies, the UKCP18 sea level projections include both surface mass balance (i.e. the balance between accumulated snowfall and ice melt) and ice dynamics (i.e. changes in rate of discharge in active ice flows) for each of the ice sheets. Finally, changes in land water storage, through processes such as groundwater extraction and reservoir impoundment make a substantial contribution to GMSL change (e.g. Church et al, 2011; Wada et al, 2012; Dieng et al, 2015).

As we move to regional scales, several additional processes come into play (Figure 2.1.1, middle column). Firstly, changes in local seawater density and/or ocean circulation leave their imprint in the shape of the sea surface. While temperature effects dominate density changes for GMSL, locally both changes in temperature and salinity are important factors (e.g. Lowe and Gregory, 2005; Pardaens et al, 2011). Due to the differing responses among climate models (Pardaens et al, 2011; Slangen et al, 2014) the spatial pattern of change associated with ocean circulation and density is highly uncertain. Following the nomenclature of Kopp et al, (2014), we refer to the combined effect of changes in global thermal expansion and the regional ocean circulation and density as "oceanographic" sea level change.

Secondly, changes in land-based ice and land water storage are also associated with spatial patterns of regional sea level change. These spatial patterns depend on the geographic distribution of the mass changes and arise from: (i) the solid Earth response to changes in local mass loading; (ii) the effect of the mass redistribution on Earth's gravity field; (iii) the combined effect of (i) and (ii) on Earth's rotation (e.g. Tamisiea and Mitrovica, 2011). Estimates of the six different mass fingerprint patterns used in the UKCP18 sea level projections are presented in section A1.1.2, following Slangen et al, (2014).

Thirdly, the ongoing response of the Earth system to the last deglaciation (which terminated approximately 10, 000 years ago) - referred to as glacial isostatic adjustment (GIA) - gives rise to a spatial pattern of sea level change across the UK with peak magnitudes of approximately +/- 1 mm per year (Figure A1.1.5). This pattern is characterised by sea level fall centred on Western Scotland and sea level rise to the south of mainland UK, with maximum values in the south east and south west. While vertical land is the dominant contribution to this pattern, gravitational and rotational effects also make a substantive contribution (Shennan et al, 2012). Due to the long adjustment timescales associated with GIA, the rates of change are constant for the time horizons presented in the UKCP18 sea level projections.

The superposition of the three different spatial elements described above, determine the sea level change for a given location in the UKCP18 time-mean sea level projections (see section A1.1 for more details). In addition to the climate change signal, coastal decision makers should be aware of the substantial interannual variations in time-mean sea level, as evidenced in tide gauge records around the UK. The future evolution of regional sea level will be a combination of the climate change signals represented by the UKCP18 time-mean sea level projections and this background variability. For this reason, information on the spatial patterns and magnitude of coastal sea level variability is provided alongside the UKCP18 time-mean sea level projections to aid interpretation of the available tide gauge records.

As we move to the local scale (Figure 2.1.1, right column), it is important to consider the potential for changes in the drivers of sea level extremes. It is well known that many of the worst and earliest effects of sea level rise will be experienced during extreme high-water events, which are usually associated with high tides combined with storm surges and may involve overtopping due to extreme wave heights. While previous studies (e.g. Lowe et al, 2009; Howard et al, 2014; Cannaby et al, 2016) have emphasised the dominance of changes in time-mean sea level in driving changes in future coastal sea level extremes, it is important to also consider changes in the extremes themselves that may arise through, for example, changes in atmospheric storminess. For this reason, the UKCP18 sea level projections consider the potential for changes in extreme surge events and the regional wave climate around the UK (sections 3.2 and 3.3).

In addition, there is potential for interaction between the changes in local time-mean sea level and tide and surge characteristics, due to the influence of water depth on the tide and surge. These effects are examined in UKCP18 by considering how past extreme surge events might play out given future increases in local time-mean sea level (section 4.3).

2.2 Overview of the UKCP18 time-mean and extreme sea level projections

The sea level projections presented in this report cover four fundamental aspects relevant to coastal water levels: (1) projections of regional time-mean sea level, i.e. the local baseline water level on which the local variability and sea level extremes are superimposed; (2) projections of changes in storm surge extremes; (3) projections of changes in local wave climate and wave extremes; (4) assessment of the potential for changes in tide and surge characteristics arising from local time-mean sea level change.

As with UKCP09, the focus of the UKCP18 sea level projections is on the 21st century (section 3). However, due to the interest in longer time horizons from some stakeholders (e.g. the nuclear energy sector) we also present exploratory time-mean sea level projections out to 2300 (section 4). Users should be aware that there is a greater degree of unquantified uncertainty for these multi-century projections. Our assessment of the potential for changes in surge and tide characteristics considers levels of future time-mean sea level change that are commensurate with multi-century time-horizons (section 4.3).

All elements of the UKCP18 sea level projections are rooted in the climate model simulations of the Coupled Model Intercomparison Project Phase 5 (CMIP5, Taylor et al, 2012). These models formed the basis of the climate projections presented in the IPCC AR5 (IPCC, 2013) and exhibit substantial improvements over their predecessor CMIP3 models (Meehl et al, 2007), including their representation of sea level (see section A2.1).

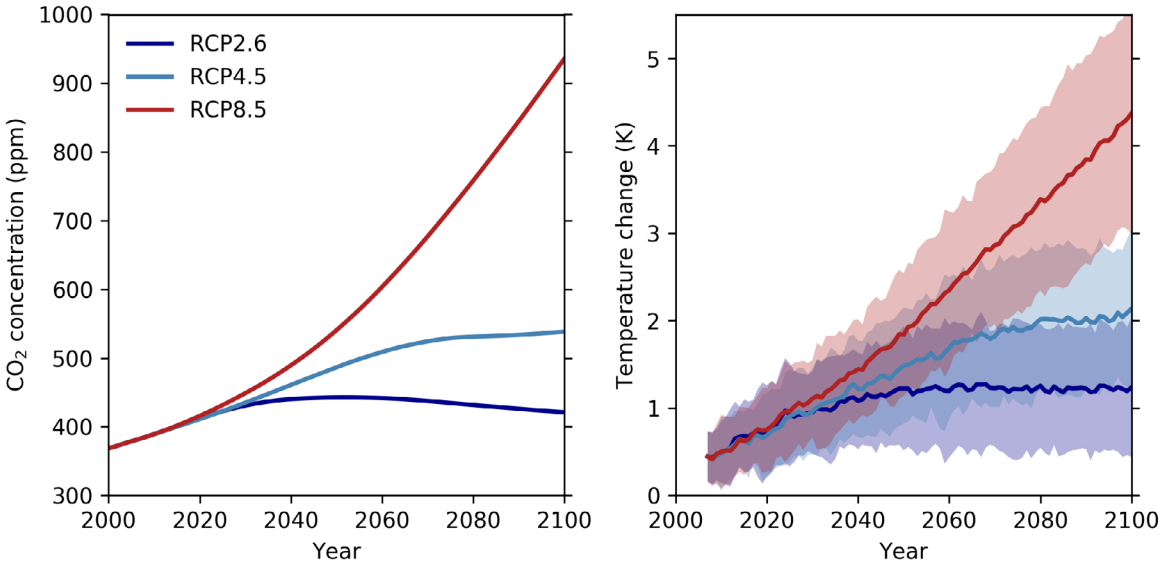

Figure 2.2.1. The UKCP18 sea level projections are based on three of the Representative Concentration Pathways (RCPs, Meinshausen et al, 2011) that formed the basis of the climate change projections presented in the IPCC AR5. (left) Carbon dioxide concentrations over the 21st century for RCP2.6, RCP4.5 and RCP8.5. (right) The associated global mean surface temperature change resulting from carbon dioxide and other climate forcings for the ensemble of CMIP5 climate models used in the UKCP18 time-mean sea level projections. Temperature change is shown relative to a 1981-2000 baseline. The shaded regions represent the projection range.

The UKCP18 time-mean sea level projections include three Representative Concentration Pathway (RCP; Meinshausen et al, 2011) climate change scenarios; RCP2.6, RCP4.5 and RCP8.5 (Figure 2.2.1). These RCPs span a larger range of climatic forcings than the SRES scenarios that were used in UKCP09 (see section 5). We do not include results for RCP6.0 because the scenario exhibits a similar global mean sea level rise at 2100 to RCP4.5 and has poorer data availability in the CMIP5 database than the other scenarios.

The UKCP18 projections of surge extremes make use of CMIP5 simulations under RCP8.5 that have been dynamically downscaled by regional atmospheric models under the EURO-CORDEX experiment (Jacob et al, 2014). We consider only RCP8.5 to maximise the climate change signal and promote the most robust statistics in our analyses. The wave projection work makes use of both global CMIP5 model simulations and a regionally downscaled EURO-CORDEX simulation for both RCP4.5 and RCP8.5.

3. 21st century projections

In this section we present 21st century projections of: (i) changes in time-mean sea level (section 3.1); (ii) changes in storm surges and extreme water levels (section 3.2); (iii) changes in the UK wave climate (section 3.3). Details of the methods and evaluation of the modelling systems are presented in sections A1 and A2, respectively.

Figure 3.1. Coastal sites that are included in the projections of changes in storm surge statistics (section 3.2). The coastal outline comes from the storm surge model grid, which is used as the basis of the data delivery for the time-mean sea level and surge projections in the UKCP18 user interface.

Our projections of 21st century sea level change focus on the coastline of the UK and in particular the sites shown in Figure 3.1, which correspond approximately to tide gauge locations. To unify the data delivery of time-mean sea level and surge projections, these are both presented on the storm surge model grid used in section 3.2. There are 775 model grid boxes around the UK coastline, and the above tide gauge sites are of particular interest because these are sites where return-level information is available along with an estimate of the local sea level variability directly from tide gauge observations. Projections at tide gauge sites use the nearest model grid box to the real tide gauge location, to ensure consistency between surge model output and the time-mean sea level projections.

3.1 Projections of time-mean sea level change

Section summary: The UKCP18 21st century time-mean sea level projections build upon the materials and methods described in the IPCC AR5. All RCP scenarios show substantial sea level rise over the 21st century. Coastal sea level projections around the UK show substantial variations associated with both the RCP climate change scenario and geographic location. In general, greater sea level rise is projected for the south of the UK, where values are similar to the global mean projections. In the north of the UK, sea level rise projections are substantially lower than the global mean and minimum values are centred on South West Scotland. For UK capital cities, projections at 2100 range from approximately 0.1 - 0.5m (Edinburgh and Belfast under RCP2.6) to 0.5 - 1.1m (London and Cardiff under RCP8.5). Coastal sea level variability is an important additional consideration, particularly for planning time-horizons that are limited to a few decades.

We define time-mean sea level as the baseline water level upon which drivers of sea level extremes - such as tides, surges and waves - are superimposed. Projections of time-mean sea level are presented as yearly values over the 21st century. The potential for changes in storm surges and wave climate over the 21st century are discussed in sections 3.2 and 3.3, respectively.

The UKCP18 time-mean sea level projections are rooted in the materials and methods described in the IPCC AR5 (Church et al, 2013) (see section A1.1 for a full description). Following the approach of the IPCC AR5, we present a range of future sea level rise for any given scenario on the basis of the 5th and 95th percentiles of the underlying process-based model projections. IPCC AR5 referred to this as the "likely range" based on their expert judgement that there was a ⅔ chance of sea level rise falling within this model range, for a given scenario. The UKCP18 interpretation of the projection ranges presented in this report is that there may be a greater than 10% chance that the real-world response lies outside these ranges and that this likelihood cannot be accurately quantified.

In the following sections, we present projections of global mean sea level and show how the UKCP18 results differ from the projections presented in the IPCC AR5 (section 3.1.1). We also discuss the potential for accelerated sea level rise from Antarctic land-based ice loss, which is a topic that has received a lot of attention since the publication of the IPCC AR5 (section 3.1.2). Regional coastal projections for the UK, which are derived from our GMSL projections, are presented in section 3.1.3.

3.1.1 Global mean sea level (GMSL) projections

The UKCP18 global mean sea level (GMSL) projections differ from the IPCC AR5 projections for two reasons: (i) we use a baseline period of 1981-2000 rather than 1986-2005; (ii) we include updated estimates of the contribution from Antarctic ice dynamics, following Levermann et al, (2014; see section A1.1). The change of baseline period results in a small +0.01m increase in projected values of GMSL. The change in Antarctic ice dynamics brings about more substantive changes to the GMSL projections, systematically increasing the projections and in particular, raising the value of the 95th percentile (i.e. the upper bound of the likely range). The 2100 values for the IPCC AR5 and UKCP18 are summarised in Table 3.1.1. A comparison of the UKCP18 projection for RCP4.5 and the available satellite altimeter observations shows good agreement in the contemporary rates of GMSL change (figure 3.1.2).

Climate scenario	Global mean sea level rise at 2100 (m)	
	UKCP18	IPCC AR5*
RCP2.6	0.29 - 0.66	0.27 - 0.61
RCP4.5	0.38 - 0.79	0.36 - 0.71
RCP8.5	0.56 - 1.12	0.53 - 0.98

Table 3.1.1. Summary of the projected global sea level change at 2100 for UKCP18 and the IPCC AR5. *Note that the IPCC AR5 values have been adjusted to the 1981-2000 baseline used in UKCP18.

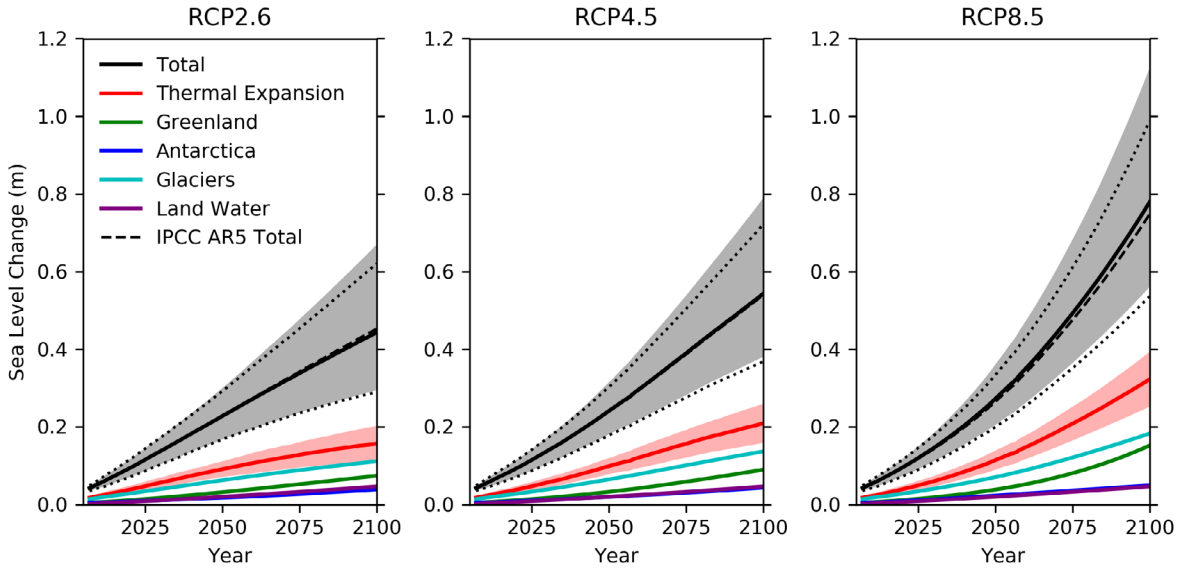

Figure 3.1.1. UKCP18 global time-mean sea level projections for the 21st century, including components as indicated in the figure legend. The corresponding shaded regions indicate the range of projections for the total and thermal expansion. Also shown is the total for the sea level projections presented in the IPCC AR5 (Church et al, 2013), with the range indicated by the dotted lines. All projections are shown relative to a 1981-2000 baseline period.

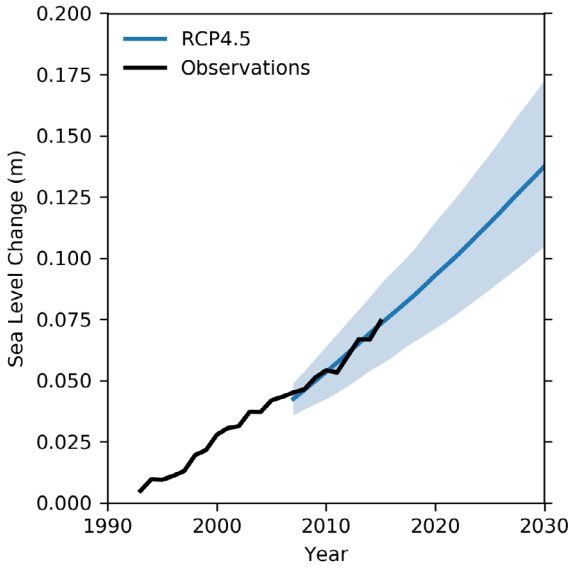

Figure 3.1.2. Comparison of the UKCP18 global time-mean sea level projection for RCP4.5 with the annual mean values from satellite altimeter observations (ESA CCI Sea Level data version 2.0; http://www.esa-sealevel-cci.org/). The sea level projections are shown relative to a 1981-200 baseline period. The satellite observations are plotted so that they match the average of the projection time series for the overlapping period of 2007-2015.

3.1.2 Potential for accelerated sea level rise from antarctic ice loss

One of the key uncertainties for 21st century sea level projections that was highlighted in the IPCC AR5 is the potential for accelerated rise from land-based ice loss. While mountain glaciers and the Greenland ice sheet are important reservoirs of land-based ice, there is limited potential for substantive increases in their mass input to the oceans over the 21st century. Therefore, the focus of the discussion in this section is on Antarctica.

It is important to note that the IPCC AR5 did not rule out future sea level rise in excess of the likely range presented for the process-based models. The statement made in this regard reads as follows (Church et al, 2013):

"We have considered the evidence for higher projections and have concluded that there is currently insufficient evidence to evaluate the probability of specific levels above the assessed likely range. Based on current understanding, only the collapse of marine-based sectors of the Antarctic ice sheet, if initiated, could cause global mean sea level to rise substantially above the likely range during the 21st century. This potential additional contribution cannot be precisely quantified but there is medium confidence that it would not exceed several tenths of a meter of sea level rise during the 21st century."

One of the important developments since the publication of the IPCC AR5 is advancement in our understanding of the potential for collapse of the West Antarctic Ice Sheet and consequent acceleration in the rate of global sea level rise. This is a predominantly marine-based ice sheet, where ice mass input to the ocean is governed primarily by ice flow processes rather than the surface mass balance (between snow accumulation and ice melt) that dominates for the East Antarctic Ice Sheet. Satellite and modelling evidence suggest that this collapse could already be underway, via a positive feedback known as 'Marine Ice Sheet Instability' (Rignot et al, 2014; Favier et al, 2014; Joughin et al, 2014). Recently, a second potential positive feedback on ice loss from West Antarctica has been proposed called 'Marine Ice Cliff Instability'. This feedback would be triggered by disintegration of the floating ice shelves around Antarctica, wherever these leave behind coastal ice cliffs taller than around 100m in height (Pollard et al, 2015; DeConto and Pollard, 2016). Such cliffs would be structurally unstable, and if they entirely collapsed, leaving behind further unstable cliffs, this could lead to self-sustaining ice losses and associated global sea level rise of order 1m by 2100 if the feedback were rapid and widespread (DeConto and Pollard, 2016). While this level of rise is well outside the IPCC AR5 "several tenths" statement, assessing the likelihood of this sequence of events is very challenging, partly because the modelling studies that produce these high rates of sea level rise depend on simple parameterisations of key processes that are very poorly understood (Edwards et al, in press). Most studies published since IPCC AR5 suggest maximum rates of about 0.4-0.5m per century for the global sea level rise contribution from Antarctica (Levermann et al, 2014; Ritz et al, 2015; Ruckert et al, 2017; Cornford et al, 2016; Clark et al, 2016) and are consistent with both the IPCC AR5 projections (Church et al, 2013) and the projections presented here.

The triggers of Antarctic dynamic change – ice shelf disintegration and basal melting – are expected to become more likely under anthropogenic warming (i.e. scenario-dependent), but their exact sensitivity is uncertain due to limitations of model resolution and process knowledge. Hence, the UKCP18 projections of Antarctic ice discharge are based on the scenario-dependent estimates of Levermann et al, (2014), with further details in section A1.1.1. Ice shelves are vulnerable to atmospheric warming through surface melting and firn compaction (Kuipers Munneke et al, 2014; Trusel et al, 2015), though the consequent likelihood of disintegration is not clear (Kingslake et al, 2017; Bell et al, 2017).

Basal melting is also expected to increase with anthropogenic warming (Timmermann and Hellmer, 2013; Kusahara and Hasumi, 2013; Hellmer et al, 2017), though future increases in stratospheric ozone due to the Montreal Protocol may have some countering effect by reducing upwelling (Waugh et al, 2013; Previdi and Polvani, 2014). However, the degree to which such triggers increase dynamic sea level contribution is expected to depend on local conditions (Ritz et al, 2015). Under the Marine Ice Sheet Instability hypothesis, for example, ice losses due to increased basal melting persist even if melt rates later decrease, but model simulations currently disagree on whether losses would continue or decrease (Favier et al, 2014; Seroussi et al, 2014a; Feldmann and Levermann, 2015; Arthern and Williams, 2017).

Projections beyond 2100 are reasonably consistent for low to medium greenhouse gas concentration scenarios (e.g. RCP2.6, RCP4.5), but become increasingly different under high scenarios, with values at 2200 under RCP8.5 that range from about 1m (Golledge et al, 2015) to several metres (DeConto and Pollard, 2016). These differences may be driven by timing of ice shelf collapse, and the degree to which resulting ice losses are mitigated or self-limiting due to local conditions (Ritz et al, 2015; Edwards et al, in press). Despite these differences in the simulated rates in the coming centuries, studies generally agree on a long-term committed sea level rise from Antarctica of several metres under all but the most aggressive mitigation scenarios (Levermann et al, 2014; Golledge et al, 2015; Feldmann and Levermann, 2015; Winkelmann et al, 2015; DeConto and Pollard, 2016; Clark et al, 2016; Pattyn, 2017). The UKCP18 extended sea level projections presented in section 4.2 also illustrate this multi-century sea level commitment.

The potential for accelerated dynamic ice discharge over the coming decades and centuries emphasises the need for close monitoring and improved modelling of the West Antarctic Ice Sheet. While Shepherd et al, (2018) have reported an acceleration in the rate of ice mass loss from West Antarctica over the last decade or so, it is unclear whether this change represents natural variability or a longer-term trend. Efforts to estimate the ice sheet mass balance must be continued, ideally supplemented with observational campaigns to monitor the ocean conditions under the ice shelves. Marine ice cliff instability has been proposed as an important potential feedback (DeConto and Pollard, 2016) and further research is required to strengthen the observational evidence for, and prevalence of, this mechanism. Ice models must continue to be improved with an emphasis on process-level understanding and making use of observational constraints when developing new projections.

3.1.3 Coastal time-mean sea level projections for the UK

The coastal sea level projections presented in this section are derived from the GMSL projections presented in section 3.1.2, as described in section A1.1. This procedure takes account of the spatial patterns of sea level rise associated with changes in land-based ice and land water storage (e.g. Tamisiea and Mitrovica, 2011; Slangen et al, 2014) and the effects of local oceanographic processes (e.g. Cannaby et al, 2016) on regional sea level for the UK. The final component for the regional projections is an estimate of the pattern of regional sea level change associated with the ongoing response of the solid Earth to the last de-glaciation (often referred to as glacial isostatic adjustment, GIA), including the effect of vertical land motion. This combination of factors results in substantial variations in projections of coastal time-mean sea level change around the UK for any given RCP scenario (Figure 3.1.3), as discussed later in this section.

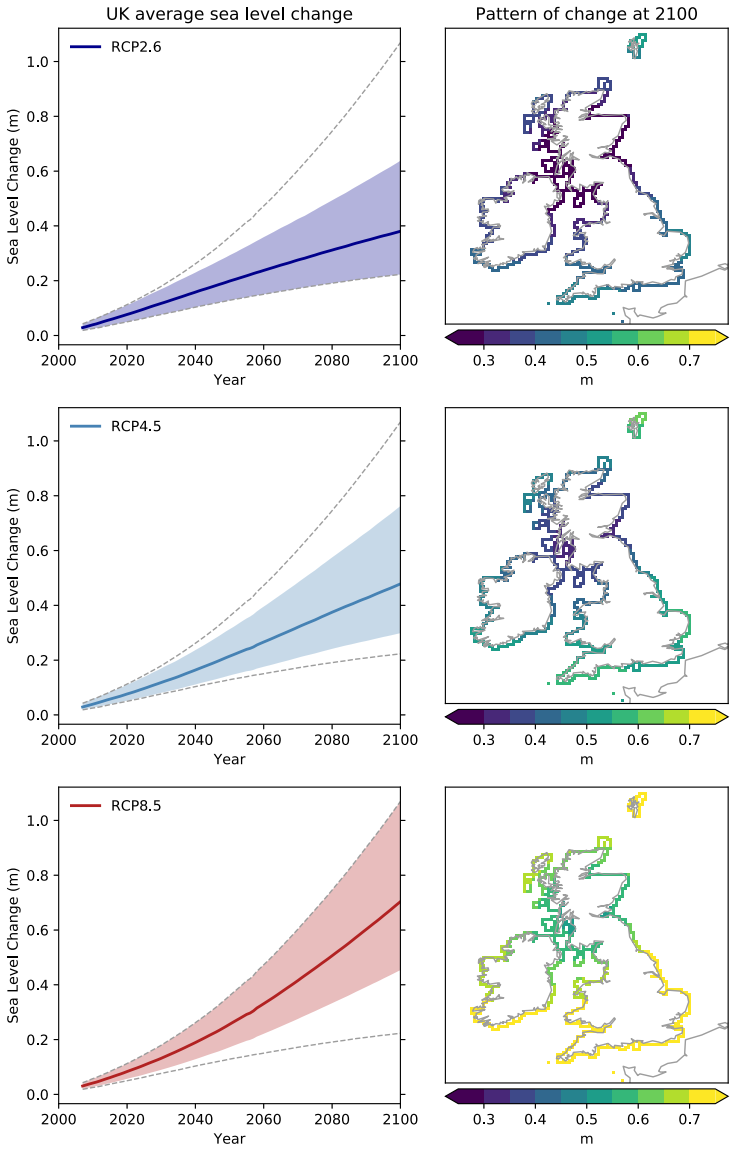

Figure 3.1.3. (left) Time series of time-mean sea level change based on the average of the UK ports listed in table 3.2.1. The solid line and shaded regions represent the central estimate and ranges for each RCP scenario as indicated in the legend. The dashed lines indicate the overall range across RCP scenarios. (right) the spatial pattern of change at 2100 associated with the central estimate of each RCP scenario. All projections are presented relative to a baseline period of 1981-2000.

The time-evolution of the UK coastal sea level projections (Figure 3.1.3) have a very similar time evolution to the corresponding GMSL time series (Figure 3.1.1). For the UK average, total sea level rise is slightly lower than for GMSL across all scenarios. For example, under RCP4.5, the UK average value at 2100 is 89% of the GMSL rise. As discussed in section 3.1, the proximity of the UK to the Greenland ice sheet means that the regional signal of this contribution is substantially reduced compared to the global mean (Figure A1.1.4). The pattern of sea level rise across the UK can be broadly characterised by a north-south gradient, with larger sea level rise to the south (Figure 3.1.3). This results in some regions of the UK coastline showing projections of time-mean sea level rise that are larger than the global average (see section 3.1.4). In addition, the range for UK coastal sea level projections is larger than for the GMSL time series, owing the additional uncertainty associated with regional processes.

Time-mean sea level projections for UK capital cities show the largest sea level rise for London and Cardiff, where the central estimates are similar to the corresponding GMSL time series. Edinburgh and Belfast show similar values for future sea level rise, which are substantially lower than the other two capital cities. The sea level projections for UK capital cities are summarised in Table 3.1.2 and Figure 3.1.4.

	London			Cardiff			Edinburgh			Belfast		
YEAR	R2.6	R4.5	R8.5	R2.6	R4.5	R8.5	R2.6	R4.5	R8.5	R2.6	R4.5	R8.5
2020	0.07 – 0.13	0.07 – 0.13	0.07 – 0.13	0.06 – 0.12	0.06 – 0.12	0.07 – 0.13	0.01 – 0.07	0.01 – 0.07	0.02 – 0.07	0.02 – 0.08	0.02 – 0.08	0.03 – 0.08
2040	0.13 – 0.26	0.14 – 0.27	0.16 – 0.29	0.12 – 0.25	0.13 – 0.26	0.15 – 0.28	0.04 – 0.16	0.05 – 0.17	0.06 – 0.20	0.05 – 0.18	0.06 – 0.18	0.08 – 0.21
2060	0.19 – 0.40	0.22 – 0.44	0.26 – 0.52	0.18 – 0.39	0.21 – 0.43	0.25 – 0.51	0.06 – 0.27	0.08 – 0.30	0.13 – 0.38	0.08 – 0.29	0.10 – 0.32	0.15 – 0.40
2080	0.24 – 0.55	0.30 – 0.63	0.39 – 0.80	0.23 – 0.53	0.28 – 0.62	0.38 – 0.79	0.07 – 0.37	0.12 – 0.45	0.21 – 0.62	0.10 – 0.40	0.15 – 0.48	0.23 – 0.65
2100	0.29 – 0.70	0.37 – 0.83	0.53 – 1.15	0.27 – 0.69	0.35 – 0.81	0.51 – 1.13	0.08 – 0.49	0.15 – 0.61	0.30 – 0.90	0.11 – 0.52	0.18 – 0.64	0.33 – 0.94

Table 3.1.2. Projected ranges of sea level rise at UK capital cities under RCP2.6, RCP4.5 and RCP8.5 relative to a baseline period of 1981-2000.

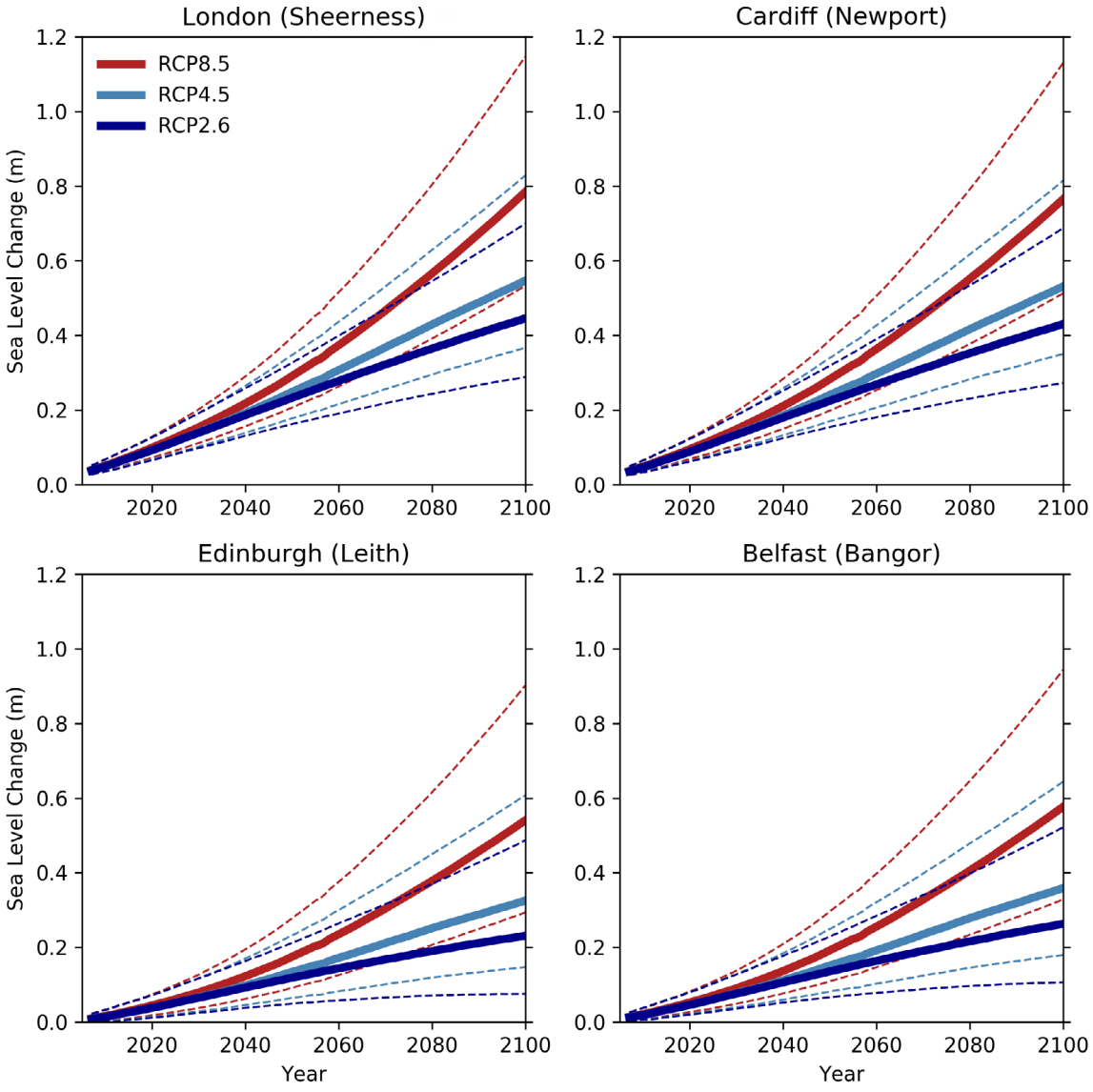

Figure 3.1.4. 21st century projections of time-mean sea level under change for UK capital cities, based on the nearest class A tide gauge location (indicated in brackets). . The solid lines indicate the central estimate and dashed lines indicate the range for each RCP as indicated in the legend. All projections are presented relative to a baseline period of 1981-2000.

3.1.4 Exploring the drivers of coastal sea level change

In this section we use two example tide gauge locations around the UK to illustrate how 21st century sea level change, and its components, vary geographically. We also explore the drivers of UK coastal sea level change, in terms of variability, climate change scenario and modelling uncertainty (following Hawkins and Sutton, 2011).

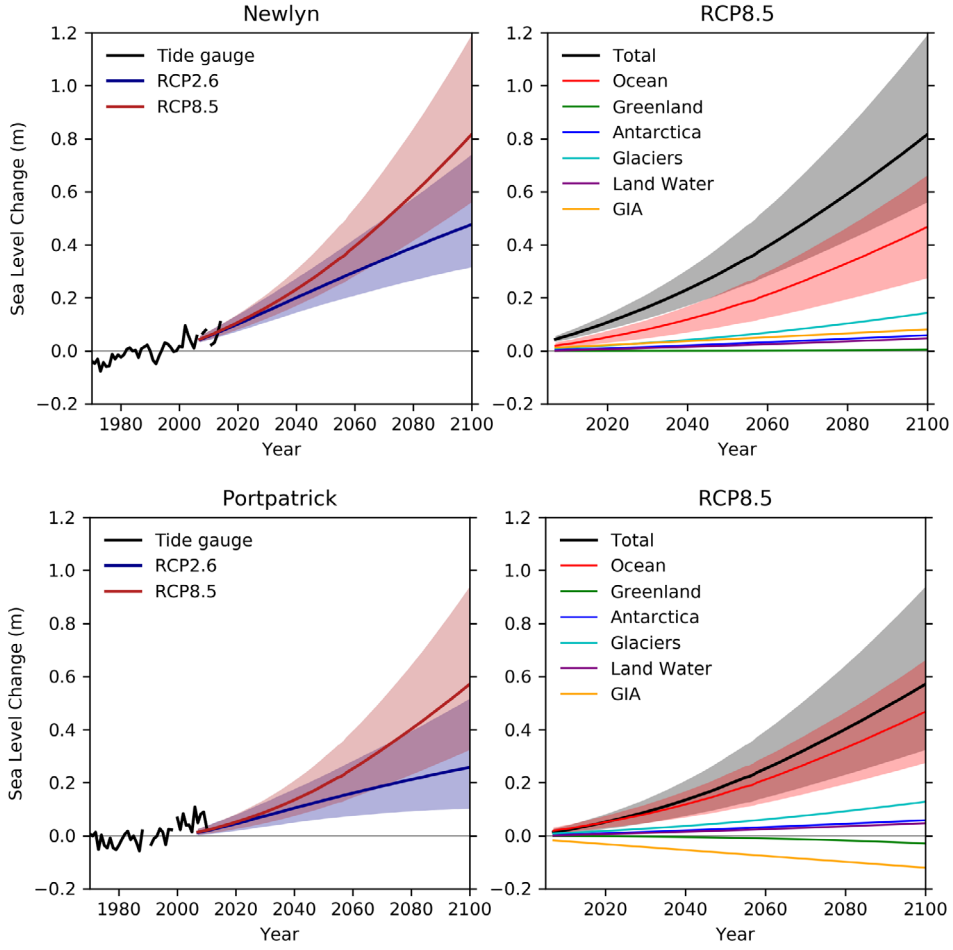

Figure 3.1.5. Regional sea level projections for example locations to illustrate the sea level variability observed at tide gauge locations and the variation in individual components. GIA and Greenland Ice Sheet have the largest contributions to variations in the projections. All time series are plotted relative to a baseline period of 1981-2000. Coloured lines indicate the central estimates according to the figure legend. Shaded regions represent the projection range for the corresponding RCP scenario (left panels) or sea level component (right panels).

Newlyn in South West England and Portpatrick in South West Scotland (see Figure 3.1 for locations) are used as example locations to illustrate the range of sea level projections across the UK (Figure 3.1.5). The total range of projected sea level rise at 2100 across all RCP scenarios is approximately 0.3 - 1.2m for Newlyn and 0.1 - 0.9m for Portpatrick. While at both sites the oceanographic component of sea level change represents the largest individual contribution, the Greenland and GIA components dominate the differences in projected sea level rise between the two sites (see section 2 for discussion of components). For Portpatrick, both the Greenland and GIA contribution to regional sea level is negative, whereas these components are approximately zero and positive for Newlyn, respectively. This result is more generally true across the UK, i.e. that geographic variations in 21st century sea level projections are dominated by the influence of Greenland and GIA.

Both Newlyn and Portpatrick show considerable year-to-year variability in the annual mean sea level observed in tide gauge records. This variability, with a typical range of about +/- 5cm is representative of tide gauge records around the UK (see section A2.5). It is important to note that this sea level variability will be superimposed on the long-term projected sea level rise. While a 5cm change is small compared to the sea level rise projections for 2100, this variability is an important consideration on shorter timescales (e.g. the next decade or two, especially for the lower emissions scenarios).

This last point is clearly illustrated in an analysis of the sea level rise uncertainty for Newlyn and Portpatrick (Figure 3.1.6), following Hawkins and Sutton (2011). Detrended tide gauge records are used to estimate the coastal sea level variability at each location, using the available annual values; 1916-2014 for Newlyn and 1968-2010 for Portpatrick. These are combined with an estimate of the uncertainty originating from the different RCP scenarios and the modelling uncertainty (i.e. the average 5th to 95th percentile range of sea level rise across all RCPs) to give a first order picture of the importance of these different factors over the 21st century. Both coastal sites present a very similar picture: the uncertainty in coastal sea level change is dominated by variability over the first decade or two, and this remains an important factor until the mid-21st century. The climate change scenario only starts to become an important player in the projected sea level change from the mid-21st century. The model uncertainty is an important component of the overall uncertainty in sea level projections throughout the 21st century.

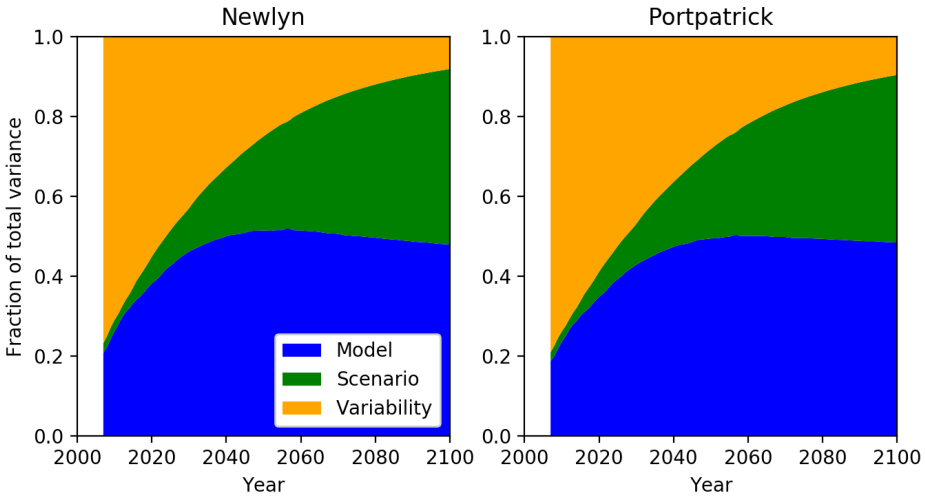

Figure 3.1.6. The fraction of sea level rise uncertainty for Newlyn (left) and Portpatrick (right) from: sea level variability (yellow); climate change scenario (green); and model uncertainty (blue), following Hawkins and Sutton (2011) based on annual mean data.

This simple analysis of sea level rise uncertainty suggests that for stakeholders who are interested in relatively short time horizons, e.g. the 2020s to 2050s, coastal sea level variability is an important consideration. The best information currently available on observed coastal sea level variability comes from the relatively sparse network of tide gauges around the UK (e.g. Figure 3.1; http://www.psmsl.org/). To aid the interpretation of the available tide gauge records and give a first-order picture of the magnitude of coastal sea level variability, we present sea level trends from a 7km resolution regional ocean model simulation (Figure 3.1.7). This model configuration has been set up to simulate interannual-to-multi-decadal sea level variability (section A1.7) around the UK and compares well with the available tide gauge observations on these timescales (section A2.5). The model simulation suggests that the largest magnitude sea level changes arising from variability occur on timescales of about 5 years, with 5th and 95th percentile trends in annual mean values that can exceed 6cm over this period. The simulations also suggest a large degree of spatial coherency in the magnitude of the variability. This suggests that the sea level variability observed at a tide gauge site is typically representative of a much longer stretch of coastline.

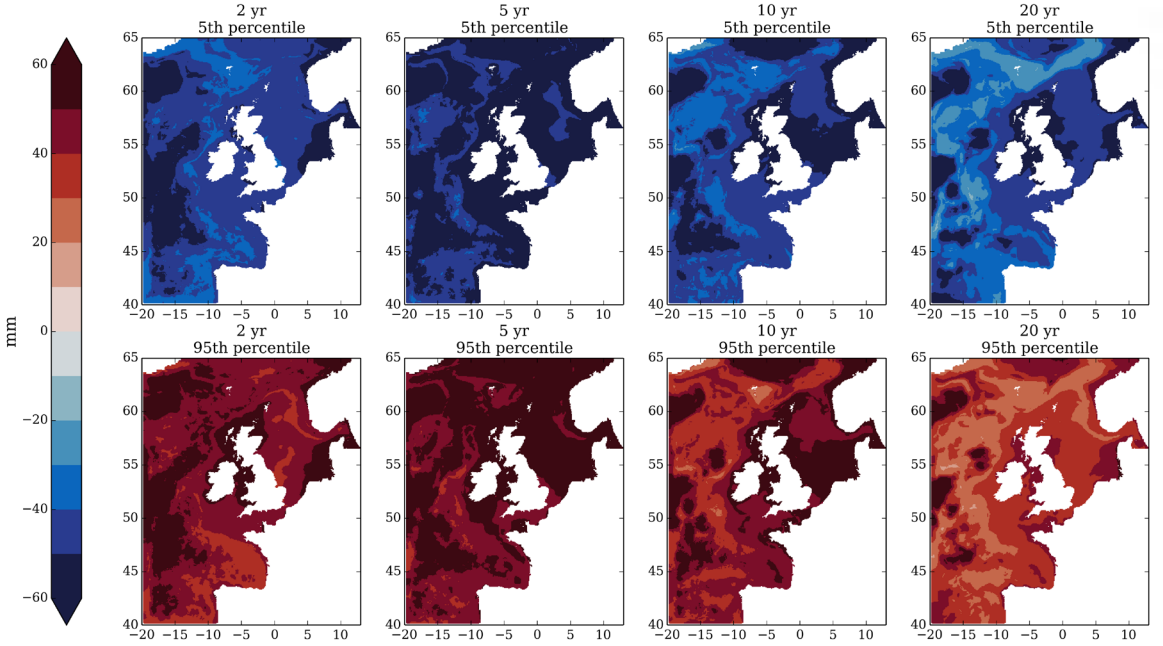

Figure 3.1.7. The 5th and 95th percentile trends in annual time-mean sea level change from a 200-year "present day" simulation using a high resolution coastal ocean model (section A1.7). Trends are expressed as the total change (mm) over each time period (years) as indicated in the figure panels.

3.2 Projections of change in storm surge and extreme water levels

Section summary: UKCP18 projections of change in extreme coastal water levels are dominated by time-mean sea level increase. There is a potential for an additional contribution due to atmospheric storminess changes over the 21st century. We present two strands of evidence to explore this additional contribution. Firstly, we present results from an ensemble of regionally-downscaled climate model simulations under RCP8.5 that samples a range of storminess change. Based on this ensemble, we present a best estimate of zero additional contribution around the UK. The largest trends across the ensemble have a magnitude of about 1 mm/yr (which is about 10% of the projected time-mean sea level rise) and can be positive (augmenting the mean sea level change) or negative (partially offsetting the mean sea level change). Secondly, we present an illustrative "high-end" projection based on the GFDL-ESM2M global model simulation under RCP8.5. Under this projection for some locations the trend in the 200-year return level due to the additional contribution can be as large 2-3 mm/yr. This simulation explores changes that might be found outside the range of the regionally-downscaled simulations and may be useful for sensitivity testing and contingency planning. However, it does not represent an upper limit on the additional contribution over the 21st century. Based on our simulations it is likely[2] that any negative additional contribution would be more than offset by regional mean sea level increase. The effect of mean sea level increase on the propagation of tide and surge is investigated separately in section 4.3.

[2] We do not quantify this likelihood, but even our lowest projections of mean sea level change under RCP8.5 would more than offset our most negative projections of surge trends.

3.2.1 RCA4 Downscaled simulations

To produce projections of the likely component of change in sea level extremes due to 21st century atmospheric storminess change, we used five CMIP5 simulations, downscaled with the SMHI RCA4 regional climate model, to drive the CS3 storm surge model (see Methods section A1.3 for details). These five models were chosen based on their ability to simulate a realistic climate over North West Europe, and they span a range of projected responses over the 21st century. Each simulation covers the period from 1970 to 2100.

Two of the five simulations exhibit significant spatially-coherent signals of 21st century change in skew surge: the HadGEM2-ES-RCA4 simulation, which exhibits a negative signal of change, and the MPI-ESM-LR-RCA4 simulation, which exhibits a positive signal of change. Maps of the 21st century trend in skew surge extremes (see section A1.3.3) are shown in Figure 3.2.1.

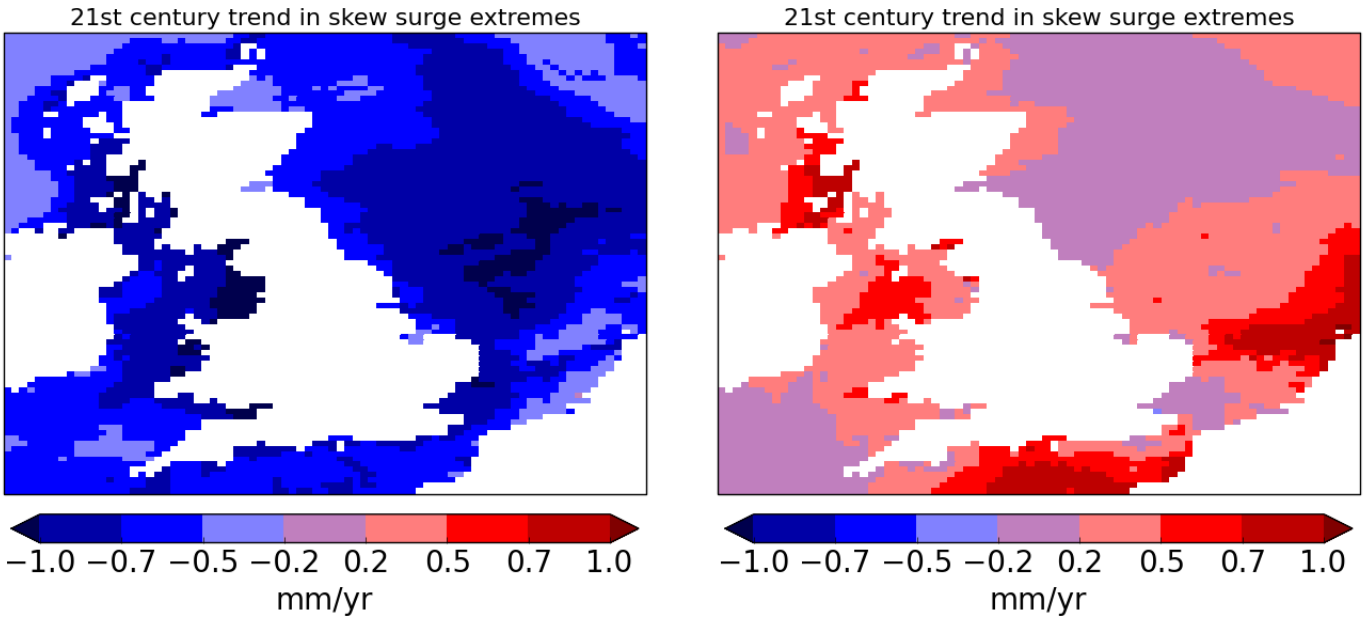

Figure 3.2.1. Projected 21st century trend in skew surge extremes diagnosed from HadGEM2-ES-RCA4 (left) and MPI-ESM-LR-RCA4 (right) simulations, shown using a colour scale that is common to both plots. The metric of change is the 21st century trend in the one-year return level (see section A1.4.1) of skew surge (see section A1.3.3), which for these simulations also applies to all other return periods (see section A1.4.2).

The use of a common colour scale helps to underscore the contrast between the two results. The spatial coherence of the patterns (uniformly negative in HadGEM2-ES-RCA4 and almost uniformly positive in MPI-ESM-LR-RCA4) suggests that these trends are the result of large-scale atmospheric storminess change over the 21st century in the driving models (see the discussion in section A1.4.2). The contrast between the two results underscores the uncertainty in model projections of large-scale atmospheric storminess change over the 21st century. Further implications of this uncertainty for users are discussed in section 3.2.2.

For comparison the current observed rate of global mean sea level increase is around 3.2 millimetres per year (2.8 to 3.6 mm/yr, Church et al, 2013) and typical projected rates averaged over the 21st century are around twice the current observed rate. Thus, we see that even the largest projected changes due to changes in storminess in the RCA4-downscaled simulations are smaller by about an order of magnitude than typical projected changes in mean sea level. We cannot be sure whether any projected changes are a response to greenhouse gas forcing or an expression of long-period internal variability (see sections 3.2.2 and A1.3.1).

Pointwise uncertainty of the fitted trend for each individual simulation

For each simulation and for each site, we fit a linear trend over the 21st century to the simulated extreme skew surges (see methods section A1.4). For a given simulation, due to variability, the simulated extreme skew surges at any given site do not exactly follow our fitted linear trend and so we can identify a range of possible trends consistent with the simulated extremes. Figure 3.2.2 shows this range for 38 sites around the UK mainland for two simulations: the MPI-ESM-LR-RCA4 simulation (in red) and the HadGEM2-ES-RCA4 simulation (in blue). The horizontal separation between vertical lines is proportional to the distance around the mainland coast (as defined by the chainage; see Batstone et al, 2013). The location of each site is shown on the map in Figure 3.1. For the MPI-ESM-LR-RCA4 simulation the most likely trend (i.e. the most consistent with the simulated extremes) is shown by the red line and the red shading shows the 5 to 95% confidence interval of the trend fitted to that simulation. For each site the shading gives a pointwise measure of the statistical significance of the diagnosed trend at that site: if the X-axis (the trend=zero line) lies well outside the shaded region then the trend is diagnosed as statistically significant at that site, for that simulation. The same applies to the HadGEM2-ES-RCA4 simulation, but read 'blue' in place of 'red'.

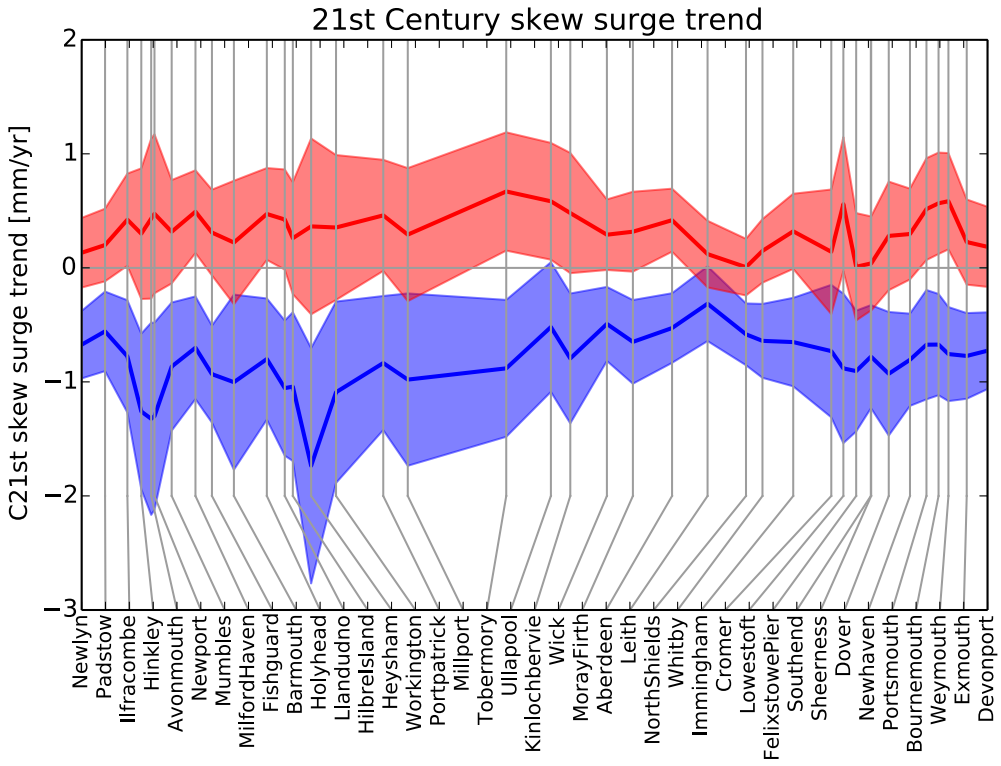

Figure 3.2.2. Projected 21st century trends in extreme of skew surge for sites of class A tide gauges around the UK mainland, in the HadGEM2-ES-RCA4 simulation (blue) and the MPI-ESM-LR-RCA4 simulation (red). This does not include time-mean sea level change and is due to projected storminess change only. The lines show the central estimates. The shading shows the uncertainty (5th to 95th percentile) in the fitted trend based on a pointwise site-by-site assessment (see main text).

As stated in the discussion of Figure 3.2.1, the two simulations, which are presented in an alternative way in Figure 3.2.2, do not agree on the size or even the sign of the change. The other three RCA4-downscaled simulations exhibit trends which are generally weaker and less spatially consistent than these two. Central estimates from each of the five simulations are shown in Figure A1.4.1. We synthesize the results from these differing simulations in section 3.2.2.

3.2.2 Best estimate of projected 21st century change in skew surge: no change

The pointwise central estimate of skew surge trend (for example as shown by the red line in Figure 3.2.2) is our best guide to the trend at an individual site for a given model simulation. However, this pointwise (local) trend may be the result of both large-scale variations in atmospheric storminess ('signal') and small-scale local chaotic effects which are not caused by any systematic change ('noise': see the discussion in section A1.4.2). In our MPI-ESM-LR-RCA4 simulation the trend is positive at nearly all of the sites around the UK coastline (see Figure 3.2.1 and Figure 3.2.2) and we conclude that this is the result of large-scale atmospheric changes over the 21st century in that simulation. A similar conclusion holds for the negative trends in the HadGEM2-ES-RCA4 simulation. This does not mean that we can necessarily attribute such change to global warming, because another (larger-scale) signal-vs-noise issue arises when we think about the causes of any large-scale atmospheric storminess change. Some of this large-scale atmospheric storminess change may be due to the effect of a warming climate on the storm tracks ('large-scale systematic change'), for example, movement or intensification or weakening of the storm tracks. But in the context of storm-track variations there are also natural variations on a wide range of time and spatial scales ('large-scale noise'). Looking at multiple simulations (such as the five RCA4-downscaled simulations we have considered here) and the natural variations in a long unforced control simulation (we plan to do this in work following on from UKCP18) are first steps towards determining whether any large-scale atmospheric storminess change is systematic change or noise.

Typical projected UK coastal skew surge trends from the RCA4-downscaled simulations (c/f Figure 3.2.2) range from about -1 mm/yr to about 0.7 mm/yr. Taking into account the disagreement (Figure 3.2.1, Figure 3.2.2 and Figure A1.4.1) between these simulations, we conclude that a trend of zero (that is, $\mu' = 0$, see section A1.4.1) is the best estimate based on the RCA4-downscaled simulations; in this case all of the change in the water level extremes during the 21st century would come from the change in the mean sea level (plus other sources such as the change in surface waves and the secondary contributions explored in section 4.3), and none of the change would come from changes in atmospheric storminess.

3.2.3 Illustrative high-end surge projection

This projection explores the size of change which might be found outside the limited range of the RCA4-downscaled simulations and is included as a tool for sensitivity testing and contingency planning. However, it is not an upper limit to the storminess-change contribution.

Some CMIP5 simulations that were not downscaled with RCA4 exhibit large signals of 21st century change in atmospheric storminess (see section 6.2). An example is the GFDL-ESM2M simulation, which has a realistic present-day North Atlantic storm track (see Evaluation section A2.2). To produce an illustrative high-end projection of the component of extreme sea level change due to atmospheric storminess changes over the 21st century we used atmospheric data from the GFDL-ESM2M simulation to drive our storm surge model. UKCP09 presented a "High-plus-plus" range of 21st century surge change based on a crude scaling of one of the CMIP3 models. Owing to the availability of higher temporal resolution data in the CMIP5 database we are able to present a surge model simulation driven directly by the GFDL-ESM2M global model, so we don't have the additional uncertainty associated with the crude scaling. GFDL-ESM2M does not evaluate quite as well as the RCA4-downscaled simulations in terms of the representation of the storm track in the north-east Atlantic (see Figure A2.2.1) and the simulation does not include a regional downscaling step[3].

[3] An RCA4-downscaled simulation of GFDL-ESM2M is available (Nikulin, pers. comm), although not at the spatial resolution of the RCA4-downscaled simulations presented here. We have not produced a surge simulation based on the downscaled GFDL-ESM2M data.

The simulated extreme skew surge events are, at most locations, slightly weaker than those in the RCA4-downscaled simulations, so that the distribution of extremes as represented by the return level curve is slightly further offset from the tide gauge curve than the RCA4-downscaled simulations, as shown in Figure A2.3.1. However, the slope of the return level curve evaluates well, suggesting that changes in the extremes will be well simulated (c/f Sterl et al, 2009). In view of the simulation of weaker extremes by this model, we considered scaling the trends. However in a comparison (not shown), of century-scale trends in extreme skew surge from the HadGEM2-ES simulation with and without the RCA4 regional downscaling step we find that although the sign of the trend is preserved by the regional downscaling step, the attenuation or amplification of the signal is not sufficiently consistent around the UK coast to justify scaling the trends in the manner of Howard et al, (2010), see also section A1.3.1.

The GFDL-ESM2M simulation has a more substantial signal of 21st century increase in skew surge than any of the RCA4-downscaled simulations, consistent with an assessment based on mean sea level pressure variability by Wade et al, (2015, see our section 6.2) and an assessment based on storm count (see Figure 6.2.2). We therefore use this model as the basis of our illustrative high-end projection. This projection lies above the range of change found in the RCA4-downscaled simulations. Nevertheless, it is physically plausible and is included as a tool for sensitivity testing and contingency planning where a higher level of protection is needed.

For this simulation the spatial coherence of the scale parameter trend, (see section A1.4.1) justifies the use of the five-parameter statistical model (see section A1.4.2). So in this case we cannot simply express the projected change as a trend in the location parameter (see section A1.4.1) which applies to all return periods. We must consider the scale parameter trend as well. This means different rates of change for different return periods. Spatial maps of the projected trend in the one-year and the 200-year return levels of skew surge are shown in Figure 3.2.3, and the uncertainty in the linear trend fit to the simulation for sites around the mainland coast is shown in Figure 3.2.4. The projected trend for coastal sites (including Jersey and Guernsey) is tabulated for convenience in table 3.2.1.

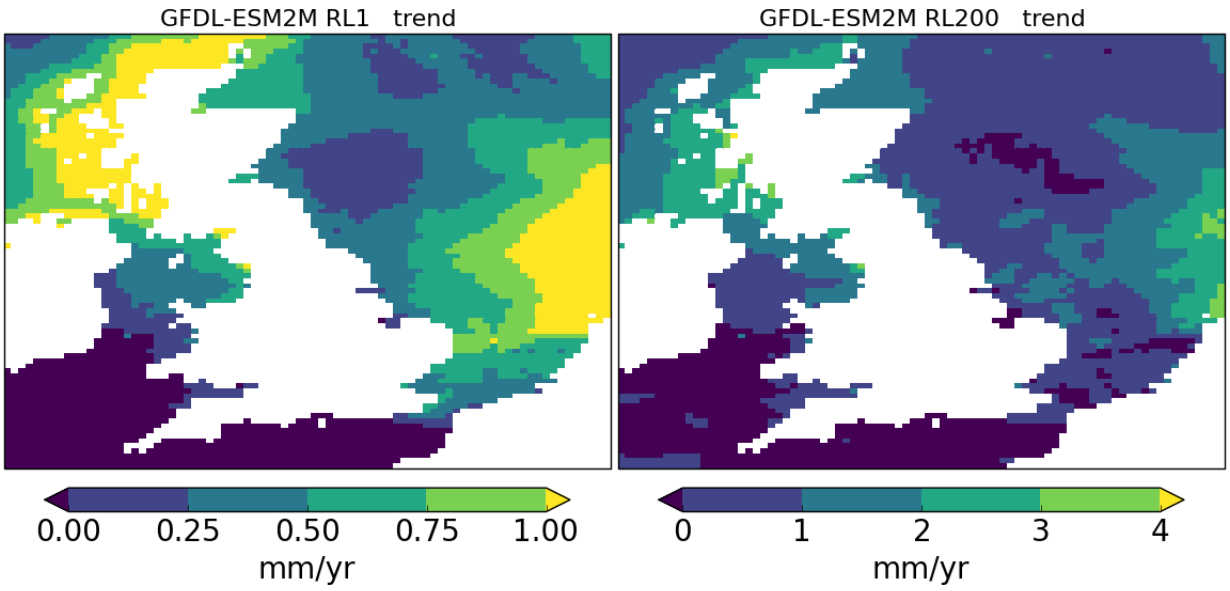

Figure 3.2.3. Spatial pattern of the illustrative high-end projection of 21st century trend in one-year return level of skew surge (left) and 200-year return level of skew surge (right). This does not include any time-mean sea level change.

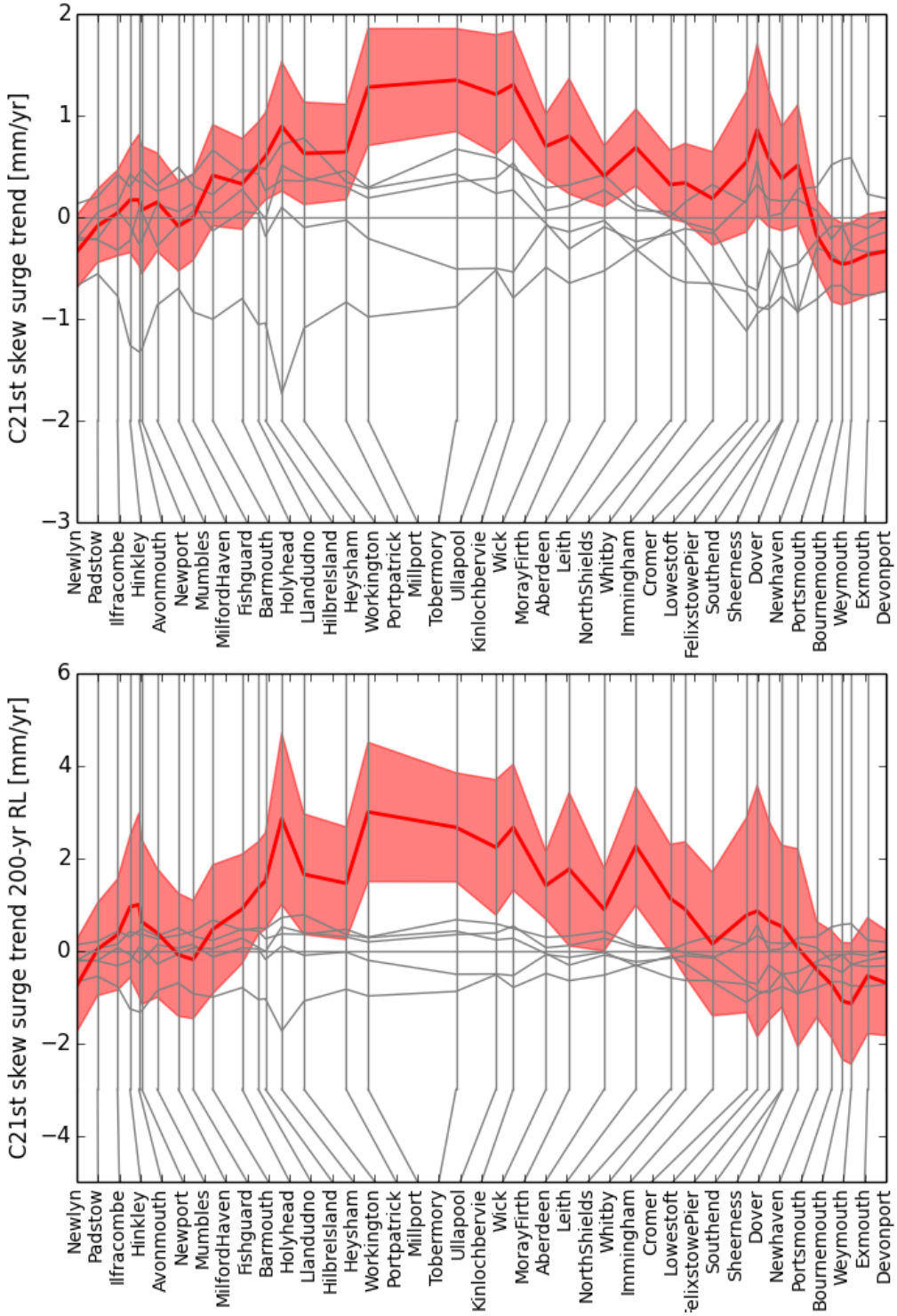

Figure 3.2.4. Illustrative high-end projection of 21st century trends in one-year return level of skew surge (top panel) and 200-year return level of skew surge (bottom panel). Lines show the central estimate. Shading shows the 5th to 95th percentile of the fitted trend. The central estimates from the RCA4-downscaled simulations are shown by the grey lines. Note the different Y-axis scales.

Site	RL1 trend mm/yr	RL200 trend mm/yr
Newlyn	-0.34	-0.76
St Marys	-0.11	-0.27
Padstow	-0.08	0.03
Ilfracombe	0.04	0.35
Hinkley	0.17	0.95
Avonmouth	0.17	1
Newport	0.07	0.63
Mumbles	0.15	0.38
Milford Haven	-0.09	-0.09
Fishguard	0	-0.19
Barmouth	0.41	0.46
Holyhead	0.33	0.91
Llandudno	0.51	1.35
Hilbre Island	0.6	1.51
Port Erin	0.38	0.89
Heysham	0.89	2.85
Workington	0.63	1.65
Portpatrick	0.64	1.46
Millport	1.28	3
Port Ellen	1	2.36
Tobermory	1.35	2.67
Ullapool	1.21	2.24

Site	RL1 trend mm/yr	RL200 trend mm/yr
Wick	0.7	1.41
Moray Firth	0.8	1.77
Aberdeen	0.4	0.89
Leith	0.69	2.27
North Shields	0.32	1.13
Whitby	0.34	0.9
Immingham	0.18	0.15
Cromer	0.54	0.77
Lowestoft	0.86	0.86
Felixstowe Pier	0.58	0.65
Southend	0.38	0.52
Sheerness	0.38	0.52
Dover	0.51	0.06
Newhaven	-0.18	-0.41
Portsmouth	-0.41	-0.73
Bournemouth	-0.46	-1.09
Weymouth	-0.44	-1.14
Exmouth	-0.37	-0.55
Devonport	-0.33	-0.7
Malin Head	1	2.02
Portrush	1.05	2.47
Bangor	0.56	1.27

Site	RL1 trend mm/yr	RL200 trend mm/yr
Stornoway	0.94	1.4
Kinlochbervie	1.3	2.67
Lerwick	0.44	0.49

Site	RL1 trend mm/yr	RL200 trend mm/yr
Jersey	-0.3	-0.66
Guernsey	-0.3	-0.82

Table 3.2.1. Illustrative high-end projection of atmospheric storminess contribution to 21st century trend in one-year and 200-year return level of skew surge at sites around the UK coast. This projection does not include any contribution from time-mean sea level change.

The values in Table 3.2.1 and Figure 3.2.4 show our illustrative high-end projection of the contribution to the average rate of extreme sea level change over the 21st century due to changes in atmospheric storminess only. Figure 3.2.4 shows that the fitted trends are statistically significantly different to zero by a pointwise assessment along much of the north coast of mainland UK. Consistent with this the trends in both location and scale parameter are found to be significant at meaningful spatial scales (see the discussion in section A1.4.1). In some locations, the size of the projected trend in the 200-year return level is between 2 and 3 mm/yr. This projection has been developed by choosing from among many model simulations the one which seems likely to give the largest change in skew surge at some locations around the UK, and is included as a tool for sensitivity testing and contingency planning where a higher level of protection is needed. Nevertheless, even with this simulation there is little 21st century increase in storminess over the south of the UK and consequently the skew surge increases in the south are small (or negative at some sites). We consider this to be an illustrative simulation only: it explores the size of change which might be found outside the limited range of the RCA4-downscaled simulations. It is not an upper limit to the storminess-change contribution, and increases in skew surge, particularly around the south of the UK, could be larger than the ones seen in this simulation - for example they might be of comparable size to the increases seen in the north of the UK in this simulation, or larger. However, we reiterate that mean sea level change is expected to be the dominant source of increase and uncertainty in extreme still water levels.

3.2.4 Projected future return level curves

We combine projections of regional mean sea level change with the best available estimates of the present-day return levels of extreme still water (still water includes the astronomical tides and surge but does not include the effect of waves) at class A tide gauge sites around the UK. We include the uncertainties in the projections of regional mean sea level change (the dominant uncertainty) but not the uncertainties in the contribution from atmospheric storminess change (which are expected to be smaller: for example the difference between the largest and smallest projected 21st century change in one-year return level at Sheerness due to storminess change only in our RCA4-downscaled ensemble is only around 10% of the uncertainty range associated with mean sea level change at Sheerness).

We do not include the uncertainties in the present-day return levels in the projections. Estimates of the uncertainty in the present-day return level curves are documented in a separate report (Environment Agency, 2018). We decided to exclude this source of uncertainty from the present work because combining this source of uncertainty with the uncertainty in the projections of mean sea level change in a meaningful way is not a straightforward task, and further scientific work is required to establish the best way to do this.

Figure 3.2.5 (left-hand panels) show the best-estimate present day return level curves and uncertainties taken from Environment Agency (2018) at four example sites around the UK. Projected future return level curves based on a simple addition of projected regional mean sea level change (for 2030, 2050 and 2100) to the best-estimate present-day return level curve are shown by the other panels. Results for other sites and other years are available through the UKCP18 user interface.

Figure 3.2.5 illustrates the fact that the uncertainties in the present-day return level curves at some sites may be larger than the uncertainties in the projected change, particularly for long return periods (i.e. low probability events). Thus, users with an interest in events with a low probability in the near future (for example the 1000-year return level for 2030) should be aware of the uncertainties illustrated in the left-hand panels of Figure 3.2.5 and documented in Environment Agency (2018).

For further discussion please see section A1.5.

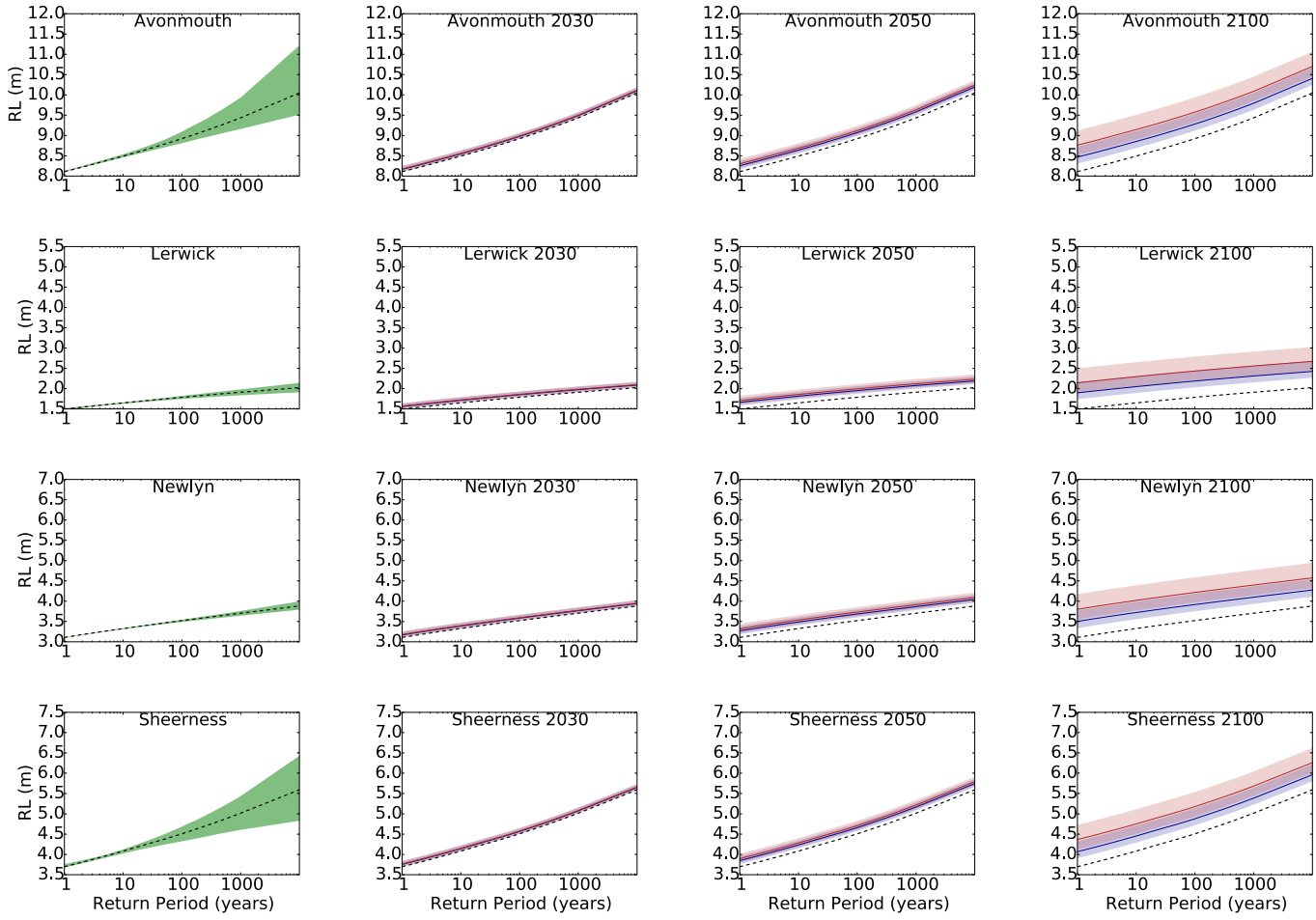

Figure 3.2.5. Projected future still water Return Level (RL) at Avonmouth, Lerwick, Newlyn and Sheerness. The present-day curve from Environment Agency (2018) is shown by the dashed black line (the lowest dashed line in each panel). Left-hand panels also show an estimate of the present-day uncertainty (green shading, showing 5th to 95th percentile). The blue (red) lines show the future return level curve under the central estimate of time-mean sea level change from the RCP2.6 (RCP8.5) scenario. The blue (red) shading shows the respective UKCP18 projection ranges. Uncertainty from the time-mean sea level projections is included. Uncertainty due to storminess changes is not included. Uncertainty in the present-day return level curves is not included in the projected future curves (see main text). Projections are shown for years 2030 (left column), 2050 (centre) and 2100 (right column). The uncertainties shown should be regarded as minimum uncertainties: for details see main text. To give sensible scales and aid comparison, we have chosen different Y-axis limits for each site, but we have adjusted such that the range of each Y-axis is 4 metres. Present-day return level curves are in ordnance datum Newlyn (ODN), which is an absolute datum. Projected future return level curves are not strictly in ODN because they are relative to the local land level, which is not fixed relative to ODN.

3.3 Projections of changes in wave climate

Section acknowledgment: The research presented in this section was funded by a National Environmental Research Council Knowledge Exchange Fellowship NE/P01321X/1 and the EU FP7 project "RISES-AM" FP7-ENV-2013-Two-Stage-603396-RISES-AM-.

Section summary: An ensemble of seven CMIP5-based global wave models is used to explore potential changes in mean and mean annual maximum significant wave height (SWH) under RCP8.5. These simulations suggest an overall decrease in mean SWH around most of the UK coastline of 10-20% over the 21st century, but the sign of change differs among models and coastal location. The focus of this section is on relative changes in projected wave conditions, and we note that the magnitude of the changes in mean and mean annual maximum (AnnMax) is similar in all seven models. By combining these relative changes with historical wave conditions from the reanalysis period, we can derive some absolute changes in SWH. This avoids biases in the climate model being compounded into erroneous change signals.

High resolution regional model projections are presented based on a single CMIP5 model under RCP4.5 and RCP8.5. This model configuration shows a similar magnitude of change to the global model simulations but provides better treatment of coastal processes and additional insights into the projected changes. The regional projections show more consistent changes across the 21st century and RCPs for the more exposed coastline, where remote generation of swell waves dominates SWH. For more sheltered sections of coastline, SWH changes are determined primarily by locally-generated waves and therefore local weather "noise" seems to dominate over the climate change signal. We note that projected changes in wave climate are inextricably linked to changes in atmospheric circulation and storminess. Given the inherent uncertainty in projections of storm track changes and the limited sample size available, the wave projections presented here should be viewed as indicative of the potential changes with low confidence.

3.3.1 Global wave model projections

As a representation of present-day conditions, the period 1980-2005 is used for the global wave model results. The future changes for this model in mean and AnnMax SWH are assessed for the period 2070-2099. In the future, mean SWH is projected to decrease (by more than 0.3m in places) across NW Europe. This reduction is seen more strongly under RCP8.5 than RCP4.5. However, a reduction in SWH is not seen in all areas: there is a drop in SWH across the NE Atlantic, while in some models (e.g. HadGEM2-ES) SWH is predicted to increase (by up to 0.2 m) in the North Sea and coastal seas. A similar analysis is repeated for the AnnMax, which shows greater spatial variability, and less consistency among models. There is no agreement in the sign of change of AnnMax SWH across the seven models considered. The magnitude of the projected change in extreme waves can exceed 1m in the future simulations.

For consistency with the surge model, future wave conditions are extracted at sites of class A tide gauges around the UK. Figure 3.3.1 shows the future change in mean and AnnMax SWH at gauge sites. It is important to note that the magnitude of change projected in both mean and AnnMax SWH is similar across all ensemble members, with no outliers. This information provides some insight into the potential contribution to total water level from future changes in surface waves.

As context for the change in wave conditions, Figure 6.2.2 shows the wave models run in comparison with other models from the CMIP5 ensemble. This suggests that the global wave models we have used here cluster around the middle / lower left quadrant (calmer, southwards shift). We are missing GFDL and MPI, which are in the upper right (stormier, northward shift). The information on storm track is not available for ACCESS1.0, and GFDL-CM3.

All the global wave-model ensemble members project a decrease in mean SWH by the end of the 21st century under RCP8.5. HadGEM2-ES and GFDL-CM3 project the largest reduction in mean SWH, around 20%. This decrease could be driven by a reduction in remotely generated swell waves and/or locally generated wind waves and seems broadly consistent with the tendency for a reduction in surface winds over the UK in CMIP5 models presented in the Land Report (Murphy et al, 2018). We note that, in contrast to the CMIP5 ensemble, the HadGEM3 PPE shows a tendency for increased surface winds over the winter season. More modest reductions of the order 5-10% are projected in CNRM, BCC-CSM1.1, and EC-Earth. Only one model (MRI) projects an increase in mean SWH: at three sites in the North Sea, and Irish Sea sites. It should be reiterated that it is in these semi-enclosed seas where the different models diverge most. Turning to the projected AnnMax SWH (lower panel of Figure 3.3.1), there is no consensus in the direction of change within the model ensemble. This is the case considering any of the UK tide gauge sites plotted. Though there is inconsistency in the direction, the magnitude of change in all models remains around 10 - 20% of the absolute SWH.

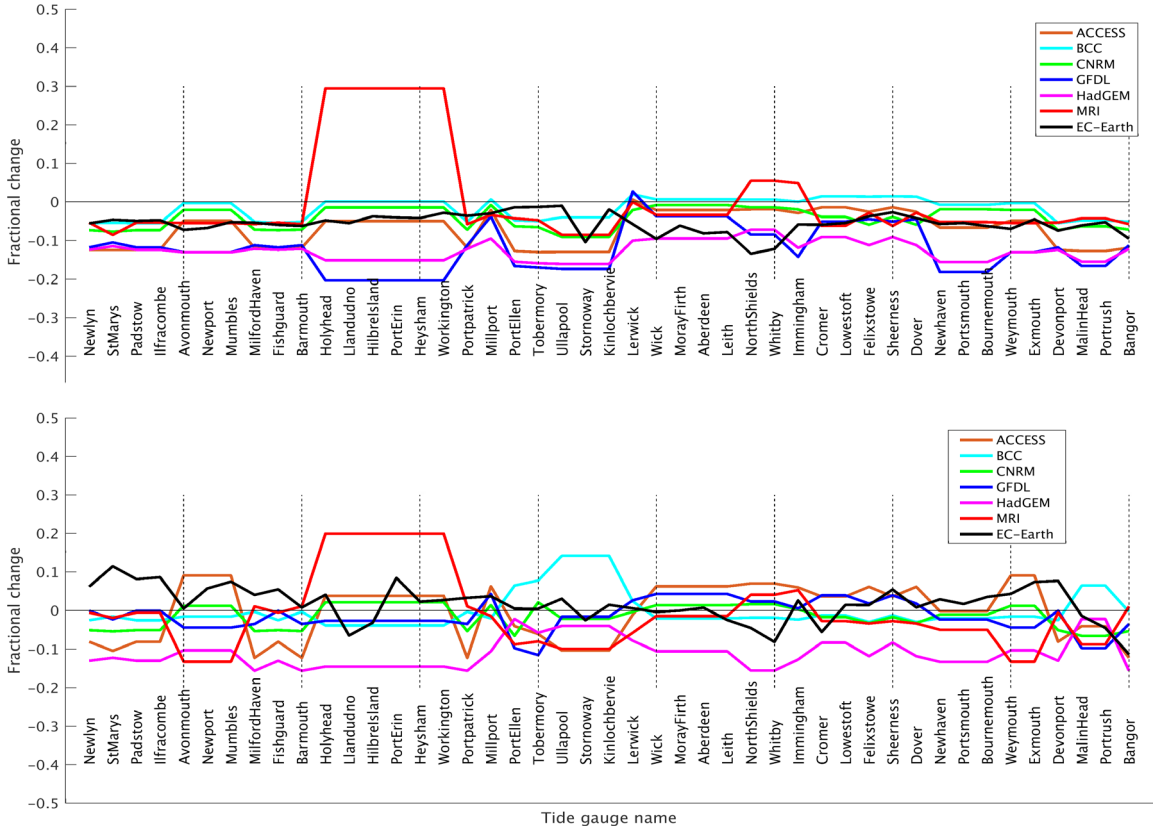

Figure 3.3.1. Fractional change in mean significant wave height (SWH, upper panel) and annual maximum wave height (AnnMax, lower panel) for class A tide gauge locations around the UK. The change is computed as the 2070-2099 average for RCP8.5 minus the 1980-2005 average from the historical simulation. Colours correspond to different CMIP5 climate models as indicated in the figure legend.

3.3.2 Regional wave model projections

As a representation of present-day conditions, the period 1981-2000 is used for the regional wave model. The future changes in mean and AnnMax SWH are assessed for the end-21st century period 2081-2100. Maps of change in SWH between the end-21st century RCP8.5 projection, and the present-day conditions are shown in Figure 3.3.2. Difference plots from global wave model (left) and regional model (right), with red (blue) colours indicating an increase (decrease) in SWH in the future. The top row shows the change in mean SWH, and the bottom row shows changes in the AnnMax. A statistical test - the Kruskal-Wallis (KW) test, see section A1.6.3 - is applied to two populations in order to mask out changes where the signal-to-noise ratio is low. Where the KW-test score exceeds 75% the absolute differences between the historical and future wave conditions are shown unmasked. In unmasked areas we are confident that the future wave conditions are different to the historic, rather than hidden by natural variability.

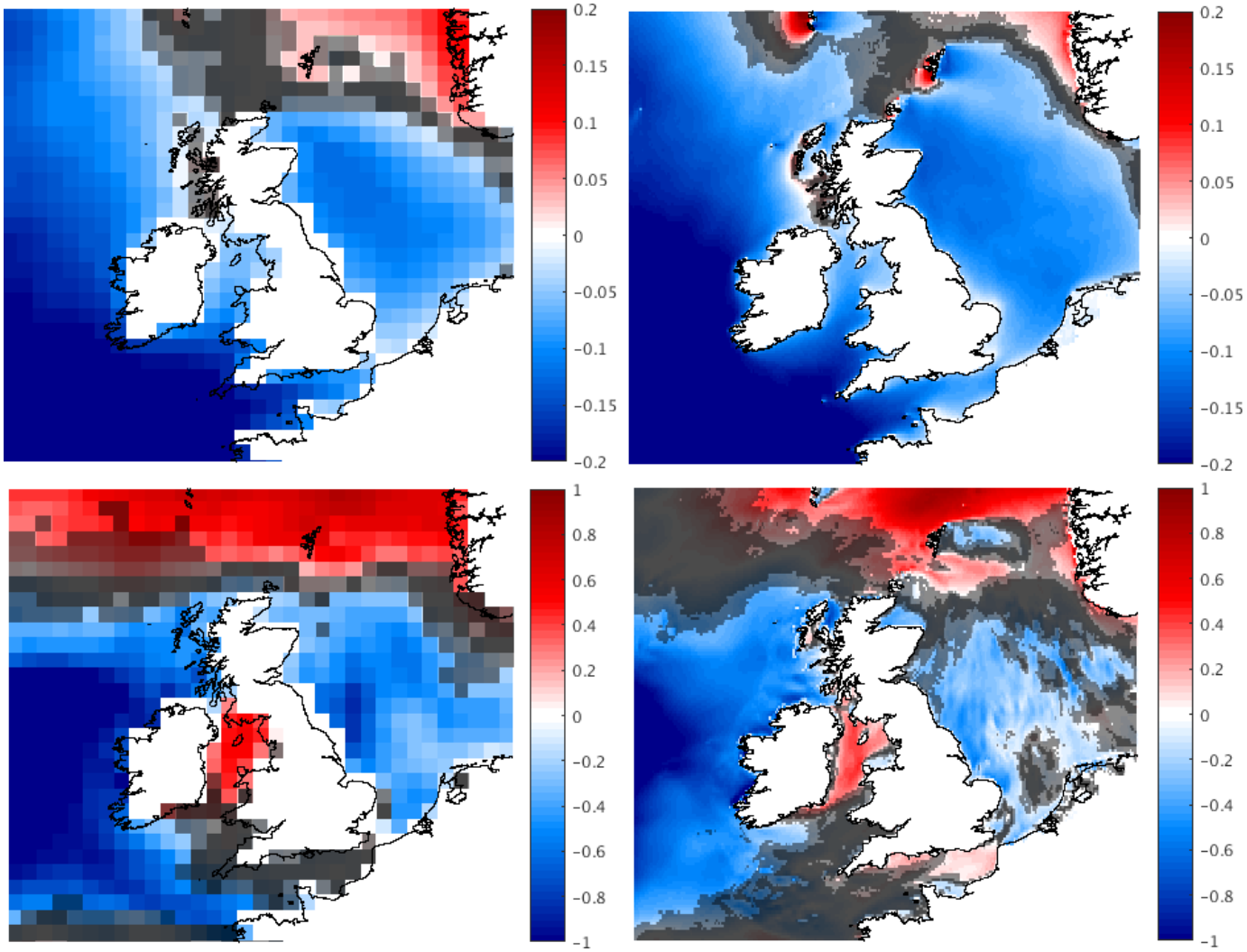

Figure 3.3.2. RCP8.5 end century change in mean SWH (top) and mean AnnMax (below). Global model (left) and regional (right). All plots show an absolute change, in metres. Grey masking indicates where natural variability is high. Where there is no masking, there is higher than a 75% chance that the future wave conditions are different to the historical conditions, rather than masked by natural variability.

It is important to first note that the global and regional wave model results are consistent in their overall direction and magnitude of change, adding confidence to this result. There is a reduction in mean SWH projected across all UK seas, with the exception of a slight increase to the North of Scotland. Average SWH is projected to reduce by around 10% around the majority of the UK coastline. The projected reduction in mean SWH is stronger in the regional wave model, and an emergent signal is present in a wider area than in the global model. SWH reduces the most to the South West of the UK and Ireland.

Projected changes in AnnMax SWH are of the order +/- 1m or 20%, but with a more complex spatial pattern than for the mean SWH. The pattern of changing AnnMax is more complicated than the mean as it is driven by passing individual storms. There are also wider areas of masking (areas where a change signal does not emerge from natural variability) for AnnMax than mean change. The AnnMax SWH is projected to increase off the south west of the UK and in parts of the Irish Sea but reduce off the west of Ireland and in the southern North Sea. This could be explained dynamically by a southward shift in the position of the storm-track (as in Wolf et al, 2015), although we note that this is at odds with our general expectation for a poleward shift in the mid-latitude jet (Barnes and Polvani, 2013). An increase in annual maximum SWH is also observed to the north of the UK, which could be related to a change in sea-ice cover due to global warming, leading to increased fetch for northerly winds in Nordic Seas.

Wave climate is driven by surface winds and is thus linked to the position of the storm track and changing fetch. How do these changes in SWH align with atmospheric storminess? Figure 6.2.1 shows that in the CMIP5 model EC-Earth, the maximum storm track shifts southwards, while decreasing in strength. The CCRA (Wade et al, 2015) finds that the CMIP5 climate model projections suggest a plausible H++ scenario for a 50 - 80% increase in the number of days of strong winds over the UK during 2070-2100 compared to the period 1975-2005. In general, the ensemble of models projects a southerly shift in the storm track over NW Europe. In the EC-Earth model, the storm track is also projected to move south. There is also a projected reduction in sea ice, increasing fetch from the Arctic (only affecting northern UK).

An increase in the AnnMax winds is also seen in the EC-Earth model. The mean wind speed change patterns are very similar to the change in mean SWH, with a low to the West / South West of Ireland, and slight increase to the north of the British Isles. The differences from historical to end-21st century RCP8.5 are of the order 0.5 m. Changes in the mean AnnMax wind speed are spatially noisy, with changes of the order +/- 1.5 m/s in places (not shown).

The direction of change in future wave climate is consistent, with the mean SWH seen to reduce in both configurations. Stronger changes are seen in the regional model than the global model. Additional simulations under RCP4.5 (not shown) show similar patterns to the RCP 8.5 projections (Figure 3.3.2). Stronger reductions in the mean SWH are observed for mid-21st century (not shown) than end-21st century, which suggests that both low-frequency internal variability and climate change may be playing a role in shaping the simulated wave response. While the UK coastline in these simulations is characterised by a future reduction in SWH, some regions of the Irish Sea and South Coast exhibit an increase in AnnMax (Figure 3.3.2). A reduction in the mean SWH, together with an increase of the extreme SWH can be visualised by considering the full probability density function. If the probability density function is widening, and spreading, the tail can move towards higher waves, while the mean conditions remain unchanged, or reduced. The prospect of a future decrease in mean SWH, and greater uncertainty associated with extreme wave events, is consistent with the findings of Aarnes et al, (2017) who analyse wave change in 6 CMIP5 models. Further discussion of the simulated wave changes can be found in Bricheno and Wolf (submitted 2018).

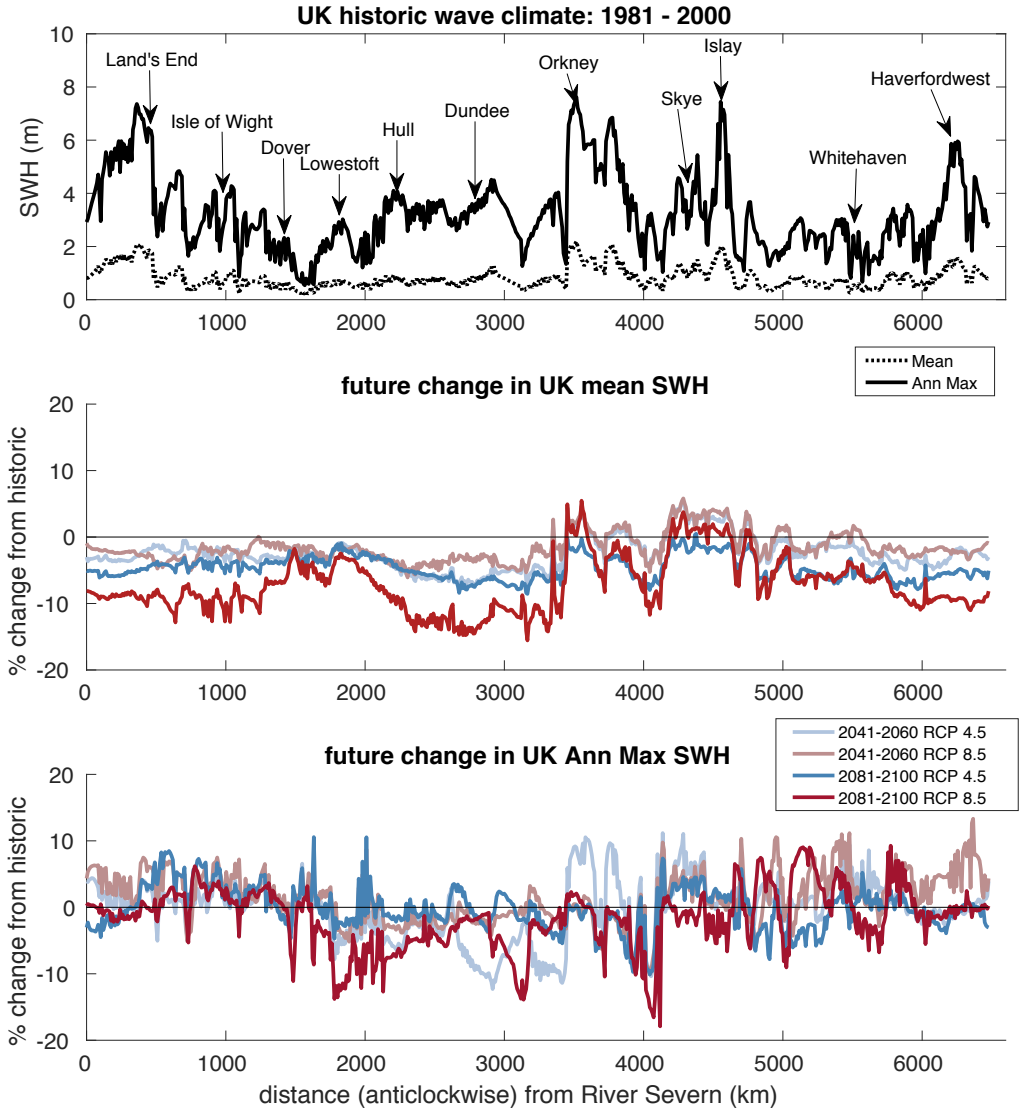

Figure 3.3.3. Coastal strip plots of historical wave climate and projected future changes for UK mainland. The top panel shows the mean SWH (dotted line) and mean AnnMax (solid line) from the historical simulation. The middle and bottom panels show percentage changes in mean SWH and AnnMax respectively, relative to a 1981-2000 baseline period. The four coloured lines represent "mid-21st century" (2041-2060) and "end-21st century" (2081-2100) change signals for RCP4.5 and RCP8.5.

In order to focus on changes in nearshore waves, figure 3.3.3 shows SWH at coastal model points. In this plot the modelled coastline of the British mainland is 'unwrapped' anticlockwise, starting and ending in the Bristol Channel. The top panel shows historical conditions of mean and AnnMax SWH along the British shoreline. This shows that the largest waves are seen on western facing coasts, including Cornwall, South West Wales, and North West Scotland. These west-facing coasts are dominated by long swell waves. Swell waves reaching the UK coastline are generated offshore, in the North Atlantic. The long period swells may have an integrative effect, as they build with storms moving across the ocean basins. The lowest wave heights are found in more enclosed seas, which are sheltered from long swells. In these semi-enclosed seas (for instance Irish Sea, North Sea) windsea waves are generated by local winds with a short fetch. In fetch-limited areas, there are short-period waves driven by local storm systems. By partitioning the wave conditions by peak period, it could be possible to isolate changes in locally generated windsea and non-local swell waves.

The middle and bottom panels of figure 3.3.3 show changes in mean and AnnMax SWH, respectively. Four coloured lines are plotted for two time slices each from RCP 4.5 and RCP 8.5. Where the four futures cluster together, and show the same direction of change, we are more confident in an emergent climate signal. As seen in the maps (Figure 3.3.2), the mean SWH is seen to reduce at most coastal sites, by of the order 10%. The four future projections are coherent in their direction of change, and the largest reduction in coastal mean SWH is seen in RCP8.5 at end-21st century.

The change in AnnMax SWH is more spatially complex, and the different time periods are also inconsistent in places. The projections of AnnMax tend to agree in direction of change (showing increased SWH) on the swell facing coasts. This is especially clear on the Cornish coast and South West England (also West of Ireland, not shown). The AnnMax wave projections diverge most strongly in the semi-enclosed seas, where wind-sea waves dominate. For example, consider the North Sea region between Hull and Orkney. In the North Sea coastal projections there is no consistent direction of change between the four future time periods. In the fetch-limited areas where local windsea waves dominate there is no clear direction of change within this single model for future projections in either RCP 4.5 or 8.5 scenario.

4. Exploratory extended projections of sea level change

In this section we present exploratory projections of time-mean sea level for the period out to 2300 and the effects such changes could have on future tide and surge characteristics. There is inherently a much larger degree of uncertainty associated with providing information on these time horizons than for the 21st century projections presented in section 3. The results should therefore be taken as illustrative of potential future changes and we have a lower degree of confidence in the absolute values reported. In section 4.1 we present the RCP extensions that are used to provide time-mean sea level projections out to 2300. Global and regional sea level projections are presented in section 4.2, based on the methods described in section A1.2. In section 4.3 we present exploratory analysis of the impact several metres of time-mean sea level rise could have on tide and surge characteristics.

4.1 Climate forcing and surface temperature response

Section summary: In this section we present the extensions to the RCP climate change scenarios that form the basis of our multi-century projections of time-mean sea level change. On these extended time-horizons there is a marked divergence between RCP8.5 and the other two climate change scenarios. RCP2.6 is the only scenario to show a decrease in CO_2 concentrations and global mean surface temperature (GMST) in the coming centuries. RCP4.5 is characterised by a slow increase in GMST after 2100 as atmospheric CO_2 concentrations stabilise. Under RCP8.5, CO_2 concentrations continue to rise rapidly after 2100 before a smooth transition to stable values after 2250. The central estimate for surface temperature change at 2300 (based on our Two Layer model simulations, section A1.2) under each scenario is approximately 1.3C, 2.4C and 8.3C relative to a 1981-2000 baseline period for RCP2.6, RCP4.5 and RCP8.5, respectively.

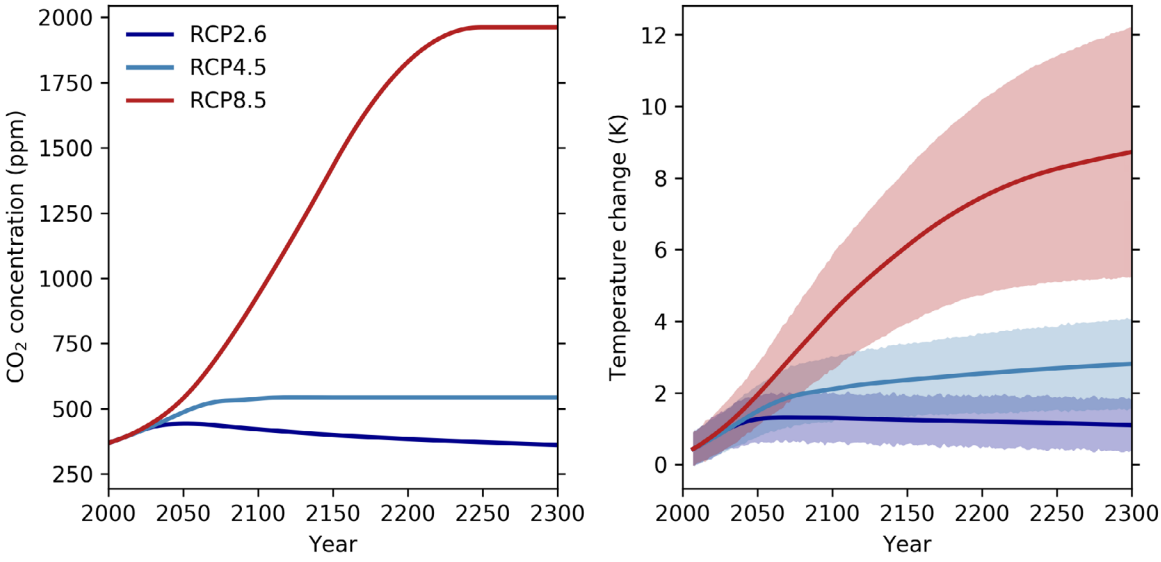

Figure 4.1. (left) Extended carbon dioxide concentrations for the coming centuries under RCP2.6, RCP4.5 and RCP8.5. (right) The associated global mean surface temperature (GMST) change for the Two Layer mode ensemble used in the UKCP18 extended sea level projections (see section A1.2 for details). Temperature change is shown relative to a 1981-2000 baseline. Shaded regions represent the projection range for the corresponding RCP scenario.

The 2300 projections presented here make use of representative concentration pathway (RCP) scenarios and their corresponding extended concentration pathways (ECPs), as described by Meinshausen et al, (2011). The ECPs are simple extensions to the RCP beyond 2100 based on the assumption of either smoothly stabilizing concentrations or constant emissions (Figure 4.1). The strong mitigation scenario RCP2.6 has constant negative CO_2 emissions after 2100, leading to the atmospheric concentration of CO_2 falling to 360 ppm by 2300. CO_2 concentrations in RCP4.5 undergo a smooth transition to constant values after 2150 by linear adjustment of emissions from 2100. The same approach was used for the RCP8.5 extension, with linear adjustment of emissions from 2150 and CO_2 stabilisation after 2250. The scenario extensions can be considered as sensitivity studies and should not be interpreted as showing the full range of post 2100 behaviour, or the most likely behaviour.

The global surface temperature response associated with the extended RCPs is evaluated using the same Two Layer model simulations that form the basis of our extended sea level projections (section A1.2). On these extended time horizons, the RCP8.5 scenario results in much larger CO_2 concentrations than the other two scenarios and a correspondingly large global mean surface temperature (GMST) response (Figure 4.1.1). This larger temperature response is also associated with very large uncertainties, reflecting the range of climate sensitivities among CMIP5 climate models (e.g. Knutti and Hegerl, 2008; Andrews et al, 2012; Collins et al, 2013). We note that these levels of surface temperature rise take climate models a long way from the regime in which they are evaluated against observations and values should therefore be interpreted with caution.

Despite the stabilisation of CO_2 concentrations in RCP4.5 from 2150, the GMST continues to rise over the coming centuries. This delayed response to CO_2 stabilisation is a well-known phenomenon of the climate system and on century timescales it is primarily associated with the slow response of the global ocean to the imposed climate forcing (Nicholls and Lowe, 2004; Knutti and Hegerl, 2008; Collins et al, 2013). RCP2.6 is the only scenario to show a decrease in GMST after peak values during the 21st century. We note that the Two Layer model simulations used in our extended time-mean sea level projections tend to slightly underestimate (of order 0.1K) the reduction of GMST at 2300 compared to the available CMIP5 climate model simulations (section A1.2, Palmer et al, 2018).

4.2 Projections of time-mean sea level change to 2300

Section acknowledgment: This research was funded by the Joint Flood and Coastal Erosion Risk Management Research and Development Programme (FCERM) of Defra, the Environment Agency, Natural Resources Wales and the Welsh Government and the flood research programme of the Scottish Environmental Protection Agency.

Section summary: In this section we present exploratory time-mean sea level projections that extend to 2300 that have been designed to be used alongside the UKCP18 21st century projections. In particular, these extended projections illustrate the long-term commitment to sea level rise for all three RCP climate change scenarios, in contrast to the global surface temperature response. We emphasise the inherent uncertainty in providing sea level projections on these time horizons and that we cannot rule-out higher values, associated with, for example, the potential of accelerated ice mass loss from West Antarctica. For London and Cardiff the projection ranges at 2300 are approximately 0.5 - 2.2m, 0.8 - 2.6m and 1.4 - 4.3m for RCP2.6, RCP4.5 and RCP8.5, respectively. The values for Edinburgh and Belfast as substantially lower, with corresponding ranges at 2300 of approximately 0.0 - 1.7m, 0.2 - 2.1m and 0.7 - 3.6m, illustrating the geographic variations around the UK. While the upper estimates of sea level rise are greater than H++ values for the 21st century (Lowe et al, 2009) they occur much later and are subject to lower confidence given the extended time horizons. As a horizon-scanning exercise the results may be useful to motivate stakeholders to think beyond 2100 and provide an approximate set of sea level change values against which vulnerabilities might be compared.

4.2.1 Global mean sea level (GMSL) projections

The time-mean sea level projections presented in this section make use of a physically-based emulator to extend CMIP5 climate model projections to 2300, as described in section A1.2. Compared to other recent studies (e.g. Palmer et al, 2015; Nauels et al, 2017) the advantage of our method is that it provides a set of extended projections that can be used alongside the UKCP18 21st century projections because they are based on essentially the same underlying CMIP5 models and give very similar values over the 21st century (Table 4.2.1). By construction, our extended projections are directly traceable to CMIP5 climate model simulations and methods of IPCC AR5 (Church et al, 2013; see section A1.2 for details).

Our extended projections show that GMSL continues to rise over the coming centuries under all RCP scenarios (Figure 4.2.1). This continued rise is a clear illustration of the long-term committed sea level rise associated with anthropogenic forcing of the climate system and the long timescale responses of the ocean (through thermal expansion) and land-based ice loss.

These directly-driven climate responses are compounded by the expectation of continued future groundwater extraction in order to maintain water availability (e.g. Wada et al, 2012; Church et al, 2013). Even under RCP2.6, the most aggressive mitigation scenario, our central estimate of GMSL sea level rise exceeds 1m at 2300. The central estimate increases to about 1.5m for RCP4.5 and exceeds 2.5m for RCP8.5.

The contribution from different components varies somewhat by scenario. Under RCP2.6 we find a similar contribution from all the major GMSL components in the central estimate. Under RCP4.5, the contributions from thermal expansion, Greenland ice loss and Glaciers become the dominant contribution for the central estimate, with total glacier mass being exhausted during the 23rd Century. The central estimate for the RCP8.5 scenario shows Glacier mass becoming exhausted around 2150 and thermal expansion and Greenland ice loss dominating the GMSL rise thereafter. While the central estimate shows a lesser contribution from Antarctica, owing to greater snow accumulated associated with a warmer atmosphere (and increased moisture transports), the large uncertainty in GMSL rise under RCP8.5 is dominated by uncertainty in the future dynamic ice discharge from Antarctica.

As one might expect, the projections of GMSL rise to 2300 are associated with much larger uncertainties than the projections over the 21st century and we have lower confidence that these uncertainties span the range of potential outcomes. At 2300 these uncertainties are approximately 0.5-1.0m for RCP2.6 and RCP4.5 and 1.5-2.0m for RCP8.5. In all cases the uncertainties are non-symmetric, with greater uncertainties on the higher levels of future sea level rise. Our extended GMSL projections show similar values to the previous work carried out as part of the Singapore's Second National Climate Change study (Palmer et al, 2015), based on version 4.1 of the MAGICC simple climate model (Wigley, 2008; Bernie et al, 2013). A more recent study, using a substantially revised version of MAGICC shows broadly similar results to those presented here for RCP2.6 and RCP4.5, but values under RCP8.5 at 2300 that are systematically larger by approximately 1-2m (Nauels et al, 2017). While a detailed comparison is left for future work, these differences illustrate the inherent uncertainty with formulating sea level projections on multi-century time horizons (see section 3.1.2 for further discussion).

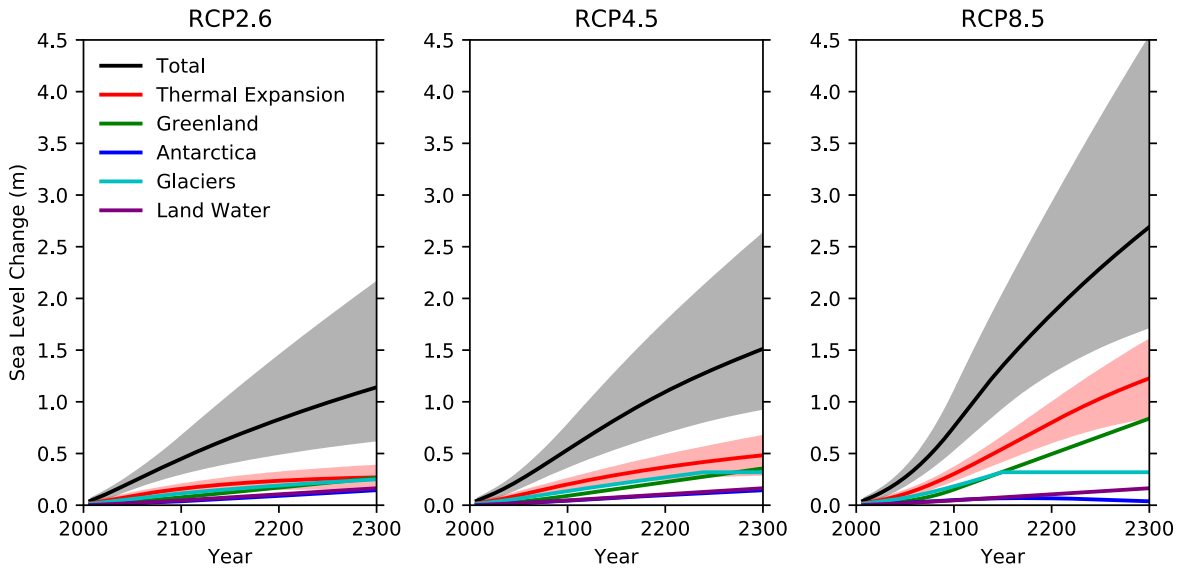

Figure 4.2.1. Time series of global time-mean sea level change to 2300 with a baseline period of 1981-2000. Individual components are indicated by the coloured lines. The projection ranges are indicated by the shaded regions for the total sea level and thermal expansion.

Table 4.2.1. Comparison of the UKCP18 21st century global time-mean sea level projections (section 3.1) and the extended projections presented in this section. Numbers beyond 2100 are quoted to the nearest 0.1m, given the lower confidence associated with projections on these extended time horizons.

	Year	RCP2.6	RCP4.5	RCP8.5
UKCP18 21st century projections	2100	0.29-0.67	0.38-0.79	0.56-1.12
Extended projections	2100	0.30-0.68	0.36-0.79	0.53-1.12
	2200	0.5-1.5	0.7-1.8	1.3-2.9
	2300	0.6-2.2	0.9-2.6	1.7-4.5

4.2.2 Coastal sea level projections for the UK

The global mean sea level projections presented in the previous section are regionalised for the UK coastline using the same approach as for the 21st century projections (section A1.1). This procedure takes account of the spatial patterns of sea level rise associated with changes in land-based ice and land water storage (e.g. Tamisiea and Mitrovica, 2011; Slangen et al, 2014) and the effects of local oceanographic processes (e.g. Cannaby et al, 2016) on regional sea level for the UK as a whole. In addition, we make use of new estimates of the pattern of regional sea level change associated with the ongoing response of the solid Earth to the last de-glaciation (often referred to as glacial isostatic adjustment, GIA; e.g. Shennan et al, 2012), including the effect of vertical land motion. This combination of factors results in substantial variations in projections of coastal time-mean sea level change around the UK for any given RCP scenario (Figure 4.2.2).

Projections of sea level rise for the UK show a very similar time-evolution to the global time series presented in the previous section. For the UK average, peak values are slightly lower than the global time series. However, some regions of the UK coastline show projections of time-mean sea level rise that are larger than the global average (Figure 4.2.3). As discussed in section 3.1, the proximity of the UK to the Greenland ice sheet means that the regional signal of this contribution is reduced compared to the global mean (Figure A1.1.4). The illustrative projections presented here all show a deceleration of sea level rise after the 21st century. However, we cannot rule out the possibility of increases in the rate of sea level rise post-2100, for example if there were a rapid loss of ice from West Antarctica (see section 3.1.2 for a discussion).

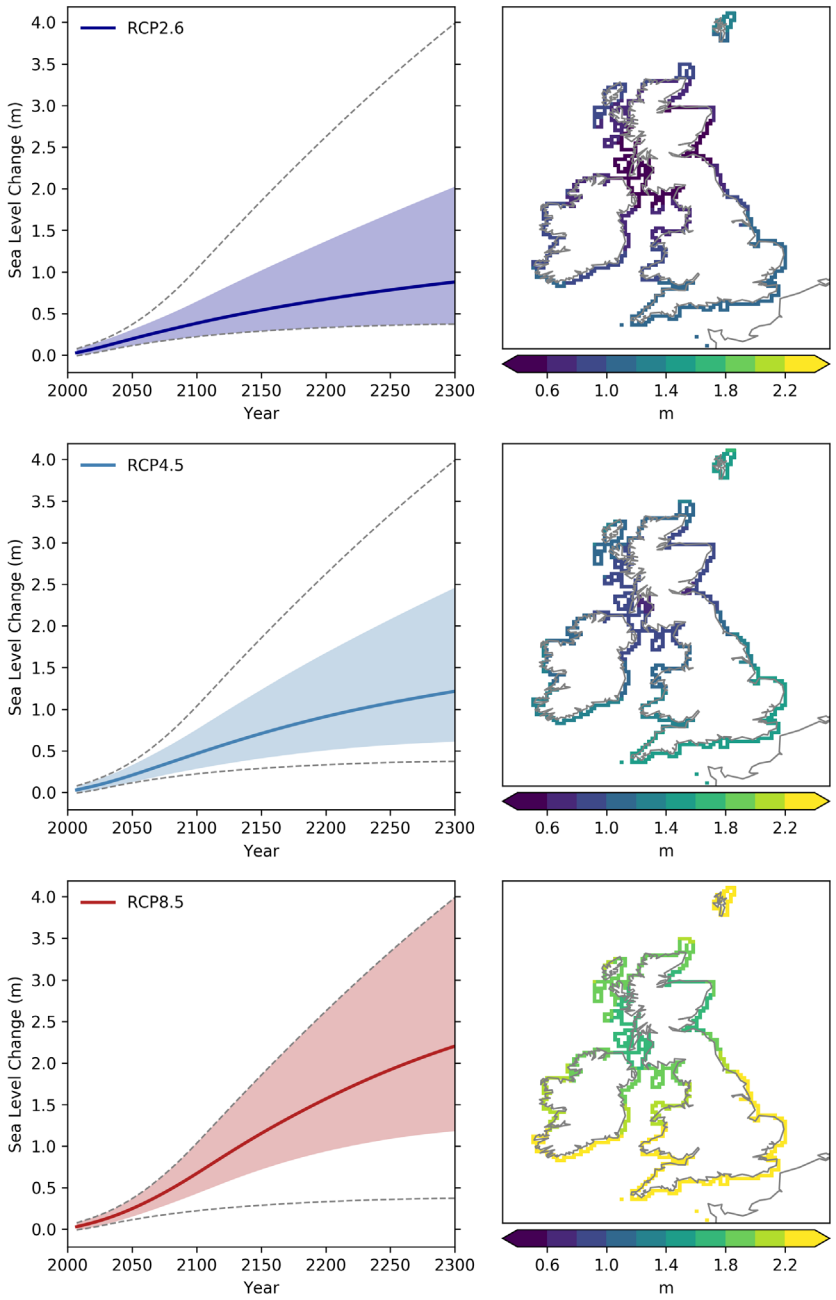

Figure 4.2.2. (left) Time series of time-mean sea level change based on the average of the UK ports listed in table 3.2.1. The solid line and shaded regions represent the central estimate and ranges for each RCP scenario as indicated in the legend. The dashed lines indicate the overall range across RCP scenarios. (right) the spatial pattern of change at 2100 associated with the central estimate of each RCP scenario. All projections are presented relative to a baseline period of 1981-2000.

The spatial variations of projected sea level rise for the UK on these extended time horizons have similar characteristics to the 21st projections (section 3.1). The magnitude of sea level change is largest to the south of the UK and for Shetland. The lowest values of sea level rise are centred on Western Scotland, with the Scottish coastline showing lower values than for the Welsh and English coastlines. These regional variations arise primarily from the spatial patterns associated with the Greenland ice sheet (Figure A1.1.4) and glacial isostatic adjustment (Figure A1.1.5).

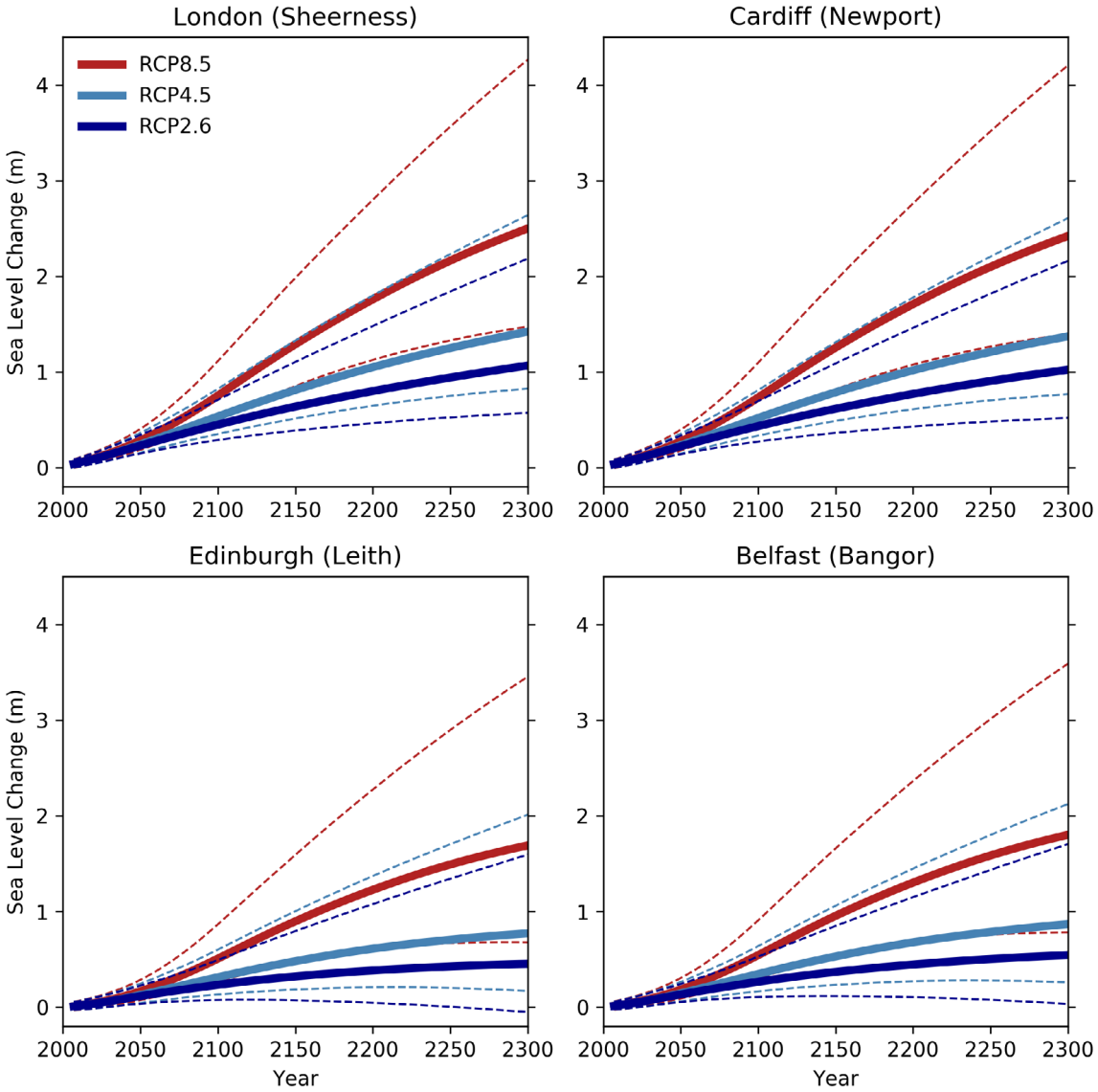

Figure 4.2.3. Time series of the time-mean sea level change for UK capital cities, based on the nearest class A tide gauge location (indicated in brackets). The solid lines indicate the central estimate and dashed lines indicate the range for each RCP as indicated in the legend. All projections are presented relative to a baseline period of 1981-2000.

Of the UK capital cities, London and Cardiff show the largest values of future sea level rise, with projected ranges at 2300 of approximately 0.5 - 2.2m, 0.8 - 2.6m and 1.4 - 4.3m for RCP2.6, RCP4.5 and RCP8.5, respectively. Edinburgh and Belfast show similar values of projected sea level rise, which are substantially lower than for London and Cardiff. Projected ranges for these cities at 2300 are approximately 0.0 - 1.7 m, 0.2 - 2.1m and 0.7 - 3.6m for RCP2.6, RCP4.5 and RCP8.5, respectively. While we expect these results to be qualitatively robust (e.g. in terms of spatial variations around the UK), absolute values of change should be treated with caution owing to the lower confidence in projections on these extended time horizons.

4.3 Potential changes in tide and surge characteristics

Section summary: Time-mean sea level rise will cause a direct increase in both low and high waters. However, since the propagation of tide and surge is dependent on water depth, there is also a potential for time-mean sea level change to have a more spatially complex effect on local tidal range and the extent of storm surges above the high tide. Here we report numerical modelling simulations which give some indication of the potential for changes in tide and surge characteristics under future time-mean sea level rise.

The results presented here should be treated as indicative of a potential secondary effect of time-mean sea level rise, rather than a detailed projection.

We find that simulated changes in the tidal range at some sites are substantial, for example more than 10cm change in the standard deviation of the tidal elevation and/or more than 10% change, consistent with previous findings (e.g. Pickering et al, 2012). However, simulated changes in skew surge are insubstantial, consistent with previous findings (e.g. Howard et al, 2010, Sterl et al, 2009).

Simulated changes in tidal range vary spatially, for example changing sign twice on the English south coast. Our spatial pattern of change in tidal range agrees well with that reported by Pickering et al, (2012), except around the Bristol Channel.

The size of the tidal response to imposed time-mean sea level change is not proportional to the size of the imposed time-mean sea level change at many sites.

Tidal response in this study is small (less than 5% change in the standard deviation of tide) on much of the Scottish coast and the northern part of the English east coast (approximately from Tobermory via Leith to Cromer) even under a large time-mean sea level increase.

4.3.1 Potential changes in tidal characteristics

Pickering et al, (2012) investigated the effect of future sea level rise on the tides of the northwest European Continental Shelf using the Dutch Continental Shelf Model version 5. They found that the M2 tidal amplitude responds to sea level rise in a spatially non-uniform manner, with substantial amplitude increases and decreases. Here we perform similar experiments with the CS3 continental shelf model driven by a set of 14 tidal constituents. We also note substantial changes in tidal range, and a spatially non-uniform response. The CS3 model (see section A1.3.3) has been in use operationally for many years and has been extensively evaluated against observations. Typical east coast M2 amplitude errors are around 10 centimetres (Furner et al, 2016; Horsburgh et al, 2008). We consider time-mean sea level (MSL) increases of up to 3 metres. Following Pickering et al, (2012) we also consider more long-term (potential millennial-scale, c/f section 3.1.2) MSL increases of up to 10 metres to investigate any non-proportionality in the response (in other words to investigate the question of whether the size of the response is proportional to the size of the MSL increase). Figure 4.3.1 shows examples of modelled changing tidal cycles at six example locations.

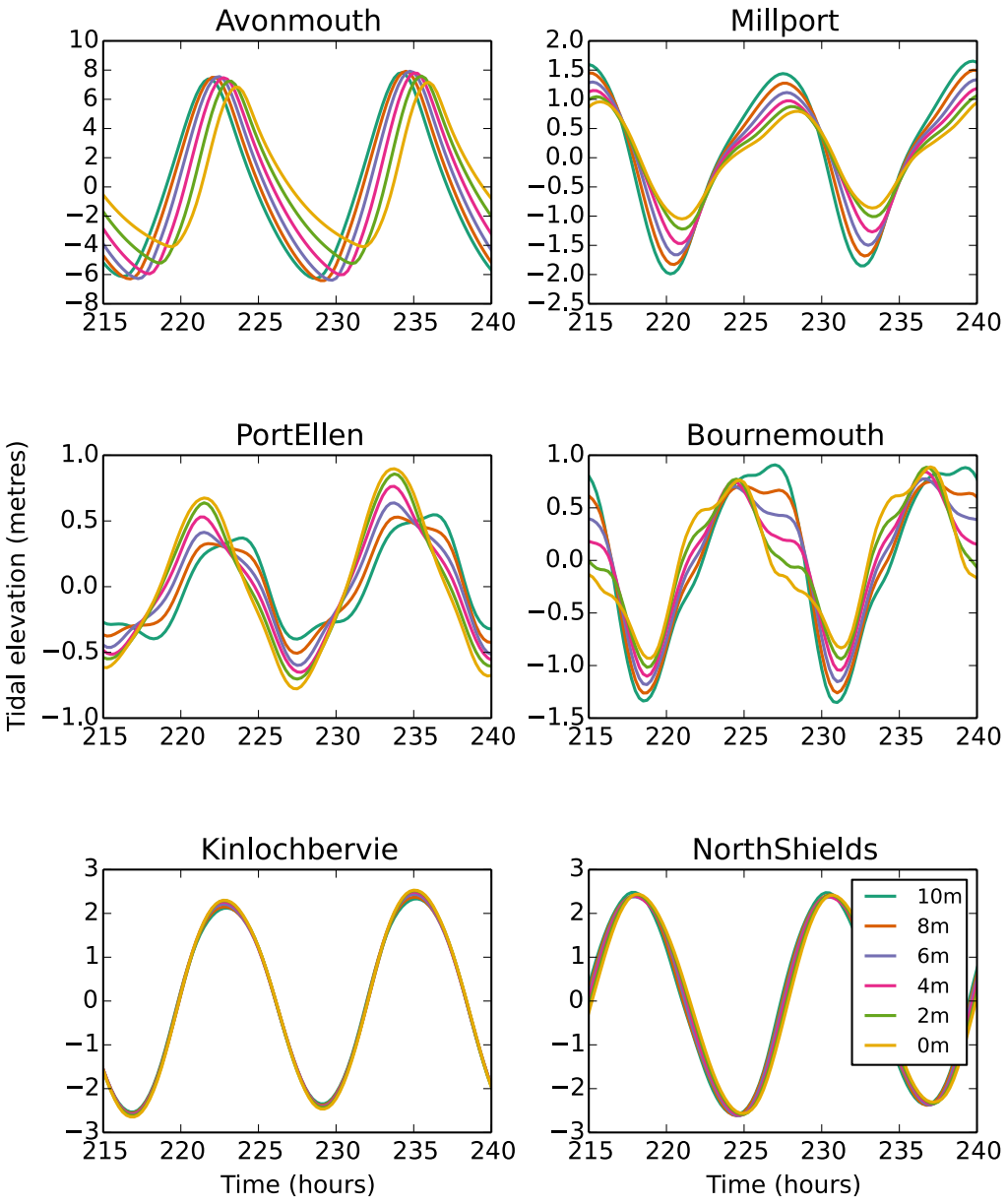

Figure 4.3.1. Example modelled changing tidal cycles at six selected locations under time-mean sea level increases of up to 10 metres, in steps of 2 metres. The legend shows the imposed time-mean sea level increase. Time is shown in hours since the 'cold' start (i.e the start of the spin-up from flat sea surface). We vary the Y-axis of these plots to accommodate the large spatial variability in the tidal range. The direct effect of the imposed time-mean sea level change is not shown: what is shown here is the tide relative to the imposed time-mean sea level. More long-term (potential millennial-scale, c/f section 3.1.2) time-mean sea level increases up to 10 metres are included as a test of the proportionality of the response. There is no implication that such high levels will be realised within the next two centuries.

It is apparent that the tidal response varies substantially between locations: for example, the response is small at North Shields compared the existing tidal range, but large at Bournemouth compared to the existing tidal range. One simple metric of tidal range is the standard deviation of the tidal elevation. A map of the modelled present-day value of this metric and a map of the changes (both absolute and expressed as a percentage of the present-day value) under 3 metres of mean sea level rise are shown in Figure 4.3.2. Significant changes, for example more than 10cm change in the standard deviation and/or more than 10% change relative to the existing standard deviation, are simulated in some places. These changes in tidal elevation will be associated with changes in the tidal currents.

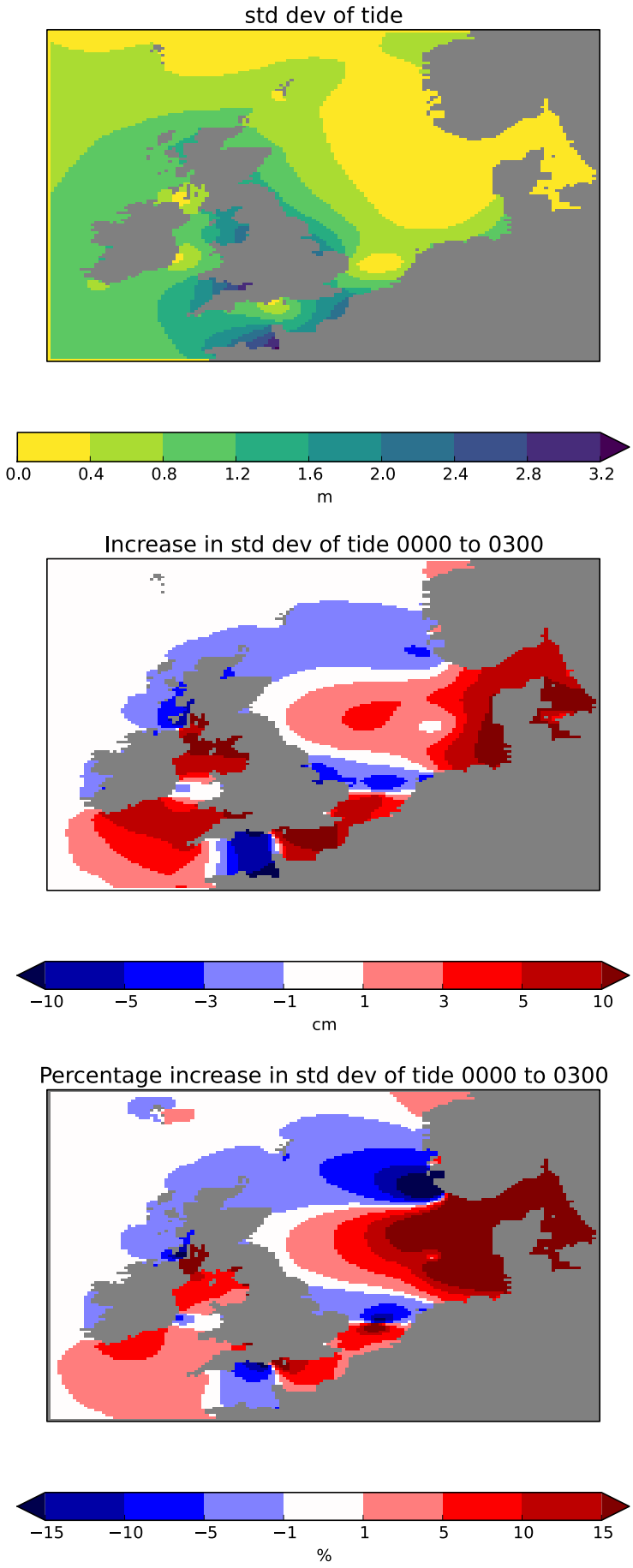

Figure 4.3.2. Modelled standard deviation of tidal elevation (top), increase in standard deviation of tidal elevation under 3 metres of time-mean sea level increase (centre) and corresponding increase expressed as a percentage (bottom). Change in the standard deviation of tidal elevation is a simple proxy for changes in the tidal characteristics and is used to indicate where the time-mean sea level change is likely to have an important secondary effect.

Comparison of this figure with Pickering et al, (2012, their figure 4 for 2m SLR) shows a strikingly similar spatial pattern of increase and decrease except for the region which spreads out from the Bristol Channel, where signs of change disagree between the two models. Flather and Williams (2000) also report an increase in tidal range in this region with a 0.5 metre MSL rise. They were using the same model that we report here. Pickering et al, (2017, 2012), on the other hand, identified a decrease using two quite different independent global and regional models. Pelling et al, (2013) again using a different model also report a decrease in the Bristol Channel with 2m SLR and a fixed coastline. Idier et al, (2017) use a substantially higher resolution model (~2km rather than ~12km) and find spatially variable increases and decreases in the Bristol Channel.

We see, then, that there is disagreement between models regarding the sign of the change in and around the Bristol Channel. More generally, Pickering et al, (2017) note that the tidal response is strongly influenced by the treatment of the coastline: a more realistic treatment of coastal recession assuming no hard coastal engineering (in contrast to the simple vertical walls used here) is capable even of reversing the sign of the tidal response at some sites. Consequently, the results presented here should be treated as indicative of a potential secondary effect of MSL rise, rather than a detailed projection. Data from the simulations is available through the user interface. Although studies with different models and treatments of coastal recession have exhibited some differences in the pattern of change, the common finding of a substantial response in the tides (which is larger than the response in the skew surge, discussed below in section 4.3.2) indicates the need for further research to constrain this effect. Future studies should include scenarios of coastline change with sea level rise (for example where land which is currently above sea level and treated as dry land becomes periodically or routinely submerged due to raised sea levels, changing the effective coastline) and scenarios of coastal engineering strategy which may have a strong effect on tidal changes (Pelling et al, 2013, Pelling and Green, 2014, Pickering, 2014, Pickering et al, 2017).

The modelled change in the standard deviation of tide under 3 metres of MSL increase at coastal sites including the sites of class A tide gauges, as a percentage of the modelled present-day value, is shown in Figure 4.3.3. Places with significant simulated changes are, for example, Millport (simulated present-day standard deviation 0.54m; change 0.11m), Avonmouth (simulated present-day standard deviation 2.94m; change 0.49m) and Portsmouth (simulated present-day standard deviation 0.96m; change 0.13m).

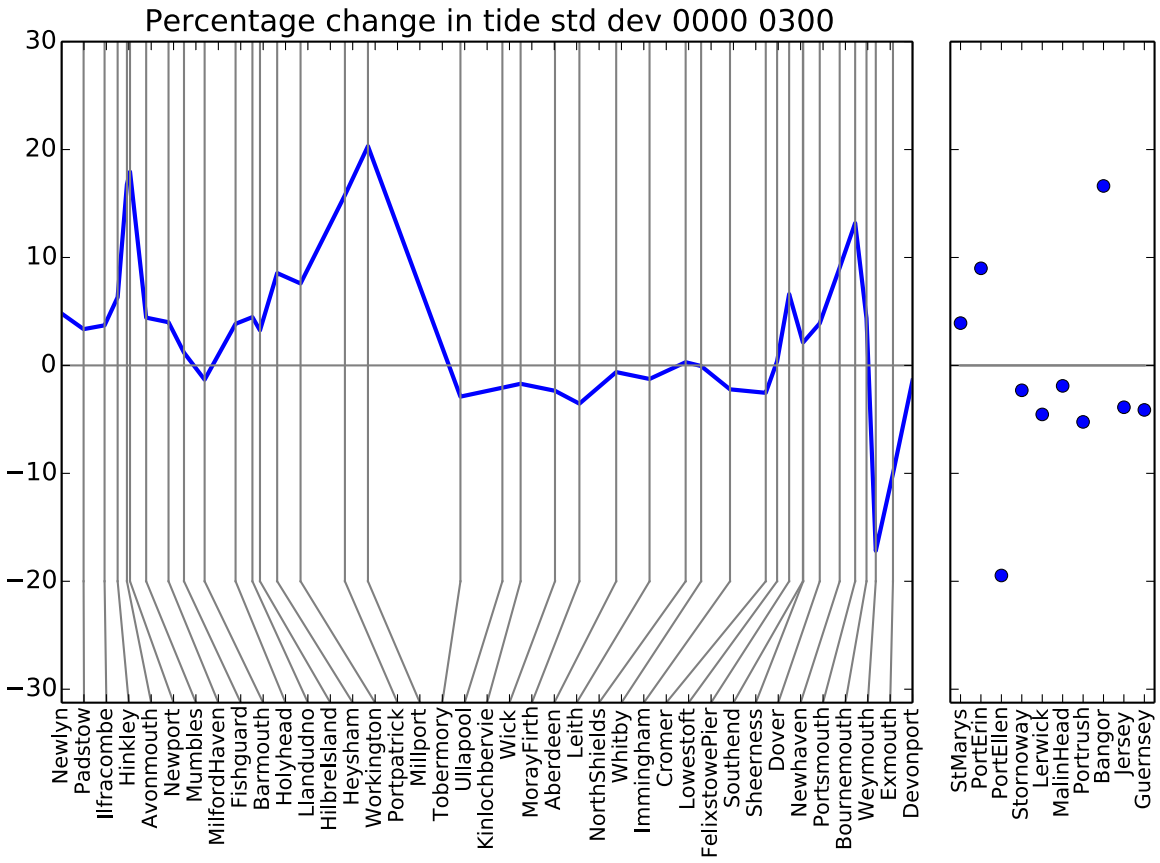

Figure 4.3.3. Modelled percentage change in the standard deviation of tide under a 3 metre increase in MSL. Both increases and decreases of more than 10% are seen in some locations.

The modelled standard deviation of the tide, normalized by the modelled present-day standard deviation, (i.e. the standard deviation with no MSL change) is shown at twelve selected sites for various imposed MSL rises in Figure 4.3.4. At several sites the response is not proportional to the time-mean sea level rise, and some sites (for example Port Ellen and Avonmouth) exhibit an inflection. This might be due to systems moving into and then out of resonance and/or migration of amphidromic points.

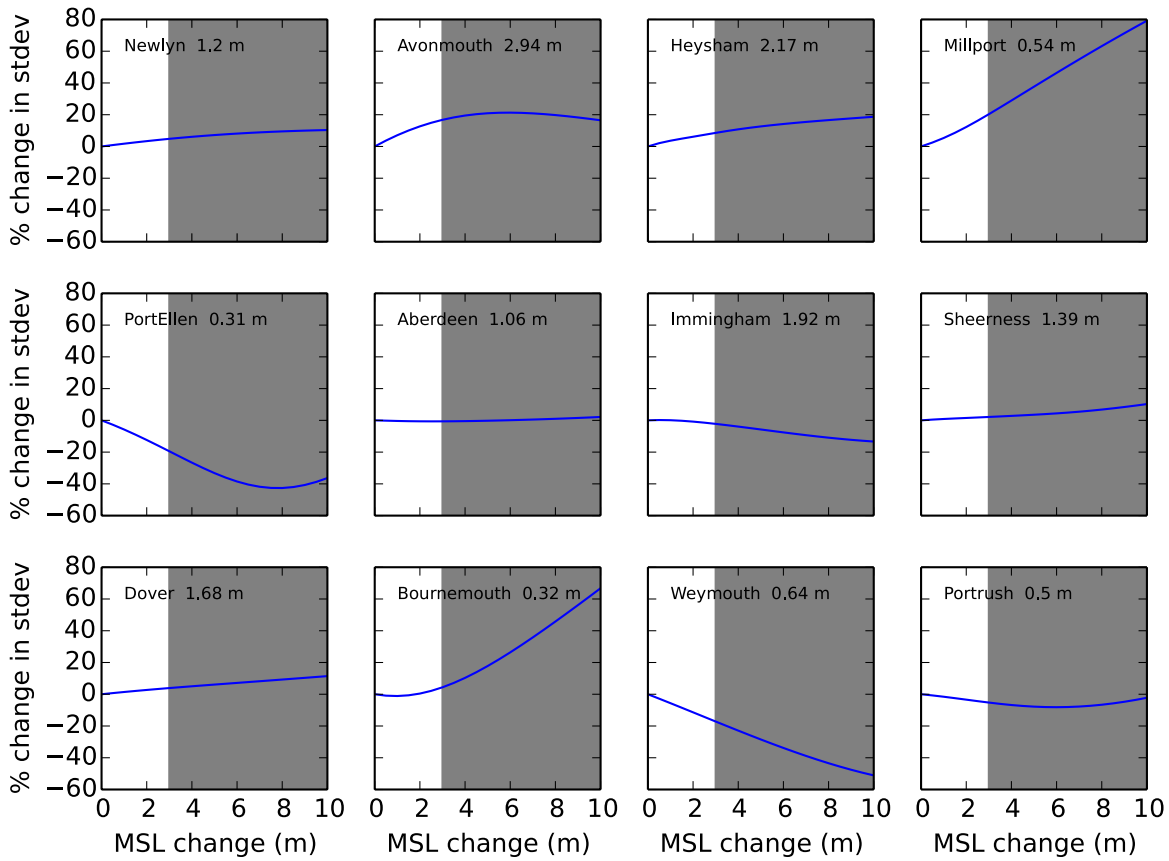

Figure 4.3.4. Change in modelled standard deviation of the tide expressed as a percentage of the modelled present-day value (which is given in the legends) against the imposed increase in MSL (from 0 to 3 m, in the white section of the plots). More long-term (potential millennial-scale, c/f section 3.1.2) MSL changes up to 10 metres (in the grey section of the plots) are also included as a test of the proportionality of the response. There is no implication that such high levels will be realised within the next two centuries.

Another simple metric of change, but a metric related to phase change rather than amplitude change, is the correlation at any given location between the simulated tides with and without mean sea level change. Strong correlation is indicative of a small or negligible change in the phase of the tides (see for example North Shields in Figure 4.3.1); weaker correlation indicates a shift of phase (see for example Avonmouth in Figure 4.3.1). For an idealised sinusoidal tidal cycle with a single frequency component, the correlation coefficient is simply the cosine of the phase difference. This gives us a simple interpretation of our correlation coefficient as a lead/lag time under an idealised sinusoidal M2 tide (the dominant tidal constituent around the UK, with period 12 hours 25 minutes). A map of this lead/lag time is shown in Figure 4.3.5. The 'future' tide with increased MSL leads the tide with present-day MSL. Some significant changes in the timing of the tide are introduced. Such changes would affect the relative times of high/low water between one port and another.

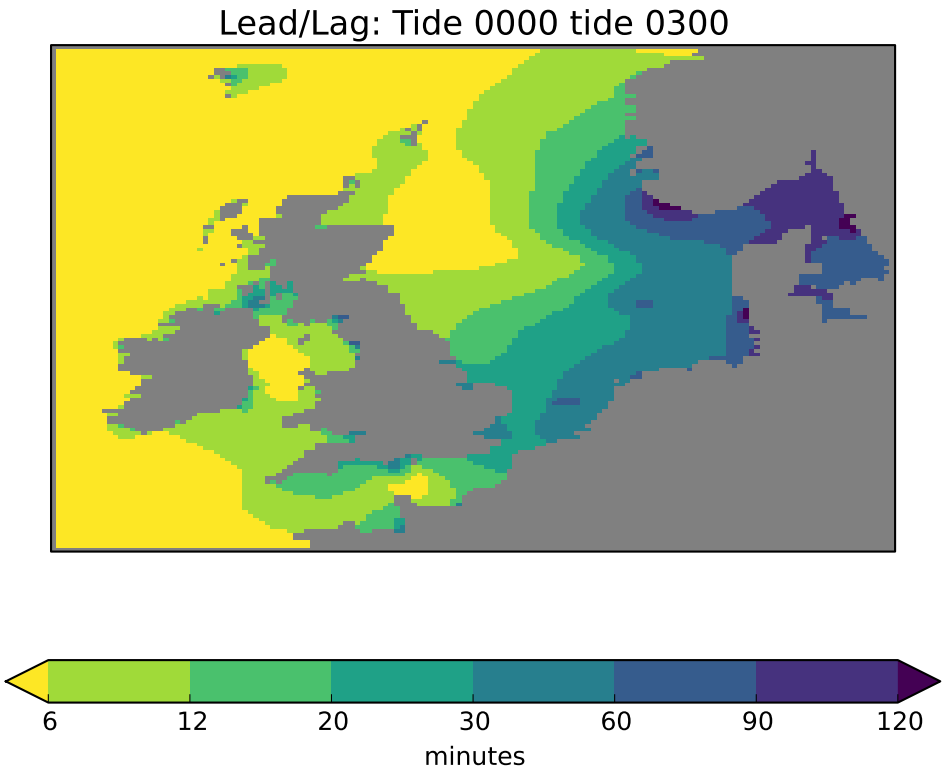

Figure 4.3.5. The correlation between simulated tide with/without 3 metres of MSL increase, interpreted as a timing difference under an idealised single-component sinusoidal M2 tide.

4.3.2 Case studies of historical surge events with imposed time-mean sea level change

Coastal engineers and researchers have amassed a wealth of information about historical coastal flooding events and the damage associated with them (for example the SurgeWatch database, Haigh et al, 2016). The case studies presented here complement the projections in section 3.2 and are intended to help users to look at potential future changes in the context of events which have already been observed.

We present three modelling case studies based on historical storm surge events. Events were chosen based on guidance from the UKCP18 user groups, storm severity, and the availability of suitable driving data. In each case, we perform numerical simulations with and without imposed mean sea level increases that span a plausible 21st century range of up to around 1 metre, and extend up to higher values of 3 metres, which could be encountered over a longer period.

Winds and sea level atmospheric pressure are taken from the Met Office global forecast model for case studies one and two, and from the SMHI-RCA4 atmospheric model driven by ERA-interim reanalysis data (Dee et al, 2011) for case study number three.

Williams et al, (2016), in a comprehensive study based on tide gauge records, showed that for the most extreme skew surges the magnitude of high water exerts little or no influence on the skew surge. In our case studies we find that mean sea level change has very little influence on the size of the skew surge. Although those two statements are not identical, they are related, and our findings are not inconsistent with the results of Williams et al, (2016).

Case study 1: 6th Dec 2013

This was the biggest event to impact the UK east coast for more than half a century. We focus on model results for the affected sites as listed in the invaluable SurgeWatch database (Haigh et al, 2015), where further details of the event can be found. The largest modelled skew surge for each site under zero, 0.5, 1, 2 and 3 metres MSL rise is shown in Table 4.3.1, along with the observed skew surge as reported on the SurgeWatch database.

Table 4.3.1. Largest skew surges (metres) associated with the event of 6th December 2013. Observed and modelled with present-day sea level; and with MSL increase of 0.5, 1, 2 and 3 metres.

	Skew Surge (m)					
Site	Observed	Model	+0.5 m	+1m	+2m	+3m
Dover	1.63	1.18	1.18	1.18	1.16	1.14
Immingham	1.61	1.59	1.6	1.61	1.61	1.59
Whitby	1.23	1.1	1.1	1.09	1.09	1.09
North Shields	1.15	0.9	0.89	0.89	0.88	0.87
Lowestoft	1.97	1.76	1.76	1.77	1.77	1.79
Newhaven	0.78	0.62	0.63	0.64	0.66	0.69
Leith	0.86	0.85	0.86	0.86	0.89	0.9
Aberdeen	0.62	0.62	0.61	0.62	0.62	0.62
Llandudno	0.7	0.77	0.79	0.78	0.76	0.75
Portsmouth	0.69	0.52	0.53	0.54	0.57	0.6
Ullapool	0.81	0.89	0.89	0.89	0.88	0.88

The fact that there is relatively little variation in skew surge (despite a substantial change in high water extremes) under the imposed MSL rise, even up to 3 metres, is underscored in Figure 4.3.6, which can be compared with Figure 4.3.4.

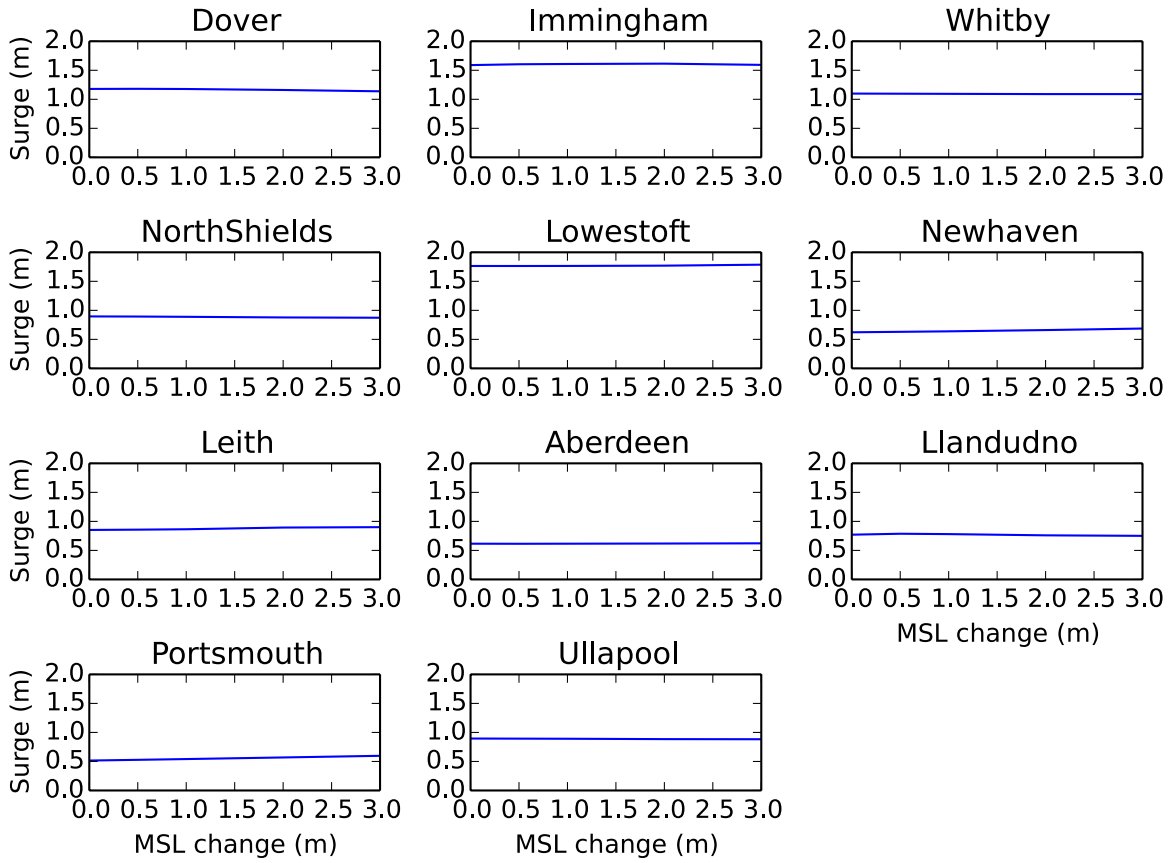

Figure 4.3.6. Case study 1. 6 Dec 2013. Modelled skew surge at affected sites vs. imposed time-mean sea level increase.

The largest modelled increase in skew surge (8 cm, which is around 15% of the modelled present-day value of 52 cm) occurs at Portsmouth. Even here, the change in tide has the dominant effect (around 28 cm) on the future extreme still water level. Details of the change at Portsmouth are shown in Figure 4.3.7. In this figure, the obvious difference between the control (no MSL change, continuous lines) and future (+3m MSL, dashed lines) simulation is due to the tidal response to the three metre MSL increase (see section 4.3.1). The MSL increase itself is not shown. If it were to be shown, it would move the dashed lines up by three metres on the Y-axis. Similarly, the MSL increase itself is not shown in Figures 4.3.8 and 4.3.9.

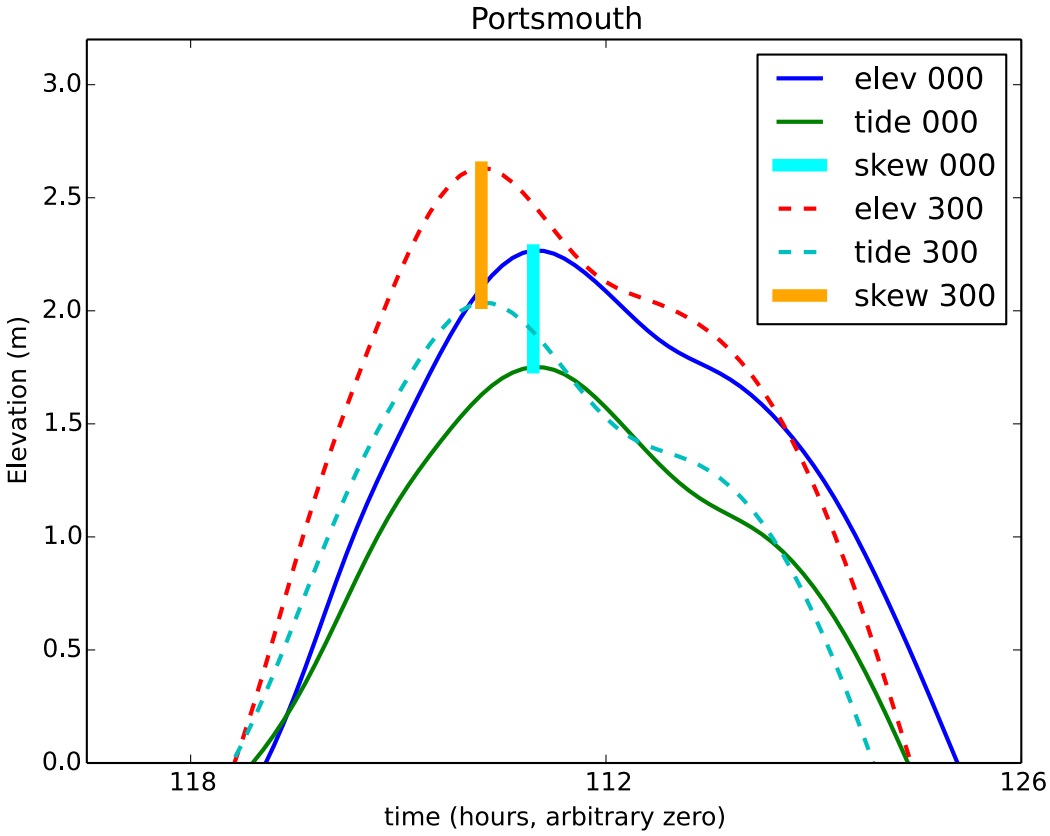

Figure 4.3.7. Simulated sea surface elevation above MSL for case study 1. 6th Dec 2013 for the zero and +3m MSL simulations. The MSL increase itself is not shown; elevations are relative to MSL.

Case study 2: 3rd Feb 2014

This event caused flooding on the south and west coasts. Again, we focus on sites listed as affected in the SurgeWatch database where further details of the event can be found. The largest modelled skew surge for each site under zero, 0.5, 1, 2 and 3 metres MSL increase is shown in Table 4.3.2, along with the observed skew surge.

Table 4.3.2. Largest skew surges (metres) associated with the event of 3rd February 2014. Observed and modelled with present-day sea level; and with MSL increase of 0.5, 1, 2 and 3 metres.

	Skew Surge (m)					
Site	Observed	Model	+0.5m	+1m	+2m	+3m
Newlyn	0.46	0.32	0.32	0.32	0.32	0.32
Fishguard	0.66	0.49	0.48	0.47	0.47	0.46
Milford Haven	0.5	0.51	0.5	0.49	0.48	0.48
Stornoway	0.4	0.57	0.58	0.57	0.6	0.57
Portpatrick	0.51	0.71	0.72	0.71	0.71	0.7
Ilfracombe	0.46	0.6	0.59	0.59	0.59	0.58
Devonport	0.46	0.3	0.31	0.31	0.31	0.32
Port Erin	0.56	0.64	0.63	0.64	0.64	0.62
Holyhead	0.49	0.57	0.58	0.57	0.55	0.54

As in case study 1 the change in mean sea level has little impact on the simulated skew surge. Simulated surges at Newlyn and Fishguard are low relative to the observations; the reason for this disparity is not clear. The simulated elevations at Holyhead are shown in Figure 4.3.8. At this location in this case, as distinct from Portsmouth in the first case study, the effect of mean sea level change on the tidal cycle is small. The effect on the skew surge is also small and consequently the imposed three-metre mean sea level increase has little secondary effect on the still water level (the primary effect is, of course, a rise of three metres).

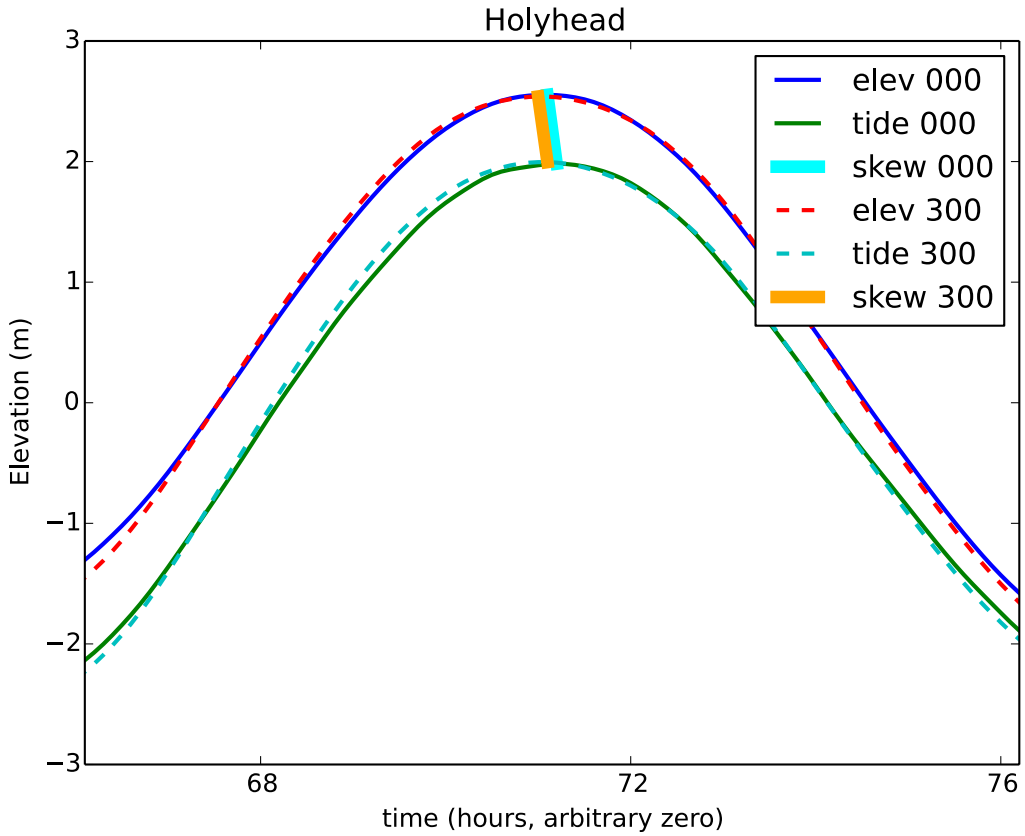

Figure 4.3.8. Simulated sea surface elevation above MSL at Holyhead with and without 3 metres of time-mean sea level increase. The MSL increase itself is not shown; elevations are relative to MSL.

Case study 3: 11th Jan 2005

In contrast to the other two case studies, this event particularly affected sites in Scotland. This event falls within the ERA interim period so we use the SMHI-ERA evaluation driving data to model this event under varying mean sea levels. The largest modelled skew surge for each affected site under zero, 0.5, 1, 2 and 3 metres MSL rise is shown in Table 4.3.3, along with the observed skew surge.

Table 4.3.3. Largest skew surges (metres) associated with the event of 11th January 2005. Observed and modelled with present-day sea level; and with MSL increase of 0.5, 1, 2 and 3 metres.

	Skew Surge					
Site	Observed	Model	+0.5m	+1m	+2m	+3m
Tobermory	1.52	0.88	0.88	0.88	0.87	0.86
Kinlochbervie	1.09	1.25	1.24	1.23	1.23	1.22
Wick	0.75	0.58	0.58	0.59	0.6	0.61
Aberdeen	0.75	0.64	0.65	0.65	0.65	0.67
Ullapool	0.93	1.14	1.15	1.16	1.16	1.16
Stornoway	0.69	0.96	0.97	0.97	0.97	0.96
North Shields	0.73	0.52	0.51	0.52	0.52	0.55
Lerwick	0.47	0.51	0.51	0.51	0.52	0.53

There is a modelled increase in the skew surge of around 3cm at North Shields under a 3m MSL increase. This is illustrated in Figure 4.3.9.

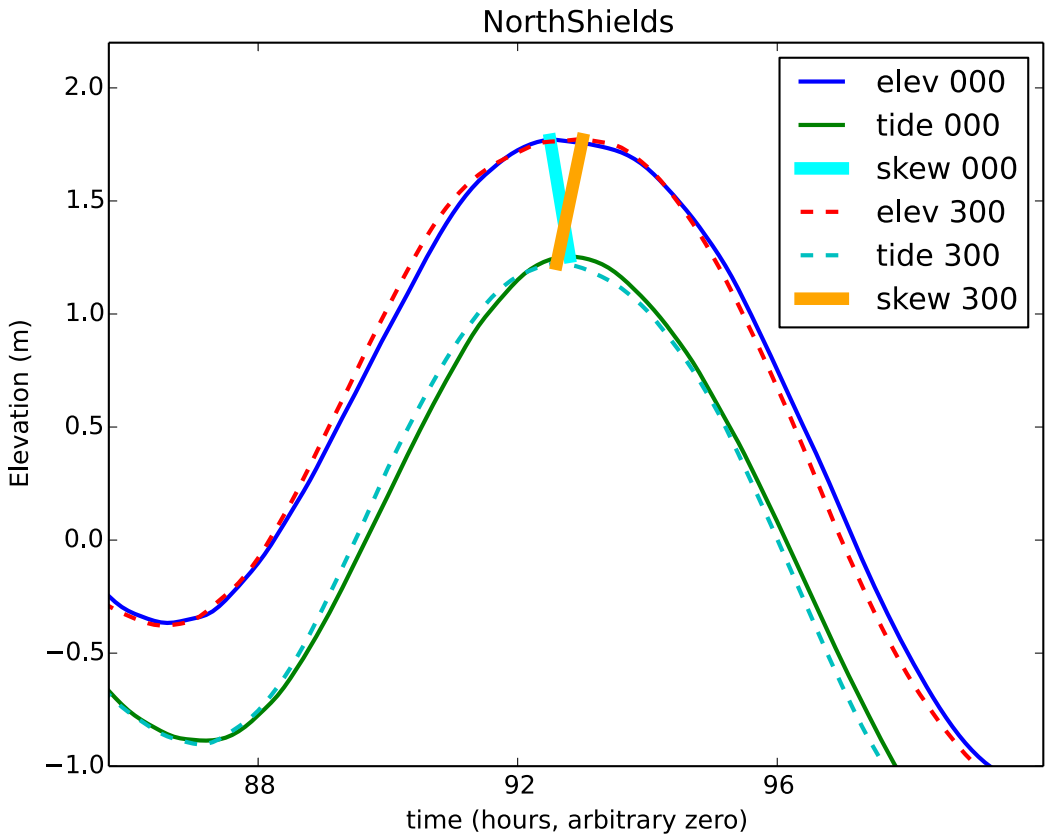

Figure 4.3.9. Simulated sea surface elevation above MSL at North Shields with and without 3 metres of time-mean sea level increase. The MSL increase itself is not shown; elevations are relative to MSL.

Like Holyhead (in case study 2), the modelled tide at North Shields is affected only very slightly by the change of MSL (this is also evident in Figure 4.3.1). The fractional increase in the skew surge is also small (less than 6%) and there are small decreases in skew surge at some of the other sites. So like case study 2, and in contrast to case study 1, the imposed three-metre mean sea level change has little secondary effect on the still water level (the primary effect is, of course, a rise of three metres).

Discussion and conclusions

In all the experiments reported here, mean sea level change is represented by a simple uniform increase to the model bathymetry. The potential change in the coastline associated with the increase in mean sea level is not modelled here. The wetting and drying algorithm described by Flather and Heaps (1975) is included, but the model land grid points are fixed and so no inundation is simulated. However, this modelling exercise does give some indication of sensitivities.

Several previous studies (e.g. Howard et al, 2010, Sterl et al, 2009) have suggested that the effect of an increased mean sea level on the characteristics of skew surge will be small and the evidence from our case studies supports this conclusion. However, some recent studies (e.g. Pickering et al, 2017; 2012, Pelling et al, 2013) have shown that the changes in the tidal cycle associated with MSL increase may be substantial, and the results of our simulations support this. Even with an unchanged skew surge, changes in the tidal cycle affect the still water level.

We conclude that tidal changes with sea level rise should therefore be the focus of further research into the secondary effect of sea level rise on extreme still water levels.

5. Comparison with UKCP09

In this section we present a comparison of the UKCP18 marine projections to the work presented as part of the UK climate projections presented in UKCP09 (Lowe et al, 2009). The 21st century projection components of UKCP09 have all been updated under UKCP18 (Table 5.1). In addition, UKCP18 provides extended projections of time-mean sea level change and explores the impacts these levels of sea level rise might have on tide and surge characteristics around the UK. The UKCP09 components on shelf coastal water properties, H++ scenarios and Thames Estuary case study have not been updated under UKCP18. However, there are ongoing efforts being carried out by the Met Office and the wider scientific community to provide updated H++ scenarios for time-mean sea level.

Science component	UKCP09	UKCP18
21st century projections of time-mean sea level (section 3.1)	Y	Y
21st century projections of storm surge (section 3.2)	Y	Y
21st century projections of wave height (section 3.3)	Y	Y
21st century projections of coastal water properties	Y	N
21st century H++ scenarios for time-mean sea level and surge	Y	N
Thames Estuary 2100 Case Study	Y	N
Extended projections of time-mean sea level (section 4.2)	N	Y
Time-mean sea level effects on tide and surge characteristics (section 4.3)	N	Y

Table 5.1. Summary of the science components included in UKCP09 and UKCP18.

UKCP09 was published following the release of the IPCC Fourth Assessment Report (Solomon et al, 2007; hereafter "AR4"). As a result, the modelling systems and scientific methods used in UKCP09 reflected the level of scientific knowledge and model capability reported in the AR4. In addition, the projections presented in both AR4 and UKCP09 were premised on the SRES (Special Report on Emissions Scenarios) climate change scenarios (IPCC Working Group 3, 2000). Since AR4 the SRES scenarios have been replaced by a different set of climate change scenarios; the RCPs (Representative Concentration Pathways), as described by Meinshausen et al, (2011) and references therein. These scenarios formed the basis of climate projections presented in the IPCC Fifth Assessment Report (Stocker et al, 2013, hereafter "AR5") and the projections presented in UKCP18.

In this section we highlight and discuss the key differences between UKCP18 and UKCP09, focussing on the 21st century projections of time-mean sea level (section 5.1) and potential changes in storm surge activity (section 5.2). We refer the reader to Palmer et al, (2016) for further discussion.

5.1 Projections of time-mean sea level change

Section summary: The time-mean sea level projections of UKCP18 are based on updated scientific methods and climate change scenarios compared to UKCP09. The most important methodological difference is the inclusion of ice dynamics in UKCP18 projections of future sea level rise, resulting in systematically larger values than presented in UKCP09. The RCP climate change scenarios used in UKCP18 span a greater range of climate forcing over the 21st century than the SRES scenarios used in UKCP09. While this results in a greater overall spread of regional sea level projections for UKCP18, we find that the modelling uncertainty for a given scenario is similar to that reported in UKCP09.

IPCC AR5 reported several substantial advances that have been made in the science of sea level change since the publication of IPCC AR4 (and UKCP09). In particular there is:

- greater confidence in projections of global mean sea level (GMSL) change, owing to improved understanding of the components of sea level.
- better agreement between processed-based models and observations.
- ice-sheet dynamical changes have been included in process-based projections of global and regional sea level change.

As noted by Palmer et al, (2016), the inclusion of ice sheet dynamics in process-based projections was the most important change between AR4 and AR5, resulting in substantially larger GMSL projections for a given climate change scenario (Table 5.1.1; Church et al, 2013).

Climate scenario	Method	Sea level change 2090-2099
SRES A1B	IPCC AR4	0.21 - 0.48m
SRES A1B	UKCP18	0.41 - 0.80m
RCP2.6	UKCP18	0.28 - 0.62m
RCP4.5	UKCP18	0.36 - 0.73m
RCP8.5	UKCP18	0.51 - 1.01m

Table 5.1.1. Projected ranges of global sea level change for the period 2090-2099. The baseline for the IPCC AR5 methods is 1980-1999 and 1981-2100 for UKCP18 methods, but this difference has a negligible impact on the results.

The difference in the climate change scenarios themselves also has an impact on the projections of future sea level rise. The RCPs span a greater range of future CO_2 concentrations and associated climate forcings than the SRES scenarios (Figure 5.1.1, Meinshausen et al, 2011). The sea level projections presented in UKCP09 made use of the SRES B1 ("Low"), SRES A1B ("Medium") and SRES A1FI ("High") scenarios. Broadly speaking, these scenarios cover a similar range of future climate change forcings as the RCP4.5 and RCP8.5 scenarios used in UKCP18. In addition, UKCP18 includes the strong mitigation scenario of RCP2.6. The central estimates of GMSL rise under SRES A1B, RCP2.6, RCP4.5 and RCP8.5 using UKCP18 methods is presented in Figure 5.1.1. As implied by the corresponding future CO_2 concentrations, projected GMSL rise for A1B lies between the projections under RCP4.5 and RCP8.5.

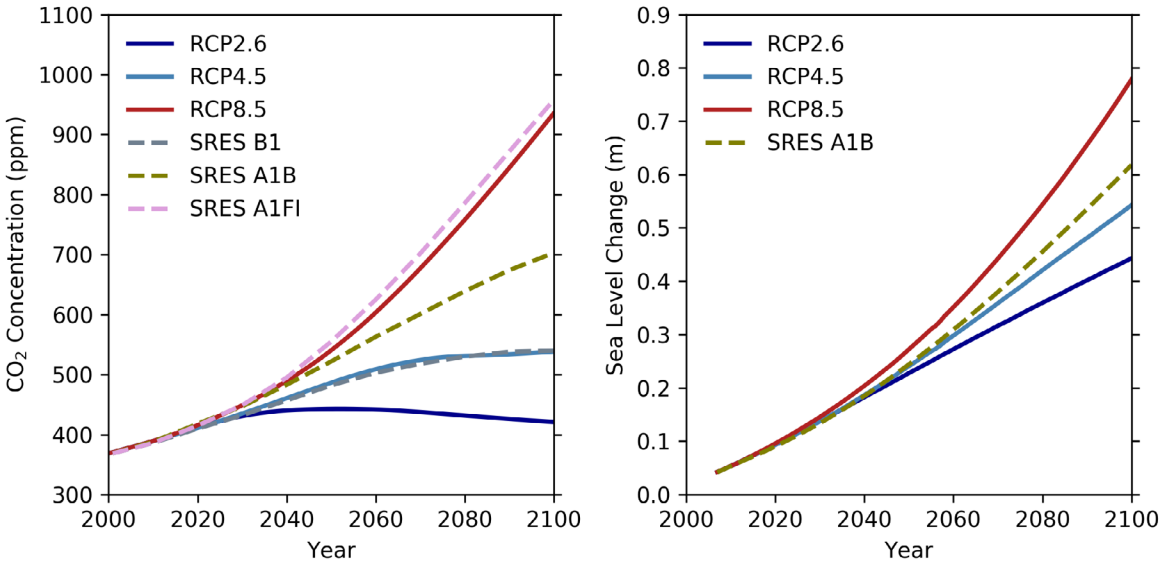

Figure 5.1.1. (left) Time series of CO_2 concentrations over the 21st century for the RCP scenarios (Meinshausen et al, 2011) and SRES scenarios (https://www.ipcc.ch/ipccreports/tar/wg1/531.htm) based on the Bern-CC Model. (right) The corresponding central estimates of time-mean sea level rise over the 21st century using UKCP18 methods for all available scenarios. The SRES A1B projection makes uses the projections of Antarctic ice dynamics from RCP4.5, but the results are not sensitive to the choice of scenario.

Moving to regional scales, we present a comparison of the 21st century time-mean sea level projections for London and Edinburgh from UKCP18 and UKCP09 (Figure 5.1.2). We can see that the inclusion of ice dynamics in the GMSL projections for UKCP18 results in local projections for the UK that are systematically larger than presented in UKCP09. The broader range of future climate forcings associated with the RCPs results in a larger overall spread in the UKCP18 projections, but the modelling uncertainty for any given scenario is similar to that presented in UKCP09.

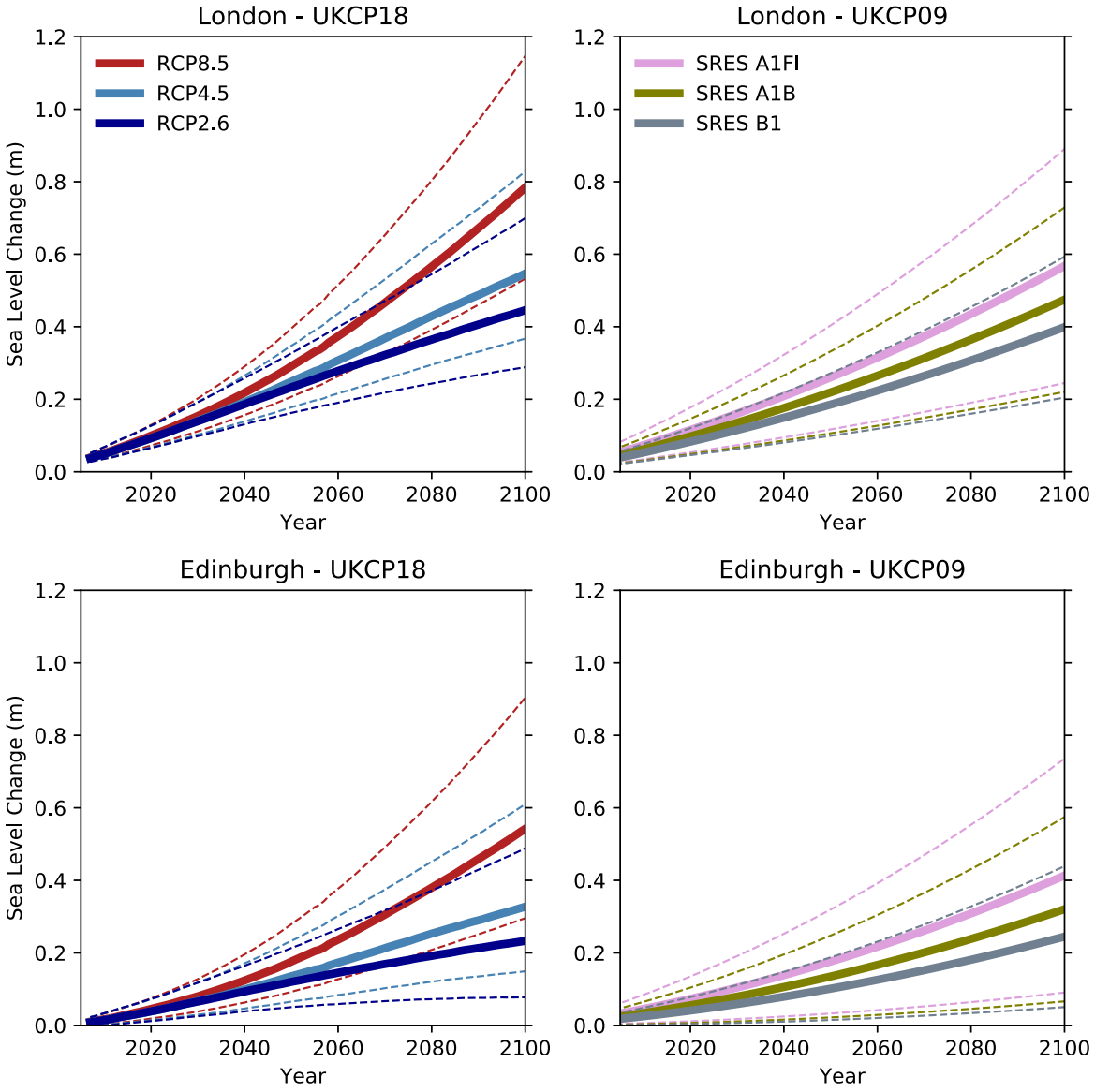

Figure 5.1.2. Time-mean sea level projections for London and Edinburgh provided under UKCP18 (left) and UKCP09 (right). SRES A1FI, SRES A1B and SRES B1 correspond to the "High", "Medium" and "Low" climate change scenarios referred to in the UKCP09 Marine Report (Lowe et al, 2009). UKCP18 results presented relative to a baseline of 1981-2000. UKCP09 results presented relative to a baseline of 1980-1999 (note that difference in baseline period equates to 1-2 mm). The solid lines indicate the central estimate and dashed lines indicate the range for each scenario as indicated in the legend.

5.2 Projections of extreme coastal still water levels

New features of UKCP18 which move beyond the guidance given in UKCP09 include illustrative combinations of projected sea level change with the best present-day estimates of extreme still water return level curves, simulations of the sensitivity of tide and surge to mean sea level increase, and case studies of past events with simulated mean sea level increase. However, unlike UKCP09, UKCP18 does not include a specific chapter focussing on the Thames Estuary.

5.2.1 Storminess component

Summary of main differences

- Perturbed-Physics Ensemble in UKCP09 replaced by Multi-Model Ensemble.
- Revised central estimate of no change in storminess contribution to extreme sea level change over the 21st century.
- Crude scaling replaced by simulation for illustrative high-end projection.
- Resulting illustrative high-end projection reduced relative to UKCP09.

In both the UKCP09 Marine and Coastal projections (Lowe et al, 2009) and UKCP18 we used a storm surge model forced by atmospheric data from an ensemble of climate model simulations of the 21st century. However, where the UKCP09 storm surge modelling used an ensemble based on a single climate model with perturbed atmospheric physics parameters (the HadRM3P perturbed physics ensemble), the UKCP18 storm surge modelling uses atmospheric data from a set of five diverse climate models selected from the CMIP5 ensemble and downscaled with the RCA4 regional climate model, plus one further CMIP5 model ***not*** downscaled through a regional climate model.

There is also an important difference in our high-end projection. UKCP09 selected a particular CMIP3 model with large projected storm track strengthening over the UK (according to one metric of storminess) and presented a high-end ("H++") 21st-century storm surge change based on two different crude scaling approaches intended to anticipate the result of downscaling that CMIP3 model, in the absence of suitable atmospheric data. In UKCP18 we select a particular CMIP5 model with large projected storm track strengthening over the UK (according to the same metric of storminess) and we present "illustrative high-end" 21st-century storm surge change results from a simulation driven directly by atmospheric data from that model. This storm surge high-end 21st century change is smaller than the "H++" high-end change reported in UKCP09. For example, the top of the UKCP09 "H++" range of increase in the 50-year return level of skew surge at the mouth of the Thames Estuary was around 0.7 metres over the 21st century. The corresponding change under our illustrative high-end projection would be less than 0.06 metres (less than 0.6 mm/year, see section 3.2.3).

Differences in statistical approach

In UKCP18 our assessment makes use of the spatial coherence of any projected change in the surge component of extreme sea level. Spatial coherence is important as it helps us assess whether any changes are the result of large-scale atmospheric changes (see section A1.4.2). Such spatial coherence was not considered in UKCP09 and results were presented for a five-parameter statistical model (see section A1.4.2) applied to the period 1950 to 2100. Thus, it is not straightforward to make a comparison with results from the UKCP18 assessment, which uses a four-parameter statistical model (see section A1.4.2) applied to a shorter period: 2007 to 2100. We used the shorter period because trends based on the period 1950-2100 may underestimate the change over the 21st century. We present a comparison in Figure 5.2.1.

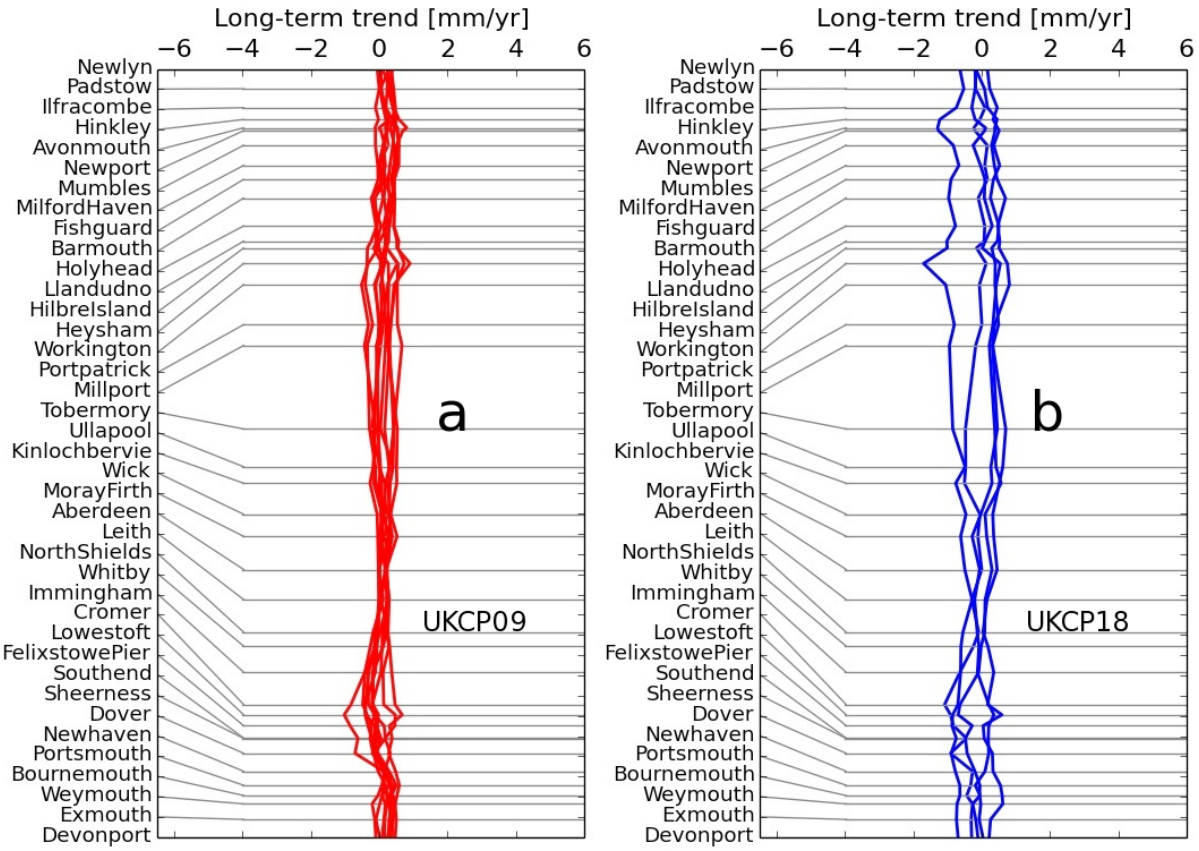

Figure 5.2.1. Comparison of diagnosed trends in one-year return level around the UK mainland in UKCP09 and UKCP18. (a): Eleven simulations of the HadRM3P perturbed physics parameter ensemble, five-parameter statistical Model, period 1950-2100, emissions scenario A1B. (b): RCA4-downscaled simulations, four-parameter statistical Model, period 2007-2100, RCP8.5.

Several factors contribute to the differences between the panels in Figure 5.2.1:

- The period over which a linear trend is assessed.
- Atmospheric model differences (HadRM3P perturbed physics parameter ensemble vs RCA4 downscaled CMIP5 simulations).
- Radiative gas/aerosol forcing differences (A1B in UKCP09; RCP8.5 in UKCP18).
- Statistical model applied (four- or five-parameter).

The increase in spread from panel (a) to panel (b) is mostly accounted for by the change in the period over which a trend is assessed, and the change of atmospheric model. These two factors contribute similar amounts to the increase in spread.

In UKCP18, in view of the disagreement between simulations, we conclude that ***no change*** is our best representative central estimate of the atmospheric storminess contribution to extreme sea level change over the 21st century, whereas UKCP09 reported changes. (Although the changes reported were small compared to the contribution from mean sea level change).

6. CMIP5 comparison with the HadGEM3 PPE

The marine projections presented in UKCP18 are rooted in the multi-model-ensemble (MME) simulations provided as part of the fifth phase of the Coupled Model Intercomparison Project (CMIP5; Taylor et al, 2012) and used in the IPCC 5th Assessment Report (e.g. Church et al, 2013). They do not use the HadGEM3 perturbed physics ensemble (PPE) that forms part of the of the UKCP18 land projections. This decision was taken for two reasons: (i) evidence from previous work suggested that the PPE would not capture the full range of sea level rise responses seen across CMIP5 models (Pardaens et al, 2011; Figure 6.1.1); (ii) the scheduling of the HadGEM3 PPE simulations did not allow sufficient time to develop sea level projections based upon those simulations. In this section we present a comparison of climate projections from CMIP5 MME and the HadGEM3 PPE for key metrics relevant to time-mean sea level, surges and waves, to establish the relationships between these two model ensembles.

6.1 Metrics relevant to time-mean sea level change

The UKCP18 time-mean sea level projections are fundamentally built upon CMIP5 model simulations of global mean surface temperature (GMST) and global thermal expansion (section A1.1). While global surface temperature is readily available from climate model simulations, global thermal expansion is not always routinely output. However, global thermal expansion is closely related to the magnitude of Earth's top-of-atmosphere radiation imbalance, via the associated changes in total ocean heat content (e.g. Kuhlbrodt and Gregory, 2012; Lorbacher et al, 2015; von Schuckmann et al, 2016). Therefore, we focus our comparisons on changes in GMST and Earth's top-of-atmosphere net radiation.

The HadGEM3 PPE shows a surface warming of GMST in the late 21st century that typically exceeds the 90% confidence interval of the CMIP5 models used in the UKCP18 time-mean sea level projections (Figure 6.1.1, left), consistent with the findings in the Land Report. However, we can see that the CMIP5 models used to supplement the HadGEM3 PPE in the land projections are well-distributed across the CMIP5 MME used in the UKCP18 sea level projections. This means there is little expectation of bias from differences in the choice of CMIP5 members. Comparisons of changes in the net radiation at top-of-atmosphere under RCP8.5 (Figure 6.1.1, right) show that the HadGEM3 PPE projections are above the CMIP5 MME average, but the two ensembles have a much greater degree of overlap than for GMST. In general, the larger rises in GMST will tend to promote greater levels of sea level rise (Church et al, 2013). Similarly, larger increases in Earth's net radiative imbalance are directly associated with greater increases in global ocean heat uptake and sea level rise through ocean expansion. Overall, we would expect the climate change signals seen in the HadGEM3 PPE simulations to be associated with global and regional sea level rise that is towards the upper end of the 90% confidence intervals of the RCP8.5 projections presented in section 3.1.

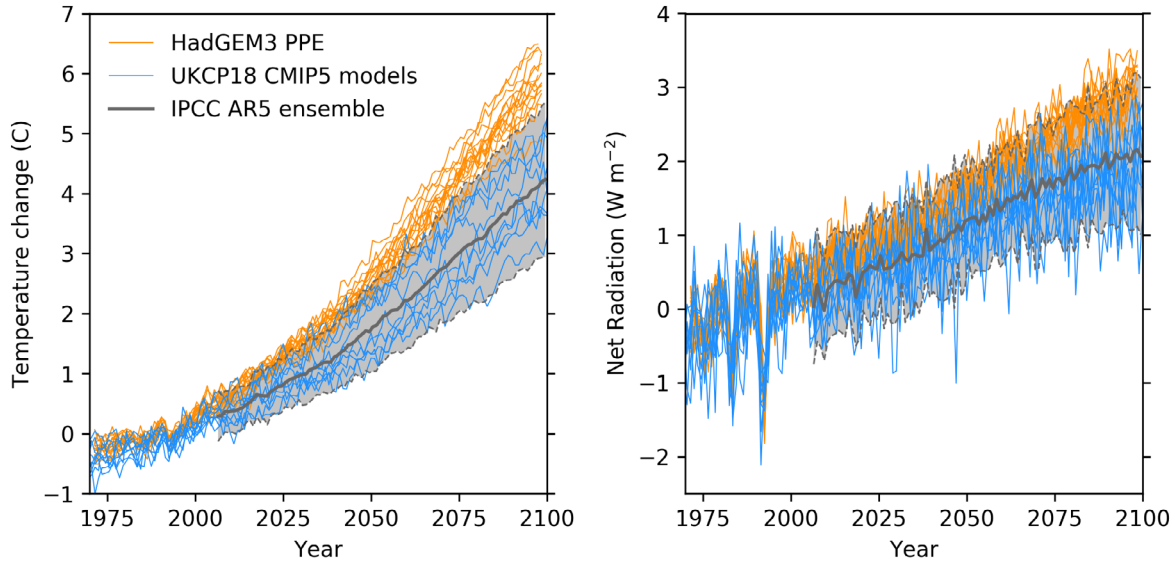

Figure 6.1.1. Time series of global mean surface temperature change under RCP8.5 for: (i) the HadGEM3 perturbed parameter ensemble of Land Strand 2 (orange); (ii) the CMIP5 models common to the UKCP18 sea level projections utilised in the Land Strand work (blue); (iii) The CMIP5 climate Model ensemble used in the UKCP18 21st century time-mean sea level projections (grey, shaded region indicates the projection range). All time series are shown relative to a baseline period of 1981-2000.

6.2 Metrics relevant to changes in storm surges and waves

We anticipate that any robust century-scale changes in the statistics of local extreme surges will be a reflection of large-scale changes in atmospheric storminess. As discussed in section A1.3.1, a great deal of research is focused on such changes. Drawing stronger links between any local changes in surge and the large-scale changes will be the subject of further work following on from UKCP18. Here we take a preliminary look at some of the evidence. One widely-used metric of storminess is the Blackmon (1976) band-pass filtered mean sea level pressure (BPF MSLP). The passage of atmospheric storms is associated with variations in mean sea level atmospheric pressure. The variability of a suitably filtered long (e.g. twenty or thirty years) time series of such variations at a given location is a metric of storminess for that location and that period. The filtering is designed to pick out the variations associated with the storms that typically drive the significant surge and/or wave events. Often the analysis is limited to a specific season, for example the northern hemisphere winter (December-January-February) season is selected here. We take a profile of this metric along the Greenwich meridian (the zero of longitude), find the latitude and strength of the maximum, and plot the 21st century changes in that strength and latitude, for some of the CMIP3 and CMIP5 model simulations, in Figure 6.2.1.

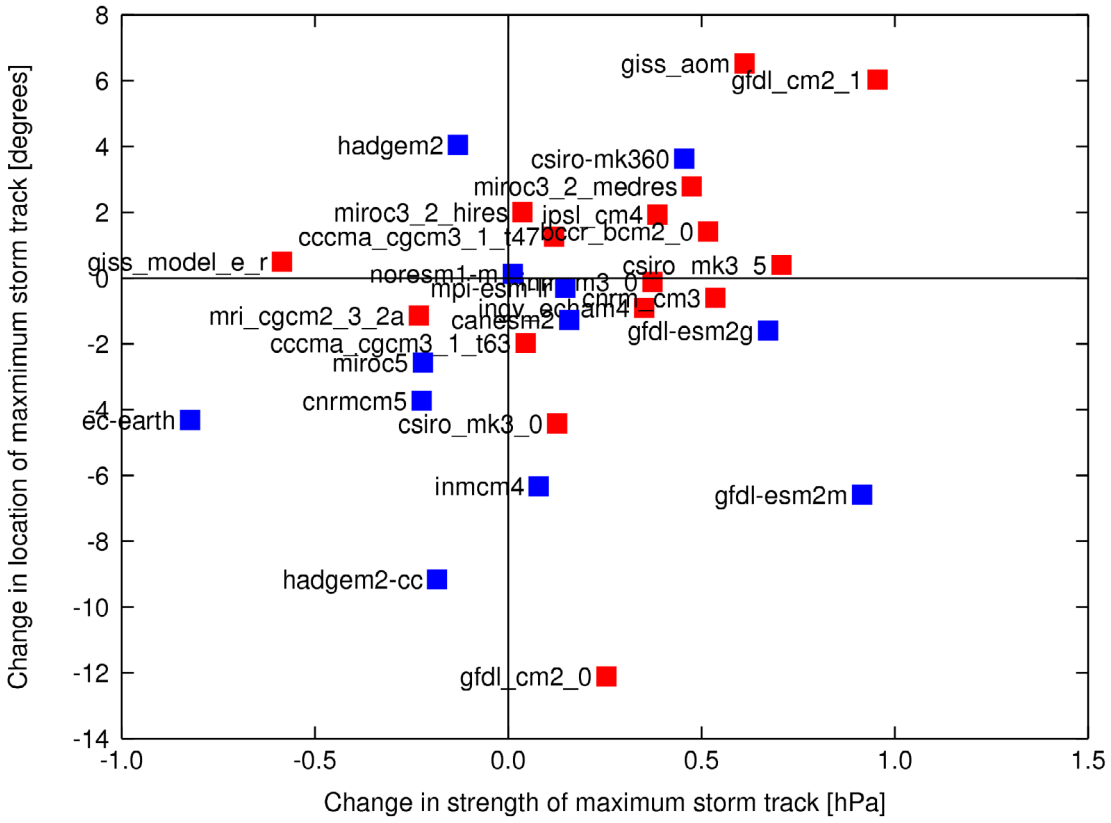

Figure 6.2.1 This is a labelled version of figure 7.1 from Wade et al, (2015), provided by Ben Harvey at the University of Reading, showing climate change responses of the latitude and strength of the December-January-February storm track at 0E. Blue and red squares represent CMIP5 (RCP8.5) and CMIP3 (SRESA1B) models respectively and the climate change response is defined as the difference between late 21st century and late 20th century values. The measure of the storm track is the 2-6 day bandpass-filtered time-mean sea level pressure: see main text for details.

It can be seen that one of the largest increases in storm track strength by this metric is exhibited by the GFDL-ESM2M model, consistent with our finding of an increase in the level of extreme surges in that simulation. An alternative commonly-used metric of storminess at a given location is a count of the number of mid-latitude cyclone centres passing close to that location. One advantage of the storm counting approach is that anticyclones, which affect the MSLP variability but are usually associated with light winds, can be explicitly excluded. Various methods are used to identify and track the movement of the centres. Figure 6.2.2 shows changes in this alternative metric of storminess. First, we evaluate the zonal mean of the number of storms per month crossing a 5-degree spherical cap around each point in a longitudinal window from 5 degrees west to 25 degrees east during December, January and February for two periods representing the climate of the recent past and the end of the 21st century. Then (as with the BPF MSLP in Figure 6.2.1), we find the latitude and strength of the maximum and plot the 21st century changes in that strength and latitude, for various sets of model simulations, in Figure 6.2.2.

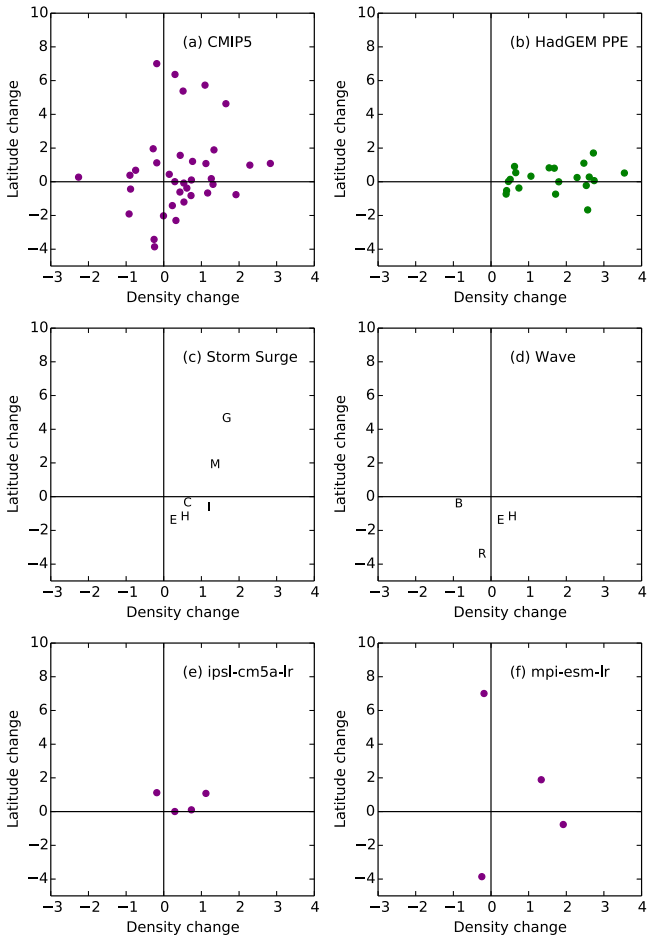

Figure 6.2.2. Simulated change in track density and change in latitude of maximum track density over the 21st century (a) for some CMIP5 Models; (b) for the HadGEM3 PPE; (c) for the Models used to simulated changes in storm surge; (d) for the Models used to simulate changes in surface waves. Panels (e) and (f) each give an indication of the range of changes within different realisations of a single Model. Letters in panels (c) and (d): B:BCC-CSM1-1, C:CNRM-CM5, E:EC-EARTH, G:GFDL-ESM2M, H:HADGEM2-ES, I:IPSL-CM5A-MR, M:MPI-ESM-LR, R:MRI-CGCM3. For full details of the axes see the main text.

A striking feature of this plot is that the difference (in the 21st-century change) between different realisations of the same model (for example the four realisations of MPI-ESM-LR shown in panel (f)) is comparable to the difference between different models. However, this may be due to inconsistent (between present-day and future) identification of the maximum (some models do not have an easily-identified single well-defined maximum). McDonald (pers comm) has studied these changes as manifest in a control simulation (i.e. a simulation with no change in radiatively-active gas forcing). The envelope of century-scale changes there was found to be significantly smaller than the envelope of forced changes seen in Figure 6.2.2 (panels (a) and (b)) implying that at least part of the change shown in Figure 6.2.2 is scenario-driven and not just long-period noise. Also noticeable comparing Figure 6.2.1 and Figure 6.2.2 is that although the strength (on the X-axis) increases for the GFDL-ESM2M simulation by either metric, the latitude of the maximum moves south by the BPF MSLP metric and north by the storm count metric. Again, this is likely associated with difficulty in correctly identifying the latitude of the peak of the track and suggests that the change in latitude is a less robust measure than the change in strength/density.

There are several possible reasons for the differences in response exhibited by the track density metric compared to the BPF MSLP metric. For example, the window of longitude considered is different. Also, the track density change could indicate a move from a few intense storms to a greater number of weak storms; this might not feature by the BPF MSLP metric. It is not obvious which metric (BPF MSLP or track density) is the most relevant to waves or surge, and the difficulty in drawing any clear parallels between the changes shown here and the results of the downscaled wave and surge simulations underscores the value of such downscaled simulations.

Both ensembles show a similar spread of track density changes, but the HadGEM3 PPE changes are all positive, whereas the CMIP5 ensemble exhibits both positive and negative changes. The HadGEM3 PPE changes are also less diverse in terms of the change in latitude. The storm tracks in the CMIP5 and HadGEM2PPE simulations are discussed in Murphy et al, 2018.

7. Acknowledgements

We would like to acknowledge the following colleagues for providing expertise and data contributions to the UKCP18 marine projections: Dr Meike Bagge[1], Dr Sarah Bradley[2], Dr Ben Harvey[3], Dr Kevin Hodges[3], Dr Jenny Hornsby[4], Prof. Kevin Horsburgh[5], Dr Volker Klemann[1], Dr Robert Lee[3], Dr Grigory Nikulin[6], Dr Jane Williams[5], Dr Simon Williams[5], Prof. Jon Tawn[7], Dr Aimée Slangen[8], Prof. Giorgio Spada[9], Dr Giuseppe Zappa[3].

1: Helmholtz Centre Potsdam, GFZ German Research Centre for Geosciences, Germany.

2: Delft University of Technology, Netherlands.

3: University of Reading, UK.

4: JBA Consulting, UK.

5: National Oceanography Centre, UK.

6: Rossby Centre, Swedish Meteorological and Hydrological Institute, Norrköping.

7: University of Lancaster, UK.

8: NIOZ Royal Netherlands Institute for Sea Research.

9: Dipartimento di Scienze Pure e Applicate (DiSPeA), Urbino University ''Carlo Bo'', Italy.

The estimates of the regional sea level change associated with glacial isostatic adjustment were developed as part of the Natural Environment Research Council consortium grant; BRITICE-CHRONO NE/J009768/1.

8. References

Aarnes, O. J., et al, (2017). Projected changes in significant wave height toward the end of the 21st century: Northeast Atlantic, Journal of Geophysical Research: Oceans, 122, 3394-3403.

Andrews, T., Gregory, J. M., M. J. Webb, M. J., and Taylor, K. E., (2012). Forcing, feedbacks and climate sensitivity in CMIP5 coupled atmosphere-ocean climate models, Geophysical Research Letters, 39, L09712, doi:10.1029/2012GL051607.

Arthern, R. J., and Williams, C. R., (2017). The sensitivity of West Antarctica to the submarine melting feedback, Geophysical Research Letters, 44, 2352–2359, doi:10.1002/2017GL072514.

Barnes, E.A., and Polvani, L., (2013). Response of the Midlatitude Jets, and of Their Variability, to Increased Greenhouse Gases in the CMIP5 Models, Journal of Climate, 26, 7117–7135, https://doi.org/10.1175/JCLI-D-12-00536.1

Batstone, C., Lawless, M., Tawn, J. A., Horsburgh, K., Blackman, D. L., McMillan, A, Worth, D., Laegar, S., and Hunt, T., (2013). A UK best-practice approach for extreme sea level analysis along complex topographic coastlines, Ocean Engineering, 71, 28-39. https://doi.org/10.1016/j.oceaneng.2013.02.003

Bell, R. E., Chu, W., Kingslake, J., Das, I., Tedesco, M., Tinto, K. J., Zappa, C. J., Frezzotti, M., Boghosian, A., and Lee, W.S., (2017). Antarctic ice shelf potentially stabilized by export of meltwater in surface river, Nature, 544, 344–348, doi:10.1038/nature22048.

Bernie, D., Lowe, J., and Smith, S., (2013). Technical Appendix: Updated projections of global emissions and temperatures. Report commissioned by the UK Committee on Climate Change in support of the fourth carbon budget review.

Bilbao, R. A. F., Gregory, J. M., and Bouttes, N., (2015). Analysis of the regional pattern of sea level change due to ocean dynamics and density change for 1993–2099 in observations and CMIP5 AOGCMs, Climate Dynamics, 45: 2647-2666. https://doi.org/10.1007/s00382-015-2499-z

Bindoff, N. L., Willebrand, J., Artale, V., Cazenave, A., Gregory, J., Gulev, S., Hanawa, K., Le Quéré, C., Levitus, S. Nojiri, Y., Shum, C. K., Talley, L. D., and Unnikrishnan, A., (2007). Observations: Oceanic Climate Change and Sea Level. In: Climate Change 2007: The Physical Science Basis. Contribution of Working Group 1 to the Fourth Assessment Report of the Intergovernmental Panel on Climate Change [Solomon, S., D. Qin, M. Manning, Z. Chen, M. Marquis, K.B. Averyt, M. Tignor and H.L. Miller (eds.)]. Cambridge University Press, Cambridge, United Kingdom and New York, NY, USA.

Blackmon, M.L., (1976). A Climatological Spectral Study of the 500 mb Geopotential Height of the Northern Hemisphere, Journal of the Atmospheric Sciences 33, 1607-1623. https://doi.org/10.1175/1520-0469(1976)033<1607:ACSSOT>2.0.CO;2

Bricheno, L.M., and Wolf, J., (submitted 2018). Future wave conditions of Europe, in response to high-end climate change scenarios, under review at Journal of Geophysical Research: Oceans.

Butler, A., Heffernan, J. E., Tawn, J. A., Flather, R. A., and Horsburgh, K. J., (2007). Extreme value analysis of decadal variations in storm surge elevations, Journal of Marine Systems, 67, 189-200. https://doi.org/10.1016/j.jmarsys.2006.10.006

Cannaby, H., Palmer, M. D., Howard, T., Bricheno, L., Calvert, D., Krijnen, J., Wood, R., Tinker, J., Bunney, C., Harle, J., Saulter, A., O'Neill, C., Bellingham, C., and Lowe, J., (2016). Projected sea level rise and changes in extreme storm surge and wave events during the 21st century in the region of Singapore, Ocean Science, 12, 613-632. https://doi.org/10.5194/os-12-613-2016

Church, J. A., and White, N. J., (2006). A 20th century acceleration in global sea level rise, Geophysical Research Letters, 33, L01602. https://doi.org/10.1029/2005GL024826

Church, J. A., White, N. J., Konikow, L. F., Domingues, C. M., Cogley, J. G., Rignot, E., Gregory, J. M., van den Broeke, M. R., Monaghan, A. J., and Velicogna, I., (2011). Revisiting the Earth's sea-level and energy budgets from 1961 to 2008, Geophysical Research Letters, 38, L18601. https://doi.org/10.1029/2011GL048794

Church, J. A., Clark, P. U., Cazenave, A., Gregory, J. M., Jevrejeva, S., Levermann, A., Merrifield, M. A., Milne, G. A., Nerem, R. S., Nunn, P. D., Payne, A. J., Pfeffer, W. T., Stammer, D., and Unnikrishnan, A. S., (2013). Sea Level Change. In: Climate Change 2013: The Physical Science Basis. Contribution of Working Group 1 to the Fifth Assessment Report of the Intergovernmental Panel on Climate Change [Stocker, T.F., D. Qin, G.-K. Plattner, M. Tignor, S.K. Allen, J. Boschung, A. Nauels, Y. Xia, V. Bex and P.M. Midgley (eds.)]. Cambridge University Press, Cambridge, United Kingdom and New York, NY, USA.

Clark, P. U., et al, (2016). Consequences of twenty-first-century policy for multi-millennial climate and sea level change, Nature Climate Change, 6, 360–369, doi:10.1038/nclimate2923.

Coles, S., (2001). An Introduction to Statistical Modeling of Extreme Values. Springer-Verlag, London, United Kingdom. https://doi.org/10.1007/978-1-4471-3675-0

Collins, M., Knutti, R., Arblaster, J., Dufresne, J.-L., Fichefet, T., Friedlingstein, P., Gao, X., Gutowski, W.J., Johns, T. , Krinner, G., Shongwe, M., Tebaldi, C., Weaver, A. J., and Wehner, M., (2013). Long-term Climate Change: Projections, Commitments and Irreversibility. In: Climate Change 2013: The Physical Science Basis. Contribution of Working Group 1 to the Fifth Assessment Report of the Intergovernmental Panel on Climate Change [Stocker, T.F., D. Qin, G.-K. Plattner, M. Tignor, S.K. Allen, J. Boschung, A. Nauels, Y. Xia, V. Bex and P.M. Midgley (eds.)]. Cambridge University Press, Cambridge, United Kingdom and New York, NY, USA.

Cornford, S. L. et al, (2016). Adaptive mesh refinement versus subgrid friction interpolation in simulations of Antarctic ice dynamics, Annals of Glaciology, 57, 1–9.

Dangendorf, S., Marcos, M., Wöppelmann, G., Conrad, C. P., Frederikse, T., and Riva, R., (2017). Reassessment of 20th century global mean sea level rise, Proceedings of the National Academy of Sciences, 114, 5946-5951. https://doi.org/10.1073/pnas.1616007114

Dee, D. P., Uppala, S. M., Simmons, A. J., Berrisford, P., Poli, P., Kobayashi, S., Andrae, U., Balmaseda, M. A., Balsamo, G., Bauer, P., Bechtold, P., Beljaars, A. C. M., van de Berg, L., Bidlot, J., Bormann, N., Delsol, C., Dragani, R., Fuentes, M., Geer, A. J., Haimberger, L., Healy, S. B., Hersbach, H., Hólm, E. V., Isaksen, L., Kållberg, P., Köhler, M., Matricardi, M., McNally, A. P., Monge-Sanz, B. M., Morcrette, J.-J., Park, B.-K., Peubey, C., de Rosnay, P., Tavolato, C., Thépaut, J.-N., and Vitart, F., (2011). The ERA-Interim reanalysis: configuration and performance of the data assimilation system, Quarterly Journal of the Royal Meteorological Society, 137, 553–597. https://doi.org/10.1002/qj.828

DeConto, R. M., and Pollard, D., (2016). Contribution of Antarctica to past and future sea level rise, Nature, 531, 591–597.

Dieng, H. B., Champollion, N., Cazenave, A., Wada, Y., Schrama, E., and Meyssignac, B., (2015). Total land water storage change over 2003–2013 estimated from a global mass budget approach, Environmental Research Letters, 10 124010, https://doi.org/10.1088/1748-9326/10/12/124010

de Vries, H., Breton, M., de Mulder, B., Krestenitis, Y., Ozer, J., Proctor, R., Ruddick, K., Salomon, J.-C., and Voorrips, A., (1995). A comparison of 2D storm-surge models applied to three shallow European seas, Environmental Software, 10, 23–42. https://doi.org/10.1016/0266-9838(95)00003-4

Edwards, T. L., Brandon, M., Durand, G., Edwards, N. R., Golledge, N. R., Holden, P. B., Nias, I., Payne, A. J., Ritz, C., and Wernecke, A., (in press). Revisiting Antarctic ice loss due to marine ice cliff instability, Nature.

Environment Agency. Coastal Flood Boundary Conditions for the UK (2018).

Favier, L. et al, (2014). Retreat of Pine Island Glacier controlled by marine ice-sheet instability, Nature Climate Change, 5, 117–121.

Feldmann, J., and Levermann, A., (2015). Collapse of the West Antarctic Ice Sheet after local destabilization of the Amundsen Basin, Proceedings of the National Academy of Sciences, 112, 14191–14196.

Flather, R. A., (1994). A storm surge prediction model for the northern Bay of Bengal with application to the cyclone disaster in April 1991, Journal of Physical Oceanography, 24, 172-190. https://doi.org/10.1175/1520-0485(1994)024<0172:ASSPMF>2.0.CO;2

Flather, R. A., (2000). Existing operational oceanography, Coastal Engineering, 41, 13–40.

Flather, R. A., and Heaps N.S., (1975). Tidal computations for Morecambe Bay, Geophysical Journal International, 42, 489–517.

Flather, R. A., and Williams, J., (2000), Climate Change Effects on Storm Surges: Methodologies and Results. In: Climate Scenarios for Water-Related and Coastal Impacts ECLAT-2 KNMI Workshop Report No. 3 KNMI, the Netherlands, 10-12 May 2000.

Forster, P. M., Andrews, T., Good, P., Gregory, J. M., Jackson, L. S., and Zelinka, M., (2013). Evaluating adjusted forcing and model spread for historical and future scenarios in the CMIP5 generation of climate models, Journal of Geophysical Research: Atmospheres, 118, 1139–1150. https://doi.org/10.1002/jgrd.50174

Furner, R., Williams, J., Horsburgh, K., and Saulter, A., (2016). NEMO-surge: Setting up an accurate tidal model. Forecasting Research Technical Report No. FRTR610 11 May 2016. Met Office, UK. https://www.metoffice.gov.uk/binaries/content/assets/mohippo/pdf/6/frtr_610_2016p.pdf

Geoffroy, O., Saint-Martin, D., Olivié, D. J., Voldoire, A., Bellon, G., and Tytéca, S., (2013a). Transient Climate Response in a Two-Layer Energy-Balance Model. Part I: Analytical Solution and Parameter Calibration Using CMIP5 AOGCM Experiments, Journal of Climate, 26, 1841-1857. https://doi.org/10.1175/JCLI-D-12-00195.1

Geoffroy, O., Saint-Martin, D., Bellon, G., Voldoire, A., Olivié, D. J., and Tytéca, S., (2013b). Transient Climate Response in a Two-Layer Energy-Balance Model. Part II: Representation of the Efficacy of Deep-Ocean Heat Uptake and Validation for CMIP5 AOGCMs, Journal of Climate, 26, 1859-1876. https://doi.org/10.1175/JCLI-D-12-00196.1

Golledge, N. R., et al, (2015). The multi-millennial Antarctic commitment to future sea level rise, Nature, 526, 421–425.

Goda, Y., (2000). Random Seas and Design of Maritime Structures. World Scientific Publishing. ISBN: 981023256X.

Good, S. A., Martin, M., and Rayner, N. A., (2013). EN4: Quality controlled ocean temperature and salinity profiles and monthly objective analyses with uncertainty estimates, Journal of Geophysical Research: Oceans, 118, 6704–6716. doi:10.1002/2013JC009067.

Gregory, J. M., Andrews, T., and Good, P., (2015). The inconstancy of the Transient Climate Response parameter under increasing CO_2, Philosophical Transactions of the Royal Society A, 373, 20140417. https://doi.org/10.1098/rsta.2014.0417.

Griffies, S. M., Yin, J., Durack, P. J., Goddard, P., Bates, S. C., Behrens, E., et al, (2014). An assessment of global and regional sea level for years 1993-2007 in a suite of interannual core-II simulations, Ocean Modelling, 78, 35-89. https://doi.org/10.1016/j.ocemod.2014.03.004

Grinsted, A., (2013). An estimate of global glacier volume, The Cryosphere, 7, 141-151. https://doi.org/10.5194/tc-7-141-2013

Haigh, I. D., Wadey, M. P., Gallop, S. L., Loehr, H., Nicholls, R. J., Horsburgh, K., Brown, J.M., Bradshaw, E., (2015). A user-friendly database of coastal flooding in the United Kingdom from 1915–2014, Scientific Data, 2, 150021. http://doi.org/10.1038/sdata.2015.21

Haigh, I. D., Wadey, M. P., Wahl, T., Ozsoy, O., Nicholls, R. J., Brown, J. M., Horsburgh, K., and Gouldby, B., (2016). Spatial and temporal analysis of extreme sea level and storm surge events around the coastline of the UK. Scientific Data, 3, 160107. https://doi.org/10.1038/sdata.2016.107

Hawkins, E., and Sutton, R., (2009). The Potential to Narrow Uncertainty in Regional Climate Predictions, Bulletin of the American Meteorological Society, 90, 1095–1108. https://doi.org/10.1175/2009BAMS2607.1

Hay, C. C., Morrow, E., Kopp, R. E., and Mitrovica, J. X., (2015). Probabilistic reanalysis of twentieth-century sea level rise, Nature, 517, 481–484. https://doi.org/10.1038/nature14093

Hellmer, H. H., Kauker, F., Timmermann, R., and Hattermann, T., (2017). The Fate of the Southern Weddell Sea Continental Shelf in a Warming Climate, Journal of Climate, 30, 4337-4350, doi: 10.1175/JCLI-D-16-0420.1.

Hemer, M. A., Wang, X. L., Weisse, R., and Swail, V. R., (2012) Advancing Wind-Waves Climate Science, Bulletin of the American Meteorological Society, 93, 791–796, https://doi.org/10.1175/BAMS-D-11-00184.1

Hemer, M. A., et al, (2013). Projected changes in wave climate from a multi-model ensemble, Nature Climate Change, 3, 471-476, doi:10.1038/nclimate1791.

Hemer, M. A., and Trenham, C. E., (2016). Evaluation of a CMIP5 derived dynamical global wind wave climate model ensemble, Ocean Modelling, 103, 190-203.

Horsburgh, K. J., Williams, J. A., Flowerdew, J., Mylne, K. and Wortley, S. (2008). The worst North Sea storm surge for 50 years: performance of the forecasting system and implications for decision makers. In: Proceedings of the 43rd Defra Flood and Coastal Management Conference 2008, Defra Flood Management Division, London.

Horsburgh, K. J., and Wilson, C., (2007). Tide-surge interaction and its role in the distribution of surge residuals in the North Sea. Journal of Geophysical Research: Oceans, 112, C08003, https://doi.org/10.1029/ 2006JC004033

Howard, T., Lowe, J. A., and Horsburgh, K. J., (2010). Interpreting century-scale changes in southern North Sea storm surge climate derived from coupled model simulations, Journal of Climate, 23, 6234-6247. https://doi.org/10.1175/2010JCLI3520.1

Howard, T., Lowe, J. A., Pardaens, A., Ridley, J., and Horsburgh, K. J., (2008). Met Office Hadley Centre Projections of 21st century Extreme Sea Levels for TE2100, Environment Agency. 54 pp.

Howard, T., Pardaens, A. K., Bamber, J. L., Ridley, J., Spada, G., Hurkmans, R. T. W. L., Lowe, J. A., and Vaughan, D., (2014). Sources of 21st century regional sea level rise along the coast of northwest Europe, Ocean Science, 10, 473-483. https://doi.org/10.5194/os-10-473-2014

Hunter, J., (2012). A simple technique for estimating an allowance for uncertain sea level rise, Climatic Change, 113, 239–252. https://doi.org/10.1007/s10584-011-0332-1

Idier, D., Paris, F., Le Cozannet,G., Boulahya, F., and Dumas, F., (2017). Sea level rise impacts on the tides of the European Shelf, Continental Shelf Research, 137, 56-71. https://doi.org/10.1016/j.csr.2017.01.007

IPCC Working Group 3 (2000). Emissions Scenarios: Summary for Policymakers. 1st ed. Geneva: IPCC, 21pp. Available at: https://www.ipcc.ch/pdf/special-reports/spm/sres-en.pdf

IPCC, (2013). Climate Change 2013: The Physical Science Basis. Contribution of Working Group 1 to the Fifth Assessment Report of the Intergovernmental Panel on Climate Change [Stocker, T.F., D. Qin, G.-K. Plattner, M. Tignor, S.K. Allen, J. Boschung, A. Nauels, Y. Xia, V. Bex and P.M. Midgley (eds.)]. Cambridge University Press, Cambridge, United Kingdom and New York, NY, USA, 1535 pp.

Jacob, D., Petersen, J., Eggert, B., Alias, A., Christensen, O. B., Bouwer, L. M., et al, (2014). EURO-CORDEX: new high-resolution climate change projections for European impact research, Regional Environmental Change, 14, 563-578. https://doi.org/10.1007/s10113-013-0499-2

Jevrejeva, S., Moore, J. C., Grinsted, A., Matthews, A. P., and Spada, G., (2014). Trends and acceleration in global and regional sea levels since 1807, Global Planetary Change, 113, 11–22. https://doi.org/10.1016/j.gloplacha.2013.12.004

Jones, C., Giorgi, F., and Asrar, G., (2011). The Coordinated Regional Downscaling Experiment: CORDEX, An international downscaling link to CMIP5, CLIVAR Exchanges, 56, 34-40. http://www.clivar.org/node/236

Joughin, I. et al, (2014). Marine Ice Sheet Collapse Potentially Under Way for the Thwaites Glacier Basin, West Antarctica, Science, 344, 735–738.

Kingslake, J., Jeremy C. Ely, J. C., Das, I., and Bell, R. E., (2017). Widespread movement of meltwater onto and across Antarctic ice shelves, Nature, 544, 349–352, doi:10.1038/nature22049.

Knutti, R., and Hegerl, G., (2008). The equilibrium sensitivity of Earth's temperature to radiation changes, Nature GeoSciences, 1, 735-743.

Kopp, R. E., Horton, R. M., Little, C. M., Mitrovica, J. X., Oppenheimer, M., Rasmussen, D. J., Strauss, B. H., and Tebaldi, C., (2014). Probabilistic 21st and 22nd century sea-level projections at a global network of tide-gauge sites, Earth's Future, 2, 383-406. https://doi.org/10.1002/2014EF000239

Kruskal, W. H., and Wallis, W. A., (1952). Use of ranks in one-criterion variance analysis, Journal of the American statistical Association, 47, 583-621.

Kuhlbrodt, T., and Gregory, J. M., (2012). Ocean heat uptake and its consequences for the magnitude of sea level rise and climate change, Geophysical Research Letters, 39, L18608, doi:10.1029/2012GL052952.

Kuipers Munneke, P. et al, (2014). Firn air depletion as a precursor of Antarctic ice-shelf collapse, Journal of Glaciology, 60, 205–214.

Kusahara, K., and Hasumi, H., (2013). Modeling Antarctic ice shelf responses to future climate changes and impacts on the ocean, Journal of Geophysical Research: Oceans, 118, 2454–2475, doi:10.1002/jgrc.20166.

Landerer, F. W., Gleckler, P. J., and Lee, T., (2014). Evaluation of CMIP5 dynamic sea surface height multi-model simulations against satellite observations. Climate Dynamics, 43, 1271-1283. https://doi.org/10.1007/s00382-013-1939-x

Legeais, J.-F., Ablain, M., Zawadzki, L., Zuo, H., Johannessen, J. A., Scharffenberg, M. G., Fenoglio-Marc, L., Fernandes, M. J., Andersen, O. B., Rudenko, S., Cipollini, P., Quartly, G. D., Passaro, M., Cazenave, A. and Benveniste, J., (in review 2017). An Accurate and Homogeneous Altimeter Sea Level Record from the ESA Climate Change Initiative, Earth Systems Science Data Discussion, https://doi.org/10.5194/essd-2017-116

Levermann, A. et al, (2013). The multimillennial sea level commitment of global warming, Proceedings of the National Academy of Sciences, 110 (34), 13745–13750.

Levermann, A., Winkelmann, R., Nowicki, S., Fastook, J. L., Frieler, K., Greve, R., Hellmer, H. H., Martin, M. A., Meinshausen, M., Mengel, M., Payne, A. J., Pollard, D., Sato, T., Timmermann, R., Wang, W. L., and Bindschadler, R. A., (2014). Projecting Antarctic ice discharge using response functions from SeaRISE ice-sheet models, Earth System Dynamics, 5, 271-293. https://doi.org/10.5194/esd-5-271-2014

Lorbacher, K., Nauels, A., and Meinhausen, M., (2015). Complementing thermosteric sea level rise estimates, Geoscientific Model Development, 8, 2723–2734, https://doi.org/10.5194/gmd-8-2723-20

Lowe, J. A., and Gregory, J. M., (2005). The effects of climate change on storm surges around the United Kingdom, philosophical Transactions of the Royal Society A, 363, 1313-1328 10.1098/rsta.2005.1570.

Lowe, J. A., Howard, T. P., Pardaens, A., Tinker, J., Holt, J., Wakelin, S., Milne, G., Leake, J., Wolf, J., Horsburgh, K., Reeder, T., Jenkins, G., Ridley, J., Dye, S., and Bradley, S., (2009). UK Climate Projections science report: Marine and coastal projections. Met Office Hadley Centre, Exeter, UK.

Meehl, G. A., Covey, C., Delworth, T., Latif, M., McAvaney, B., Mitchell, J.F., Stouffer, R.J., and Taylor, K.E., (2007). The WCRP CMIP3 multimodel dataset: A new era in climate change research, Bulletin of the American Meteorological Society, 88, 1383–1394. https://doi.org/10.1175/BAMS-88-9-1383

Melet, A., Meyssignac, B., Almar, R., and Le Cozannet, G., (2018). Under-estimated wave contribution to coastal sea level rise, Nature Climate Change, 8, 234-239. doi:10.1038/s41558-018-0088-y.

Meinshausen, M., Smith, S. J., Calvin, K. V., Daniel, J. S., Kainuma, M. L. T., Lamarque, J.-F., Matsumoto, K., Montzka, S. A., Raper, S. C. B., Riahi, K., Thomson, A. M., Velders. G. J. M., and van Vuuren, D., (2011). The RCP Greenhouse Gas Concentrations and their Extension from 1765 to 2300, Climatic Change, https://doi.org/10.1007/s10584-011-0156-z

Menéndez, M., and Woodworth, P. L., (2010). Changes in extreme high water levels based on a quasi-global tide-gauge data set, Journal of Geophysical Research, 115, C10011. https://doi.org/10.1029/2009JC005997

Meyssignac, B., Slangen, A. B., Melet, A., Church, J. A., Fettweis, X., Marzeion, B., Agosta, C., Ligtenberg, S. R., Spada, G., Richter, K., Palmer, M. D., Roberts, C. D., and Champollion, N., (2017). Evaluating Model Simulations of Twentieth-Century Sea level Rise. Part II: Regional Sea level Changes, Journal of Climate, 30, 8565–8593. https://doi.org/10.1175/JCLI-D-17-0112.1

Murphy, J.M, Harris, G.R., Sexton, D.M.H, Kendon, E.J, Bett, P.E, Clark, R.T, Eagle, K.E., Fosser, G., Fung, F., Lowe, J.A., McDonald, R.E., McInnes, R.N., McSweeney, C.F, Mitchell, J.F.B., Rostron, J.W., Thornton, H.E., Tucker, S. and Yamazaki, K., (2018). UKCP18 Land Projections: Science Report.

Nauels, A., Meinshausen, M., Mengel, M., Lorbacher, K., and Wigley, T. M. L., (2017). Synthesizing long-term sea level rise projections – the MAGICC sea level model v2.0, Geoscientific Model Development, 10, 2495-2524, https://doi.org/10.5194/gmd-10-2495-2017, 2017

Nicholls, R. J., and Lowe, J. A., (2004). Benefits of mitigation of climate change for coastal areas, Global Environmental Change, 14, 229-244.

O'Dea, E., Furner, R., Wakelin, S., Siddorn, J., While, J., Sykes, P., King, R., Holt, J., and Hewitt, H., (2017). The CO5 configuration of the 7 km Atlantic Margin Model: large-scale biases and sensitivity to forcing, physics options and vertical resolution, Geoscientific Model Development, 10, 2947–2969. https://doi.org/10.5194/gmd-10-2947-2017

Palmer, M., Lowe, J., Bernie, D., Calvert, D., Gohar, L., and Gregory, J., (2015). Long Term Projections of Sea Level, Temperature and Rainfall Change, in Singapore's Second National Climate Change Study – Phase 1. http://ccrs.weather.gov.sg/publications-second-National-Climate-Change-Study-Science-Reports

Palmer, M., Howard, T., Tinker, J., and Lowe, J., (2016). Marine Projections, Met Office Hadley Centre Technical Note 100, 12pp.

Palmer, M. D., Harris, G. R., and Gregory, J.M., (2018). Extending CMIP5 projections of global mean temperature and sea level rise due to thermal expansion using a physically-based emulator, Environmental Research Letters, 13, 84003. https://doi.org/10.1088/1748-9326/aad2e4

Pardaens, A. K., Gregory, J. M., and Lowe, J. A., (2011). A model study of factors influencing projected changes in regional sea level over the twenty-first century, Climate Dynamics, 36, 2015–2033. https://doi.org/10.1007/s00382-009-0738-x

Pattyn, F., (2017). Sea level response to melting of Antarctic ice shelves on multi-centennial timescales with the fast Elementary Thermomechanical Ice Sheet model (f.ETISh v1.0), The Cryosphere, 11, 1851–1878.

Pelling, H.E., Mattias Green, J.A., and Ward, S.L., (2013). Modelling tides and sea level rise: To flood or not to flood. Ocean Modelling, 63, 21-29.

Pelling, H.E., and Green, J.A.M., (2014). Impact of flood defences and sea level rise on the European Shelf tidal regime. Continental Shelf Research, 85, 96–105.

Perrette, M., Landerer, F., Riva, R., Frieler, K., and Meinshausen, M., (2013), A scaling approach to project regional sea level rise and its uncertainties. Earth System Dynamics, 4, 11-29, https://doi.org/10.5194/esd-4-11-2013

Pickering, M., 2014. The Impact of Future Sea level Rise on the Tides. University of Southampton, UK, Ocean and Earth Science, 347. https://eprints.soton.ac.uk/367040/

Pickering, M.D., N.C.Wells, K.J.Horsburgh, J.A.M.Green. The impact of future sea level rise on the European Shelf tides, Continental Shelf Research Volume 35, 1 March 2012, Pages 1-15. https://doi.org/10.1016/j.csr.2011.11.011

Pickering, M. D., Horsburgh, K. J., Blundell, J. R., Hirschi, J. J.-M., Nicholls, R. J., Verlaane, M., and Wells, N. C., (2017). The impact of future sea level rise on the global tides. Continental Shelf Research. Volume 142, Pages 50-68. https://doi.org/10.1016/j.csr.2017.02.004

Pollard, D. et al, (2015). Potential Antarctic Ice Sheet retreat driven by hydrofracturing and ice cliff failure, Earth and Planetary Science Letters, 412, 112–121.

Previdi, M., and Polvani, L. M., (2014). Climate system response to stratospheric ozone depletion and recovery. Quarterly Journal of The Royal Meteorological Society. 140 (685), 2401–2419.

Ray, R. D., and Douglas, B. C., (2011). Experiments in reconstructing twentieth-century sea levels., Progress in Oceanography, 91, 496–515. https://doi.org/10.1016/j.pocean.2011.07.021

Rignot, E., Mouginot, J., Morlighem, M., Seroussi, H., and Scheuchl, B., (2014). Widespread, rapid grounding line retreat of Pine Island, Thwaites, Smith, and Kohler glaciers, West Antarctica, from 1992 to 2011, Geophysical Research Letters, 41, 3502–3509, doi:10.1002/2014GL060140.

Rio, M.-H., Mulet, S. and Picot, N., (2014). Beyond GOCE for the ocean circulation estimate: Synergetic use of altimetry, gravimetry, and in situ data provides new insight into geostrophic and Ekman currents, Geophysical Research Letters 41, 8918-8925. doi:10.1002/2014GL061773.

Ritz, C. et al, (2015). Potential sea level rise from Antarctic ice-sheet instability constrained by observations, Nature, 528, 115–118.

Ruckert, K. L., Shaffer, G., Pollard, D., Guan, Y., Wong, T. E., Forest, C. E., and Keller, K., (2017). Assessing the Impact of Retreat Mechanisms in a Simple Antarctic Ice Sheet Model Using Bayesian Calibration, PLoS ONE, 12(1): e0170052. doi:10.1371/journal.pone.0170052.

Roberts, C.D., Calvert, D., Dunstone, N., Hermanson, L,. Palmer, M. D., and Smith, D., (2016). On the Drivers and Predictability of Seasonal-to-Interannual Variations in Regional Sea Level, Journal of Climate, 29, 7565–7585, https://doi.org/10.1175/JCLI-D-15-0886.1

Roberts-Jones, J., Fieldler, E. and Martin, M. J., (2012). Daily, Global, High-Resolution SST and Sea Ice Reanalysis for 1985–2007 Using the OSTIA System, Journal of Climate, 25, 6215–6232. doi: http://dx.doi.org/10.1175/JCLI-D-11-00648.1

Scaife, A. A., Arribas, A., Blockley, E., Brookshaw, A., Clark, R. T., Dunstone, N., Eade, R., Fereday, D., Folland, C. K., Gordon, M., Hermanson, L., Knight, J. R., Lea, D. J., MacLachlan, C., Maidens, A., Martin, M., Peterson, A. K., Smith, D., Vellinga, M., Wallace, E., Waters, J., and Williams, A., (2014). Skillful long-range prediction of European and North American winters, Geophysical Research Letters, 41, 2514–2519. https://doi.org/10.1002/2014GL059637

Shaw, T. A., Baldwin, M., Barnes, E. A., Caballero, R., Garfinkel, C. I., Hwang, Y.-T., Li, C., O'Gorman, P. A., Rivière, G., Simpson, I. R., and Voigt, A., (2016). Storm track processes and the opposing influences of climate change, Nature Geoscience, 9, 656–664. https://doi.org/10.1038/ngeo2783

Shennan, I., Milne, G., and Bradley, S., (2012). Late Holocene vertical land motion and relative sea level changes: lessons from the British Isles, Journal of Quaternary Science, 27, 64-70. https://doi.org/10.1002/jqs.1532

Shepherd, A., and the IMBIE Team, (2018). Mass balance of the Antarctic Ice Sheet from 1992 to 2017, Nature, 558, 219–222. https://doi.org/10.1038/s41586-018-0179-y

Shepherd, T. G., (2014). Atmospheric circulation as a source of uncertainty in climate change projections, Nature Geoscience, 7, 703–708. https://doi.org/10.1038/ngeo2253

Slangen, A. B. A., Carson, M., Katsman, C. A., Van de Wal, R. S. W., Köhl, A., Vermeersen, L. L. A., and Stammer, D., (2014). Projecting twenty-first century regional sea level changes, Climatic Change, 124, 317-332. https://doi.org/10.1007/s10584-014-1080-9

Slangen, A. B., Meyssignac, B., Agosta, C., Champollion, N., Church, J. A., Fettweis, X., Ligtenberg, S. R., Marzeion, B., Melet, A., Palmer, M. D., Richter, K., Roberts, C. D., and Spada, G., (2017). Evaluating model simulations of twentieth-century sea level rise. Part I: Global mean sea level change, Journal of Climate, 30, 8539–8563. https://doi.org/10.1175/JCLI-D-17-0110.1

Solomon, S., Qin, D., Manning, M., Alley, R. B., Berntsen, T., Bindoff, N. L., Chen, Z., Chidthaisong, A., Gregory, J. M., Hegerl, G. C., Heimann, M., Hewitson, B., Hoskins, B. J., Joos, F., Jouzel, J., Kattsov, V., Lohmann, U., Matsuno, T., Molina, M., Nicholls, N., Overpeck, J., Raga, G., Ramaswamy, V., Ren, J., Rusticucci, M., Somerville, R., Stocker, T. F., Whetton, P., Wood, R. A., and Wratt, D., (2007). Technical Summary. In: Climate Change 2007: The Physical Science Basis. Contribution of Working Group 1 to the Fourth Assessment Report of the Intergovernmental Panel on Climate Change [Solomon, S., D. Qin, M. Manning, Z. Chen, M. Marquis, K.B. Averyt, M. Tignor and H.L. Miller (eds.)]. Cambridge University Press, Cambridge, United Kingdom and New York, NY, USA.

Spada, G., and Stocchi, P., (2007). SELEN: A Fortran 90 program for solving the "sea level equation", Computers and Geosciences, 33, 538-562. https://doi.org/10.1016/j.cageo.2006.08.006

Seroussi, H., et al, (2014). Sensitivity of the dynamics of Pine Island Glacier, West Antarctica, to climate forcing for the next 50 years, The Cryosphere, 8, 1699–1710.

Sterl, A., Van den Brink, H., de Vries, H., Haarsma, R., and van Meijgaard, E., (2009). An ensemble study of extreme storm surge related water levels in the North Sea in a changing climate, Ocean Science, 5, 369–378. https://doi.org/10.5194/os-5-369-2009

Stocker, T. F., Qin, D., Plattner, G.-K., Alexander, L. V., Allen, S. K., Bindoff, N. L., Bréon, F.-M., Church, J.A., Cubasch, U., Emori, S., Forster, P., Friedlingstein, P., Gillett, N., Gregory, J. M., Hartmann, D. L., Jansen, E., Kirtman, B., Knutti, R., Krishna Kumar, K., Lemke, P., Marotzke, J., Masson-Delmotte, V., Meehl, G. A., Mokhov, I. I., Piao, S., Ramaswamy, V., Randall, D., Rhein, M., Rojas, M., Sabine, C., Shindell, D., Talley, L. D., Vaughan, D. G., and Xie, S.-P., (2013). Technical Summary. In: Climate Change 2013: The Physical Science Basis. Contribution of Working Group 1 to the Fifth Assessment Report of the Intergovernmental Panel on Climate Change [Stocker, T.F., D. Qin, G.-K. Plattner, M. Tignor, S.K. Allen, J. Boschung, A. Nauels, Y. Xia, V. Bex and P.M. Midgley (eds.)]. Cambridge University Press, Cambridge, United Kingdom and New York, NY USA.

Strandberg, G., Bärring, L., Hansson, U., Jansson, C., Jones, C., Kjellström, E., Kolax, M., Kupiainen, M., Nikulin, G., Samuelsson, P., Ullerstig, A., and Wang, S., (2014). CORDEX scenarios for Europe from the Rossby Centre regional climate model RCA4. SMHI Internal Report Meteorology and Climatology, 116. Available: https://www.smhi.se/polopoly_fs/1.90273!/Menu/general/extGroup/attachmentColHold/mainCol1/file/RMK_116.pdf

Tamisiea, M. E., and Mitrovica, J. X., (2011). The moving boundaries of sea level change: Understanding the origins of geographic variability. Oceanography, 24, 24–39. https://doi.org/10.5670/oceanog.2011.25

Taylor, K. E., Stouffer, R. J., and Meehl, G. A., (2012). An Overview of CMIP5 and the experiment design, Bulletin of the American Meteorological Society, 93, 485-498. https://doi.org/10.1175/BAMS-D-11-00094.1

Timmermann, R., and Hellmer, H. H., (2013). Southern Ocean warming and increased ice shelf basal melting in the twenty-first and twenty-second centuries based on coupled ice-ocean finite-element modelling, Ocean Dynamics, 63, 1011–1026, doi:10.1007/s10236-013-0642-0.

Tinker, J., Lowe, J., Holt, J., Pardaens, A., and Wiltshire, A., (2015). Validation of an ensemble modelling system for climate projections for the northwest European shelf seas, Progress in Oceanography, 138, 211-237. https://doi.org/10.1016/j.pocean.2015.07.002

Tinker, J., Lowe, J., Pardaens, A., Holt, J., and Barciela, R., (2016). Uncertainty in climate projections for the 21st century northwest European shelf seas, Progress in Oceanography, 148, 56-73. https://doi.org/10.1016/j.pocean.2016.09.003

Tinker, J., Palmer, M. D., Howard, T. P., Lowe, J., and Copsey, D., (in preparation). Quantifying Coastal Sea Level Variability around the UK.

Tolman, H. L., (2009). User manual and system documentation of WAVEWATCH III TM version 3.14. Technical note, MMAB Contribution 276, 220pp.

Trusel, L. D., et al, (2015). Divergent trajectories of Antarctic surface melt under two twenty-first-century climate scenarios, Nature, 8, 927-932, doi:10.1038/ngeo2563.

Von Schuckmann, K., Palmer, M. D., Trenberth, K. E., Cazenave, A., Chambers, D., Hansen, J., Josey, S., Kosaka, Y., Loeb, N., Mathieu, P.-P., Meyssignac, B., and Wild, M., (2016). An imperative to monitor Earth's energy imbalance, Nature Climate Change, 6, 138-144. doi:10.1038/nclimate2876.

Wada, Y., vanBeek, L. P. H., Sperna Weiland, F. C., Chao, B. F., Wu, Y.-H., and Bierkens, M. F. P., (2012). Past and future contribution of global groundwater depletion to sea level rise, Geophysical Research Letters, 39, L09402. https://doi.org/10.1029/2012GL051230

Wade, S., Sanderson, M., Golding, N., Lowe, J., Betts, R., Reynard, N., Kay, A., Stewart, L., Prudhomme, C., Shaffrey, L., Lloyd-Hughes, B., and Harvey, B., (2015). Developing H++ climate change scenarios for heat waves, droughts, floods, windstorms and cold snaps. https://www.theccc.org.uk/wp-content/uploads/2015/10/Met-Office-for-the-ASC-Developing-H-climate-change-scenarios-for-heatwaves-droughts-floods-windstorms-and-cold-snaps3.pdf

Wakelin, S. L., Artioli, Y., Butenschön, M., Allen, J. I., and Holt, J. T., (2015). Modelling the combined impacts of climate change and direct anthropogenic drivers on the ecosystem of the northwest European continental shelf, Journal of Marine Systems, 152, 51-63.

Waugh, D. W., et al, (2013). Recent Changes in the Ventilation of the Southern Oceans, Science, 339, 568–570.

Wigley, T. M. L., (2008), MAGICC/SCENGEN 5.3: User Manual (version 2) http://www.cgd.ucar.edu/cas/wigley/magicc/UserMan5.3.v2.pdf

Williams, J., Horsburgh, K., Williams, J., and Proctor, R., (2016). Tide and skew surge independence: new insights for flood risk, Geophysical Research Letters, 43, 6410-6417. https://doi.org/10.1002/2016GL069522

Williams, K. D., Copsey, D., Blockley, E., Bodas-Salcedo, A., Calvert, D., Comer, R. E., Davis, P., Graham, T., Hewitt, H. T., Hill, R., Hyder, P., Ineson, S., Johns, T. C., Keen, A. B., Lee, R. W., Megann, A., Milton, S. F., Rae, J. G. L., Roberts, M. J., Scaife, A., Schiemann, R., Storkey, D., Thorpe, L., Watterson, I. G., Walters, D. N., West, A., Wood, R. A., Woollings, T., and Xavier, P. K., (2018). The Met Office Global Coupled model 3.0 and 3.1 (GC3.0 and GC3.1) configurations, Journal of Advances in Modeling Earth Systems, 10, 357-380. https://doi.org/10.1002/2017MS001115

Winkelmann, R., et al, (2015). Combustion of available fossil fuel resources sufficient to eliminate the Antarctic Ice Sheet, Science Advances, 1 (8), e1500589–e1500589.

Wolf, J., Lowe, J., and Howard, T., (2015). Climate downscaling: local mean sea level, surge and wave modelling. In: Nicholls, R.J., Dawson, R.J., Day, S.A., (eds.) Broad scale coastal simulation: new techniques to understand and manage shorelines in the third millennium. Dordrecht, Springer, 79-102, 398pp. (Advances in Global Change Research, 49).

Zappa, G., Hoskins, B. J., and Shepherd, T. G., (2015). Improving climate change detection through optimal seasonal averaging: The case of the North Atlantic jet and European precipitation, Journal of Climate 28, 6381-6397.

Zappa, G., et al, (2013). A multimodel assessment of future projections of North Atlantic and European extratropical cyclones in the CMIP5 climate models, Journal of Climate 26, 5846-5862.

A1. Methods

A1.1 21st century regional time-mean sea level projections

Section summary: In this section we present the materials and methods used to produce the regional time-mean sea level projections for UKCP18. The starting point is the projections of global mean sea level (GMSL) presented in the IPCC Fifth Assessment Report (AR5). These global changes are regionalised for the UK by considering the spatial patterns associated with each of the components of global sea level and also assessing the contribution to local sea level change associated with ongoing glacial isostatic adjustment (GIA, sometimes referred to as "post-glacial rebound). Our method goes beyond the global and regional projections presented in AR5 by: (i) using a more recent scenario-dependent estimate of the contribution from Antarctic ice dynamics; (ii) using a regression-based approach to projections of oceanographic regional sea level change; (iii) including multiple estimates of the regional "mass fingerprints" and GIA changes; (iv) incorporating an improved statistical treatment of the regional sea level uncertainties that is directly traceable to the AR5 GMSL projections.

A1.1.1 Global mean sea level (GMSL) projections

The regional time-mean sea level projections presented in UKCP18 are rooted in the process-based global mean sea level (GMSL) projections described in the IPCC Fifth Assessment Report of Working Group 1 (AR5; Church et al, 2013). The only difference in the GMSL projections used in UKCP18 is that we update the estimate of the sea level contribution from Antarctic ice dynamics following the work of Levermann et al, (2014). In this section we present a brief synopsis of the AR5 methods and provide a comparison with the UKCP18 GMSL projections for the 21st century. We refer the reader to Church et al, (2013) and the associated supplementary materials (available at http://www.climatechange2013.org/report/full-report/) for a more complete discussion.

The GMSL projections presented in AR5 (Church et al, 2013) include estimates of the contribution from: (i) ocean thermal expansion; (ii) mass changes in the Greenland Ice Sheet; (iii) mass changes in the Antarctic Ice Sheet; (iv) mass changes in other ice caps and glaciers; (v) changes in sea level related to projections of groundwater extraction and reservoir impoundment. The ice sheet terms are further broken down into a contribution from surface mass balance and a contribution from ice dynamics, resulting in a total of seven individual components of GMSL change. There were three major advances in the sea level science reported in AR5 compared to the previous IPCC Fourth Assessment Report (AR4, Bindoff et al, 2007). The first was the demonstration of closure of the GMSL budget, i.e. the summation of observation-based estimates of terms (i) - (v) was consistent with an independent estimate of GMSL change based on a tide-gauge reconstruction for the period 1971-2008 (Church et al, 2011). The second was the demonstration of better agreement between process-based model estimates of GMSL change and observations. The third was the inclusion of scenario-independent estimates of the contribution from ice dynamics (i.e. changes in the flow of ice into the ocean) for both Greenland and Antarctica, which led to systematically larger GMSL projections than were reported in IPCC AR4, as discussed by Palmer et al, (2016).

The AR5 processed-based GMSL projections are based upon the output of 21 CMIP5 (Taylor et al, 2012) global climate models under the Representative Concentration Pathway climate change scenarios (RCPs; Meinshausen et al, 2011).

The mean and standard deviation of the time series of global thermal expansion and global surface temperature change (relative to a 1986-2005 baseline) were used to generate a Monte Carlo[4] distribution of sea level projections, assuming a normal distribution. Global thermal expansion was used directly from the model ensemble, and global surface temperature change was used to estimate the response of glaciers and ice sheet surface mass balance terms via established parameterisation schemes (see Church et al, 2013 for further details). A member of the Monte Carlo analysis with a relatively large thermal expansion would also have a relatively large global surface temperature change, with corresponding changes for the glacier and ice sheet mass balance terms. A range of literature and observation-based scenarios were used as the basis of distributions for ice sheet dynamics and projections of changes in groundwater, with no dependency on the climate change scenario for these terms. The 5th to 95th percentile range of the simulated total sea level change estimated using this method was presented as the “likely range”, using the expert judgement and calibrated likelihood language of IPCC AR5 (see section 3.1 for further discussion).

UKCP18 deviates from the IPCC approach to GMSL by using an updated approach to assess the Antarctic ice dynamic contribution to future sea level rise. Levermann et al, (2014) have published scenario-dependent estimates of Antarctic dynamic ice discharge, based on five different ice sheet models. For UKCP18, we update the methods presented in AR5 by including a parameterisation of Levermann et al, (2014) results (Figure A1.1.1). This is achieved using a log-normal fit (i.e. of the form Ae^N, where A is a constant and N is a normal distribution with a mean of zero) to the percentiles they give from probability distribution functions for the sea level contribution at 2100 (see their table 6, "shelf models” with time delay). All percentiles are reproduced to within +/- 0.01m by our fits, except that the 95th-percentile for RCP2.6 is 0.26m in the fit (given as 0.23m in their table). The precision of the AR5 projections themselves is no greater than 0.01m (see Church et al, 2013, SM1.2), so we judge this to be adequate, and the additional error for RCP2.6 to be tolerable. We use the 5th to 95th percentile range of Levermann et al, (2014) and choose values at 2100 from our scenario-dependent log-normal probability distribution functions instead of the scenario-independent uniform 5th-95th distribution used in the AR5. The time-dependence is then obtained as in the AR5 (see Church et al, 2013, SM1.6).

An outcome of the parameterisation of the Levermann et al, (2014) results is that the UKCP18 sea level projections do not represent any correlation between global surface temperature change and dynamic ice sheet discharge from Antarctica. However, as discussed by Levermann et al, (2014), the uncertainty in their projections was dominated by differences in the spatial pattern of warming across CMIP5 models (in particular how much warming was manifested in the Antarctic region), rather than differences across the RCP scenarios. A positive correlation between global surface temperature change and Antarctic dynamic ice discharge will tend to reduce the net contribution from Antarctica, through larger snow accumulation associated with a warmer atmosphere. In that sense, the lack of correlation in the UKCP18 projections will tend to promote more precautionary (i.e. slightly larger) projections of the net contribution from Antarctica.

The impact of implementing this representation of Levermann et al, (2014) in the UKCP18 GMSL projections is relatively modest. The largest impact is in raising the values of the 95th percentile of total sea level rise for all three scenarios presented in UKCP18, with the greatest increase for RCP8.5 of about 15cm at 2100 (see Table 3.1.1).

[4] A Monte Carlo method essentially makes random draws from an underlying distribution many times in order to build up a picture of the combined uncertainties.

One of the main limitations discussed by Levermann et al, (2014) is the assumption of linearity of ice sheet response, since the coarse resolution models used are not capable of representing the self-accelerating grounding line retreat associated with marine ice sheet instability (MISI, see section 3.1.2). This assumption of linearity becomes problematic under scenarios where MISI plays a substantive role in the rate of mass input from Antarctica. In general, MISI is expected to play a larger role for the higher emissions scenarios and on multi-century time horizons (see section 3.1.2). Golledge et al, (2015) have conducted higher resolution ice sheet model simulations under RCP scenarios that explicitly account for MISI and these simulations exhibit an acceleration of the ice mass input from Antarctica in all scenarios (Figure A1.1.2). However, the computational expense associated with the higher resolution means that only two model simulations are available for each scenario (Figure A1.1.2), which presents challenges for estimating the uncertainty associated with these projections. Levermann et al, (2014) was chosen as the basis of the UKCP18 projections in preference to Golledge et al, (2015) owing to: (i) the more comprehensive treatment of uncertainty arising from choice of ice sheet model and the spatial pattern of future warming; (ii) the suitability for the UKCP18 Monte Carlo methods used to combine uncertainties.

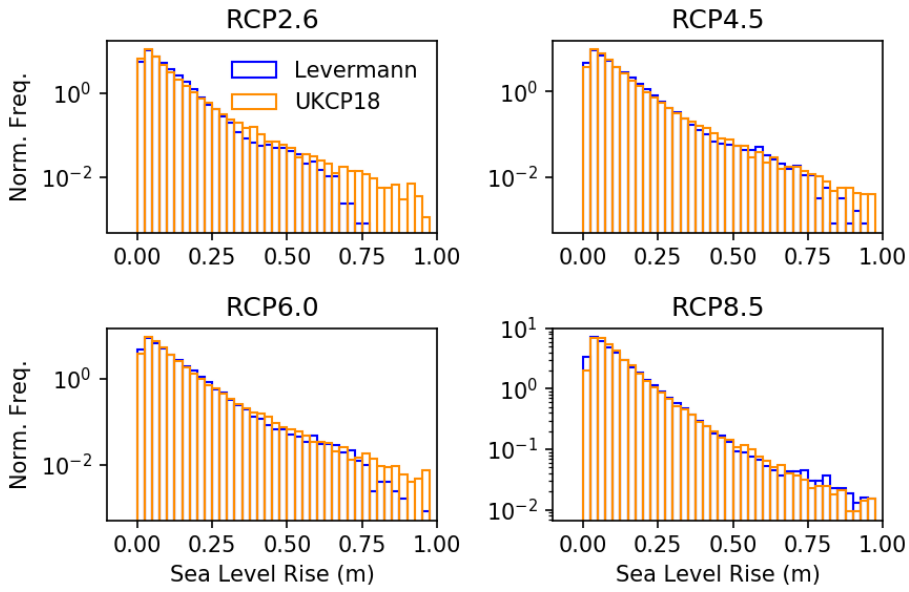

Figure A1.1.1. Comparison of the normalised frequency distribution of sea level rise from Antarctic ice dynamics at 2100, from: Levermann et al, (2014; blue); UKCP18 log-normal fit (orange). Note the log-scale on the Y-axis.

The UKCP18 projections of sea level rise from Antarctic ice mass loss show a lower scenario dependency than Golledge et al, (2015) and DeConto and Pollard (2016) (Figure A1.1.2). Projected ice mass input from Antarctica arises from both changes in surface mass balance (the difference between snowfall accumulation and surface melting) and changes in the dynamic ice discharge. The lower end of the range of UKCP18 projections reflect situations where the response is dominated by substantially increased snow accumulation on Antarctica (associated with increased atmospheric moisture transports). The upper end of the range of projections reflect situations where the response is dominated by increased dynamic ice discharge from Antarctica.

While the UKCP18 projections do not capture the same tendency for acceleration of Antarctic ice mass loss seen in other studies (e.g. Ritz et al, 2015; Golledge et al, 2015; DeConto and Pollard, 2016), the projections at 2100 presented by Golledge et al, (2015) fall well within the UKCP18 range. The study of DeConto and Pollard (2016) shows similar values to UKCP18 under RCP2.6, but substantially larger values under RCP4.5 and RCP8.5 (Figure A1.1.2). As discussed in section 3.1.2, the additional instability processes accounted for in DeConto and Pollard (2016) might be an important element of the future evolution of Antarctic ice sheet mass loss. However, the surface melt rates - one of the prime drivers of ice shelf collapse - used by DeConto and Pollard (2016) are 5-10 times higher than the CMIP5-based projections estimated by Trusel et al, (2015). Hence, the DeConto and Pollard (2016) results are shown here for context, rather than being incorporated into the UKCP18 sea level projections.

Since the IPCC AR5 GMSL projections were formulated relative to a baseline period of 1986-2005 it is necessary to carry out a small adjustment to the component time series to provide projections across UKCP18 for a common baseline period of 1981-2000. This is achieved on the basis of the average difference between the two baseline periods computed using four tide-gauge reconstructions of GMSL (Church and White, 2011; Ray and Douglas, 2011; Jevrejeva et al, 2014; Hay et al, 2015). The result is an offset of +0.011m for the total sea level, which is then applied across components according to the proportion of sea level change that each accounts for in the first decade of the projections (assuming that these are representative of the earlier period). These proportions are: 40.5% for Thermal Expansion; 9.5% for Antarctica; 12.5% for Greenland; 27% for Glaciers and 10.5% for Land Water.

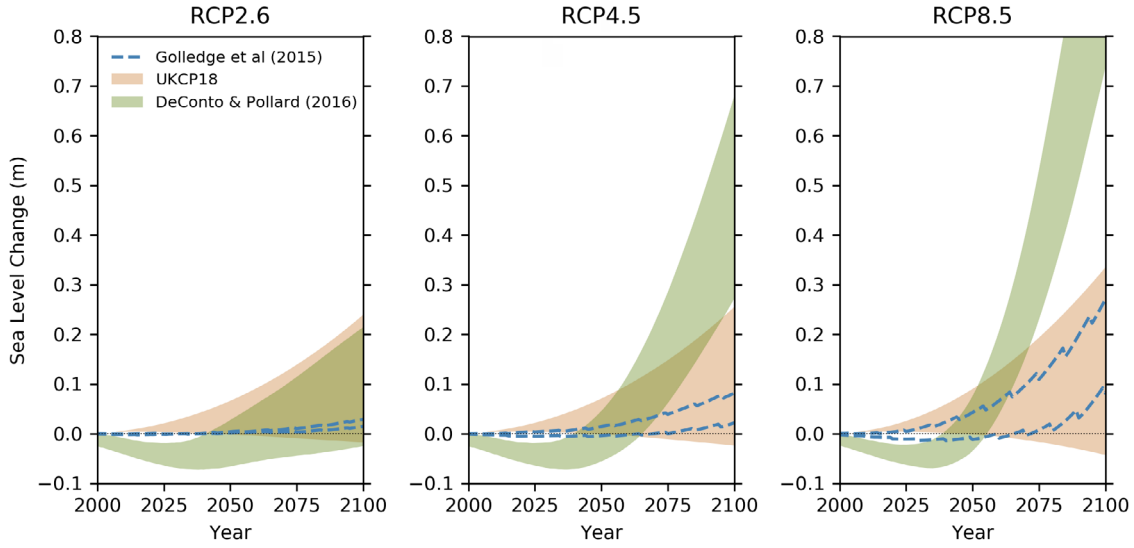

Figure A1.1.2. Projections of the net Antarctic contribution to global time-mean sea level change over the 21st century for UKCP18 (orange), Golledge et al, (2015; blue dashed); DeConto and Pollard (2016; green, from their Figure 5b). All time series are presented relative to a baseline of 1981-2000. The two simulations for each RCP scenario performed by Golledge et al, (2015) are indicated by the dashed lines. Shaded regions represent the 5th to 95th percentiles for UKCP18 and the standard deviation for DeConto and Pollard (2016).

A1.1.2 From global to regional projections

The regional sea level projections, like the global projections, make use of a Monte Carlo approach to estimate uncertainty. Before describing the mechanics of the Monte Carlo assessment, we explain how the eight spatial patterns of regional sea level change are accounted for, the first seven of which are directly related to the components of the GMSL projections described in the previous section (Table A1.1.2).

Table A1.1.2. Summary of the regional sea level components and associated methods.

Sea level component	Method
(i) Oceanographic	Regression slopes between local oceanographic sea level and global thermal expansion (Figure A1.1.3) are computed for all mainland UK coastal locations for each CMIP5 model (on the model's native grid). Each value is assigned a probability weighting to ensure equal sampling across CMIP5 models in the Monte Carlo step. This regression-based approach differs from the regional sea level projections presented in AR5, which estimated the climate change signal from the local difference between the periods 1986-2005 and 2081-2100.
(ii) Glaciers	AR5 time series of mass addition from glaciers are combined with the corresponding mass fingerprint, which is drawn at random from two independent model estimates (Slangen et al, 2014; Spada and Stocchi, 2007). Linear interpolation is used to extract the local fingerprint value at each coastal grid point. This approach differs from AR5 in using two mass fingerprint estimates.
(iii) Greenland - surface mass balance	AR5 time series of mass addition from surface mass balance are combined with the corresponding mass fingerprint, which is drawn at random from two independent model estimates (Slangen et al, 2014; Spada and Stocchi, 2007). Linear interpolation is used to extract the local fingerprint value at each coastal grid point. This approach differs from AR5 in using two mass fingerprint estimates.
(iv) Antarctica - surface mass balance	AR5 time series of mass addition from surface mass balance are combined with the corresponding mass fingerprint, which is drawn at random from two independent model estimates (Slangen et al, 2014; Spada and Stocchi, 2007). Linear interpolation is used to extract the local fingerprint value at each coastal grid point. This approach differs from AR5 in using two mass fingerprint estimates.
(v) Greenland - ice dynamics	AR5 time series of mass addition from ice dynamics are combined with the corresponding mass fingerprint, which is drawn at random from two independent model estimates (Slangen et al, 2014; Spada and Stocchi, 2007). Linear interpolation is used to extract the local fingerprint value at each coastal grid point. This approach differs from AR5 in using two mass fingerprint estimates.
(vi) Antarctica - ice dynamics	Levermann et al, (2014) time series of mass addition from ice dynamics are combined with the corresponding mass fingerprint, which is drawn at random from two independent model estimates (Slangen et al, 2014; Spada and Stocchi, 2007). Linear interpolation is used to extract the local fingerprint value at each coastal grid point. This approach differs from AR5 in using two mass fingerprint estimates and in using a different time series of mass addition.
(vii) Groundwater extraction	AR5 time series of mass addition are combined with a single estimate of the mass fingerprint from Slangen et al, (2014).
(viii) Glacial isostatic adjustment (GIA)	We make use of a 15-member ensemble of the total effect of GIA on regional sea level provided by the BRITICE_CHRONO project (Bradley, pers. comm.). A single estimate is drawn at random from the data and linear interpolation is used to extract the local value at each coastal grid point. This approach differs from AR5 in using regional observationally-constrained estimates of GIA.
Inverse barometer	This component is assessed from the AR5 supplementary data files as having a negligible contribution (~ 1% of the forced signal) and is not included. This is consistent with the approach taken in UKCP09.

The first component is that associated with regional changes in ocean circulation and density. Circulation changes leave their imprint in the shape of the sea surface, while local changes in ocean temperature and salinity affect the water column density and therefore sea surface height through volume changes. We adopt the nomenclature of Kopp et al, (2014) and refer to the combined effect of global thermal expansion and these local effects as the "oceanographic" component of regional sea level change. Following previous studies (e.g. Perrette et al, 2013; Bilbao et al, 2015), we estimate the oceanographic component of regional sea level by establishing linear regression relationships between local sea level and global thermal expansion in a number of CMIP5 climate models (Figure A1.1.3). These relationships vary both by CMIP5 climate model and geographic location around the UK, due to a spatial pattern of change that is highly uncertain (e.g. Pardaens et al, 2011; Slangen et al, 2014). Since we cannot be confident in the ability of coarse resolution CMIP5 models to reliably estimate the spatial pattern of change within UK waters, we compute regression relationships for all UK coastal grid boxes for each CMIP5 model. During the Monte Carlo step, we take a conservative approach of randomly drawing a CMIP5 model and coastal grid box to determine the local oceanographic sea level change by combining the regression slope with the time series of global thermal expansion (see section A 1.1.3 for details).

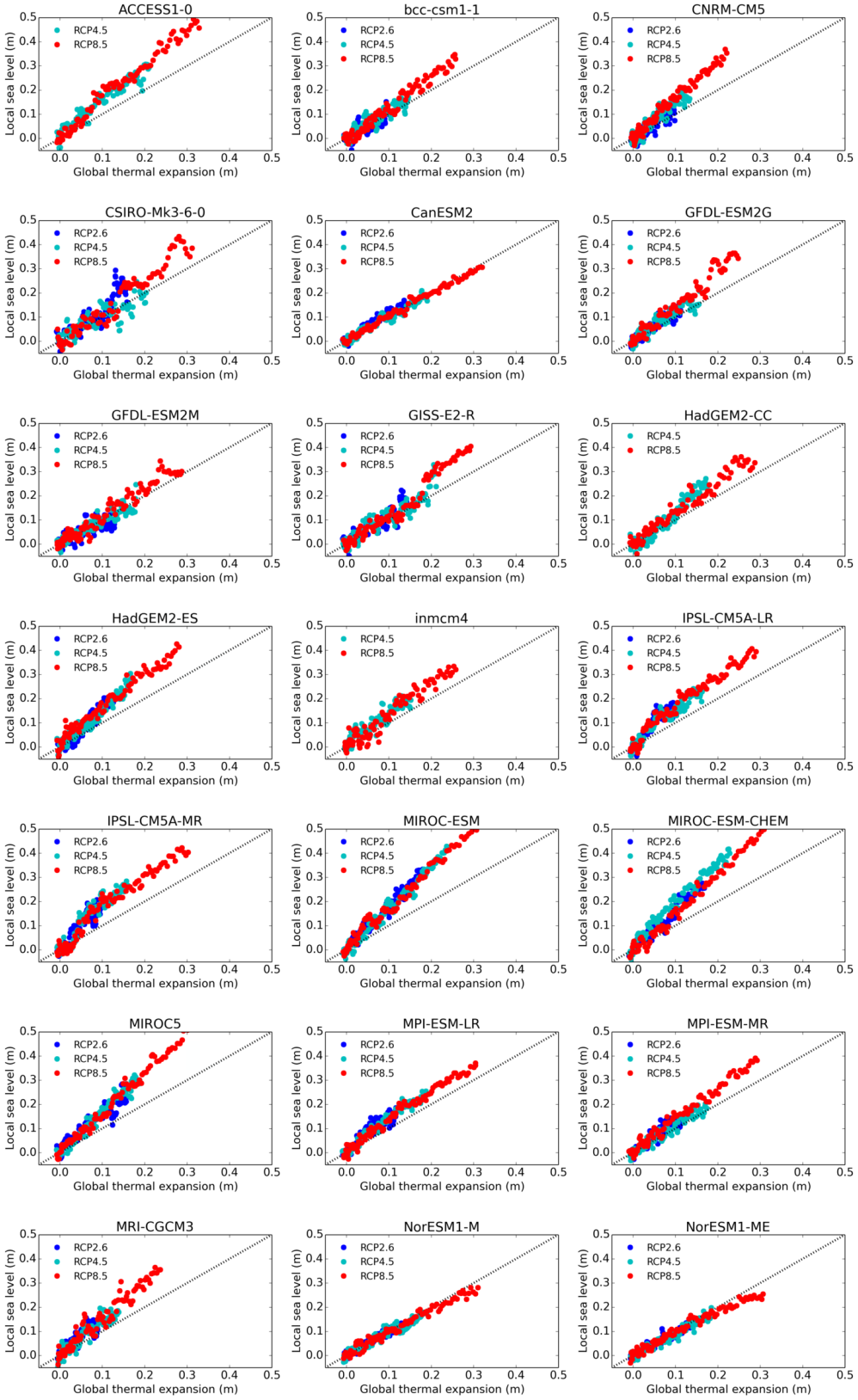

Figure A1.1.3. Regression relationships between local oceanographic sea level and global thermal expansion for Newlyn for the period 2007-2100. Relationships are plotted for all available simulations: RCP2.6 (blue); RCP4.5 (cyan); and RCP8.5 (red). For comparison, the dotted line shows the 1:1 relationship.

The six components of ocean mass addition (Table A1.1.2 ii-vii) are associated with spatial "fingerprints" of change that are dependent of the geographic distribution of the mass loss and arise from a combination of factors (e.g. Tamisiea and Mitrovica 2011).

The first factor is a localised response of the solid Earth to changes in the mass load, causing a positive vertical land motion and sea level fall when ice mass is lost and added to the ocean. The second factor is the effect of the total mass redistribution on Earth's gravity field. Both factors promote a near-field sea level fall and a far-field rise for a loss of ice mass. The third factor is the rotational effect (caused by the first two factors), which also leaves an imprint in the shape of the sea surface. In general, these physical effects are well understood and accurately simulated by the geophysical models that simulate these processes. However, in order to have some representation of the uncertainty in the fingerprint patterns, we use two independent sets of fingerprints, estimated following Slangen et al, (2014) and Spada and Stocchi (2007). In doing so, we incorporate an estimate of the uncertainty in the mass fingerprints, which is an aspect not included in the regional sea level projections reported in AR5. All fingerprint estimates use the same geographic mass distributions of Slangen et al, (2014). For the purposes of this study, we will refer to the six spatial patterns as "mass fingerprints" (Figure A1.1.4). The UK is in a region where there is a strong gradient in the Greenland ice sheet loss fingerprint, so that a small change in the pattern can have quite a substantial impact on the results. For the Antarctic, the UK is in the far field and there is less impact from uncertainty in the spatial pattern.

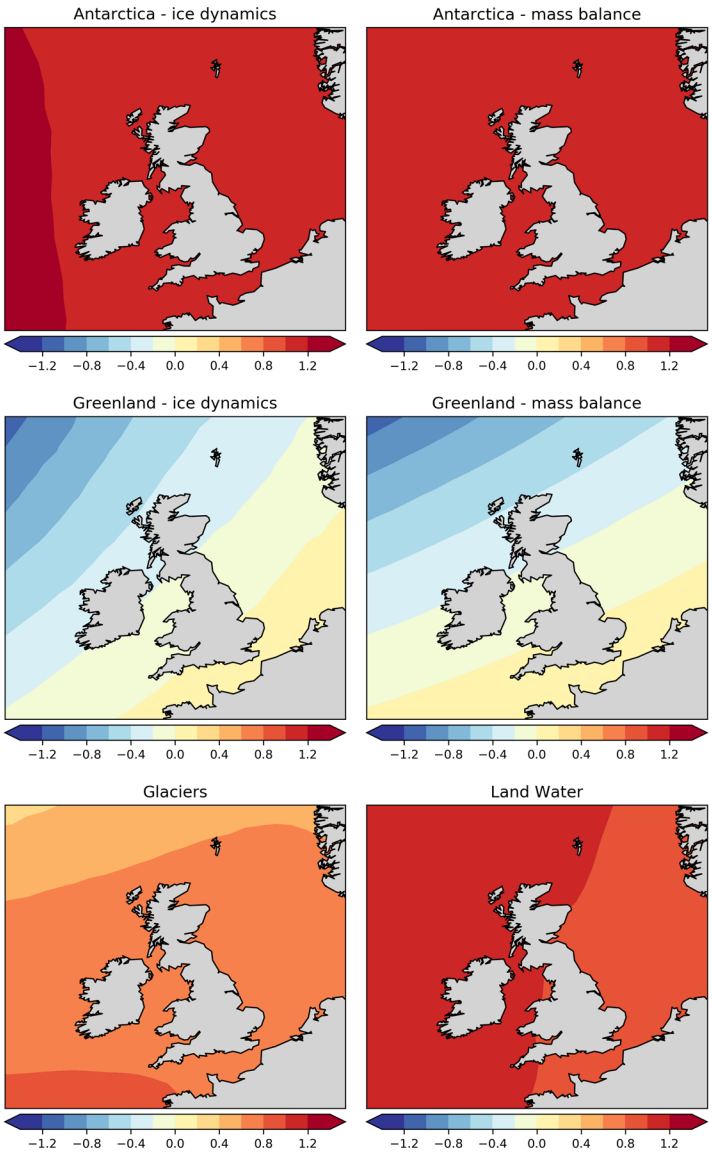

Figure A1.1.4. Sea level "mass fingerprints" for the UK region associated with changes in land ice mass and water changes, updated from Slangen et al, (2014). These spatial patterns arise from the response of the lithosphere, gravity field and Earth's rotation to changes in the surface mass distribution (Tamisiea and Mitrovica, 2011). Fingerprints represent the proportion of sea level change that is experienced locally for a unit increase in global sea level (no units).

The final component of regional sea level change is that associated with glacial isostatic adjustment (GIA, e.g. Church et al, 2013), which is sometimes referred to as "post-glacial rebound". This phenomenon occurs due to the very slow response of Earth's mantle material to the removal of land ice mass following the last glacial maximum, about 21 thousand years ago. While the largest effect from GIA for the UK is on vertical land motion, there is also a substantive contribution from changes in Earth's gravity field and rotational effects (Shennan et al, 2012). For the UK, this component of regional sea level change is characterised by negative values centred over eastern Scotland (indicating sea level fall relative to the land) and positive values for the southern UK (indicating sea level rise relative to the land) (Figure A1.1.5). The UKCP18 regional sea level projections make use of an ensemble of estimates of the effect of GIA on sea level from the NERC BRITICE_CHRONO project (Sarah Bradley, pers. comm.).

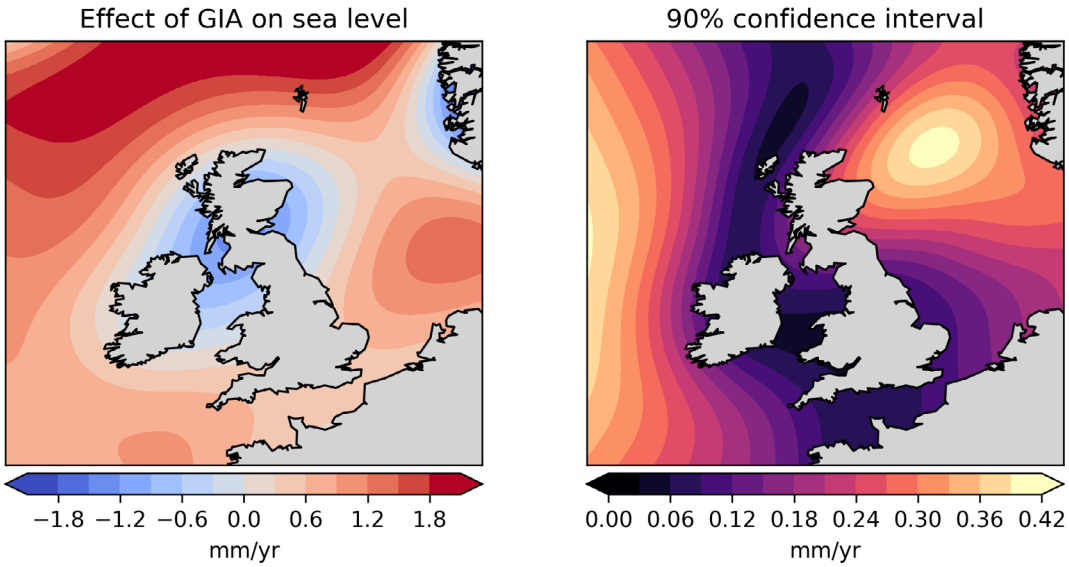

Figure A1.1.5. (left) The mean of 15 estimates of the ongoing regional relative sea level change associated with glacial isostatic adjustment (GIA), in mm/yr. (right) the associated 90% confidence interval, assuming a normal distribution, in mm/ yy. Data provided from the NERC BRITICE_ CHRONO project (Sarah Bradley, pers. comm.).

Changes in patterns of atmospheric circulation and the associated atmospheric pressure loading are projected to have a small negative sea level contribution for the UK of up to about 1cm (Church et al, 2013) over the 21st century. For the purposes of UKCP18, this term is assessed to be a negligible contribution and is omitted from our projections, as it was for UKCP09. However, changes in air pressure and wind speed are included when we look at storm surges, in section A1.3.

A1.1.3 Combining the regional sea level components

One of the key advances over the UKCP18 regional projections compared to previous studies (e.g. Church et al, 2013; Slangen et al, 2014; Cannaby et al, 2016) is that they are directly traceable to the IPCC AR5 GMSL projections and use the same Monte Carlo approach to combining uncertainties. A Monte Carlo method makes random draws from an underlying distribution many times in order to build up a picture of the combined uncertainties. The GMSL projections presented in IPCC AR5 used a Monte Carlo size of 450 thousand for each of the RCP climate change scenarios. Each realisation of the Monte Carlo makes a random draw of a component time series, based on assumptions about the underlying distributions (see Church et al, 2013, 13.SM.1). We note here again that global thermal expansion and the glacier and ice sheet surface mass balance time series (both inferred from CMIP5 time series of global surface temperature change) were treated as perfectly correlated.

Each instance of the Monte Carlo results in a total sea level change that is the sum of these randomly drawn components. The large number of realisations used provides robust information on the 5th, 50th and 95th percentiles of GMSL change for each RCP scenario.

The basis of the UKCP18 regional sea level projections is the IPCC AR5 GMSL Monte Carlo, with the Antarctic ice dynamics component updated based on the work of Levermann et al, (2014), as discussed in section A1.1.1. The Monte Carlo procedure for the regional sea level projections is shown schematically in Figure A1.1.6. The first step is to randomly draw a set of global time series from the GMSL Monte Carlo. The mass addition time series (glaciers, ice sheets and land water) are then combined with their corresponding fingerprints from the set provided following Slangen et al, (2014) or Spada and Stocchi (2007) at the specified latitude and longitude. This selection is made at random, but the same model is used for all fingerprints to preserve any correlated errors. The only exception to this procedure is for the land water fingerprint, where the only estimate available is from Slangen et al, (2014).

The time series of global thermal expansion is combined with a regression coefficient drawn at random across all CMIP5 models and all UK coastal grid boxes (a total of 930 values from 21 models). An example of these regression relationships is provided for Newlyn in South West England (Figure A.1.1.3), to illustrate the different regression slopes across the 21 CMIP5 models used. The random draw is weighted so that there is an equal chance of drawing each CMIP5 model, irrespective of how many grid boxes they have adjacent to the UK coast. The regression slopes range from about 0.8 to 2.0 and are largely insensitive to the RCP scenario. This approach differs from that used in UKCP09, where a spatial average around the UK was taken to determine the regression slope between local sea level and global thermal expansion. The UKCP18 is more conservative, in the sense that it retains the uncertainty associated with both the choice of CMIP5 model and the range of regression slopes around the UK coastline, for a given CMIP5 model.

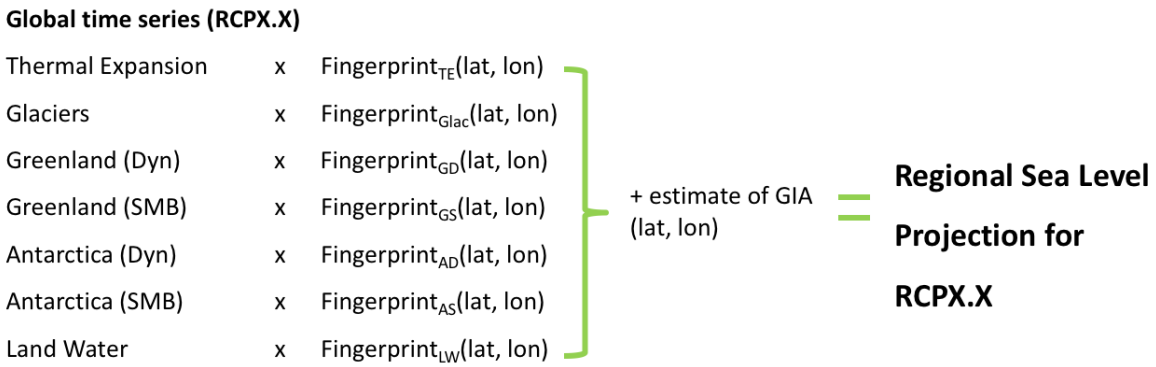

Figure A1.1.6. Schematic to illustrate how the different time series are combined with the corresponding fingerprints.

The different "fingerprint" values are effectively scaling factors for their corresponding GMSL time series. The scaled time series are then added to give the time series projection of total sea level rise for the RCP-dependent terms at the specified latitude and longitude. Finally, a random draw is made from the 15-member ensemble of GIA estimates at the specified latitude and longitude. This final component is not dependent on the RCP climate change scenario.

This procedure is then repeated 100 thousand times in order to provide robust estimates of the 5th, 50th, and 95th percentile projections of regional sea level change for each RCP scenario. The reproducibility of the Monte Carlo was assessed by repeating the whole process 30 times for two example locations that span the range of sea level projections across the UK (Newlyn and Port Patrick). The standard deviation of the 30 estimates of projected sea level at 2100 for the 5th, 50th and 95th percentiles does not exceed 1mm, 1mm and 3mm, respectively in any RCP scenario. The finalised UKCP18 projections used a fixed random seed to ensure total consistency and reproducibility across all scenarios and coastal locations.

It is important to note that there are a variety of additional geophysical processes not included in the UKCP18 regional sea level projections that can affect local sea level change, e.g. those that result in vertical land movement, such as sediment compaction/movement, other sources of subsidence, and even tectonic activity. Where vertical land motion data is available (for example, from differential GPS stations or satellite interferometry) this information should be incorporated into site-specific assessments of future sea level change.

A1.2 Exploratory extended time-mean sea level projections to 2300

Section summary: There are a small number of stakeholders who can make use of sea level information on time horizons that extend beyond the end of the 21st century, e.g. the nuclear energy sector. We use a physically-based emulator to extend CMIP5 projections of global surface temperature and global thermal expansion out to 2300. The global surface temperature projections are used as the basis for projections of ice mass addition, using the same methods as presented in IPCC AR5. This emulated ensemble forms the basis of the extended regional sea level projections. The approach taken is designed to provide a set of projections that can be used seamlessly with the UKCP18 21st century sea level projections. However, the post-2100 projections should be considered as having lower confidence than the 21st century projections.

A1.2.1 A physically-based emulator approach

The first step in this process is to generate CMIP5 model time series of global thermal expansion and global surface temperature change that extend to 2300. Only 5 CMIP5 models have both variables available on this time horizon for RCP2.6, RCP4.5 and RCP8.5 (i.e. less than 25% of the number of models used as the basis of the 2100 projections). Our approach is to use the simple two-layer energy balance model (e.g. Geoffroy et al, 2013a, b; Gregory et al, 2015) as a physically-based emulator for individual CMIP5 model simulations (Figure A1.2.1). We implement the two-layer model parameter tunings from Geoffroy et al, (2013a) and estimate the forcings for each CMIP5 model following Forster et al, (2013). Global surface temperature change is output directly from the two-layer model (Figure A1.2.1). Global thermal expansion is computed from emulated time series of total ocean heat content using CMIP5-model specific expansion efficiencies[5] estimated by Lorbacher et al, (2015). A more complete discussion of the methods and emulator performance is documented by Palmer et al, (2018).

[5] Expansion efficiency is a number relating a change in total ocean heat content to global thermal expansion, i.e., the amount that global sea level will rise as the ocean warms by a given amount.

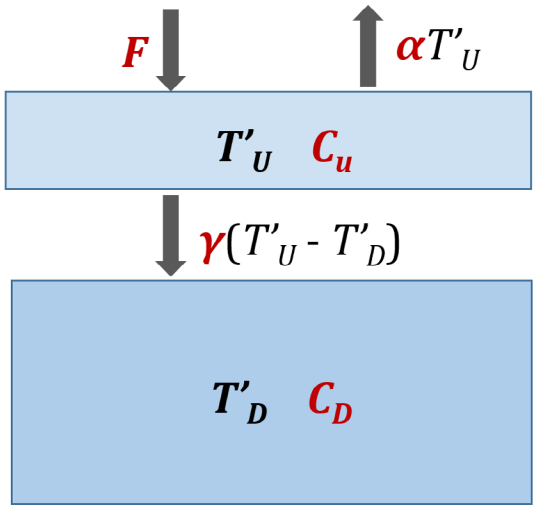

Figure A1.2.1. A physically-based emulator: the two-layer energy balance model. The model consists of an upper ocean layer (which represents surface temperature and the atmosphere), and a deep ocean layer. F is the radiative forcing at top-of-atmosphere, α is the climate feedback parameter, γ is the heat exchange coefficient. T'_U and T'_D represent temperature perturbations from a pre-industrial equilibrium state. Prognostic variables are indicated in black and tuneable parameters indicated in red. Figure reproduced from Palmer et al, (2018).

We apply the physically based emulator to 14 CMIP5 models to generate ensembles of projections to 2300 for global surface temperature and global thermal expansion under RCP2.6, RCP4.5 and RCP8.5 (Figures A1.2.2 and A1.2.3). These 14 CMIP5 models were the largest ensemble we could obtain that had both two-layer model parameter tunings available (Geoffroy et al, 2013a) and estimates of expansion efficiency with which to convert total ocean heat content change into global thermal expansion (Lorbacher et al, 2015). An estimate of the two-layer model discrepancy (i.e. the additional random uncertainty arising due to imperfect emulation of CMIP5 models) is quantified for each RCP and factored into the ensemble spread. The central estimate of the emulator ensemble shows good agreement with the IPCC AR5 global projections over the 21st century and the emulator spread compares favourably to the spread of those CMIP5 models with data available to 2300. However, we note that under RCP2.6 the two-layer model tends to overestimate time series post-2100 values compared to the available CMIP5 models. This may result in slightly larger projections of future global and regional sea level rise than if we were able to use a complete set of CMIP5 projections to 2300 and so may be considered conservative.

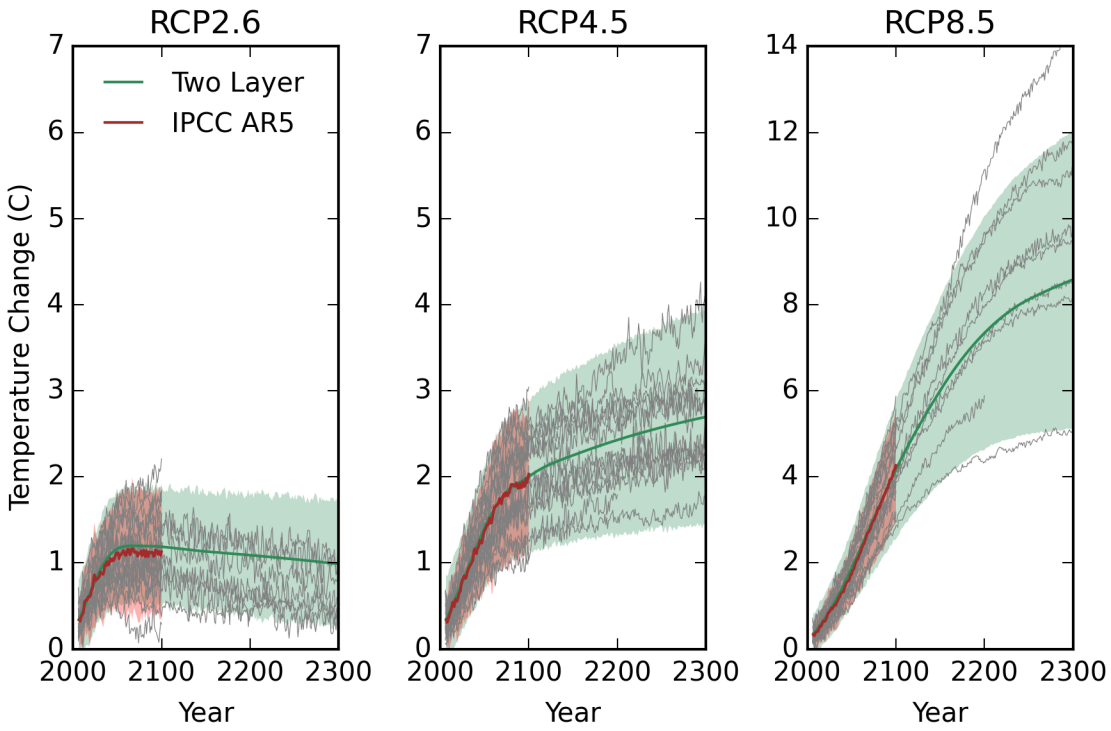

Figure A1.2.2. Ensemble projections of global surface temperature change (C) relative to a baseline period of 1986-2005. Time series include: (i) the 21-member CMIP5 ensemble used for sea level projections in IPCC AR5 (red, shaded regions indicate 5th to 95th percentile range); (ii) the 14 member two-layer model ensemble (green, shaded regions indicate 5th to 95th percentile range); (iii) individual CMIP5 model projections (grey lines). Figure reproduced from Palmer et al, (2018).

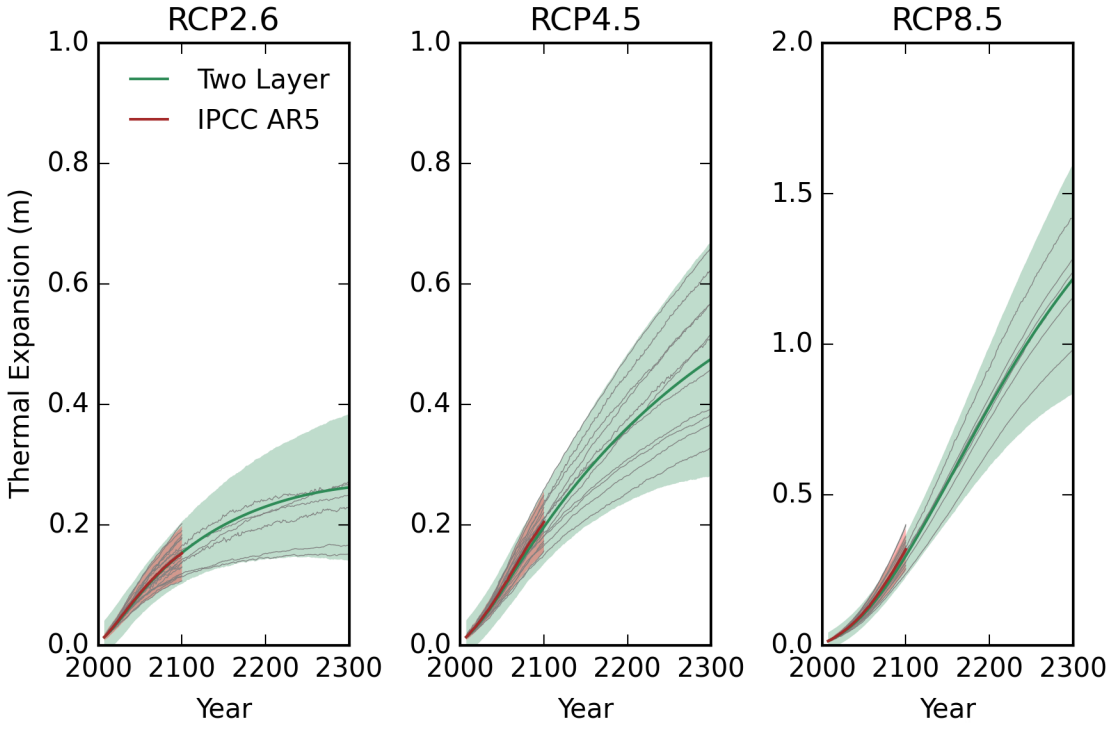

Figure A1.2.3. As figure A1.2.2, but for the global time-mean seal level change associated with thermal expansion (m). Figure reproduced from Palmer et al, (2018).

A1.2.2 Estimating the mass component time series

The approach to estimating the sea level mass components is focussed on consistency with the IPCC AR5 21st century projections, in order to provide a set of extended projections that can be used "seamlessly" with the 21st century projections. We retain the same relationships between global surface temperature and the glacier and Antarctica surface mass balance terms. However, the total contribution from glacier melt is capped at a value of 0.32m to reflect current estimates of total glacier volume (Grinsted, 2013). For Greenland surface mass balance, Greenland ice dynamics and Land Water storage changes, the rates at 2100 from the IPCC AR5 projections are held constant between 2100 and 2300. The projections for Antarctic ice dynamics use the same log-normal fit to the results of Levermann et al, (2014) as used for the UKCP18 21st century projections (see section A1.1.1 for more details) with rates held constant between 2100 and 2300. The methods are summarised in Table A1.2.1. It is important to note the role of expert judgement in this approach and other estimates of post 21st century sea level rise.

Mass component	Method
Antarctica: surface mass balance	The same relationship with global surface temperature used in the IPCC AR5 21st century projections is applied out to 2300 (Church et al, 2013).
Antarctica: ice dynamics	A statistical fit to the Levermann et al, (2014) results (see section A1.1.1) is used up to 2100 with rates held constant between 2100 and 2300.
Greenland: surface mass balance	The same relationship with global surface temperature used in the IPCC AR5 (Church et al, 2013) is used up to 2100 with rates held constant between 2100 and 2300.
Greenland: ice dynamics	The IPCC AR5 21st century projections mass loss rates at 2100 are held constant between 2100 and 2300 (Church et al, 2013).
Glaciers	The same relationship with global surface temperature used in the IPCC AR5 21st century projections is applied out to 2300 (Church et al, 2013), with a cap on the total sea level equivalent of 0.32m to reflect current estimates of global glacier volume (Grinsted, 2013).
Land Water storage	The IPCC AR5 21st century projections rates at 2100 are held constant between 2100 and 2300 (Church et al, 2013).

Table A1.2.1. A summary of methods used for each mass component time series post 2100.

As with the IPCC AR5 projections, a Monte Carlo approach of 450 thousand sets of global sea level component projections is generated for each of the RCP scenarios, which forms the basis of the extended regional sea level projections. A comparison of the extended projections of GMSL with the 21st century projections values are presented in Table A1.2.2.

	Year	RCP2.6	RCP4.5	RCP8.5
21st century projections	2100	0.29-0.67m	0.38-0.79m	0.56-1.12m
Extended projections	2100	0.30-0.68m	0.36-0.79m	0.53-1.12m
	2200	0.49-1.46m	0.69-1.78m	1.27-2.93m
	2300	0.62-2.17m	0.92-2.64m	1.71-4.55m

Table A1.2.2. A comparison of the UKCP18 21st century and extended projections. All values are change in total sea level relative to a baseline period of 1981-2000.

A1.2.3 From global to regional projections

For our post-2100 projections we follow an identical method to generate the regional sea level projections to that outlined in section A1.1.2, again based on a regional Monte Carlo of 100 thousand realisations. The rates of glacial isostatic adjustment (GIA) are assumed to remain constant over the coming centuries, which is reasonable, given the millennial-timescale associated with this process.

One of the additional assumptions for the extended projections is that the regression relationships between local sea level and global thermal expansion in CMIP5 models for the 21st century are representative of the following two centuries. We assess this by looking at a subset of models with data available to 2300 and conclude that this is a reasonable first-order approximation (e.g. Figure A1.2.5) based on the physical time constants of response. Any errors introduced by this assumption are small compared to overall uncertainties of the projected changes.

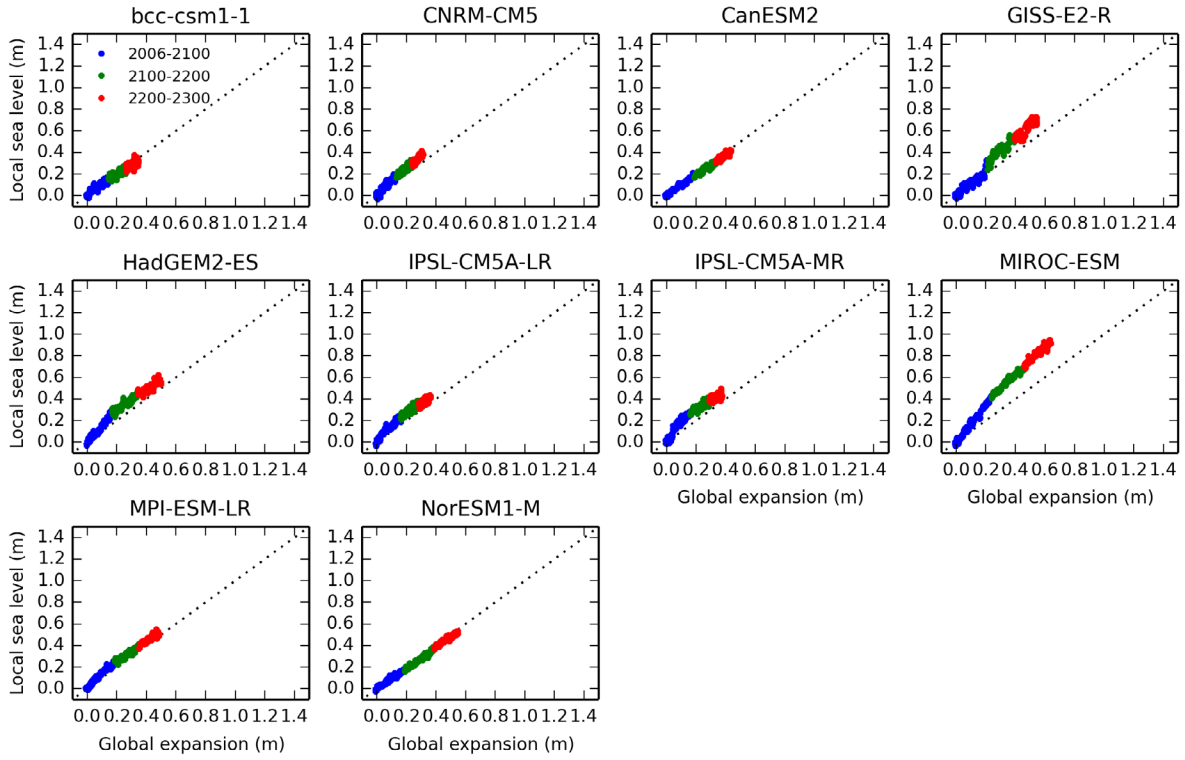

Figure A1.2.5. Regression plots of the relationship between local oceanographic sea level and global thermal expansion for Newlyn (South West England) for all CMIP5 models with data available to 2300 under RCP4.5 based on annual mean data. Colours correspond to the periods 2006-2100 (blue), 2100-2200 (green) and 2200-2300 (red). For comparison, the dotted line indicates the 1:1 relationship.

A1.3 Storm surge modelling

Section summary: Our modelling strategy is similar to that of UKCP09, but with an important difference: whereas UKCP09 used atmospheric simulations from a perturbed physics ensemble of a single coupled atmosphere-ocean general circulation model, we use atmospheric simulations from a set of diverse coupled atmosphere-ocean general circulation models in an effort to span the range of structural uncertainty.

Storm surges are short-lived increases in local water level above that of the tide. They are driven by atmospheric pressure gradients and winds, typically in shallow seas. When they occur at or near a high tide large surges are liable to cause flooding. Previous extreme surge events, such as that during winter 1953, have led to a considerable loss of life and damage to property around the coastline of the southern North Sea. In England alone more than 300 people died and 24,000 properties were seriously damaged in the 1953 coastal flooding event. Thus, as is well-recognised, many of the worst and the earliest effects of sea level rise will be experienced during extreme high water events, which may also involve overtopping due to extreme wave heights. Many previous studies (e.g. Lowe et al, 2009, Sterl et al, 2009) have indicated that the change in local relative mean sea level will be the primary contributor to the changes in the extremes, as it has been in the past (Menéndez and Woodworth, 2010). However there is also a potential for a change in atmospheric storminess to drive a change in the statistics of storm surge. Such a change in storminess will depend on changes in the mid-latitude storm tracks.

A1.3.1 Atmospheric drivers of storm surge

The position of the North Atlantic storm track, and the characteristics which include the detailed path of individual storms and their strength have a major impact on the timing and pattern of storm surges.

There is large uncertainty and little consensus in the response of the storm tracks to global warming. Many diverse competing processes in the climate system have the potential to drive changes in the storm tracks (see for example the review by Shaw et al, 2016). Among the competing processes are the following (adapted from Shaw et al, 2016):

- As climate warms, surface shortwave cloud radiative changes increase the equator-to-pole temperature gradient, but at the same time, longwave cloud radiative changes reduce this gradient.
- Some idealised simulations have shown that warming of the tropical upper troposphere increases equator-to-pole temperature gradient and shifts the storm tracks poleward. However, Arctic surface warming decreases lower tropospheric equator-to-pole temperature gradient and shifts the storm tracks equatorward.
- In coupled atmosphere-ocean models, warming of the polar lower stratosphere due to ozone hole recovery decreases equator-to-pole temperature gradient and shifts the storm tracks equatorward; however, increased greenhouse gases lead to warming of the tropical upper troposphere, cooling of the lower stratosphere and a poleward storm track shift.
- Latent heat transport increases in mid-latitudes in coupled atmosphere-ocean models, in response to increased CO_2, consistent with thermodynamic arguments. However, total energy transport does not change by as much because the increased latent energy transport is partially compensated for by decreased dry static energy transport.
- Changes in mean available potential energy, which are related to changes in storm track intensity, are sensitive to competition between changes in equator-to-pole temperature gradient and vertical stratification.

This diversity and competition makes projections of the storm track response to climate change less robust than, for example, the global mean temperature response (Shepherd, 2014). There are substantial differences between models in the way simulated atmospheric circulation responds to imposed greenhouse gas forcing. In UKCP09 this uncertainty was addressed by producing storm surge model simulations forced by an ensemble of climate models. This ensemble was generated by adjusting the atmospheric physics parameters of a single climate model. The resulting range of extreme-sea level response (as measured by the change in sea level extremes due to change in atmospheric storminess alone) was found to be small. For some metrics, the range of response sampled by a perturbed physics ensemble (PPE) is not the same as the range of response sampled by a multi-model ensemble (MME). Two examples are the regional mean sea level response, discussed by Pardaens et al, (2011), where the PPE range is smaller than the MME range, and the north-east Atlantic atmospheric storminess response as measured by band-pass filtered atmospheric pressure at sea level, discussed by Lowe et al, (2011), where the PPE and MME exhibit different responses in terms of the intensity and latitude of the maximum variability near the UK.
The resourcing and timing of the UKCP18 marine work did not allow for forcing with both PPE and MME and so, in view of the small size of the range of response found using a PPE in UKCP09, in UKCP18 we elected to address the storm-track-response uncertainty by forcing the storm surge model with data from several different climate models (i.e. a limited multi-model ensemble).

However, the results of this exercise should not be regarded as a probabilistic projection of the storm surge response, but rather a limited sample of possible responses. Furthermore, since we do not have available a long control simulation with which to assess the internal variability, and since we use only a single realization of each model simulation, we cannot be sure whether any projected changes are a response to greenhouse gas forcing or an expression of long-period internal variability. However, we note that from a coastal engineering point of view this is largely immaterial, as long as the projected changes show a realistic potential of the real world. The question of the size of the forced signal versus the internal variability is a priority for further work. The range produced should be taken as a minimum estimate because of potential uncertainties that the method does not sample.

The atmospheric data which we use to drive our storm surge model is hosted by the CMIP5 database. The horizontal resolution of most General Circulation Models (GCMs; also referred to as global climate models) making CMIP5 centennial projections is of order 1-2°. This limits their ability to represent extreme weather events and the effect of local forcing features such as coastlines, which can modulate the large-scale climate on local scales. One way to address this is to downscale the global simulation using a Regional Climate Model (RCM).

Five models contributing to the CMIP5 database were selected (Strandberg et al, 2014) and downscaled using the Swedish Meteorological and Hydrological Institute (SMHI) Rossby Centre regional atmospheric model (RCA4) as part of the Euro-Cordex initiative (Jones et al, 2011). We used output (surface wind and mean sea level pressure) from these five regional climate simulations (henceforth "RCA4-downscaled" simulations) to force our storm surge model. A schematic illustrating this experimental design is shown in Figure A1.3.1. We selected the representative concentration pathway RCP8.5 as this is expected to give the largest signal of change and is the primary scenario used in the atmospheric UKCP18 Land Strand simulations. As seen in section 3, where we examine the results, there is actually little future trend evident in storm surges for this scenario. Since lower emission scenarios are expected to give a lower response, there is little reason to expect a significant forced change from lower emission scenarios if it is not found in RCP8.5. Thus, for storm surge we do not run simulations using other scenarios. The five models selected are: CNRM-CM5, EC-EARTH, IPSL-CM5A-MR, HadGEM2-ES and MPI-ESM-LR. We refer to surge model projections based on these five models downscaled by RCA4 as CNRM-CM5-RCA4, EC-EARTH-RCA4, IPSL-CM5A-MR-RCA4, HadGEM2-ES-RCA4 and MPI-ESM-LR-RCA4 respectively. These models are listed in table A1.3.1. Due to the limited availability of suitable temporal-resolution data from regional downscaling experiments, the only regional model we use is SMHI RCA4 and so we cannot assess the sensitivity of our findings to the use of a different regional model. The five global models were selected for downscaling by the Euro-Cordex project (Jones et al, 2011) from the CMIP5 models on the basis of their ability to simulate a realistic climatology, particularly for the European region, but they do not necessarily exhibit a large 21st century change in the atmospheric drivers of extreme surge. UKCP18 did not have any say in which models were downscaled by the Euro-Cordex project; we simply used the most appropriate available data.

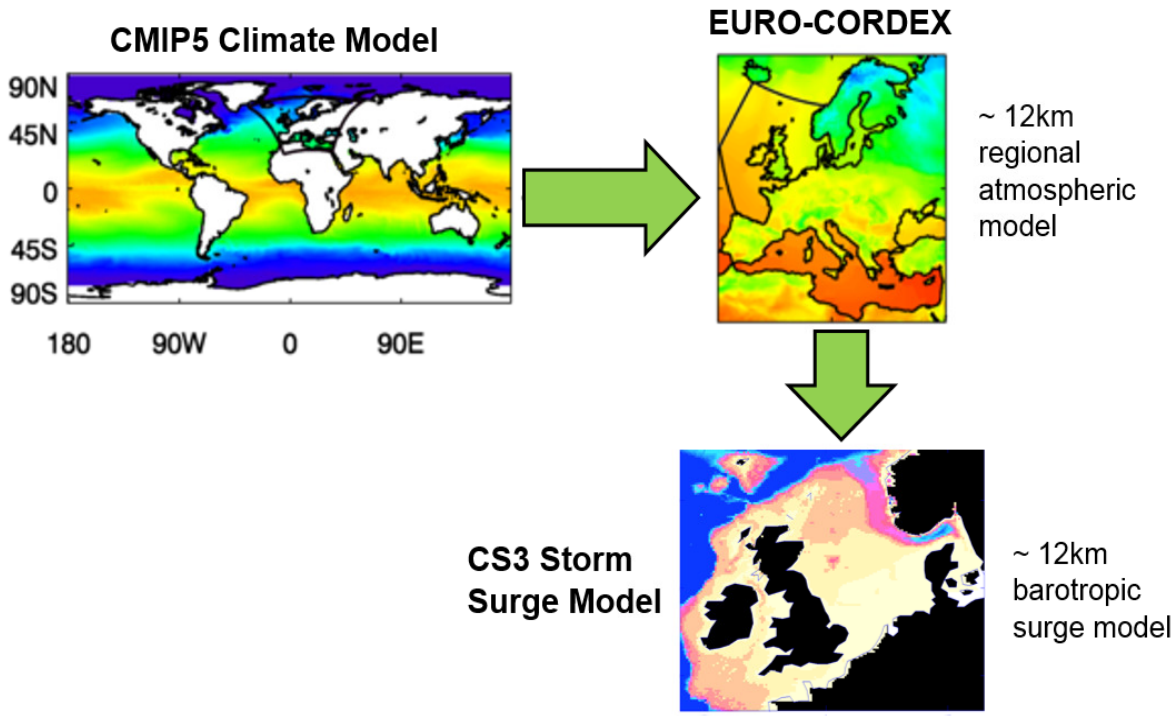

Figure A1.3.1 Schematic diagram showing the experimental design of the UKCP18 surge simulations..

Whilst there are good reasons for using regional model data for the 21st-century projections, there are global model simulations which exhibit a larger century-scale change in the storm track around the UK than the five global models underlying the RCA4-downscaled simulations. In particular the GFDL-ESM2M global simulation exhibits a large increase in storm track intensity in winter as measured by band-pass-filtered mean sea level pressure (BPF MSLP, Figure 6.2.1) variability and a substantial northward shift in the maximum storm track intensity as measured by a count of storms crossing the zero of longitude (Figure 6.2.2). Thus, in order to capture a wider spread of century-scale response, we additionally analyse the response of the surge model when driven directly by data from the global GFDL-ESM2M 21st century RCP8.5 simulation.

Howard et al, (2010) showed that the trends in surge extremes from a surge model driven directly by global climate model data correlated with those from the surge model driven indirectly by the same global climate model downscaled through a regional model, at least for the southern North Sea coast of the UK. In their study, for that location, they found that the signal of change was attenuated by missing out the regional downscaling step. In our own comparison (not shown), of century-scale trends in extreme skew surge from the HadGEM2-ES simulation with and without the RCA4 regional downscaling step we likewise find that the sign of the trend is preserved by the regional downscaling step, but the attenuation or amplification of the signal is not sufficiently consistent around the UK coast to justify applying any scaling to the GCM-only trend.

A1.3.2 Atmospheric models

The regional model we have chosen to focus on is the Swedish Meteorological and Hydrological Institute (SMHI) Rossby Centre regional atmospheric model, RCA4 with EUR-11 domain shown in Figure A1.3.2. The horizontal resolution is 12.5 km, comparable to the horizontal resolution of the surge model. Further details of the atmospheric model can be found in Strandberg et al, (2014). From the atmospheric model, near-surface wind components at the highest temporal resolution available on the CMIP5 database (6-hourly intervals) and sea level atmospheric pressure (3-hourly intervals) are spatially interpolated onto the surge model grid. To avoid smoothing (and thus reducing the intensity of) the representation of the atmospheric storms we do not perform any temporal interpolation. A wind field update frequency as low as this (only once in six hours) would be considered deficient by contemporary storm surge forecasting standards and we accept that this is a potential source of bias. However, we find that the system evaluates adequately against observations (see section A2.3) and we do not anticipate that this potential shortcoming will have a significant effect on projections of future trends, since any bias would exist in both present-day and future simulations. Furthermore, a power spectral density analysis (not shown) of a long sample of surge residuals at several ports does not show any signal with exactly six-hour frequency such as might be associated with production of spurious residuals due to the jumps in forcing at six-hourly intervals: the spectrum looks very similar to that of a model forced with one-hourly data.

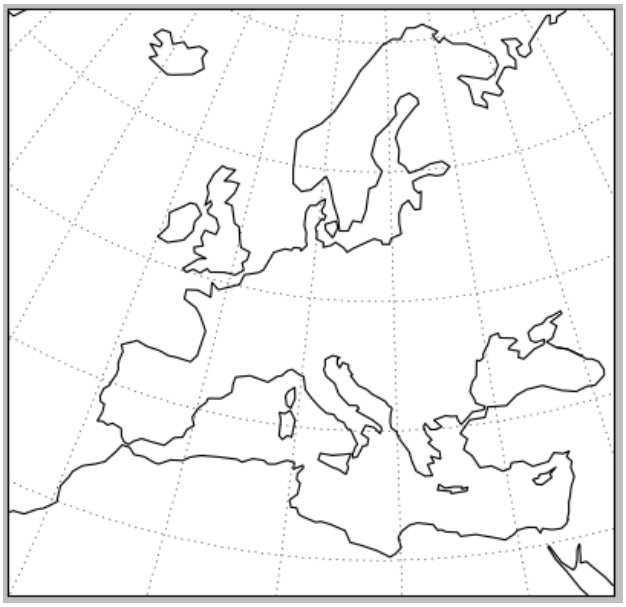

Figure A1.3.2. The EUR-11 domain of the regional atmospheric model. The model does not use a regular latitude-longitude grid. Lines of latitude and longitude are shown (dotted, at ten degree intervals) to illustrate the extent of the domain.

For the global model GFDL-ESM2M the spatial resolution is approximately 200km, and the available temporal resolution of the sea level pressure fields 6 hourly and surface winds 3 hourly.

Atmospheric driving model	Horizontal resolution of atmospheric simulation	Temporal resolution of surge model driving data in hours: (SLP, surface winds)	Global model included in land strand augmentation?
CNRM-CM5-RCA4	0.11 degrees	(3, 6)	Yes
EC-EARTH-RCA4	0.11 degrees	(3, 6)	Yes
IPSL-CM5A-MR-RCA4	0.11 degrees	(3, 6)	Yes
HadGEM2-ES-RCA4	0.11 degrees	(3, 6)	--
MPI-ESM-LR-RCA4	0.11 degrees	(3, 6)	No
GFDL-ESM2M	200 km	(6, 3)	No*

Table A1.3.1 Atmospheric models used to drive the CS3 surge model. *The Land Strand augmentation uses GFDL-ESM2G because it has a slightly better evaluation by some metrics. Here we choose GFDL-ESM2M because it exhibits a stronger signal of increase in the extreme surges.

A1.3.3 The CS3 surge model

The simulated winds and surface pressure described above are used to drive the National Oceanography Centre's ~12km resolution barotropic storm surge model (CS3). The model produces a numerical simulation of the North Sea tides and surges, and is described in detail by Flather (1994) and Flather (2000).
The model uses a regular latitude-longitude grid and covers the northwest European continental shelf from 12 degrees west to 13 degrees east in 1/6 degree steps and 48 degrees north to 63 degrees north in 1/9 degree steps. The domain is shown in Figure A1.3.2.

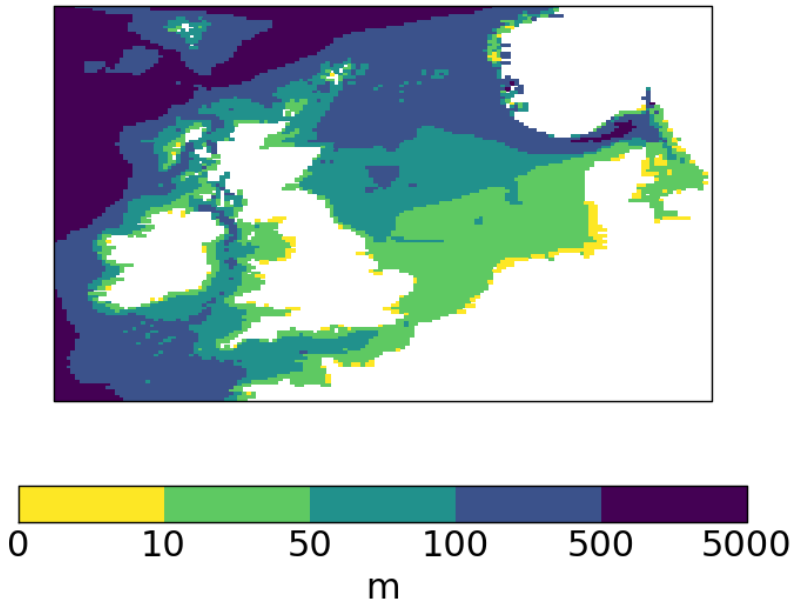

Figure A1.3.3. The domain of CS3. Colours show the bathymetry in metres.

Tidal input at the model open offshore boundaries consists of the fourteen largest tidal constituents. (The tide at any location can be thought of as being a combination of several different waves each having different characteristic oscillation periods. These are referred to as constituents). Modelled surge residuals are derived by subtracting a tidal model simulation from one forced by both tide and atmospheric forcing. Since winds are most effective at generating surge in shallow water, peaks in surge residual are consistently obtained 3–5 hours prior to the predicted high water (Horsburgh and Wilson, 2007). A more significant and practical measure than the surge residual is the skew surge (see Figure A1.3.4), which is the difference between the elevation of the predicted astronomical high tide and the nearest (in time) experienced high water (e.g. de Vries et al, 1995). “Experienced high water” here refers to either observed or modelled high water. Williams et al, (2016) have demonstrated independence of high water level and skew surge for the most extreme events.

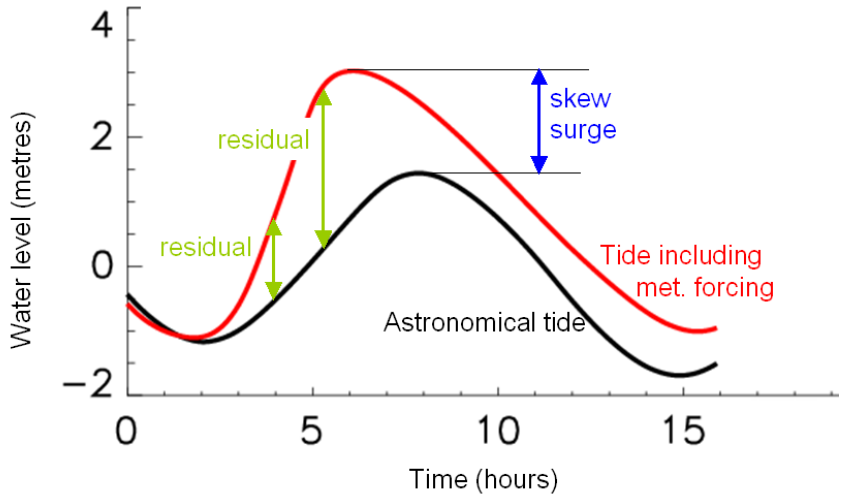

Figure A1.3.4 Schematic showing how residual and skew surge are calculated, and how skew surge is related to still water level.

A1.4 Statistical model for analysis of storm surge changes

A1.4.1 Generalised extreme value (GEV) statistical model

There are strong arguments (e.g. Coles, 2001) for using a GEV distribution as a statistical model of the behaviour of extremes such as the annual maximum skew surge. In its stationary form, the GEV distribution is a three-parameter distribution.

- The location parameter, μ is the level (for example in the case of skew surge, the water level relative to the astronomical high tide level) which is expected to be exceeded once per year on average. Even in an unchanging climate, such exceedances would not be distributed uniformly in time. There would be some years with no exceedances of the location parameter, some with just one, and some with more than one, but in the long run we would expect an average of one exceedance of the location parameter per year. This definition is often used to define the 'one-year return level' and that is the convention we adopt here[6]. In other words, the one-year return level is the same as the location parameter.
- The scale parameter, σ is a measure of the spread of the extremes. It determines the slope of the return-level curve around a return period of one year (see for example the return level plots in Figure A2.3.1). In the simplest GEV distribution, the Gumbel distribution, the scale parameter is the difference between the one-year return level and the e-year (approximately 2.72 year) return level.
- The shape parameter, ξ determines the curvature of the return-level curve. For more detail see for example Coles (2001).

To analyse century-scale change we use one of two non-stationary forms of the GEV distribution:

- A four-parameter statistical model with μ_o, σ, ξ and a linear trend, μ', in the location parameter (so that $\mu(t)=\mu_o+\mu' t$).
- A five-parameter statistical model with μ_o, σ_o, ξ, and linear trends, μ' and σ', in both location and scale parameters (so that $\mu(t)=\mu_o+\mu' t$ and $\sigma(t)=\sigma_o+\sigma' t$).

The shape parameter, ξ, is not allowed to vary over time in our statistical models. It is reasonable to treat the shape parameter as constant over time because: (i) there needs to be a very clear change in distributional shape over the data for statistically significant evidence to be found and (ii) evidence from wide-ranging environmental applications of extreme value methods suggests that the shape parameter tends not to change with covariates (Tawn, pers. comm). In our case, the covariate is time.

[6] An alternative definition, which is sometimes seen, of the N-year return level as "the level which is exceeded in any given year with probability 1/N", is approximately the same as our definition for long return periods but becomes meaningless when we speak of the one-year return level.

Our statistical analysis is based on the R-largest approach (e.g. Coles, 2001), which uses the R largest independent skew surge events each year. This is a well-recognised approach for sea level in the presence of underlying trends (e.g. Lowe et al, 2009, Cannaby et al, 2016, Butler et al, 2007). For a discussion of the choice of R see Coles (2001). Following Coles (2001) we take R to be five. We ensure independence by considering only skew surge events that are separated by at least sixty hours. Using the five largest independent events each year instead of just the annual maximum gives a more statistically robust analysis. To those data we fit a joint distribution statistical model for the five largest events, with four or five parameters as described. From this, we obtain a generalized extreme value statistical model of the annual maxima.

We choose the four-parameter statistical model for the RCA4-downscaled simulations and the five-parameter statistical model for the GFDL-ESM2M simulation. These choices are justified in section A1.4.2. The UKCP09 surge analysis used the five-parameter statistical model throughout. In either case the trend in location parameter is identically the trend in the one-year return level. Under the five-parameter statistical model, trends at other return periods are modified by the trend in scale parameter. However, under the four-parameter statistical model the location parameter trend applies to all return periods and can thus be thought of as a trend in all of the extremes.

A1.4.2 Selection of four or five parameter GEV statistical model for storm surge analysis

Section summary: We assess the spatial coherence of trends in skew surge. Spatial coherence in the trend in location parameter (μ') supports the four parameter GEV statistical model for the RCA4-downscaled simulations. Spatial coherence in the trends in both location and scale parameters (μ' and σ') supports the five parameter GEV statistical model for the GFDL-ESM2M simulation.

The pointwise central estimate (as shown, for example, by the blue line in Figure 3.2.2) is our best guide to the trend at an individual site for a given simulation (the HadGEM2-ES-RCA4 simulation in the case of the blue line in Figure 3.2.2). However, this pointwise (local) trend may be the result of both large-scale variations in atmospheric storminess ('signal') and small-scale local chaotic effects which are not caused by any systematic change ('noise', for example an increase at one site due to more storms happening to coincide with high tide at that site during the latter part of the 21st century). Such noise exists over a range of spatial and temporal scales. With or without a signal, if we analyse each coastal site around the UK independently, some of them will show significant change due to the local noise.

Taking a wider view, the proportion and spatial coherence of sites exhibiting change of consistent sign is a useful guide to whether the cause is signal or local noise. Here we use this guide to determine the appropriate number of parameters for our statistical model.

Results from the RCA4-downscaled surge simulations in the projections section of the report are from the four-parameter statistical model in which only the location parameter is allowed to change, whereas results from the GFDL-ESM2M simulation are from the five-parameter statistical model because we find (as shown in this subsection) that:

1. In the case of a trend in the location parameter the signal is widespread, at least in some of the RCA4-downscaled surge simulations.
2. There is insufficient evidence for a scale parameter trend in the RCA4-downscaled simulations on any meaningful spatial scale.
3. There is evidence of widespread trends in both location and scale parameters in the GFDL-ESM2M simulation.

RCA4-downscaled simulations: location parameter.

We begin by showing in Figure A1.4.1 the central estimate of the 21st-century trend in the location parameter for each of the RCA4-downscaled simulations for mainland class A tide gauge sites as calculated using the four-parameter statistical model.

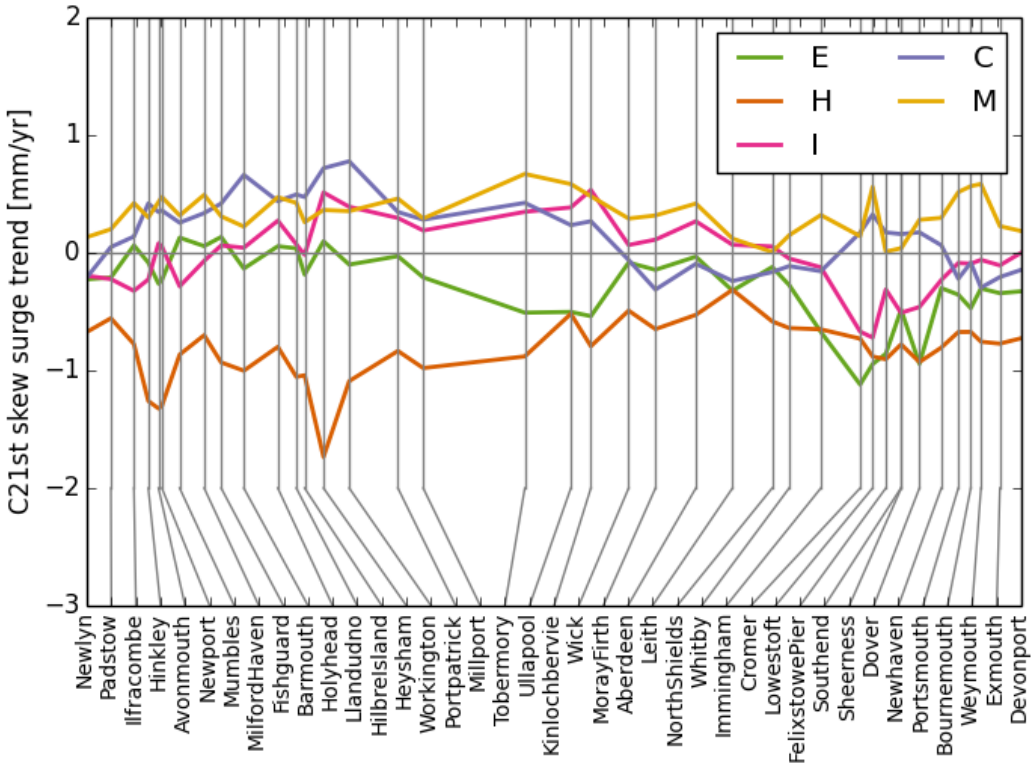

Figure A1.4.1. 21st century trend in one-year return level of skew surge as projected by the RCA4-downscaled simulations for class A tide gauge sites around the UK mainland. Key: C: CNRM-CM5-RCA4, E: EC-EARTH-RCA4, I: IPSL-CM5A-MR-RCA4, H: HadGEM2-ES-RCA4, M: MPI-ESM-LR-RCA4.

These features stand out from Figure A1.4.1:

(1) The simulations do not generally agree with each other.
(2) The trend is negative everywhere in the HadGEM2-ES-RCA4 simulation.
(3) The trend is positive almost everywhere in the MPI-ESM-LR-RCA4 simulation.

Features (2) and (3) suggest that the sum of the trends over all of the ports will be a suitable simple, non-local statistic to test for a spatially-coherent trend in individual simulations. We shuffle the years into a random order and recalculate this statistic (the sum – over all of the class A tide gauge sites – of the diagnosed trend in the location parameter) based on the shuffled years. We do this many (128) times to give an empirical cumulative distribution function (ECDF) of the statistic. Then we consider the position of the actual value (obtained from the unshuffled years) within this distribution. This is known as a spatial block bootstrap. If the actual value is outside the distribution (or very near either end of the distribution) then we regard the result as statistically significant. This test assumes that there is no significant short-term autocorrelation over time (i.e. one year is assumed effectively independent of the previous year). Consistent with this assumption, our results are not sensitive to resampling in blocks of five years instead of individual years. Figure A1.4.2 shows this test for each of the five simulations. The distribution is shown by the dots and the actual value (unshuffled years) is shown by the vertical line.

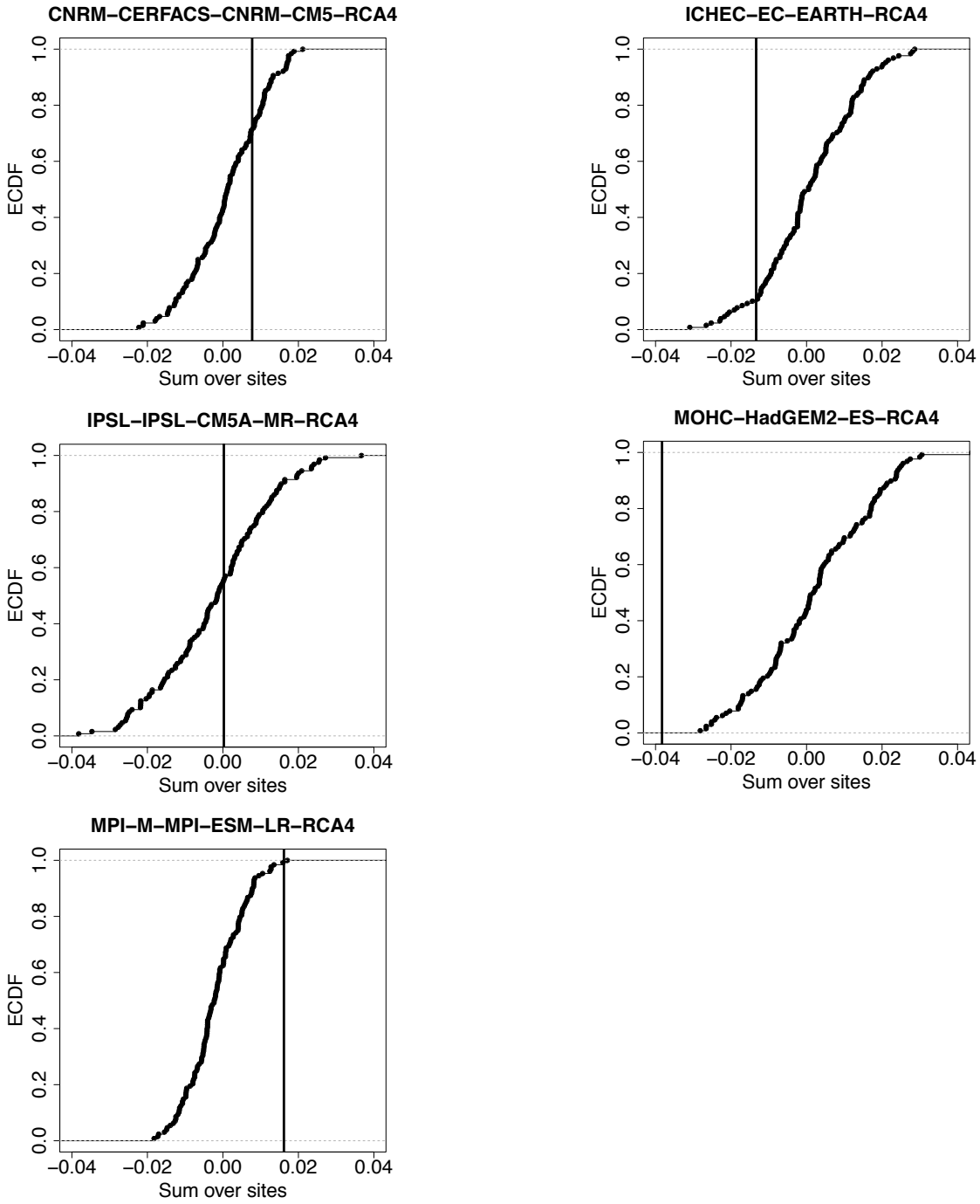

Figure A1.4.2. Significance testing of UK-wide trend in location parameter. The empirical cumulative distribution function from a spatial block bootstrap of the sum of trends over all UK class A tide gauges is shown for each of the RCA-downscaled simulations. The value of the sum from each simulation is shown by a vertical line. For full details see text.

We can see that if we had considered the HadGEM2-ES-RCA4 simulation in isolation we would have found the (negative) trend in location parameter in that simulation to be statistically significant at the spatial scale of the whole of the UK coastline. Similarly, if we had considered the MPI-ESM-LR-RCA4 simulation in isolation we would have found the (positive) trend in location parameter in that simulation to be statistically significant at the spatial scale of the whole of the UK coastline.

We conclude that there is support for the use of the fourth parameter (μ', the trend in location parameter) for the RCA4-downscaled simulations.

RCA4-downscaled simulations: scale parameter

Having found evidence supporting the use of the four-parameter statistical model for the RCA4-downscaled simulations, we turn now to the five-parameter statistical model which includes the trend in the scale parameter. In Figure A1.4.3 we show the scale parameter trend around the mainland coast for each of the RCA4-downscaled simulations. Location parameter and scale parameter are both allowed to change in this five-parameter statistical model, but we're only looking at the scale parameter changes in this plot.

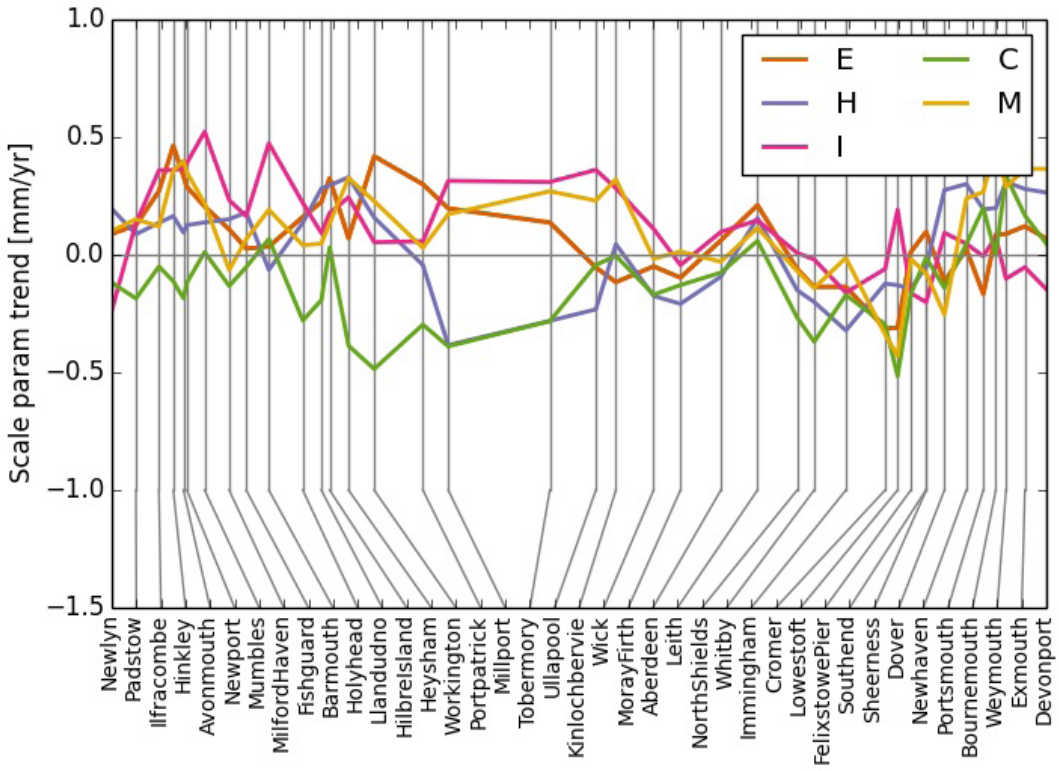

Figure A1.4.3. 21st century trend in scale parameter of skew surge as projected by the RCA4-downscaled simulations for class A tide gauge sites in the framework of the five-parameter statistical model which accommodates change in both location and scale parameters. Key: C: CNRM-CM5-RCA4, E: EC-EARTH-RCA4, I: IPSL-CM5A-MR-RCA4, H: HadGEM2-ES-RCA4, M: MPI-ESM-LR-RCA4.

Some remarks on Figure A1.4.3:

1. In contrast to the location parameter, we see that no RCA4-downscaled simulation shows a consistent trend in scale parameter on the spatial scale of the whole of the UK.
2. There is no suggestion of a statistically significant increase in scale parameter on the English east coast (including the Thames estuary), in any RCA4-downscaled simulation.
3. There is perhaps a hint of a small decrease in scale parameter on most of the east coast: the trend is negative (or tiny) in all RCA4-downscaled simulations at Cromer, Immingham, Whitby and North Shields.

To put this analysis on a more formal basis we first consider the sum over all sites, with significance assessed by comparison with randomised results from shuffled years (not shown), as we did for the location parameter trend. In contrast to the location parameter trend (and consistent with remark 1 above), we do not find a significant signal in any RCA4-downscaled simulation on the spatial scale of the entire UK coastline for the trend in the scale parameter. However, that test does not tell us about any signal on an intermediate spatial scale (somewhere between the whole-coastline scale and the non-credible single site scale). We applied several tests (not shown) but found no compelling evidence for any intermediate-spatial-scale signal in the scale parameter trend in the RCA4-downscaled simulations.

We conclude that there is insufficient support for the use of the fifth parameter (σ', the trend in scale parameter) for the RCA4-downscaled simulations. Consequently, in the main report we show results from the four-parameter statistical model applied to the RCA4-downscaled simulations.

Why not report the diagnosed trends in the scale parameter anyway, even though they are not statistically significant? There are three reasons:

1. Statistical reason: having shown that the scale parameter trend is not significant, including it in the statistical model constitutes overfitting.
2. Precautionary reason: wherever the scale parameter trend is negative, it pulls down the location parameter trend if both are allowed.
3. Pragmatic reason: with a trend in the location parameter only, the interpretation of the results is simplified: the same trend applies to all return periods.

GFDL-ESM2M simulation: statistical model selection

We applied the same set of tests (not shown) to the GFDL-ESM2M simulation. Here we found evidence of (positive) trends in both location and scale parameters at credible spatial scales. We conclude that the use of the five-parameter statistical model is justified for this simulation. Consequently, in the main report we show results from the five-parameter statistical model applied to the GFDL-ESM2M simulation.

A1.5 Projected future return level curves

In section 3.2.4 we show projected future return level curves of still water level. A return level curve of still water level can be thought of as one representation of the probability distribution of the annual maximum still water, which could alternatively be represented by a plot of the cumulative distribution function or a plot of the probability density function. Whilst such a distribution is readily understood in the context of extreme events which are well-modelled by a random process with a fixed mean and variance, it is less clear how it should be interpreted in the context of a projected future mean sea level which is itself uncertain. If the probability distribution of the future mean sea level were known in full (which it is not), we could convolve the two distributions to give a distribution of the uncertain future extremes. An additional complication is that the projected future mean sea level and its uncertainty increase over time. Several authors (for example Hunter, 2012) have presented approaches to dealing with these issues and addressing them will form part of the work following on from UKCP18, but not the work presented here.

A further complication is that the present-day distribution of the annual maximum still water is itself uncertain: although we can fit a statistical model to the observed maxima, there is uncertainty in the fitted parameters and a deeper uncertainty about the suitability of the statistical model (there is analogous deep uncertainty in the suitability of computer models for projection of future mean sea level). Thus, the present-day return level curves are themselves uncertain (Environment Agency, 2018), but we do not include that uncertainty here. Nor do we include the uncertainty in the contribution from atmospheric storminess (recall that our central estimate of this contribution is zero, c/f section 3.2). We do however include the uncertainty in the projected regional time-mean sea level change, which is generally much larger than the range of modelled contribution from storminess change.

A1.6 Wave modelling

Section summary: In UKCP09, a perturbed physics ensemble from a single model (HadCM3) was used to drive the wave model WAM. In this work, an ensemble of 7 CMIP5 models is used to drive a global wave model in order to explore potential changes in wave climate around the UK. Three CMIP5 models are common to both the surge and wave projection work. The historical wave climate is compared with projections from RCP4.5 and RCP8.5 over the 21st century. The change in both average and extreme wave conditions are considered, with the latter most pertinent to coastal erosion and flood events. In addition, a regional atmosphere and regional wave model are used to provide downscaled climate projections for a single CMIP5 model. These simulations are used to assess the value added from high resolution wave projections around the UK coastline.

A1.6.1 Global wave model simulations

In addition to storm surges, wind-generated surface waves are important drivers of local extreme water levels. The surface wave field is made up of a spectrum of individual waves, which can be separated in terms of period into, long-period swell (often remotely generated), and locally forced windsea. The windsea waves are short and steep, and indicative of local wind conditions. The swell waves are representative of wind conditions in the wider North Atlantic, where most UK storms originate. Significant wave height (SWH) is a useful summary statistic to describe the average wave height in a spectral wave field. To investigate changes in average and extreme wave conditions, a mean and annual maximum (AnnMax) SWH are presented.

The COWCLIP community (Coordinated Ocean Wave Climate Projections; (www.jcomm.info/cowclip) aims to generate and share wave climate projections. An ensemble of global wave projections has been made publically available, as described by Hemer et al, (2012). This dataset consists of climate-model-driven global wave model simulations, which can be used to explore the influence of climate variability and change on the global wave field. The wave models analysed here are driven by climate projections from the fifth phase of the Coupled Model Intercomparison Project (CMIP5) Taylor et al, (2012).

The global models are analysed for the "historical" period (1980 - 2005) and "end-century" (2070-2099). Two future scenarios are compared: RCP4.5 and RCP8.5. We use a subset of the CMIP5 models utilised in the Land Strand projections (Table A1.6.1). These global wave models have a grid resolution of the order 1 degree and are driven directly by global climate model winds and ice-cover, with no intermediate downscaling step.

Climate model forcing	Project / data source
ACCESS1.0 (sister model of ACCESS 1-3)	COWCLIP
BCC-CSM1.1	COWCLIP
CNRM-CM5*	COWCLIP
EC-Earth*	RISES-AM
GFDL-CM3	COWCLIP
HadGEM2-ES*	COWCLIP
MRI-CGCM3	COWCLIP

Table A1.6.1. the seven CMIP5 models used to drive the global wave model simulations, and the data sources. * indicates that the model is also used in the surge model projections.

Six of the global wave model simulations have been carried out by CSIRO Oceans and Atmosphere Flagship. This data constitutes the Australian contribution to the Coordinated Ocean Wave Climate Project (COWCLIP). A global 1 degree implementation of WaveWatch III (v3.14) was forced with surface winds (at 3-hourly resolution) and sea-ice concentrations (linearly interpolated from monthly data). The model description and evaluation of the CMIP5 historical simulations are detailed in the submitted manuscript (Hemer and Trenham 2016). The global wave model simulations are forced with fields taken directly from each CMIP5 model, and wave data used in this report is 6-hourly SWH.

In addition to COWCLIP simulations additional set of simulations, forced by the EC-Earth model, were performed at the National Oceanography Centre as part of the EU RISES-AM project. The wave model configuration used was similar but not identical to the COWCLIP simulations. The simulations based on EC-Earth used the spectral wave model WaveWatch III version 3.14, (Tolman 2009; hereafter "WW3"). WW3 is a state-of-the-art 3rd generation wave model developed at NOAA/NCEP. Two model implementations were set up using WaveWatch III: (i) a global wave model domain, and (ii) a higher resolution nested domain covering the North East Atlantic. The global configuration consists of a Spherical Multiple Cell grid with a resolution of 0.703° (longitude) x 0.469° (latitude), extending from approximately 80 N to 80 S. The global wave model is forced by 3-hourly 10m winds and daily sea ice cover. The wave model in configured to use 36 directional bins (giving a directional resolution of 10 degrees) and 30 frequency bins, using a logarithmic distribution, with a minimum frequency of 0.04118 Hz. This spectral model approach is typical for wave applications, and a standard the wave growth and dissipation are driven using source terms. The source terms described in Tolman (2009) were chosen, to represent energy input and dissipation by bottom friction, depth-limited wave breaking and whitecapping following Cannaby et al, (2016). JONSWAP is used for dissipation by bottom friction and Battjes and Janssen for depth-limited breaking, with the dissipation constant set to the default value of 1. Ice in the global model is represented as a fractional cover between zero and one.

A1.6.2 Regional wave model simulations

The global wave models presented in section A1.6.1 have a relatively coarse resolution of the order 1° in latitude and longitude. These simulations are suitable to areas of deep water, away from the coast. However, higher resolution is required to capture coastal geometry, complex bathymetry, and shallow water wave transformations that are important for a complete representation of the total wave field around the UK coastline. Dynamical downscaling of atmospheric driving data using a regional climate model brings advantages including better resolution of deep low pressure systems and high winds which drive the largest waves. Adequate representation of these phenomena is particularly important for the UK, where small scale storm systems dominate the weather. Therefore, to investigate changing wave conditions at the coast, a regional wave model can be used to gain better representation of small-scale features, local-effects and peak wind speeds.

The EC-Earth model used in section A1.6.1 to force a global wave model, is also downscaled through a regional atmosphere model. The regional wave model runs were performed for the RISES-AM- project (Project ID: 603396. Funded under: FP7-ENVIRONMENT). These simulations make use of regional atmospheric models run under Euro-CORDEX. The 0.11° resolution regional atmospheric model, RCA4 with EUR-11 domain is used, which is the same regional climate model as used in the UKCP18 surge projections (Figure A1.3.2). The regional wave model is a configuration of WaveWatch III version 3.14, (Tolman 2009), and is forced at the surface by 6-hourly 10m winds.

The low temporal resolution of these winds may limit the ability to catch fast-moving systems crossing enclosed regional seas. This may reduce the skill in representation of growing seas with fetch-limited waves. The regional wave model domain covers 35.5N to 62.5N and -16.E to 10.5E (figure A1.6.1). The regional wave model is one-way nested, with no information being passed back to the global model. This configuration uses a regular latitude-longitude grid at 0.083° x 0.083° (~ 12 km) resolution. Further information and model evaluation are contained in Bricheno and Wolf (submitted 2018).

The regional wave model is forced at the surface with the downscaled EC-Earth atmosphere. Full wave spectra produced by the global wave model are provided to the regional wave model at the open boundaries at an hourly frequency. There is no ice cover in the regional wave model, and the model physics is configured as for the global simulation above. Unresolved islands are represented by a partial obstruction to the propagating wave energy. These are standard assumptions for regional wave modelling in this area, and we believe the added value of the regional model is relevant to improving coastal resolution, while not deteriorating the quality of the global wave model. The model simulations presented here are limited to a representation of offshore waves and will not include nearshore transformation processes such as wave set-up, run-up, and swash.

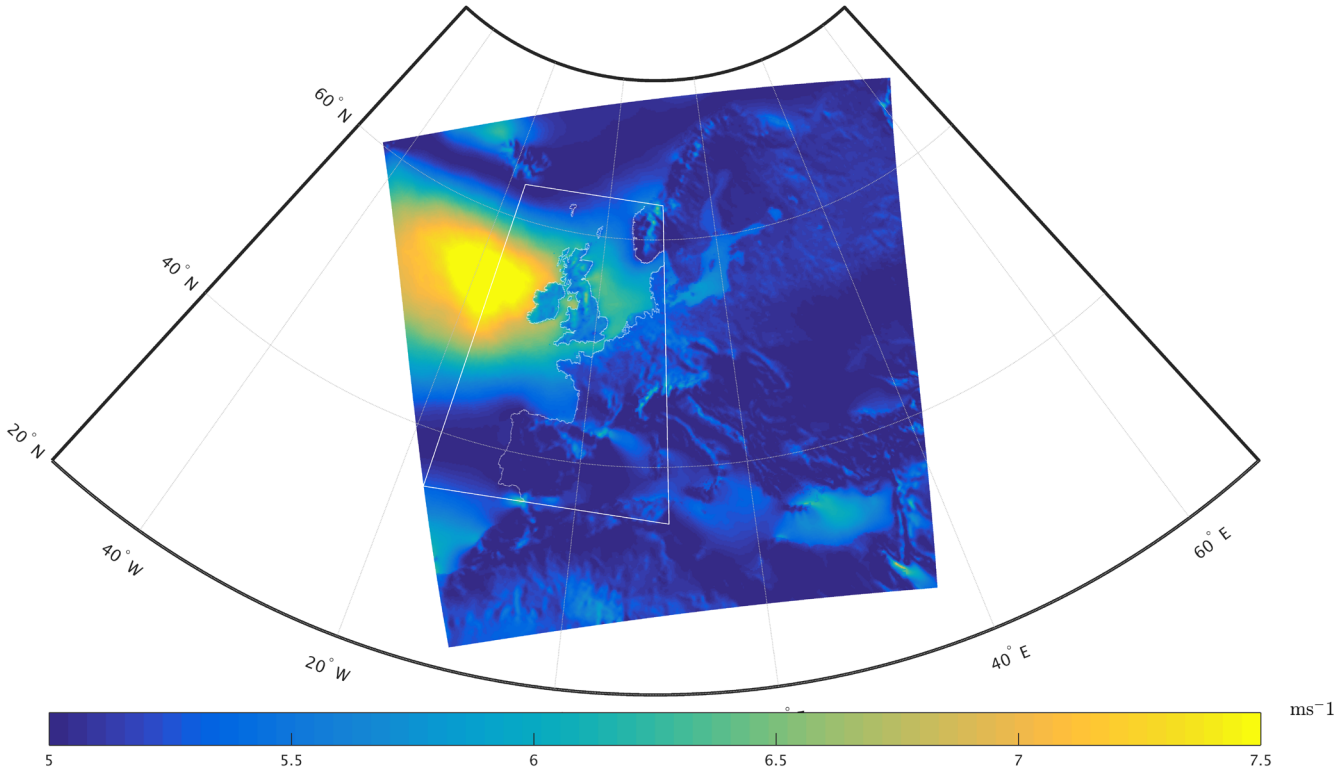

Figure A1.6.1. RCA regional climate model annual average wind speed (coloured), and wave model domain outlined in white.

Continuous simulations have been run with the regional wave model covering the period 1970 - 2100. After 2005 the `future' scenarios diverge and we have investigated two possible scenarios: RCP4.5 and RCP8.5. The future wave projections have been run continuously from 2006 to 2100. However, as the present-day refers to a model climatology (and not historical weather conditions), a hindcast has also been run forced by ERA-Interim winds for the period 1979-2015. This hindcast period is first used to validate the model performance (See section A2.4).

Years run	Global wind forcing
1979-2015	ERA_interim
1970-2005	Historical EC-Earth
2006-2100	RCP 4.5 EC-Earth
2006-2100	RCP 8.5 EC-Earth

Table A1.6.2. Summary of wave model simulations for section A1.6.2.

In order to focus on coastal changes, SWH at the closest model point to land is taken, and plotted in an 'unwrapped' coastal strip (see for example figure 3.3.1). The x-axis for these plots represents a progression anti-clockwise around the UK mainland, beginning at the Bristol Channel. The coastal strip plots, as well as showing the baseline ("historical") wave conditions, show a percentage change in both mean and AnnMax. Similarly, the multimodel ensemble plots show a relative change to the historical baseline. The coastal strip plots are set in context by the maps in figure A1.6.2.

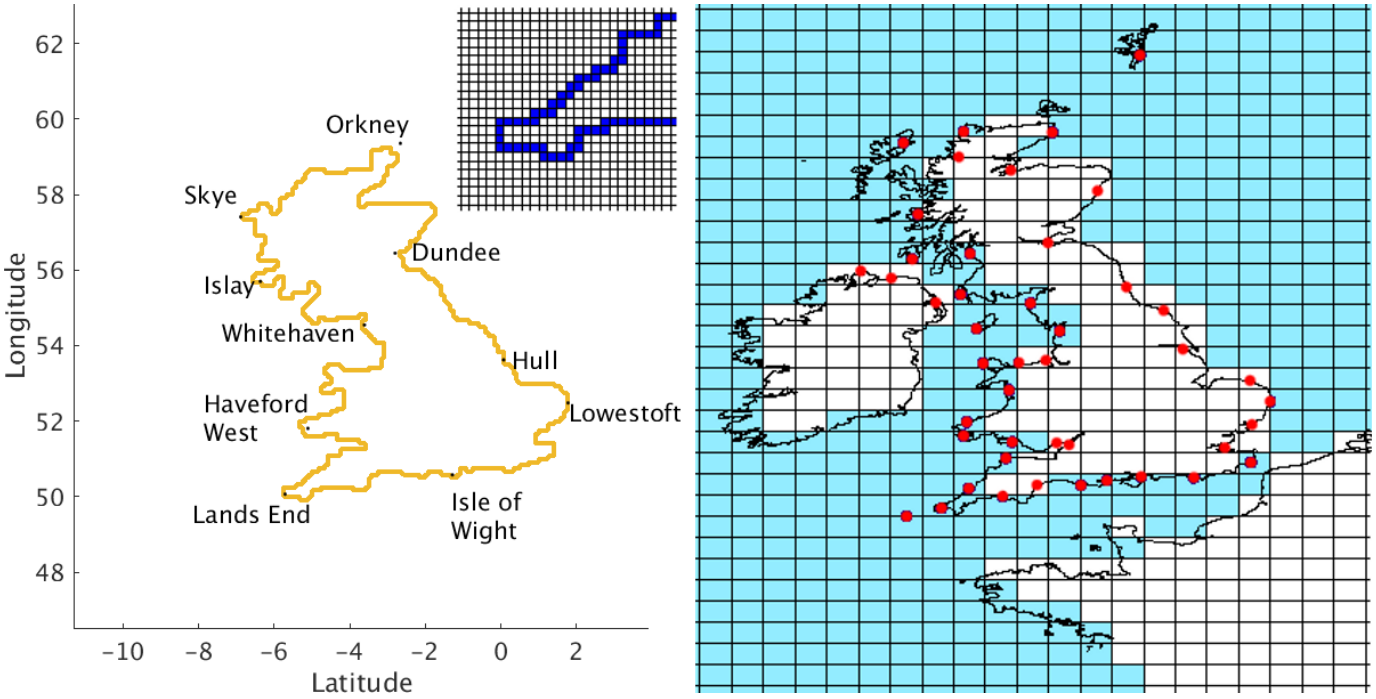

Figure A1.6.2. Regional wave model grid points where coastal strip plots are extracted from (left), and locations of class-A gauges used, with corresponding global wave model grid (right). An inset showing the regional model resolution around SW England is shown in the left-hand panel.

A1.6.3 Statistical methods

Zappa et al, (2015) suggested that a climate-related signal emerges sooner from the natural variability if seasonal averages rather than an annual mean are used to examine the climate response. This suggests that by considering extreme winter waves, we may be able to see emergent signals more easily than by looking at the annual means.

To minimise the impact of internal natural variability, thirty-year averages of mean and mean annual maximum (AnnMax) SWH are taken. The maps plotted in section 3.3 show the absolute change between the historical period (1981-2000) and end century (2081-2100). A masking has been applied to regions where there is a poor signal-to-noise ratio. Following the approach used by Wakelin et al, (2015), the Kruskal-Wallis test (Kruskal and Wallis 1952) test is applied to SWH - where the change between two simulations is small compared with inter-annual variability.

Wave height has a very large range, dependent on whether conditions are calm, or a storm is passing. This leads to a large variability in SWH, making any change signal in wave conditions hard to identify from the noise. In order to separate out physical changes from a noisy background, statistical methods such as a Kruskal-Wallis test (Kruskal and Wallis 1952) can be used. This is a non-parametric test to determine whether one sample population is significantly different from another. Applying a KW-test to compare a distribution of future wave height with the recent past, we can assess whether the modelled wave conditions have changed in a statistically significant way.

In Figure 3.3.2 black shading is used where the KW-test falls below 50 %, grey shading indicates a KW-test score of between 50% and 75 %. Where there is no shading, there is higher than a 75% chance that the future wave conditions are different to the historical conditions, rather than masked by natural variability.

A1.7 Shelf seas modelling

Section summary: UK tide gauge records clearly illustrate the year-to-year variability in coastal sea level that will be superimposed on the longer-term sea level rise. In this section we make use of a high resolution coastal ocean model to estimate the magnitude and spatial characteristics of coastal sea level variability around the UK. This information is designed to aid the interpretation of tide gauge records and to be used alongside the UKCP18 regional time-mean sea level projections.

Tide gauge records of sea level around the UK are characterised by substantial variations on both interannual and decadal timescales. This variability has been linked to large-scale climatic drivers, such as the North Atlantic Oscillation (Roberts et al, 2016). UK tide gauge records show year-to-year changes in annual mean sea level of several cms, which means that variability is an important consideration for coastal decision makers who are often working on timescales of a few decades or shorter. Since there are relatively few long continuous tide gauge records around the UK coast, we use simulations from a 7km model of the European Shelf Seas in order to gain insights into the magnitude and spatial coherence of sea level variability around the UK. This information is designed to be complementary to the time-mean sea level projections discussed in the previous sections and to aid the interpretation of the available tide gauge records (e.g. to determine how far along the coast observed variability characteristics can be extrapolated). Here we present a brief overview of the modelling strategy and model configurations. We refer the reader to Tinker et al, (in preparation) for further information.

A1.7.1 Model configurations

In order to estimate the spatial characteristics of coastal sea level variability around the UK we make use of simulations from a state-of-the-art global coupled climate model (HadGEM3 GC3.0) and a 7km resolution regional European Shelf Seas Model (NEMO CO6) in a "nested" model configuration (Figure A.1.7.1). A long present-day control run of HadGEM3 GC3.0 is used to simulate about 270 years of climate and weather variability. This simulation is then dynamically downscaled using the NEMO CO6 regional ocean model to provide greater regional detail and important shelf seas processes that are missing from the global climate model, most notably tides. The modelling approach used here is very similar to that used in the UKCP09 European continental shelf waters projections.

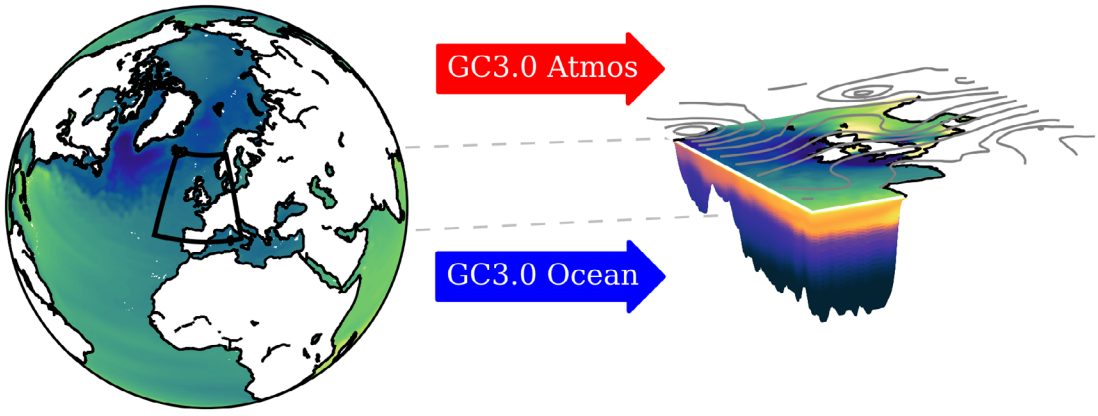

Figure A1.7.1. Schematic of the "nested" model configuration showing how HadGEM3 GC3.0 (left, showing surface elevation) is used to drive Nemo Coastal Ocean version 6 (CO6, right, showing surface elevation at a particular stage of the tide, the boundary temperature structure (from HadGEM3) and the time-mean sea level pressure contours (also from HadGEM3). HadGEM3 atmospheric (red arrow) and oceanic (blue arrow) model output are used to drive NEMO CO6, which uses climatological data for the boundary at the Baltic Sea and rivers.

Table A1.7.1. Summary of the model configurations.

	HadGEM3 GC3.0	NEMO CO6
Main reference	Williams et al, (2018)	O'Dea et al, (2017)
Domain extent	Global	40°4' N, 19° W to 65° N 13° E
Horizontal resolution (atmosphere)	N216 grid, ~50 km for UK	N/A
Horizontal resolution (ocean)	ORCA025 grid, ~15 km for UK	1/9° x 1/15° grid, ~7km for UK
Ocean vertical grid	75 z-coordinate levels	50 sigma-levels (i.e. terrain following)

The HadGEM3 GC3.0 climate model is essentially the same physical model as the 3.1 version being used for the UKCP18 Land Projections. One of the main improvements of the 3.1 version over 3.0 is a reduction in the well-documented Southern Ocean warm bias (see Williams et al, 2018 for a discussion). Of particular relevance here is the skill of HadGEM3 GC3.0 in representing important aspects of climate and weather variability the UK region, such at the North Atlantic Oscillation (Scaife et al, 2014).

The NEMO CO6 model is a state-of-the-art regional European Shelfs Seas model and is very similar to the configuration described by O'Dea et al, (2017). This model forms the basis of the Met Office operational ocean forecasts and has much improved performance over the previous POLCOMMS system (O'Dea et al, 2017), which was used in UKCP09. Atmospheric, oceanic and riverine model output from HadGEM3 GC3.0 are used to produce the lateral and surface boundary conditions, following a similar approach to Tinker et al, (2015; 2016). The NEMO CO6 model is forced with sub-daily surface fields with daily forcing of the lateral ocean open boundaries and riverine inputs. This "one way" nested model is run for approximately 270 years. The first 70 years is discarded as spin-up owing to substantial drifts in sea level and shelf water properties. The remaining 200 years is used to characterise the spatial patterns and magnitude of coastal sea level variability around the UK, in conjunction with the available tide gauge observations.

A2. Model evaluation

A2.1 Time-mean sea level

Section summary: CMIP5 climate models, which form the basis of the time-mean sea level projections in UKCP18, show a marked improvement in their simulation of observed sea level compared to the previous generation of CMIP3 models. The CMIP5 models are able to capture well the observed large-scale horizontal variations in time-mean oceanographic sea level. The models show a diverse representation in spatial patterns and magnitude of interannual variability with some comparing remarkably well with satellite observations. In terms of global mean sea level, CMIP5 model simulations are able to reproduce the majority of the observed rise over the 20th Century and capture the acceleration since the 1960s. Comparisons with individual tide gauge records show that regional sea level trends are also captured, with best agreement during the latter half the 20th Century.

A2.1.1 Spatial patterns of oceanographic sea level in CMIP5 models

Landerer et al, (2014) have assessed the ability of 33 CMIP5 models (Taylor et al, 2012) to replicate the time-mean, seasonal cycle and spatial patterns of variability of sea level using satellite altimeter observations. The authors note that the CMIP5 simulations of sea level are markedly improved compared to those of CMIP3 models (Meehl et al, 2007), which formed the basis of the IPCC 4th Assessment Report (Bindoff et al, 2007) and the UKCP09 sea level projections (Lowe et al, 2009). We present a similar analysis to that of Landerer et al, (2014), including results for only those CMIP5 models that are used to determine the oceanographic sea level response in the UKCP18 sea level projections (Figures A2.1.1 and A2.1.2), as described in section A1.1.2.

In general, the subset of CMIP5 models used in UKCP18 do a good job of capturing the observed large-scale spatial characteristics of the time-mean oceanographic (i.e. the shape of the sea surface that arises from horizontal variations in sea water density and ocean circulation) sea level and show spatial correlations with the satellite data ranging from 0.96-0.98 (Figure A2.1.1; Landerer et al, 2014). While the multi-model mean presented by Landerer et al, (2014) shows a spatial correlation of 0.99 and modest biases in time-mean sea level that rarely exceed 0.2m, individual CMIP5 models often show biases of up to 0.5m. These biases tend to be largest in tropical regions and the Southern Ocean and are thought to relate to documented biases in the corresponding wind stress fields (Landerer et al, 2014). In general, the simulations of time-mean sea level from higher resolution models show the best agreement with satellite altimeter observations (Figure A2.1.1; Landerer et al, 2014).

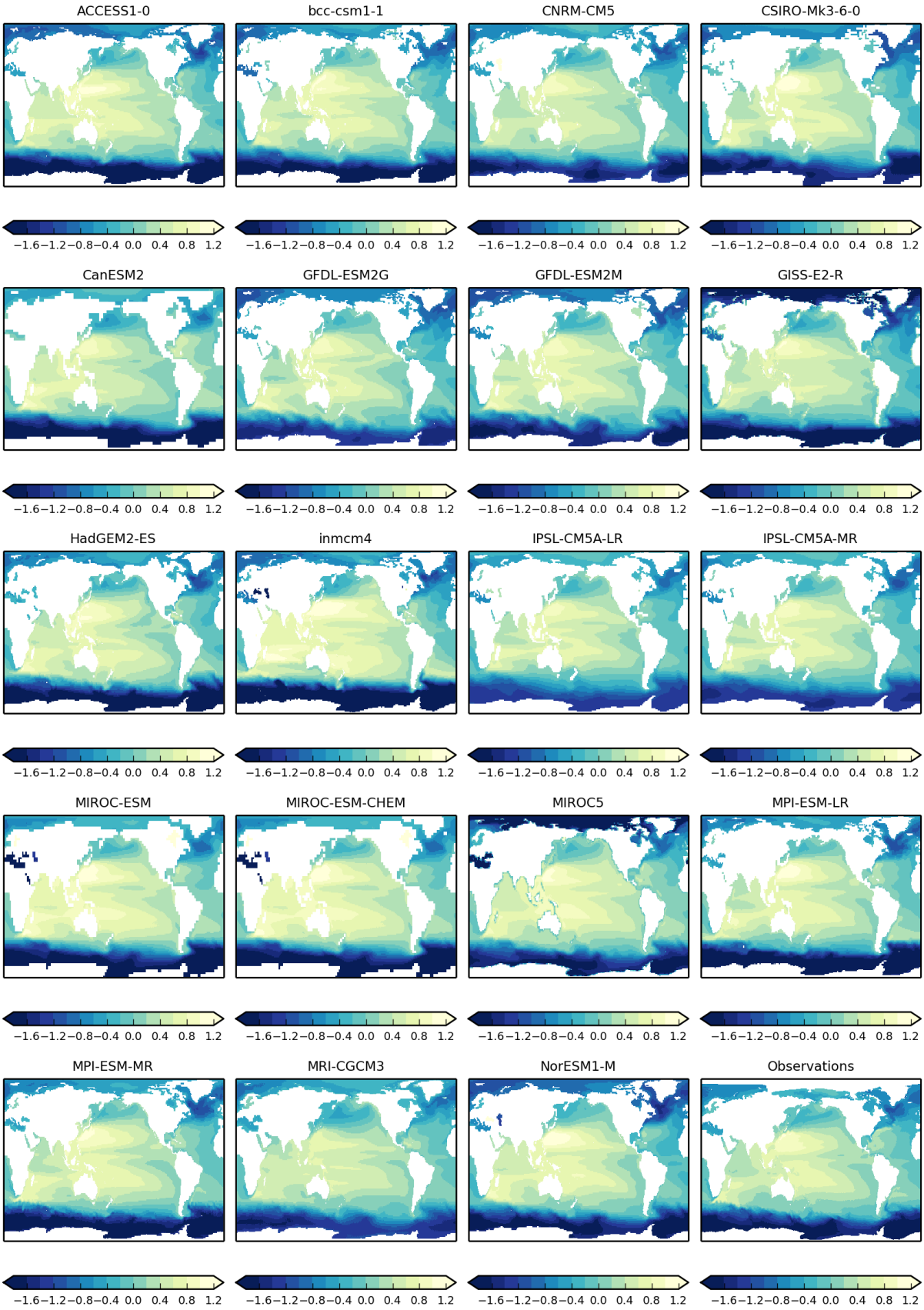

Figure A2.1.1. Variations in the shape of the sea surface (in metres) that arise from water properties and ocean circulation ("oceanographic" sea level) for the CMIP5 models used in the UKCP18 regional projections. HadGEM2-CC and NorESM1-ME are not shown because they give very similar results to their sister models HadGEM2-ES and NorESM1, respectively. The observations come from the AVISO+ level 4 estimate of mean dynamic topography (the estimate of the sea surface height above the geoid). All panels show the time-mean for the period 1993-2012, when CMIP5 model results use data from the historical simulations for the period 1993-2005 and RCP4.5 thereafter. For the purposes of the model comparison, all panels are set to have an area-weighted average of zero. The representation of coastlines in each panel is indicative of the underlying model resolution.

The comparison of interannual variability of oceanographic sea level in CMIP5 models with satellite observations shows a diverse representation among the models (Figure A2.1.2). Much of the real-world sea level variability on these timescales is dominated by the mesoscale eddy activity, i.e. the "ocean weather systems", an aspect of the ocean dynamics that is parameterised in CMIP5 models. This lack of eddy representation in CMIP5 models leads to an underestimated sea level variability, particularly in eddy rich regions such as western boundary currents (e.g. the Gulf Stream) and the Southern Ocean. Despite this, some models do a remarkably good job of capturing both the spatial patterns and magnitude of interannual sea level variability. As noted by Landerer et al, (2014), there is no obvious relationship between those models that show most skill in simulating the time-mean sea level (Figure A2.1.1) and those that do the best job of simulating interannual sea level variability (Figure A2.1.2).

It is important to stress that the large-scale pattern of the time-mean sea level (Figure A2.1.1) is an emergent property of the climate models. Errors in the shape of the sea surface can reflect deficiencies in the ocean water mass properties, their distribution, and/or the mean ocean circulation. The comparison of variability is somewhat hampered by the lack of explicit representation of mesoscale eddies in the simulations, but it shows just how much variability can differ between models and it also shows that some models do a remarkably good job. Since we do not use the CMIP5 models to estimate sea level variability around the UK, any deficiencies in this aspect will not directly impact our time-mean sea level projections. The diversity of model representation can be seen as a strength of the CMIP5 multi-model ensemble: it helps to span the climate change uncertainty, and results in a broad range of emergent patterns of oceanographic sea level change (e.g. Slangen et al, 2014; Bilbao et al, 2015). There is potential for using observed ocean changes to reduce the uncertainty in future projections of oceanographic sea level and this remains the subject of ongoing research.

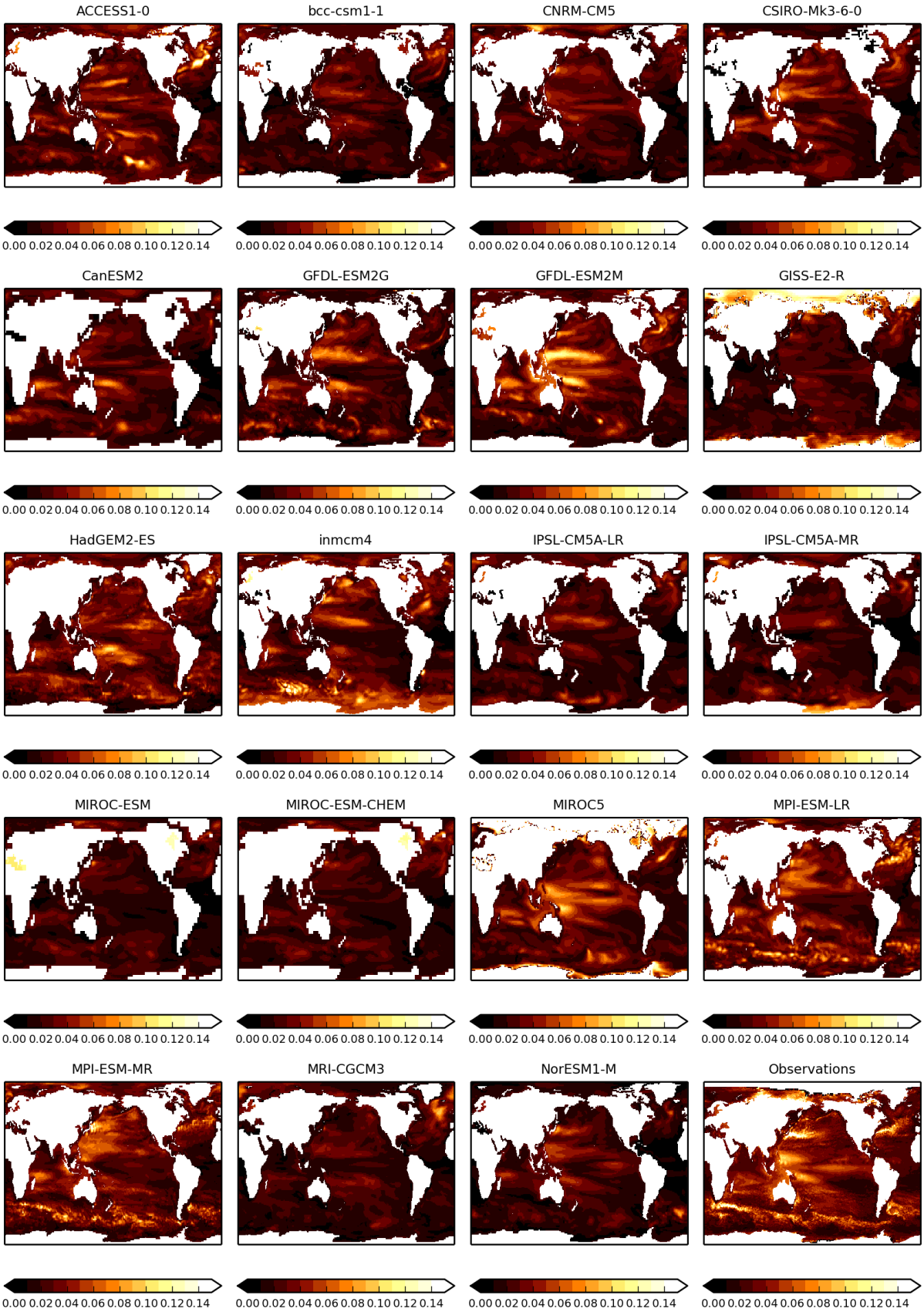

Figure A2.1.2. The standard deviation of annual-mean sea surface height (metres) for the model simulations shown in Figure A2.1.1, highlighting the spatial patterns and magnitudes of interannual sea level variability. The satellite altimeter observations come from the ESA CCI Sea Level data version 2.0 (http://www.esa-sealevel-cci.org/). All data are for the period 1993-2012, inclusive.

A2.1.2 CMIP5 simulations of sea level change over the 20th century

CMIP5 model simulations of historical sea level change over the 20th Century have been evaluated in a two-part study by Slangen et al, (2017) and Meyssignac et al, (2017). The authors carried out a detailed comparison of sea level simulations of 12 CMIP5 models with the available observations over the period 1900-2015, focussing on tide-gauge based reconstructions of global mean sea level (GMSL) and individual tide gauge records. The two studies included all components of the global sea level budget, with CMIP5 model-derived ice mass terms and representation of the associated spatial fingerprints (see section A1.1.2). Here, we present the key findings of those studies and refer the reader to the manuscripts for more details.

Slangen et al, (2017) found that CMIP5 model simulations are able to explain 50% ± 30% of the mean observed change in GMSL over the 20th Century (Figure A2.1.3a), which rises to 75% ± 38% when accounting for model biases relating to the documented non-equilibrium response of the ice sheets and deep ocean not represented in models (Figure A2.1.3b). In addition, a more recent tide-gauge based GMSL reconstruction (Dangendorf et al, 2017) shows a lesser rate of sea level rise over the first half of the 20th Century and suggests a more favourable comparison with the CMIP5 model simulations. In any case, the model simulations generally compare favourably with GMSL reconstructions for the latter half of the 20th Century and capture the observed acceleration of sea level rise over this period (Figure A2.1.3).

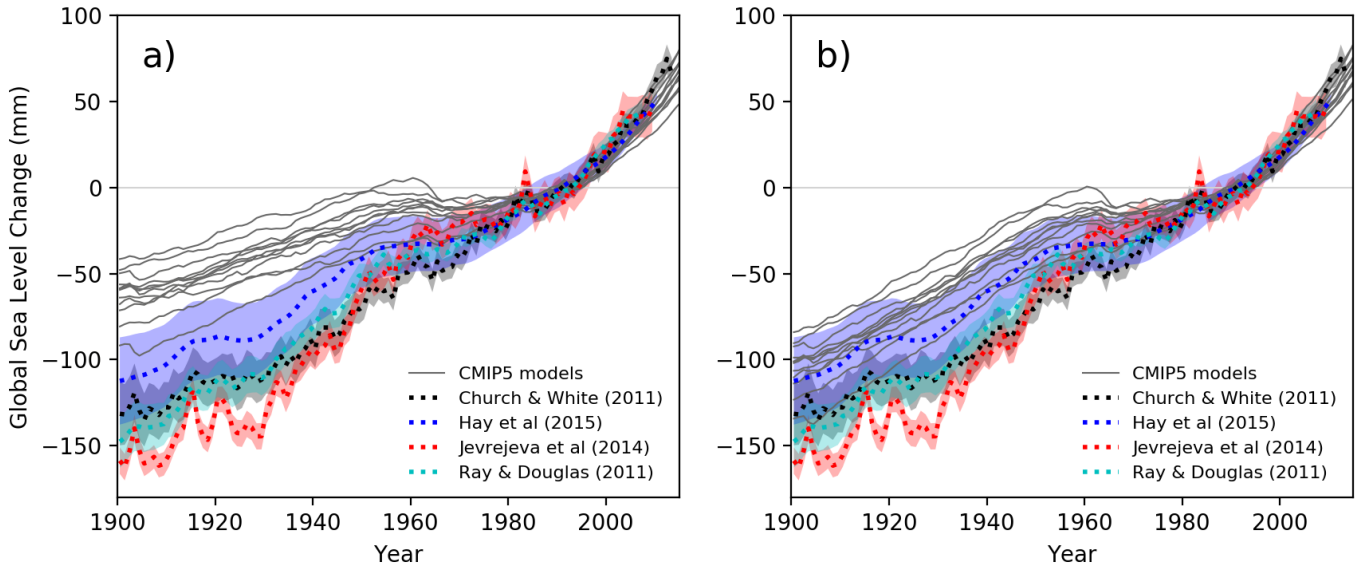

Figure A2.1.3. Adapted from Slangen et al, (2017). Modelled total sea level change (1900–2015; mm) for 12 CMIP5 models (grey lines) compared to observational reconstructions, relative to a baseline period of 1980–2000, showing models (a) excluding and (b) including proposed corrections for glaciers and ice sheets. Observational reconstructions (dotted lines) are Church and White (2011) in grey, Hay et al, (2015) in blue, Jevrejeva et al, (2014) in red, Ray and Douglas (2011) in cyan; shading indicates observational uncertainty (5th to 95th percentiles). © American Meteorological Society. Used with permission.

At local scales, the CMIP5 models are able to capture some of the inter-decadal variations in sea level rise at a number of tide gauge locations around the world, associated with changes in climatic forcing over the 20th Century, (Figure A2.1.4, e.g. Key West, Midway Island, Fremantle). They also seem to capture the magnitude of sea level variability at many tide gauge locations (Figure A2.1.4, blue shaded regions compared to variability in black lines). Similar to the global results, the agreement between tide gauge observations and CMIP5 model simulations tends to be improved during the latter half of the 20th Century. Meyssignac et al, (2017) note that glacial isostatic adjustment (GIA) dominates spatial variations in the long-term rate of sea level rise at tide gauge locations and emphasise the need to consider non-climatic processes, such as groundwater extraction, in order to fully account for observed local sea level change.

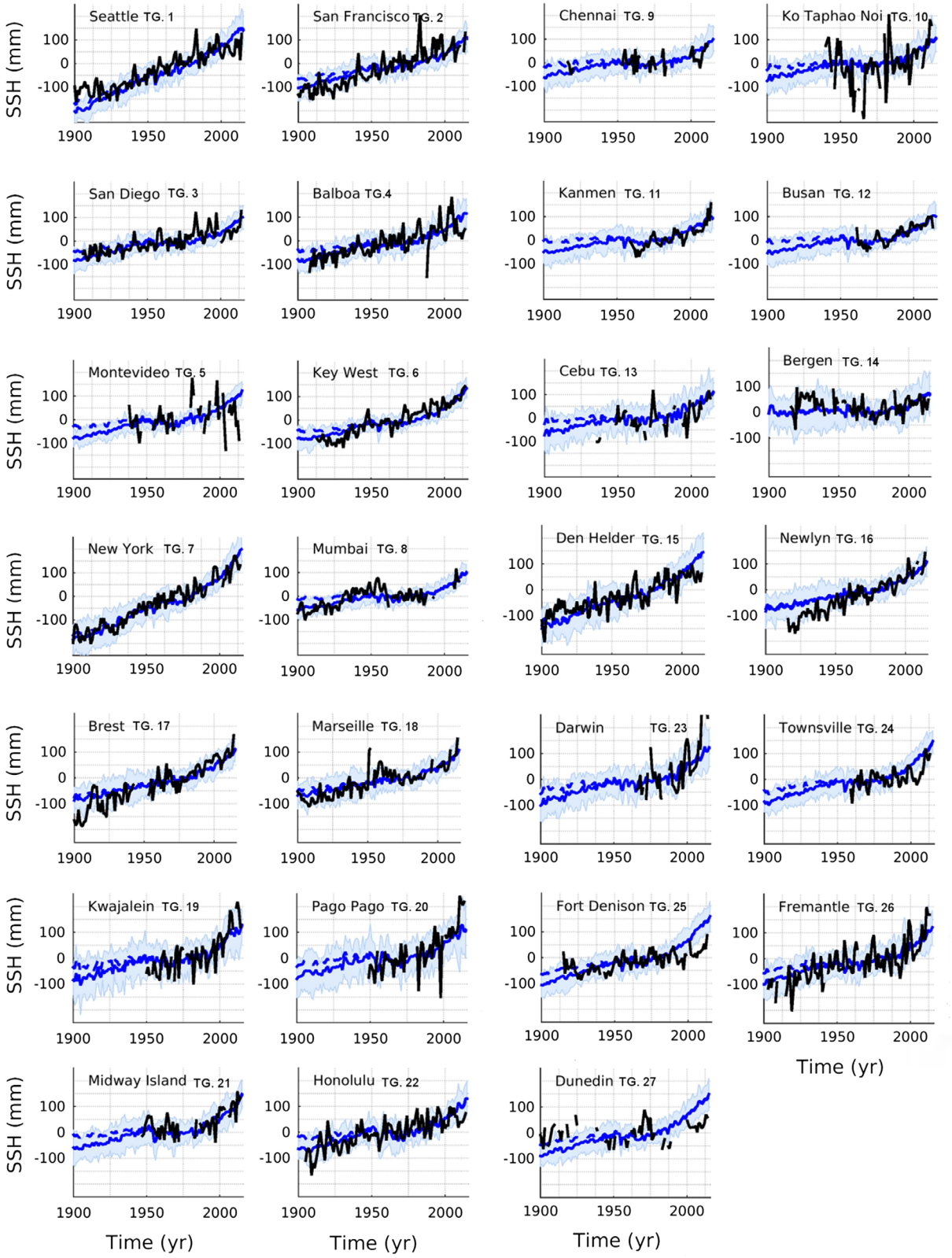

Figure A2.1.4. Reproduced from Meyssignac et al, (2017). Total simulated annual local sea level with (blue solid curve) and without (blue dotted curve) the proposed correction for glaciers and ice sheets at tide gauge stations against tide gauge records (black curve). The shaded blue areas represent the ensemble spread (5th to 95th percentile range) of the simulated sea level. © American Meteorological Society. Used with permission.

A2.2 Evaluation of atmospheric driving data

Five global models (CNRM-CM5, EC-EARTH, IPSL-CM5A-MR, HadGEM2-ES, MPI-ESM-LR) were selected from the CMIP5 models for downscaling by the Swedish Meteorological and Hydrological Institute regional climate model RCA4 (see section A1.3.2) as part of the Euro-Cordex project on the basis of their ability to simulate a realistic climatology, particularly for the European region. For our purpose the simulation of the storm track is of particular relevance. To assess this, in Figure A2.2.1 we compare one metric of storminess as realized in the historical simulations by the global models selected for downscaling by RCA4 with the corresponding reanalysed data from ERA-interim (Dee et al, 2011). Also shown is GFDL-ESM2M. All CMIP5 models with available data are shown by the 'cloud' of grey lines in the background of each panel. The Y-axis is the zonal mean of number of storms per month crossing a 5 degree spherical cap around each point in a longitudinal window from 5 degrees west to 25 degrees east during December, January and February for a period representing the climate of the recent past (1976-2005 for the CMIP5 models and 1980-2009 for the reanalysis data). Using this metric, we can see that storm track biases are large in some of the CMIP5 models. Zappa et al, (2013) found that the storm-track response of a subset of models with low biases was similar to the mean response of all of the CMIP5 models, suggesting that the broad features of the North Atlantic and European response are only weakly sensitive to the historical biases. By comparing our selected models with the cloud, we can see that all six models in our selection have relatively small biases, and the five models selected for downscaling by RCA4 are in good (in some cases very good) agreement with the observations, which are shown by the black line in each panel.

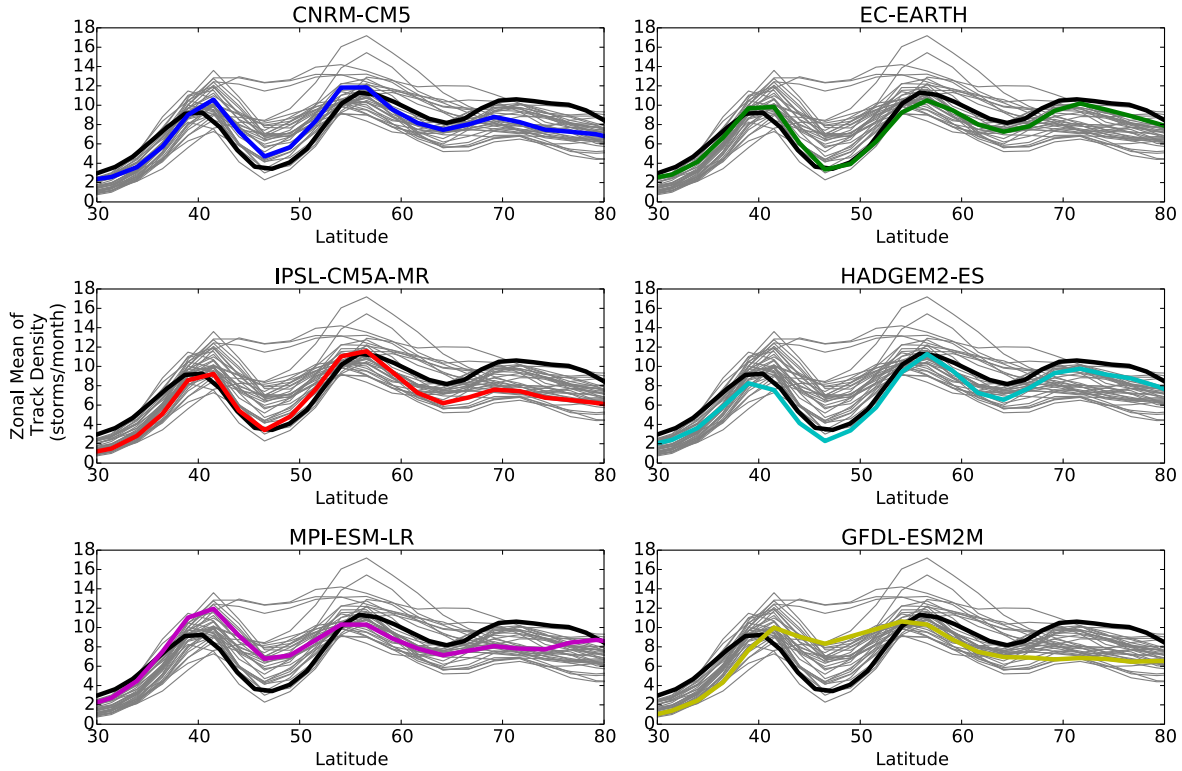

Figure A2.2.1. Evaluation of the north-east Atlantic storm tracks in the five driving GCMs which were selected for downscaling by RCA4, and in GFDL-ESM2M. December-January-February (DJF) zonal mean storm track density (zonal mean of number of storms per month crossing a 5 degree spherical cap around each point in a longitudinal window from 5 degrees west to 25 degrees east) in the CMIP5 historical simulation (coloured solid lines). The black line shows ERA-interim data, regarded here as 'truth' (i.e. the best available guide to the real-world behaviour). The grey lines show all CMIP5 models with available data. For full details see text.

A2.3 Evaluation of storm surge model

Section summary: Our simulations are downscaled from general circulation models which evaluate well against observed storm tracks (see section A2.2). Simulated skew surges show a similar relationship between changes of intensity and changes of frequency of extreme events to the relationship seen in the tide-gauge records; in other words, the variability of the extremes is well-simulated.

The components of our storm surge modelling system have been extensively evaluated: a very similar surge model (CS3X) is used operationally to provide coastal flood warnings in the UK as part of the Storm Tide Forecasting Service (STFS), and model performance is routinely monitored at the National Oceanography Centre Liverpool by comparing forecast results with observations every month. Typical root-mean-square errors are about 10cm (e.g. Furner et al, 2016 and http://www.ntslf.org/storm-surges/storm-surge-model). The operational model has been shown to perform particularly well during extreme storm surges in the southern North Sea (Horsburgh et al, 2008), forecasting surge in the Thames estuary to within 10cm when driven by re-analysed meteorology. Further evaluation of the modelling system was reported in UKCP09 (Lowe et al, 2009) and TE2100 (Howard et al, 2008).

To make a comprehensive comparison of simulated extremes with observations for the historical period, we compare return level curves of skew surge from nine tide gauges with the corresponding data from the nearest grid-point in the surge model, in Figure A2.3.1. We show model data for the historical simulations (1971-2005 inclusive) by each of the RCA4-downscaled models (yellow in the figure), model data for a simulation driven by reanalysed data (ERA-interim, 1981-2009 inclusive, Dee et al, 2011, black in the figure) and the tide gauge data (in red). In this context, a historical simulation means only that the radiatively-active gas concentration is based on observations, whereas the reanalysis is an attempt to reconstruct the weather of a period consistent with assimilation into a numerical weather prediction model.

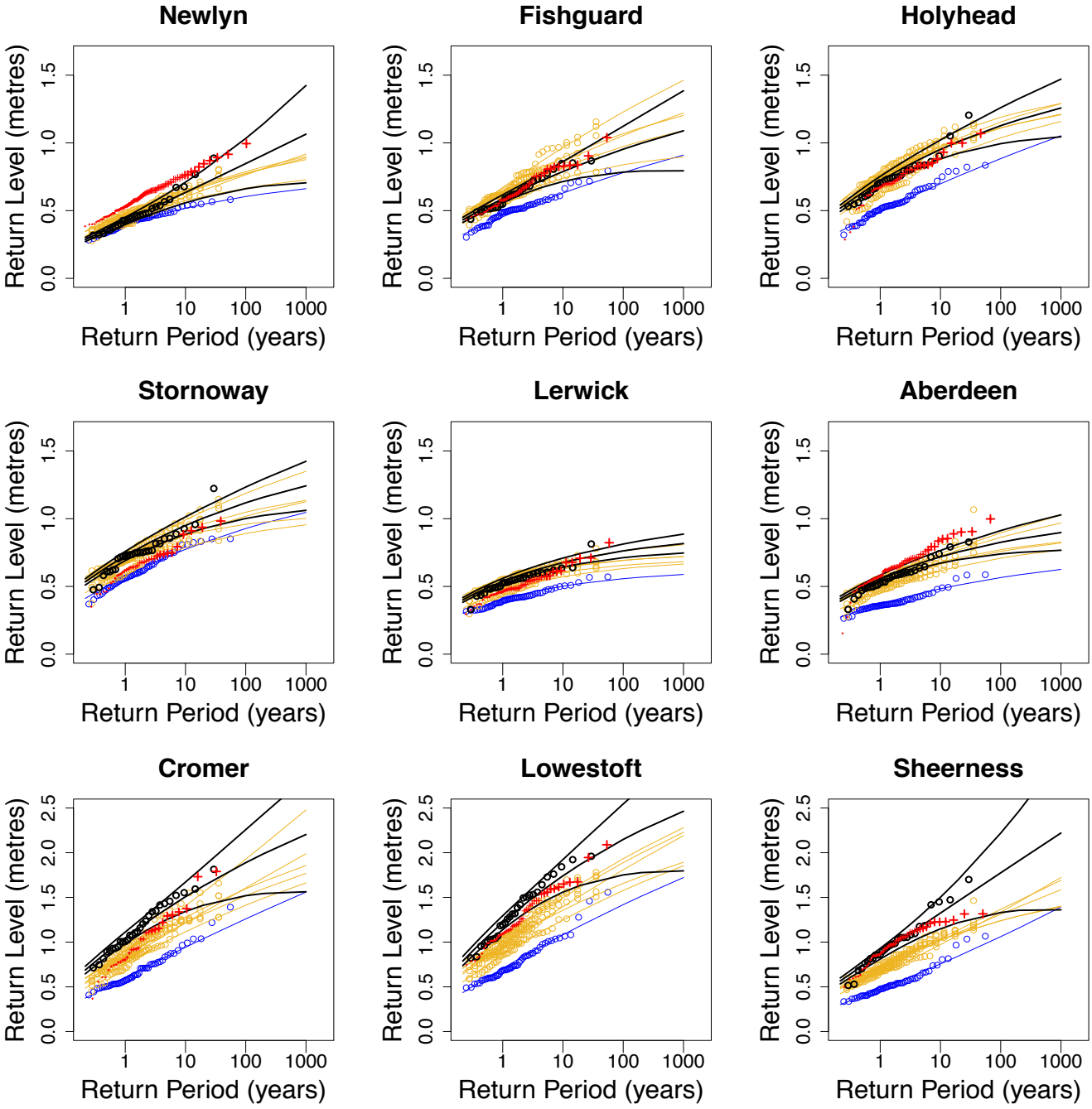

Figure A2.3.1. Skew surge return level plots for evaluation. Red points: observed annual maxima of skew surge from tide gauges. Black points: 29 simulated annual maxima (1981-2009 inclusive) from ERA interim evaluation simulation. Black lines: maximum likelihood estimator and 5th and 95th percentile fitted curve based on the 5 largest events per year from ERA interim evaluation simulation. Yellow points: 35 annual maxima (1971-2005 inclusive) from historical simulations by each of the RCA4-downscaled simulations. Yellow lines: maximum-likelihood fit based on the 5 largest events per year from historical simulations by each of the RCA4-downscaled simulations. Blue points: 35 annual maxima (1971-2005 inclusive) from the GFDL-ESM2G historical simulation. Blue lines: maximum-likelihood fit based on the 5 largest events per year from the GFDL-ESM2G historical simulation. Analysed tide gauge data courtesy of National Oceanography Centre Liverpool.

From Figure A2.3.1 we can see that:

(1) The skew surge extremes from the RCA4-downscaled simulations are in places offset from the observed surges (for example at Newlyn by about 15cm). This size of bias is not unusual in surge modelling (see for example Sterl et al, 2009, their figure 3). The bias may be associated with the more complex coastline around the tide gauge, which will not be well-represented in the model (c/f Batstone et al, 2013, and our Figures 3.1 and A1.3.3). The bias is generally larger in the GFDL-ESM2M simulation (which does not include the regional downscaling step). However, a more important consideration is that:

(2) For any given site, the gradients of all of the fit lines at return period of one year are all comparable (with the possible exception of the GFDL-ESM2M gradient at Aberdeen), i.e. within each panel of Figure A2.3.1 all lines are near-parallel at the one-year return period. This indicates that the models evaluate well (see again Sterl et al, 2009) as it means that the models show a similar relationship between ***changes of intensity*** and ***changes of frequency*** of extreme events to that relationship seen in the tide-gauge record for any given site.

A2.4 Global and regional wave models

Global wave models forced by CMIP5 "historical" simulations are compared against a corresponding ERA-Interim reanalysis forced simulation, to evaluate their skill in reproducing the observed wave climate. All 7 models used are seen to be capable of capturing the spatial patterns in mean and annual maximum wave climate, with above 95% correlation. The models show some degree of bias when compared with reanalysis data, with the mean wave heights biased low, and annual maxima biased high. There is no evidence of spatial correlations between the model biases and the signals of wave climate change projected.

The multi-model approach used here is an improvement on the perturbed physics, single model approach used in UKCP09. Our ensemble approach allows a wider coverage of the uncertainties regarding the representation of North Atlantic storm track strength and position. Though some absolute bias exists in the CMIP5-forced wave models, we can make useful projections by combining the baseline conditions with the relative changes projected.

A new global and regional wave model configuration is assessed using wave buoy observations of significant wave height (SWH), wave period, and wave direction. The temporal variability is well captured by the model, as indicated by the low root-mean-square error. Significant wave height is slightly under-predicted in the model, especially during high wave events. For SWH there is little skill gained when moving from the coarse-grid to the higher resolution models, however, the results have more granularity and coastal detail. The wave direction is seen to improve significantly in the higher resolution model.

Both global and regional configurations are then driven by the EC-Earth climate model, as this has been assessed to be the best model at capturing storm track and spatial patterns of baseline wave conditions.

A2.4.1 Global wave model simulations

As well as forcing the global wave model with winds from 6 CMIP5 climate models, the same configuration was also run with surface forcings from NCEP CFSR historical atmospheric reanalysis (http://cfs.ncep.noaa.gov/cfsr/). In this way, wave model performance can be evaluated against real weather events. The global wave model configuration has been evaluated in detail in Hemer et al, (2013), and Hemer and Trenham (2016). Their reanalysis run of Hemer (2013) slightly overpredicts annual mean SWH over northern Europe by of the order 0.3 m, with the largest biases seen over open ocean areas, including the North Atlantic. The overestimation of SWH is greater during winter months, with higher positive biases recorded in the North Atlantic basins during winter. Hemer and Trenham (2016) evaluate an ensemble of CMIP5 global wave models, finding the multi-model mean SWH is biased low, by of the order 0.5m, with largest errors seen in the Southern Ocean and North Atlantic.

In the present work, our global wave model simulations forced by the "historical" CMIP5 model data show biases in the wave climate compared to corresponding simulations forced by the ERA-Interim reanalysis. Mean and annual maximum (AnnMax) SWHs for the historical period 1981-1999 from the COWCLIP models were compared against the wave climate in the reanalysis run. While the climate models include (to our best knowledge) the important climate forcings for the historical period, each CMIP5 model includes essentially random internal climate variability; the models are "free-running" and are not tied to real-world short-term individual weather events by data assimilation in the way that the ERA-Interim reanalysis is. Therefore, we can only compare the statistical representation of wave climate, rather than individual events.

Analysis of CMIP5 models by Zappa et al, (2013) shows that too many cyclones are found in the east Atlantic, which would lead to an overprediction of strong winds in this area (confirmed by the positive biases in AnnMax seen in table A2.4.1. When compared with the ERA-Interim run (which we are treating as historical 'truth'), all but one of the CMIP5 models were biased low when comparing the mean SWH. However, many members of the model ensemble were also seen to over-estimate the AnnMax SWH. These biases arise primarily from deficiencies in the CMIP5 models' ability to simulate the position of the storm track, and the intensity of local wind fields. Those CMIP5 models performing the best at capturing the position of the storm track (with respect to ERA-Interim cyclone track position at 0 degrees E) are HadGEM2-ES, EC-Earth, and GFDL CM3. The storm track is too far south in BCC, CNRM and MRI-CGCM3. ACCESS is not assessed in Zappa et al, (2013). It is important to note that the biases in the 7 models evaluated are not spatially correlated with the change signals observed in those models, i.e. we can separate out the relative changes from the model biases. This is the case for both the patterns of mean and AnnMax SWH change.

Model name	% bias in mean SWH (direction)	% bias in AnnMax SWH (direction)
ACCESS	31.5% (negative)	14.7% (positive)
BCC	26.8% (negative)	17.1% (positive)
CNRM	35.2% (negative)	26.7% (positive)
EC-Earth	5% (positive)	13% (positive)
GFDL CM3	29.4% (negative)	16.7% (negative)
HadGEM	33.4% (negative)	16.7% (positive)
MRI	13.0% (positive)	34.6% (positive)

Table A2.4.1. Percentage bias in historical wave conditions from 7 COWCLIP models, compared with ERA-Interim run.

Given these CMIP5 limitations, our analysis of future projections focuses on relative changes in the wave field, rather than absolute changes. We also want to use this dataset to investigate how wave climate changes around the UK coast. This means that accurately representing the spatial patterns of SWH will be an important metric of skill. As we are considering relative future changes to already biased models the spatial correlation patterns are likely more important than the percentage bias and root-mean-square error (rmse). By this metric, EC-Earth, ACCESS and GFDL are found to be the 'best' models for wave patterns in NW Europe (Table A2.4.2). As we are interested in properly representing the patterns of extreme waves, AnnMax is deemed most important. Here, EC-Earth is found to be the stand-out best performing model in recreating the wave patterns found in the ERA-Interim reanalysis. Decadal-timescale changes in the global wave field can arise through natural variability (e.g. Melet et al, 2018).

Model name	mean	AnnMax	Rank mean	Rank AnnMax
ACCESS	0.983	0.969	2nd	2nd
BCC	0.969	0.954	6th	7th
CNRM	0.979	0.963	=3rd	4th
EC-Earth	0.979	0.981	=3rd	1st
GFDL	0.985	0.966	1st	3rd
HadGEM	0.978	0.962	5th	=5th
MRI	0.975	0.962	7th	=5th

Table A2.4.2. Spatial correlations between ERA-Interim forced (Dee et al, 2011) and CMIP5 "historical" forced global wave models.

A2.4.2 Regional wave model

Next, the regional wave model skill will be evaluated in parallel with the global model. In this section the global configuration of WaveWatch III is compared with the regional model nested within it. The regional model receives swell from the global model but is forced with local winds. There will also be differences between how the two models represent water depth and coastlines, due to the differing grid resolutions. The two configurations are driven by ERA-Interim reanalysis winds for a historical period (1979 - 2015) and then compared to evaluate the performance of both models and impacts of dynamical downscaling. A large set of wave buoy observations (a total of 1,804,906 records) were used. The buoys used for validation cover a range of water depths, and wave exposure. The data are managed by The Met Office, and CEFAS WaveNet. The exact locations and time period covered for model evaluation is presented in table A.2.4.3. Figure A.2.4.2. shows the wave buoy locations, and correlation between modelled and observed significant wave height.

Buoy	latitude	longitude	Start date	End date
Poole	50°38'.02N	1°43'.13W	17th Dec 2003	present
Liverpool	53°32'.01N	3°21'.30W	13th Nov 2002	present
Moray	57°57'.98N	3°19'.99E	29th Aug 2008	present
Hebrides	57°17'.53N	7°54.85W	23rd Feb 2009	present
Scilly	49°49'.00N	6°32.78W	11th Oct 2014	25th Mar 2016
S. Knock	51°34'.23N	1°34.76E	15th Jan 2010	5th Feb 2016
Belmullet A	54°17.08'N	10°16.21'W	15th Jan 2010	present
Belmullet B	54°14.03'N	10°8.57'W	15th Dec 2009	17th Apr 2015
Belmullet C	54°13.50'N	10°5.52'W	10th Sep 2014	17th Apr 2015
K1	48°42.00'N	12°24.00'W	5th Jan 2006	present
K2	51°00.00'N	13°30.00'W	5th Jan 2006	present
K4	54°31.80'N	12°21.00'W	5th Jan 2006	present
K5	59°06.00'N	11°24.00'W	5th Jan 2006	present
K7	60°42.00'N	4°30.00'W	5th Jan 2006	present

Table A2.4.3. Locations of buoy data used for wave model validation and the start/end date of observations.

A linear regression is fitted to the modelled SWH (plotted in red), and the `perfect' 1:1 line is also shown in black. This fit demonstrates an under-prediction in the most extreme wave heights in both model configurations, though it is slightly reduced at higher resolution. This is not unexpected as the simulated winds tend to underestimate extreme events, due to the atmospheric model missing small-scale (in space and time) features. The average root mean square error for the global model is 0.76m, reducing to 0.73m in the regional model. There is also a modest improvement in the R-squared correlation, from 0.90 to 0.91, as the model resolution increases.

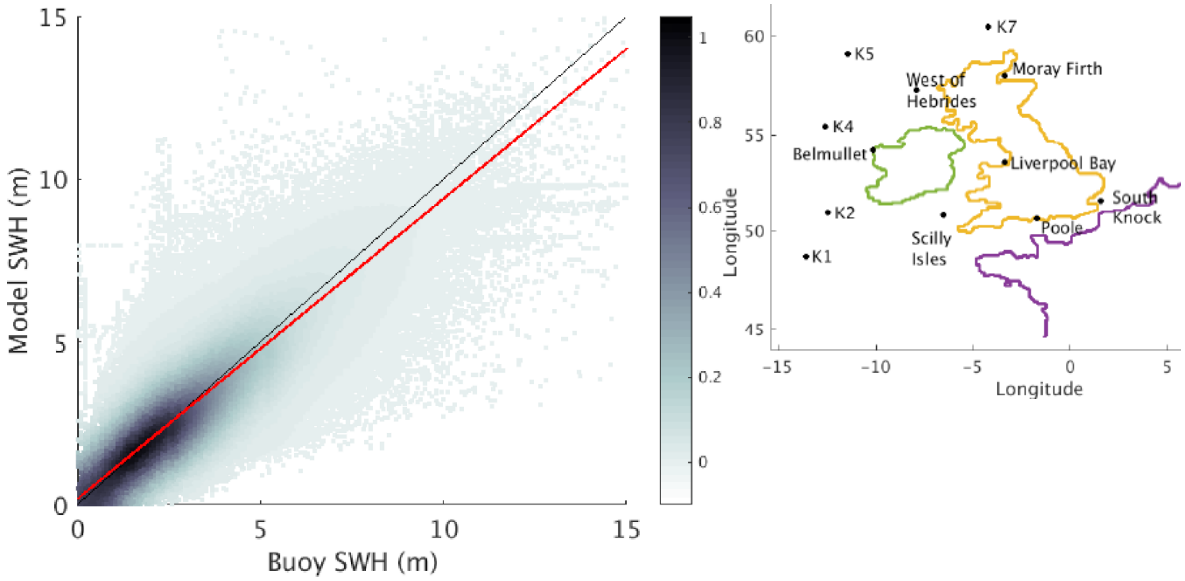

Figure A2.4.2. Left: Scatter plot coloured by density of observed vs. modelled significant wave height for the regional wave model. A linear fit is shown in red, and the 1:1 line in black. Right: locations of buoys used for model verification.

To examine the model performance at contrasting sites, the individual buoy sites are considered separately. A detailed statistical validation of the SWH and mean direction can be found in Bricheno and Wolf (submitted 2018). By considering an individual buoy, the model's ability to capture temporal variability can be tested. For example, the K2 buoy has a root mean square error of 0.85m, and a range between 0.2 and 18m. Figure A2.4.3 shows a time series at K2 from 1998 to 2015. Both global and regional model configurations capture the variability, with a small positive bias (+2.6%). At this site, the R-squared correlation is 0.87 in the global model and 0.85 in the regional model. Figure A2.4.4 presents a comparison between modelled and observed wave direction. The high resolution wave model is seen to produce better estimates of wave period and direction at both offshore and shallow water buoy sites. Improved spatial resolution in semi-enclosed seas produces a more detailed picture of coastal change.

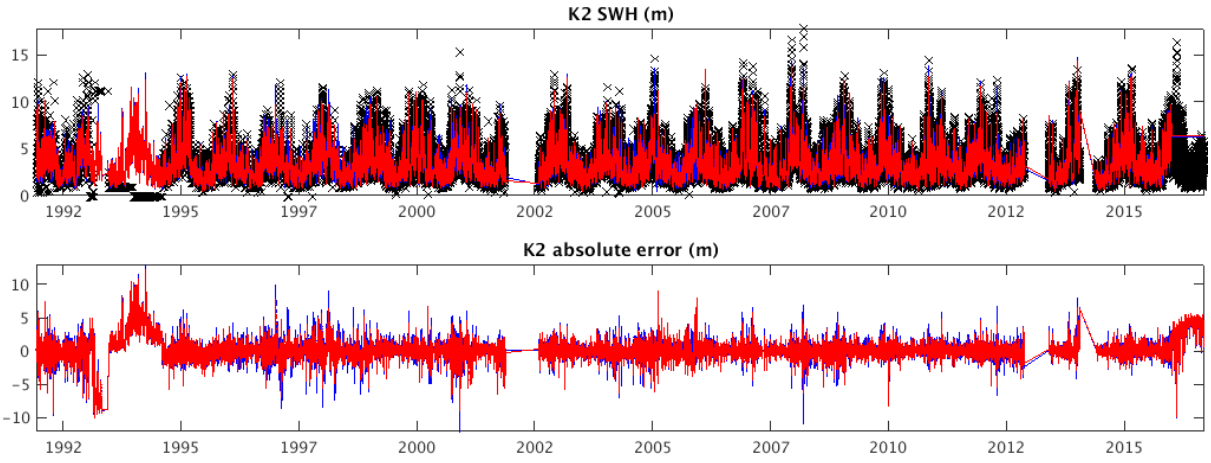

Figure A2.4.3. time series of SWH at the K2 buoy site. Blue: global wave model. Red: regional wave model. Black: observations (top). Difference between model and observations (below).

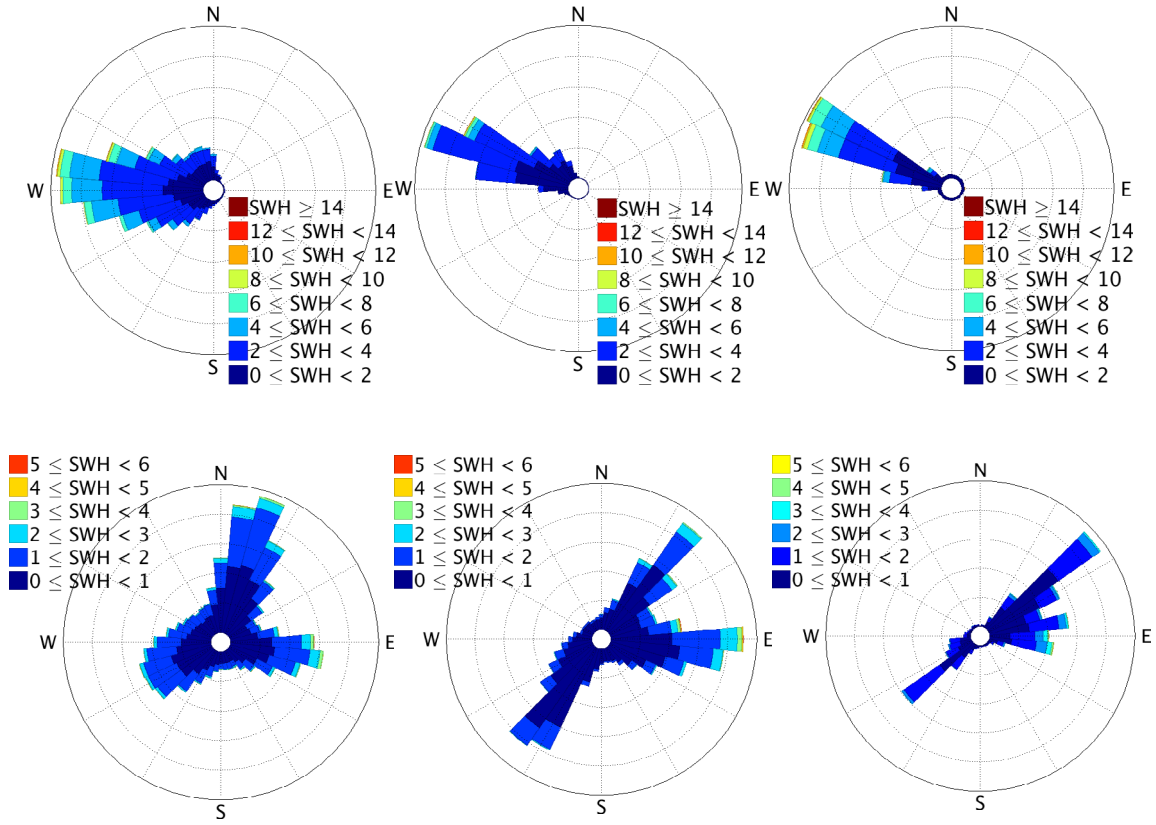

Figure A2.4.4. Wave roses from Belmullet (top) and Moray Firth (below) showing impact of model resolution. From left to right: global model, regional model, buoy.

Dynamical downscaling of the wave simulations has a more striking impact on wave direction. In seven out of nine sites considered the wave direction is better modelled with high resolution. This improvement is particularly strong at shallow, sheltered sites where coastal geometry and model bathymetry are poorly resolved in the global wave model. Figure A2.4.4 illustrates the results for 2 example locations using a “wave rose”, i.e. a polar plot, showing how wave height and direction are typically distributed at a particular location. A longer bar in each 10 degree directional bin indicates more of the waves approaching from this direction. The roses show the direction which waves are approaching the buoy from and are coloured by significant wave height. At the Belmullet site (Figure A2.4.4, upper row), the high resolution model better represents the narrow range of wave directions seen at this buoy.

In the Moray Firth (Figure A2.4.4, lower row) the regional model is better able to capture the multidirectional wave spectra, and again the wave directions have a sharper focus at higher resolution. To conclude, the regional wave model is capable of capturing a full range of wave conditions from calm to stormy. This is true for sheltered and exposed sites, experiencing swells, windsea, and bimodal conditions. There is no consistent bias or drift observed in the model, giving confidence in its ability to be used for making projections of future wave climate.

A2.5 Simulation of UK coastal sea level variability

Section summary: The UKCP18 shelf seas model simulation of coastal sea level variability is assessed against UK and European tide gauges. The model is able to capture the majority of the observed interannual variability, accounting for between about 60% and 100% of the UK tide gauge values. The model shows significant skill in capturing the spatial variations in the magnitude of sea level variability, with a spatial correlation of 0.7 with UK and European tide gauges. Overall, the evaluation gives us confidence in the utility of the UKCP18 coastal model simulations for providing information on the spatial patterns and indicative magnitude of sea level variability around the UK.

In this section we present a comparison of the UKCP18 NEMO CO6 shelf seas model simulation with the available tide gauge data from the UK, Ireland and mainland Europe. The UKCP18 shelf seas model is used to provide a spatially continuous estimate of coastal sea level variability around the UK and aid the interpretation of the available tide gauge records. Further details on the model configuration and experimental design are available in section A1.7.

An indicative set of UK tide gauge records and corresponding shelf seas model simulated time series is presented in Figure A2.5.1. Tide gauges are selected on the basis of geographical coverage and the series length. All time series are linearly detrended in order to focus on sea level variability, rather than secular change signals. The shelf seas model simulation generally does a good job of reproducing the magnitude and temporal characteristics (see Tinker et al, in prep) of the UK tide gauges, and accounts for between about 60% and 100% of the observed variability (Figure A2.5.1).

Across the larger European domain, the shelf seas model does a good job of capturing the spatial variations in the magnitude of observed sea level variability, with a spatial correlation of 0.7 based on the selected tide gauge records (Figure A2.5.2). The model generally underestimates the observed variability, by an average of about 1 cm. Overall, the comparison gives us confidence in the ability of the shelf seas model to capture spatial variations in the magnitude of coastal sea level variability and aid the interpretation of the available tide gauge records. For example, to provide guidance on the length of coastline for which a tide-gauge estimate of sea level variability is likely to be representative.

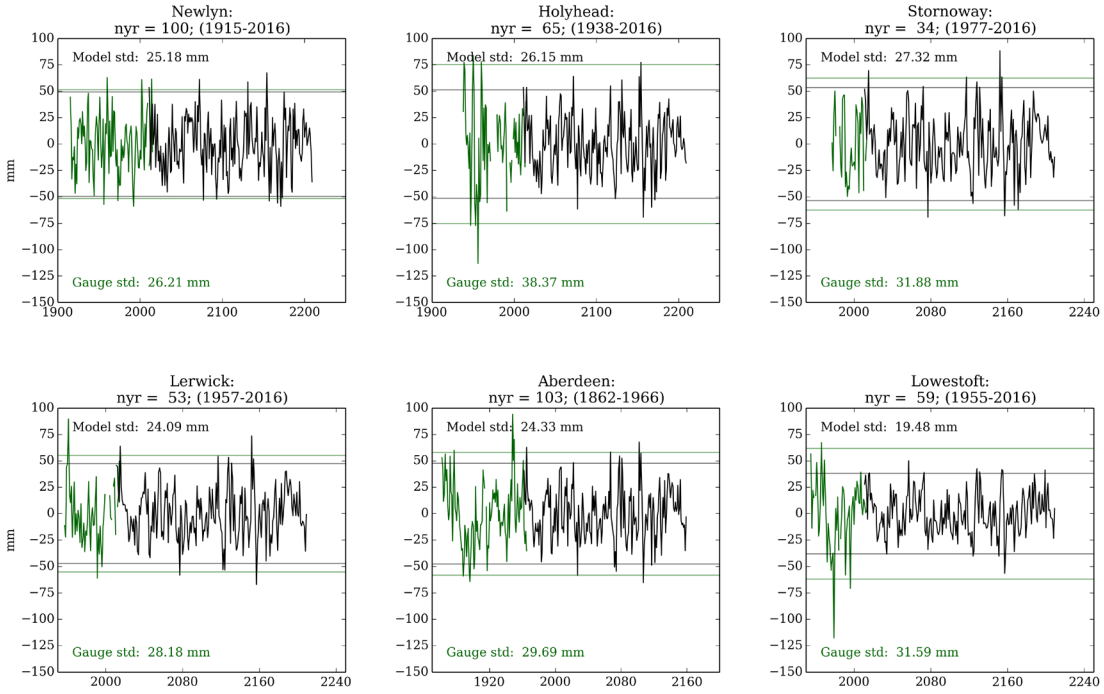

Figure A2.5.1. Observed and simulated interannual sea level variability (all time series have been linearly detrended). Tide gauges (green) are compared to the nearest model grid box (black) for a number of tide gauges around the UK, with interannual standard deviations (σ) given (horizontal lines indicate the 5th to 95th percentile range). Model simulations are appended to the end of each tide gauge record to aid comparison.

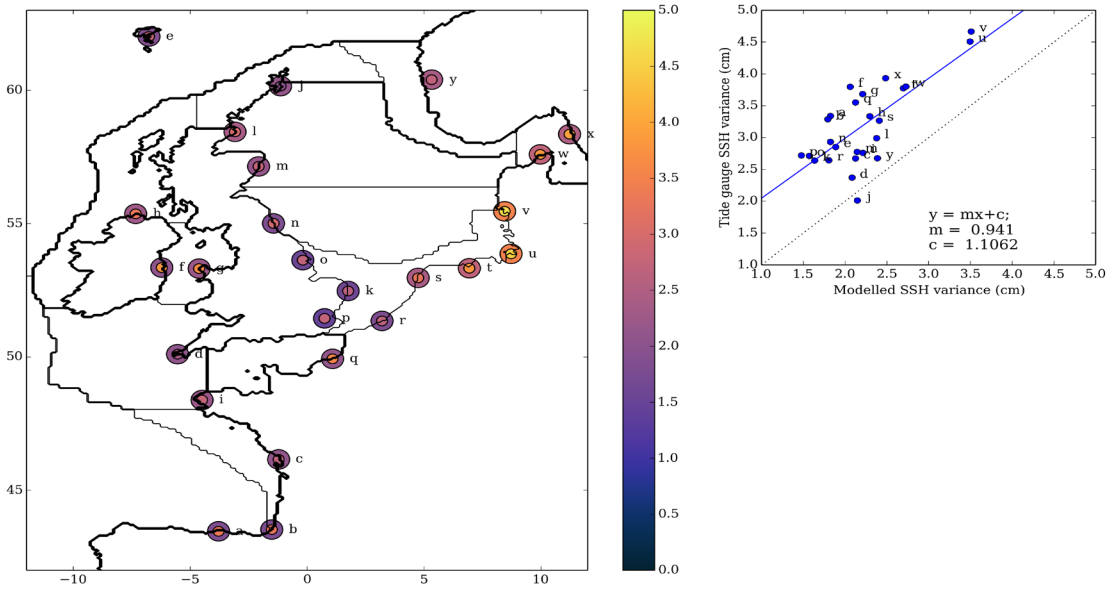

Figure A2.5.2. Spatial comparison of variance of the observed and simulated tide gauge records. All time series have been detrended using a 20-year high-pass filter. Only locations with tide gauge records longer than 45 years are included. Left: observed (inner circle) and simulated (outer circle) tide gauge variability (standard deviation). Right: Scatter plot showing the linear relationship between these observed and simulated tide gauge data.

A more complete assessment of the NEMO CO6 model is presented in Tinker et al, (in preparation) and summarised in Table A2.5.1. This more holistic assessment gives us greater confidence in the shelf model simulations in general and suggests opportunities for future work to consider the variability of on-shelf circulation and water properties (and their drivers).

Model variable	Observation data set (and reference)	Summary
Sea surface temperature	OSTIA (Roberts-Jones et al, 2012).	Interannual variability of the model and observations overlaps, but the model tends to be too cold. Biases are typically < 1 °C.
Temperature and salinity	EN4 quality-controlled temperature and salinity profiles (Good et al, 2013).	Model shows modest biases, generally < 1 °C and < 1 salinity (no units), compared to observations, tending to be too cold and too saline.
Spatial pattern of time-mean oceanographic sea level	AVISO+ Mean Dynamic Topography (Rio et al, 2014).	Very good spatial agreement (spatial correlation > 0.9).
Spatial pattern of interannual variability of oceanographic sea level	ESA Sea level anomaly CCI (Climate Change Initiative) (Legeais et al, in review 2017).	Good qualitative agreement in the spatial patterns of variability.

Table A2.5.1. A summary of model evaluation presented in Tinker et al, (in preparation).

A3. Outlook for further work

During the process of assembling this report we developed a list of future scientific research topics that would benefit the user and advance the understanding of UK coastal flood risk. The list can be regarded as a series of recommendations to the research community that has been developed by the author team with input from the UKCP18 Peer Review Panel.

- UKCP18 and previous studies have highlighted the substantial uncertainty associated with the current baseline flood risk from extreme sea level events, typically expressed in terms of return level curves. Future work should explore approaches to combining the uncertainties in return level curves with the uncertainties in time-mean sea level change to present a more holistic view of the overall uncertainty.
- One of the key uncertainties for time-mean sea level change highlighted in this report is the future contribution of Antarctic ice mass loss, particularly from dynamical ice processes on the West Antarctic Ice Sheet. Future work should consider a range of projections of Antarctic ice dynamic discharge as these become available, noting that this is a rapidly moving field of research. Assessments of the potential for accelerated sea level rise from Antarctica should also be incorporated into efforts to generate new H++ scenarios for global and UK sea level change.

- More work is needed to improve our understanding of the current and future risks of coastal flood events associated with drivers of extreme coastal water levels, particularly storm surges and waves. This includes elucidating the relationships between atmospheric storminess and extreme storm surge events around the UK. The development of storyline approaches is a useful framework in this context and could be used, for example, to explore the spread in changes in storminess over the UK and the associated changes in future flood risk. We note that there is currently very active discussion on different types of storyline approach among the research and stakeholder communities.
- Given the limitations of climate models to represent shelf sea processes, ocean dynamical downscaling should be explored to extract more reliable information on the emergent patterns of oceanographic sea level change. Downscaled simulations are also potentially a way to include realistic expressions of sea level variability with the emergent climate change signals, which may offer increased utility to coastal stakeholders.
- If there is demand for more detailed information on sea level change beyond the 21st century, it would be useful to generate extended time-horizon model projections using several different modelling approaches that include suitably sophisticated process representation (such as the two-layer model used in UKCP18). These simplified climate models are well suited to exploring a wide range of climate scenarios and this may also constitute a useful avenue of future research.

Acknowledgement

We thank the UKCP18 Peer Review Panel, chaired by Sir Professor Brian Hoskins, for their continued valuable input during the project, and specifically in reviewing and commenting on the final reports. The Peer Review Panel consisted Professor Mat Collins, Professor Jim Hall, Dr Ed Hawkins, Professor Gabi Hegerl, Dr Erik Kjellström, Professor Christoph Schär, Professor Ted Shepherd, Dr Claudia Tebaldi, Professor Dr Bart Van Den Hurk and Prof Sybren Drijfhout.

The UKCP18 Project is part of the Met Office Hadley Centre Climate Programme funded by BEIS and Defra.